1997

High precision measurement of a atmospheric trace gases using fourier transform infrared spectroscopy

Michael Brian Esler
University of Wollongong

HIGH PRECISION MEASUREMENT OF ATMOSPHERIC TRACE GASES USING FOURIER TRANSFORM INFRARED SPECTROSCOPY

A thesis submitted in fulfilment of the

requirements for the award of the degree

DOCTOR OF PHILOSOPHY

from

UNIVERSITY OF WOLLONGONG

by

MICHAEL BRIAN ESLER, B.Sc. (Hons.)

Department of Chemistry, 1997

Acknowledgments

I would like to express my sincere gratitude to my supervisors, colleagues and friends who have provided invaluable assistance in the course of this study:

- My three supervisors Assoc.Prof. David Griffith, Dr Stephen Wilson and Dr Paul Steele for interest in the project and their complementary and broad ranging expertise,

- The CSIRO Division of Atmospheric Research for financial support of the UoW/CSIRO PhD scholarship, and GASLAB for material and scientific support,

- The Cape Grim Baseline Station and the Bureau of Meteorology for financial support of project costs, and for scientific support,

- My colleagues in the atmospheric chemistry group especially Ian Jamie, Frances Phillips and Peter Mueller for their companionship and stimulating discussion,

- My fellow students and dear friends Susan Hunt, Keiryn Bennett and Karin Maxwell for accompanying me on the PhD adventure,

- My lovely wife Jo for daring to marry a PhD student and for her unwavering support.

Publications

Sections of the work described in this thesis have been reported in the following patent and publications:

- M.B. Esler and D.W.T. Griffith (inventors), 'Method and Apparatus for Measuring Gas Concentrations and Isotope Ratios in Gases', University of Wollongong (applicant). Australian Provisional Patent Application filed 18 December, 1996; U.S.A. and Canadian Patent Applications filed December 1996; International (PTC) Application filed December 1997.

- M.B. Esler, D.W.T. Griffith, S.R. Wilson and L.P. Steele, 'Carbon Monoxide, Nitrous Oxide, Methane and Carbon Dioxide - Trace Gas Analysis by Fourier Transform Infrared (FTIR) Spectroscopy' in *Baseline Atmospheric Program Australia 1994-95*, edited by R.J. Francey, A.L. Dick and N. Derek, pp. 117-18, Bureau of Meteorology and CSIRO Division of Atmospheric Research, Melbourne, Australia, 1996.

- M.B. Esler, D.W.T. Griffith, S.R. Wilson and L.P. Steele, 'Precise Measurement of Trace Gas Mixing Ratios and $^{13}CO_2/^{12}CO_2$ Isotope Ratios in Air Using FTIR Spectroscopy', *Eos Transactions, American Geophysical Union*, 77(22), Western Pacific Geophysics Meet. Suppl., W5, 1996.

- M.B. Esler, S.R. Wilson, D.W.T. Griffith and L.P. Steele, 'Cape Grim Trace Gas Monitoring Using Fourier Transform Infrared Spectroscopy' in *Baseline Atmospheric Program Australia 1996*, edited by W.J. Bouma and A.L. Dick, Bureau of Meteorology and CSIRO Division of Atmospheric Research, Melbourne, Australia, 1997, (in press).

- D.W.T. Griffith, M.B. Esler and S.R. Wilson, 'Isotopic Analysis of Atmospheric Trace Gases by FTIR Spectroscopy', in *Proceedings 11th International Conference on Fourier Transform Spectroscopy, Athens, Georgia, August 1997*, Ed. J. de Haseth, American Institute of Physics, 1997, (in press).

Abstract

Studies in recent years have revealed that the global atmosphere is undergoing rapid change due to anthropogenic activities, potentially leading to climate change through greenhouse warming, and to harmful stratospheric ozone depletion. There is a need for more and better measurements of the atmospheric trace gases implicated in these processes, so that the global anthropogenic impact can be quantified and, if possible, minimised. The three main anthropogenic greenhouse gases are carbon dioxide, methane and nitrous oxide. Nitrous oxide is also implicated in stratospheric ozone depletion. Carbon monoxide, while not directly a greenhouse gas, is intimately connected with the oxidative state of the atmosphere.

Measurements of the background atmosphere mixing ratios and of biosphere-atmosphere fluxes of trace gases typically employ some ensemble of Gas-Chromatography (GC), Non-Dispersive Infrared (NDIR) spectroscopy and Tunable Diode Laser (TDL) spectroscopy instrumentation. If, in addition, stable isotope ratio data are to be retrieved, Isotope-Ratio-Mass-Spectrometry (IRMS) instrumentation is required. These instruments all provide high-precision measurements. However, their usual single-species focus, their variety of detector response functions, calibration requirements, varying degree of mobility, as well as their complexity and expense, seriously constrains the accumulation of data in both laboratory and field investigations.

This thesis reports the development of a method of trace gas and isotope ratio analysis based on $1cm^{-1}$ resolution FTIR spectroscopy, deployable in both laboratory and field applications. The species CO_2, CH_4, CO and N_2O may be analysed simultaneously in a single air sample using this method. Its mixing ratio analytical precision is in all cases superior to or competitive with that of the more usual methods mentioned above. In addition, the FTIR instrument may be used to measure the stable isotope ratio $\delta^{13}C$ of CO_2 in ambient air to a geophysically useful degree of precision; still exceeded, however, by that attainable using IRMS.

The novel FTIR method relies on calibration using synthetically calculated absorbance spectra and a chemometric multivariate calibration algorithm, Classical Least Squares (CLS). Careful experimental design and control of the instrument environment also contributes to the high degree of precision achieved.

The overall conclusion is that $1cm^{-1}$ resolution FTIR spectroscopy is a powerful method for the simultaneous determination of trace gas mixing ratios in air, and of the isotope ratio $\delta^{13}CO_2$.

TABLE OF CONTENTS

Chapter One: Introduction

1.0 Background

The need to accurately and precisely measure the abundances of atmospheric trace gases as well as to monitor the rate at which they are changing due to natural and anthropogenic activities is now well accepted. The information gained from trace gas measurements is critical in understanding the present state of the atmosphere and in constraining projections of the future evolution of the atmosphere and climate. Since we, humankind, have proven capable of perturbing the Earth's atmosphere significantly, it is essential that trace gas measurements be made and that models of their transport and chemistry be constructed. These efforts to understand the atmosphere will inform the profoundly important political decisions needed to deal with the global consequences of our actions.

There is a need for reliable, inexpensive, but precise and accurate, trace gas analytical instrumentation to make these measurements. This work presents a novel analytical technique, based on Fourier Transform InfraRed (FTIR) spectroscopy, for the simultaneous, precise and accurate measurement of four of the most important atmospheric trace gas species CO_2, CH_4, N_2O and CO as well as for the isotopic ratio $^{13}C/^{12}C$ in CO_2.

1.1 Constituents and Structure of the Earth's Atmosphere

Compared to its radius, 6370km, Earth's atmosphere is a very thin layer of gas, ~100km, divided into four sub-layers, the troposphere, stratosphere, mesosphere and

thermosphere. Atmospheric pressure falls off exponentially with altitude, and more than 99% of the mass of the atmosphere is contained in the lowest ~50km, within the troposphere and the stratosphere, illustrated in Figure 1.1. The troposphere is the lowest layer, about 15km thick on average, and contains 90% of the mass of the atmosphere. Within the troposphere, temperature decreases with height, giving rise to efficient vertical mixing of gases (*tropos* = turning, Gk.). Separating the troposphere from the stratosphere above it is the tropopause, where the temperature undergoes an inversion. The stratosphere is typically 30-40km thick, and is characterised by increasing temperature with altitude, resulting in very slow vertical mixing and a vertically stratified structure (*stratus* = layered, Lat.).

Solar radiation passes through the atmosphere mainly in the form of visible light but also in the form of infrared (IR) and ultraviolet (UV) radiation. Much of the potentially harmful UV radiation is filtered out before reaching the earth's surface. Similarly, all of the outgoing energy, mostly IR radiation emitted by the earth's surface, passes through the atmosphere before reaching space. Some is trapped within the atmosphere and serves to warm the planet. The biosphere is the very thin "shell", lying between the atmosphere above and the lithosphere below, and contains all known life. Virtually all life depends directly or indirectly on the atmosphere for its continued existence via temperature regulation and the supply of O_2 and CO_2. (The few exceptions are some deep rock and deep sea-floor dwelling bacteria which have little apparent dependence on the atmosphere or the sun).

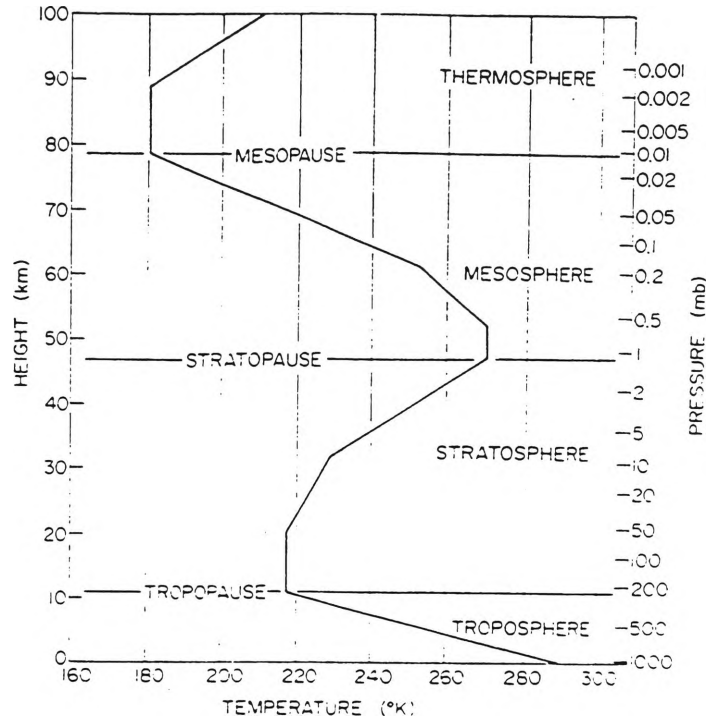

Figure 1.1. Vertical temperature and pressure structure of the atmosphere, (from [Wallace and Hobbs, 1977]).

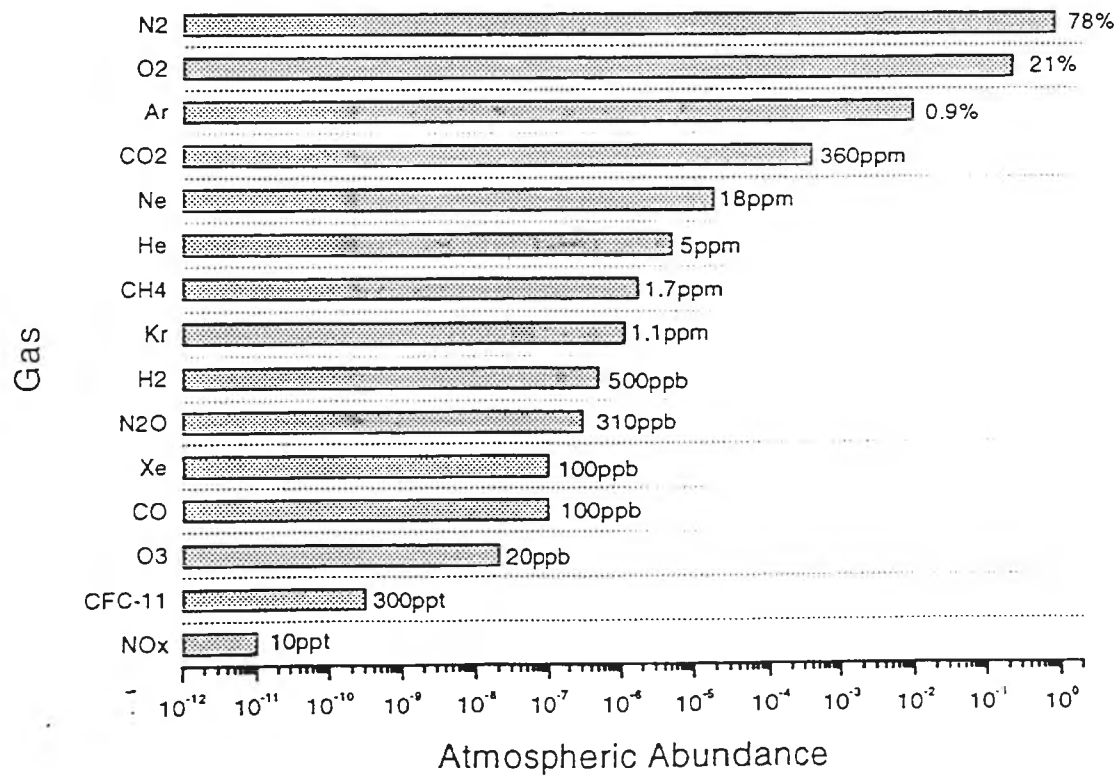

Figure 1.2. Composition of dried, unpolluted air by mole fraction. (ppm=μmol mol^{-1}, ppb=nmol mol^{-1}, ppt=pmol mol^{-1}.)

Earth's atmosphere consists almost entirely of nitrogen gas, ~78%, which is relatively inert, and of oxygen gas, ~21%, an oxidant. These two species, along with water vapour which varies from 3ppm to 4% by volume, constitute about 99% of the total atmosphere, as illustrated in Figure 1.2. Most of the remaining 1% is made up of the inert noble gases which play little part in atmospheric chemistry. Of the remainder, most is the relatively inert gas carbon dioxide, currently 360ppm in unpolluted air (ppm represents the mole fraction parts per million (10^6) or μmol/mol). This is followed by methane, 1700ppb (parts per billion (10^9) or nmol/mol), hydrogen 500ppb, nitrous oxide 310ppb, and carbon monoxide, about 50ppb in unpolluted southern hemisphere air. Recent studies indicate that this handful of trace species may wield an influence on the earth's climate that is vastly out of proportion to their atmospheric abundance (for example [*IPCC*, 1996]). CO_2, CH_4 and N_2O are the three most important anthropogenic greenhouse gases. CO, while not directly a major greenhouse gas, is intimately involved with the oxidative state of the atmosphere and hence indirectly influences global phenomena such as the greenhouse effect.

1.2 Anthropogenic Perturbation of the Atmosphere

The impact of humankind on the global atmosphere has occurred almost entirely since the beginning of the Industrial Revolution in the eighteenth century, and parallels the exponential growth of the human population since that time. The global population was approximately 0.6 billion (i.e.10^9) in 1700, 0.9 billion in 1800, 1.5 billion in 1900 and is ~5 billion in 1997 [*Graedel and Crutzen*, 1993]. Anthropogenic effects on the atmosphere are usually delineated into the distinct but related areas: urban pollution, acid rain, stratospheric ozone depletion, and the greenhouse effect. The present work is

concerned principally with the last two of these and urban pollution and acid rain will not be discussed further.

1.2.1 Stratospheric Ozone Depletion

Ozone exists in the clean troposphere at mixing ratios of < 50 ppb (parts per billion (10^9) by volume) and is present at higher concentrations, >1-10 ppm (ie. parts per million (10^6) by volume), in the stratosphere. (The volumetric mixing ratio ppb is equivalent to the mole fraction nmol mol^{-1} and ppm is equivalent to µmol mol^{-1}). In the stratosphere ozone filters out nearly all UV radiation of wavelengths less than 290nm (UV-A) which, if it reached the ground, would be lethal to living organisms. It also partially filters out UV-B radiation (290-320) which is associated with skin cancers in humans.

Ozone is formed in the stratosphere by photolysis of oxygen followed by the reaction of atomic oxygen with molecular oxygen:

$$O_2 + h\nu \rightarrow O\cdot + O\cdot \qquad (1.1)$$

$$O_2 + O\cdot \rightarrow O_3 \qquad (1.2)$$

Ozone is removed from the stratosphere by several natural sink processes. Briefly, about 20% of ozone loss is through the direct reaction:

$$O\cdot + O_3 \rightarrow O_2 + O_2 \qquad (1.3)$$

and the rest through a catalytic route:

$$X\cdot + O_3 \rightarrow XO + O_2 \qquad (1.4)$$

$$\underline{XO + O \rightarrow X\cdot + O_2} \qquad (1.5)$$

$$O\cdot + O_3 \rightarrow O_2 + O_2 \qquad (1.6)$$

The catalyst may be one of the species X· = H·, ·OH, NO, Cl· or Br·. These species all exist naturally in the stratosphere as a result of tropospheric sources of water and methane for H· and ·OH , nitrous oxide for NO, methyl chloride, CH_3Cl, for Cl· and methyl bromide, CH_3Br for Br·. However, the naturally occurring Cl· and Br· results in negligible O_3 loss.

In recent decades anthropogenic emission of CFCs (chlorofluorocarbons) and the brominated CFCs has supplemented the natural supply of Cl· and Br· to the stratosphere so that the ozone balance has shifted. Declining ozone column abundances have been observed, particularly at high latitudes where the additional factor of polar stratospheric clouds has resulted in transient springtime so-called "ozone holes" [*Hofmann et al.*, 1994]. Global emissions of CFC's are now being phased out under the Montreal Protocol. The positive effect of this has already been observed at baseline monitoring stations including the Australian station at Cape Grim, Tasmania [*Elkins et al.*, 1993; *Elkins et al.*, 1996]. Global emissions of N_2O, however, are still increasing leading to increased stratospheric ozone destruction through catalysis by NO.

1.2.2 Radiative Forcing and the Greenhouse Effect

Virtually all the radiant energy reaching the Earth is IR, visible and UV radiation emitted mainly from the photosphere of the sun which may be considered as behaving like a blackbody radiator at ~5780K, as illustrated in Figure 1.3. If all of this radiation were absorbed at the Earth's surface, thereby warming the surface, its average intensity would be approximately 343 Wm^{-2} (see Figure 1.4). However, only about 70% is absorbed, the other 30%, 103 Wm^{-2}, being reflected by clouds, the earth's atmosphere and surface back into space. So the net incoming solar radiation is 240 Wm^{-2}. The earth's surface

and atmosphere, being much colder than the sun, emits radiation at infrared wavelengths, behaving like a blackbody radiator at ~250K (Figure 1.3). Some of the infrared radiation from the surface is absorbed and re-emitted by greenhouse gas molecules in the troposphere, warming the surface further and warming the troposphere. If the earth is to maintain a constant temperature on average, the net outgoing infrared radiation which escapes into space from the top of the atmosphere must match the net incoming solar radiation, i.e. it must be 240 Wm^{-2}. The result is that although the net energy flux is zero, the trapping of radiation by the troposphere results in a warming effect at the surface. For the earth it is this effect that keeps the surface and troposphere comfortably warm, at a global average temperature of about 15°C, approximately 33°C warmer than it would otherwise be (e.g. [*Graedel and Crutzen*, 1993]).

A greenhouse gas is one which absorbs IR radiation within the frequency range of terrestrial emissions not already removed by absorption by water vapour. As illustrated in Figure 1.3, this window through which radiation may escape into space is the region 7-15μm (or about 1400-700cm^{-1}), almost coinciding with the peak intensity of terrestrial emissions. Terrestrial radiation of wavelengths longer than 15μm and shorter than 7μm is almost completely absorbed by tropospheric H_2O. The species H_2O, CO_2, CH_4, N_2O and O_3 absorb infrared radiation of various frequencies within the 1400-700cm^{-1} window. CO_2 absorbs very strongly at 700-800cm^{-1} (~14μm) and less strongly but significantly in terms of greenhouse warming at 900-1100cm^{-1} (~10μm) [*IPCC*, 1995]. Both CH_4 and N_2O absorb strongly near 1300cm^{-1} (~8μm), and ozone absorbs very strongly near 1050cm^{-1} (~9.5μm). Water, characteristically, absorbs infrared radiation (although not to extinction) at many frequencies throughout the 1400-700cm^{-1} region. The other trace

gas which is the subject of the present work, CO, absorbs infrared radiation but is not a greenhouse gas. CO absorbs near 2050cm^{-1} (~5μm), well beyond the spectral range of terrestrial emissions.

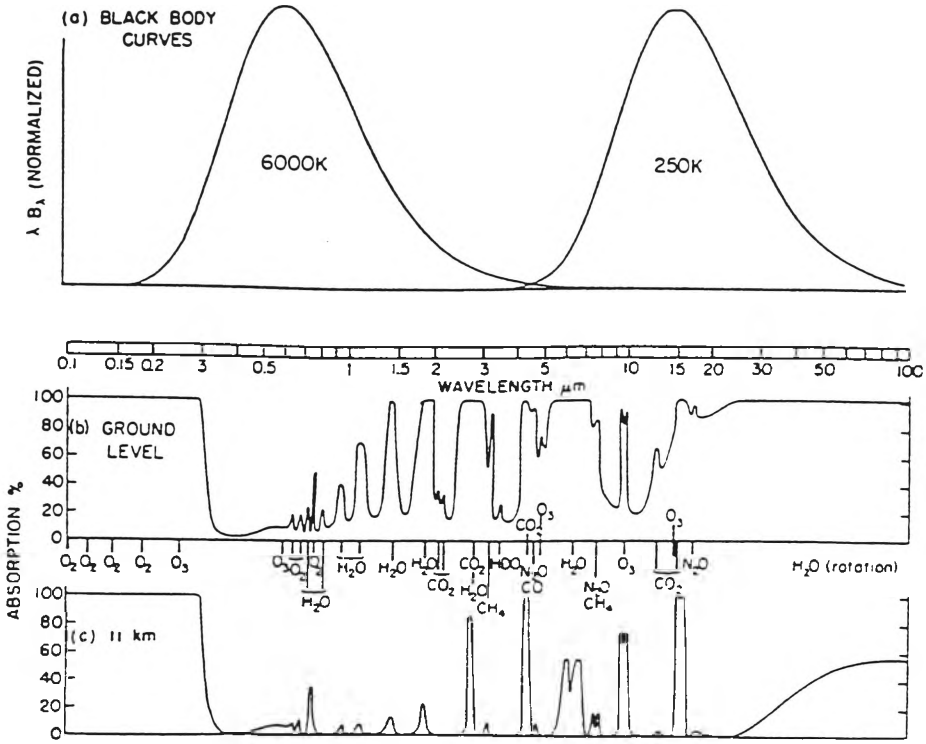

Figure 1.3. Atmospheric absorptions. (a) Black-body curves for 6000 K (the approximate temperature of the Sun) and 250 K (approximately the average temperature of the earth's atmosphere). (b) Atmospheric absorption spectrum for a solar beam reaching ground level. (c) The same for a beam reaching the tropopause (from [*Goody and Yung*, 1989]).

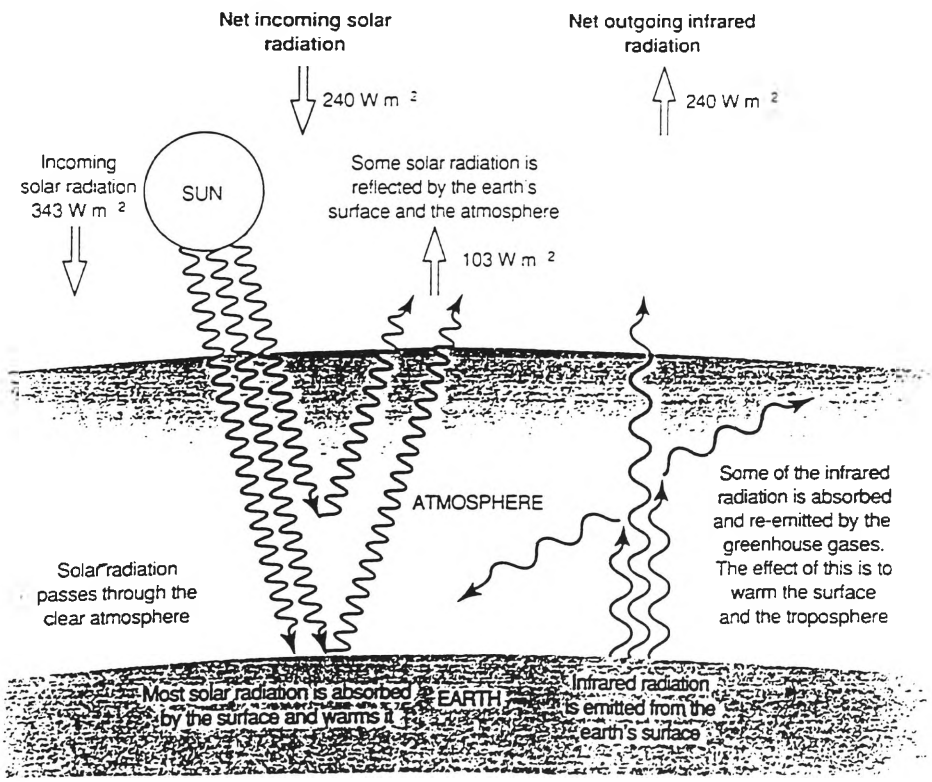

Figure 1.4. Simplified illustration of the global long-term radiative balance of the atmosphere (from [*IPCC*, 1995]).

The most abundant greenhouse gases are water vapour, (by far the most important), CO_2, CH_4, N_2O and O_3. These species are all naturally occurring and the result of their warming behaviour on the Earth is called the *natural* greenhouse effect.

While the average net radiative flux at the top of the earth's troposphere remains constant, the system is in radiative balance. If there is a change to the average net radiation, *radiative forcing* is said to occur. The climate system will slowly change to re-establish the radiative balance. Not all radiative forcing is a greenhouse effect. Radiative forcing may occur because of either a change in incoming solar radiation or in outgoing infrared radiation. For example, the steadily increasing luminosity of the sun over the earth's lifetime, a positive radiative forcing, is an example of the former. The eruption of Mt Pinatubo in 1991 resulted in an increase in the amount of aerosol particles in the stratosphere which took several years to return to pre-Pinatubo levels. This resulted in less solar radiation reaching the troposphere and a radiative forcing of about -4 Wm^{-2} a year after the eruption, cooling the earth's surface by perhaps 0.5 °C [*IPCC*, 1995].

Radiative forcing directly due to the greenhouse effect is related to changes in outgoing infrared radiation rather than incoming solar radiation. For example, an increase in CO_2 to double the pre-industrial concentration, with no other changes, will result in a global radiative forcing of about +4 Wm^{-2} due to the trapping of more infrared radiation in the atmosphere, directly warming the Earth's surface by at least 1°C on average [*IPCC*, 1995]. Increases in the tropospheric concentrations of other greenhouse gases such as CH_4, N_2O and the CFC's in particular, will also result in positive radiative forcing and potential climate change. While these gases, apart from the CFC's, do have natural

tropospheric sources, the industrial and agricultural activities of humankind is resulting in increases in the levels of these gases which, compared to their pre-industrial levels and their geological record, are extremely rapid. The report of the Intergovernmental Panel on Climate Change (IPCC) published recently concludes that "The balance of evidence suggests a discernible human influence on global climate" [*IPCC*, 1996].

1.2.2.1 Global Warming Potentials

The Global Warming Potential (GWP) of a trace gas is the time integrated radiative forcing from the instantaneous release of 1kg of the trace gas expressed relative to that of 1kg of a reference gas, usually CO_2. These are listed for a range of gases in Table 1.1. There are two main factors which account for differences in species GWPs.

Firstly, the strength with which a species absorbs infrared radiation and the part of the spectrum in which the absorption occurs. There is approximately 600 times as much CO_2 in the troposphere as there is CH_4, by mass. As seen from above the troposphere some of the CO_2 absorption bands are already saturated and addition of further CO_2 can cause more absorption only at the non-saturated edges of these bands. The integrated absorption, and hence additional radiative forcing, still increases with added CO_2, but not linearly. A similar effect occurs if a molecule absorbs in a spectral region already largely saturated by some other species, such as CO_2 or water vapour. The relationship between added CH_4 and additional radiative forcing is much closer to being linear since CH_4 is much less abundant than CO_2 and none of its absorption bands is close to saturation.

Secondly, greenhouse gases persist in the troposphere for different lengths of time depending on the mode of their destruction or removal. The species which have the

longer lifetimes will have an impact for a longer period. Thus, all other things being equal, their time integrated impact will be greater. Related to this, the time period over which the integration is performed will effect the GWP. For example, methylchloroform is an intense absorber relative to N_2O, but is much shorter lived than N_2O. Thus over a 20 year window, its GWP is greater than N_2O's, but is much less over a 500 year period.

Species	Formula	Lifetime	Global Warming Potential		
			20 years	100 years	500 years
Carbon dioxide	CO_2	50-200*	1	1	1
Methane	CH_4	12±3	56	21	6.5
Nitrous oxide	N_2O	120	280	310	170
CFC-11	$CFCl_3$	~50	4900	3800	1400
CFC-12	CF_2Cl_2	102	7800	8100	4200
CFC-113	C2F3Cl3	85	4900	4800	2300
Carbon tetrachloride	CCl_4	42	1900	1400	500
Methylchloroform	CH_3CCl_3	54	300	100	35

Table 1.1. Global Warming Potentials, referenced to the absolute GWP for CO_2. The typical uncertainty is ±35% relative to the CO_2 reference [*IPCC*, 1995; *IPCC*, 1996; *Schimel et al.*, 1996]. *No single lifetime for CO_2 can be defined because of the different rate of uptake by different sink processes.

The combination of GWPs and knowledge of the anthropogenic change in greenhouse gases since pre-industrial times allows an estimate of the radiative forcing resulting from each of the species, Figure 1.5. In order of importance the main anthropogenic greenhouse gases are CO_2, CH_4, N_2O and the various halocarbons. It is on these species that the science must focus in order to inform current and future policy decisions which may have major human and economic ramifications.

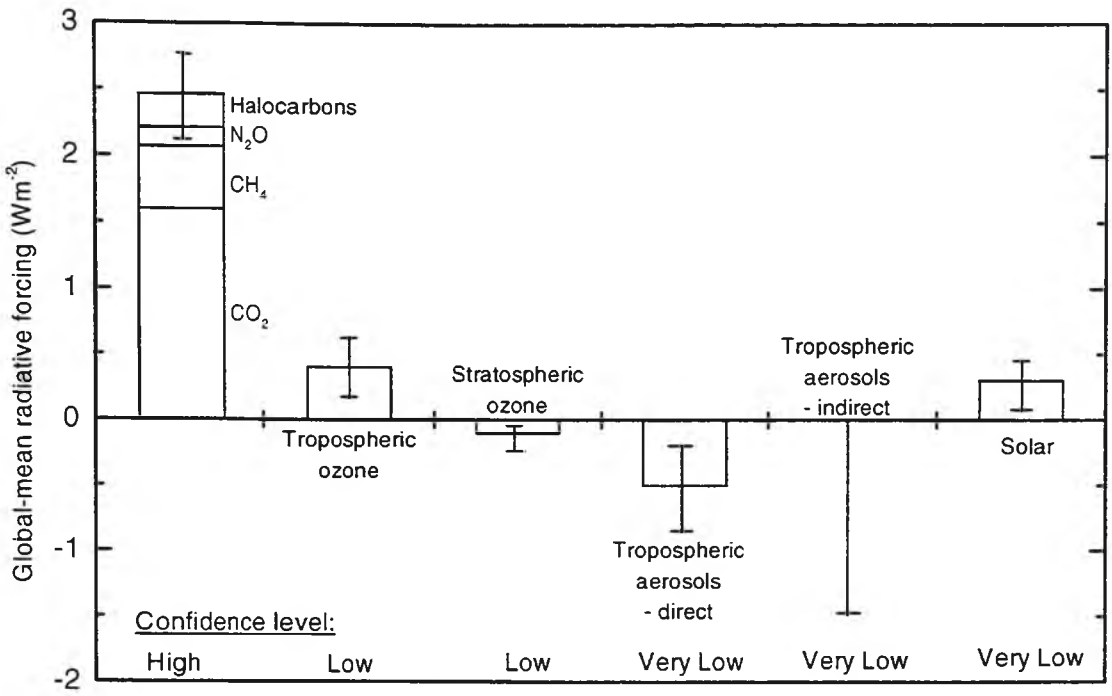

Figure 1.5. Estimates of the globally averaged radiative forcing due to changes in greenhouse gases and aerosols from pre-industrial times to the present day and changes in solar variability from 1850 to the present day. The height of the bar indicates a mid-range estimate of the forcing whilst the lines showe the possible range of values. An indication of the relative confidence level in the estimates is given below each bar [*IPCC*, 1996].

1.3 Carbon Dioxide

Carbon dioxide is the most important anthropogenic greenhouse gas. It is involved in large atmosphere-biosphere-hydrosphere fluxes of carbon but has remained at a constant average tropospheric mixing ratio over recent millennia until about 200 years ago. Its atmospheric burden has been increasing since the Industrial Revolution, mainly due to fossil fuel combustion emissions. The following sections review the geophysical significance of atmospheric carbon dioxide, the global CO_2 budget, the historical record of its atmospheric mixing ratio, and current methods for its analysis.

1.3.1 Geophysical Significance: The Carbon Cycle

Carbon dioxide accounts for more than 99% of the total carbon in the atmosphere. It plays a central role in the cycling of the element carbon between its various reservoirs in the atmosphere, biosphere (bacteria, fungi, plants animals whether terrestrial or marine), hydrosphere (oceans, rivers, lakes) and lithosphere (rocks, earth's crust and interior). The largest of these reservoirs by far is the lithosphere containing perhaps ~150×10^6 GtC (gigatons of carbon) in the form of elemental and organic carbon and carbonates originally formed by oceanic deposition as well as carbon in the planet's interior present from the time of its formation [*Wayne*, 1991]. Interaction between the lithosphere and the other reservoirs is relatively small and slow, limited to oceanic sedimentation, weathering of carbonate and silicate rocks and volcanism. The hydrosphere is the next largest planetary reservoir of carbon containing ~38000 GtC in the form of dissolved CO_2, (HCO_3^- and CO_3^{2-} ions) [*Wayne*, 1991]. The dissolution of CO_2 by the ocean and its release back into the atmosphere are in dynamic equilibrium; about 120 GtC yr^{-1} are transferred each way. Apart from this $CO_{2(g)} \leftrightarrow HCO_3^-{}_{(aq)}$ equilibrium occurring mainly in the top 100m of the ocean, the hydrosphere turns over its carbon slowly relative to its size, the deeper (than 100 m) ocean receiving organic and inorganic carbon mainly from dead marine biota and depositing carbon as ocean floor sediment.

The biosphere and atmosphere reservoirs, while much smaller than lithosphere and hydrosphere, completely dominate the latter in terms of the speed and quantity of carbon cycling occurring. For shorter time scales (i.e. less than geological) the biosphere-atmosphere system can be considered as a closed loop in isolation from the geochemical reservoirs because of the large differences in carbon flux and time constants involved.

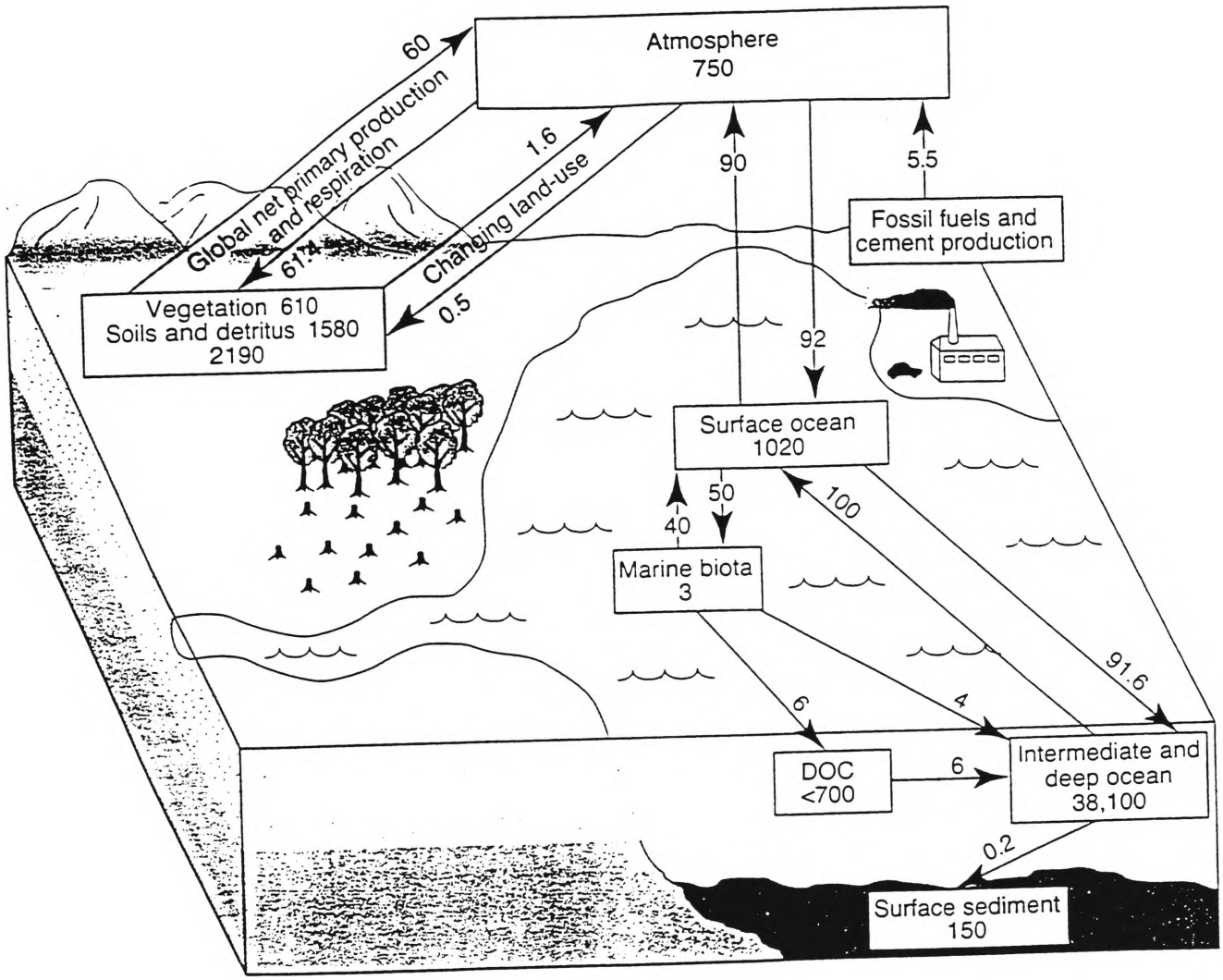

Figure 1.6. The global carbon cycle, showing the reservoirs (in GtC) and fluxes (GtC/yr) relevant to the anthropogenic perturbation as annual averages over the period 1980 to 1989. The component cycles are simplified and subject to considerable uncertainty (from [*IPCC*, 1995]).

These more rapid parts of the carbon cycle are illustrated in Figure 1.6. The atmosphere, containing 750 GtC mainly in the form of CO_2, exchanges 20% of its contents with the ocean and terrestrial biosphere every year. Terrestrial vegetation exchanges about 10% of its carbon with the atmosphere annually. Marine biota, which contain ~3GtC, annually process more than 15 times their own carbon content mainly by exchange with the atmosphere through carbon dioxide dissolved in the surface ocean layers.

Uptake of CO_2 in the biosphere is by photosynthesis by terrestrial and marine plants and micro-organisms. The chemistry of photosynthesis can be simplistically summarised as the reduction of carbon dioxide to carbohydrate, represented as $(CH_2O)_n$:

$$nCO_2 + nH_2O \xrightarrow{h\nu} (CH_2O)_n + nO_2 . \qquad (1.7)$$

The reverse process is respiration, whereby CO_2 is returned to the atmosphere,

$$(CH_2O)_n + nO_2 \rightarrow nCO_2 + nH_2O + \text{heat} . \qquad (1.8)$$

Ice core and sediment studies have shown that the carbon cycle is capable of persisting in a near steady state for millennia, (alternating with periods of glaciation), where the large carbon exchanges are nearly balanced and the size of the reservoirs constant [*Graedel and Crutzen*, 1993]. The burning of fossil fuels by humankind in the last two centuries is a significant perturbation to the steady state that has characterised recent millennia. The carbon flux into the atmosphere due to fossil fuel burning has grown from virtually zero prior to the Industrial Revolution to its present level of 5.5 GtC yr^{-1} for the period 1980-89 (see Table 1.2) and without a matching sink term to balance it. Anthropogenic changes to land use (mainly forest clearing) in recent centuries has also resulted in a net source term of biomass carbon to the atmosphere, currently estimated to be ~1 GtC yr^{-1}. The response of the carbon cycle to this anthropogenic disturbance may well be played out in the coming decades, centuries and millennia through global climate change

resulting from the CO_2 greenhouse effect. There is currently a strong effort by the atmospheric modelling community to answer the two related questions that arise from the recent recognition of the unknown consequences of anthropogenic perturbation of the carbon cycle [*Kattenberg et al.*, 1996]. They are the forward modelling question:

> "For a given CO_2 emission scenario, how might atmospheric CO_2 concentrations change in the future?"

and the reverse modelling question:

> "For a given (desirable/tolerable) CO_2 concentration profile in time leading to stabilisation at some future point, what anthropogenic emissions are implied?"

Real measurements over as much time as possible of real atmospheric, biospheric and oceanic parameters and phenomena, particularly of the trace gas species which are the subject of this work, are essential in providing data and realistic constraints to such models.

1.3.2 Sources and Sinks: The Carbon Dioxide Budget

The amount of carbon introduced to the atmosphere due to anthropogenic fossil fuel combustion and cement production during the period 1980-89 is reasonably well quantified, due to the keeping of emission inventories, at 5.5±0.5 GtC yr^{-1} (see Table 1.2). The other major anthropogenic source term, due to changes in tropical land use, is difficult to measure or model, and so is more uncertain at 1.6±1.0 GtC yr^{-1}. The sink terms describe the fate of all this extra carbon and its subsequent partitioning among the various reservoirs. Global monitoring of tropospheric CO_2 mixing ratios has determined fairly precisely that just under half of the anthropogenic emissions, 3.2±0.2 GtC yr^{-1}, remain in the atmosphere and result in the increasing levels of CO_2 witnessed since the Industrial Revolution, an increase from ~280 ppmv CO_2 in 1800 to ~360 ppmv CO_2 in

1997. The distribution of the remaining ~3.9 GtC yr^{-1} is much less well determined. The estimated budget of carbon dioxide perturbations for 1980-89 is summarised in Table 1.2.

CO_2 sources	**GtC/yr**
(1) Emissions from fossil fuel combustion and cement production	5.5 ± 0.5
(2) Net emissions from changes in tropical land use	1.6 ± 1.0
(3) Total anthropogenic emissions (1)+(2)	7.1 ± 1.1
Partitioning amongst reservoirs	
(4) Storage in the atmosphere	3.3 ± 0.2
(5) Oceanic uptake	2.0 ±0.8
(6) Uptake by Northern Hemisphere forest regrowth	0.5 ± 0.5
(7) Inferred sink (CO_2 fertilisation, nitrogen fertilisation, climatic effects); [(1) + (2)] - [(4) + (5) + (6)]	1.3 ± 1.5

Table 1.2. Averaged annual budget of CO_2 perturbations for 1980 to 1989. Fluxes and reservoir changes of carbon are expressed in GtC/yr, error limits correspond to an estimated 90% confidence interval [*IPCC*, 1996]

The ~3.9 GtC yr^{-1} not accounted for by atmospheric storage must be distributed among other sink terms to balance the budget. Experimental and modelling exercises have estimated net oceanic uptake somewhat uncertainly at 2.0±0.8 GtC yr^{-1}. The net ocean-atmosphere flux is difficult to determine because it is a very small term compared to the gross ocean-atmosphere fluxes involved, ~120 GtC yr^{-1}. Similarly, a sink term of 0.5±0.5 GtC yr^{-1} is ascribed to regrowth of forest in the northern hemisphere. The final term in Table 1.2, sometimes called the "missing sink", is basically determined by difference to account for the storage of whatever carbon is left over. CO_2 fertilisation refers to the effect of stronger plant growth in an atmosphere which is richer in CO_2. Similarly nitrogen fertilisation refers to stronger plant growth (and therefore increased carbon storage) due mainly to intentional use of agricultural fertilisers. Climatic effects

refers to decadal time-scale fluctuations in climate, whereby plant photosynthesis is more active in warmer periods than in cold, storing more carbon.

An important research imperative currently is the more precise determination of the partitioning between oceanic and terrestrial carbon sinks [*Ciais et al.*, 1995a; *Ciais et al.*, 1995b; *Francey et al.*, 1995b]. It is thought that the terrestrial sinks may not be as large or longlasting as the oceanic sinks. Terrestrial carbon storage relies on plant growth. There are two ways in which increased plant growth is limited in its long term capacity to absorb more of the atmospheric CO_2 burden. Firstly, plant lifetime is typically on the scale of decades. The death or harvest of a plant may result in most of its carbon being rereleased into the atmosphere. Secondly, the maximum potential size of the terrestrial reservoir is relatively small. The oceanic reservoir is already known to be about 50 times as large as the terrestrial reservoir. Deep ocean storage of CO_2 as HCO_3^- and CO_3^{2-} is potentially a much larger sink and likely to be effective on a longer time scale than is terrestrial carbon storage. The uncertainty in the oceanic sink term is large, 2.0±0.8 GtC yr^{-1}. The higher end of this range implies that the oceanic sink dominates terrestrial storage as a means of reducing the atmospheric carbon burden. Modelling of future climate change should correspondingly focus closely on ocean-atmosphere dynamics of carbon storage. If, however the oceanic sink is closer to 1.2 GtC yr^{-1}, the lower end of the range, terrestrial carbon storage is the dominant term. The limited size of the terrestrial reservoir and its relatively short turnover time implies a far more serious future scenario of greenhouse related climate change if this is the case [*Tans et al.*, 1993].

1.3.3 Historical Record

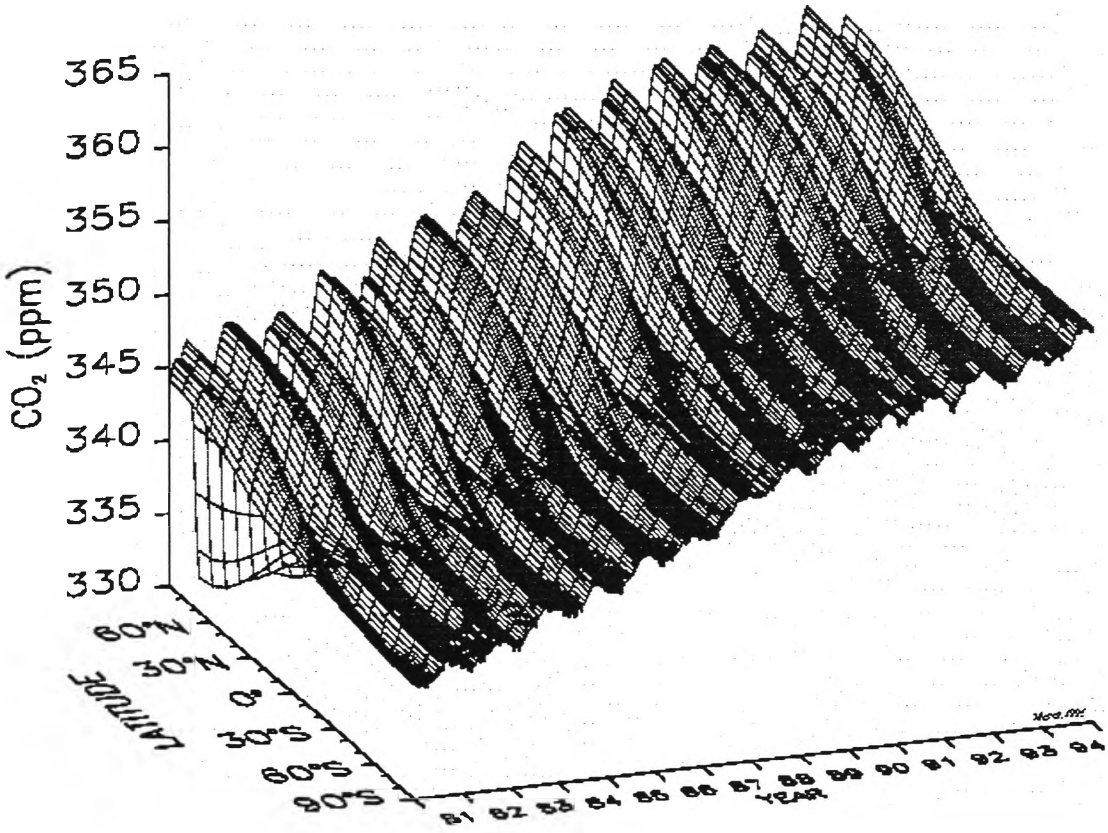

Figure 1.7. Three dimensional representation of the global distribution of atmospheric carbon dioxide in the marine boundary layer for the period 1981 through 1994 assuming no variation with longitude. Data from the NOAA/CMDL Global Cooperative Air Sampling Network were used. The surface represents data smoothed in time and latitude. (From Carbon Cycle Group, NOAA/CMDL website: http://ccg1.cmdl.noaa.gov)

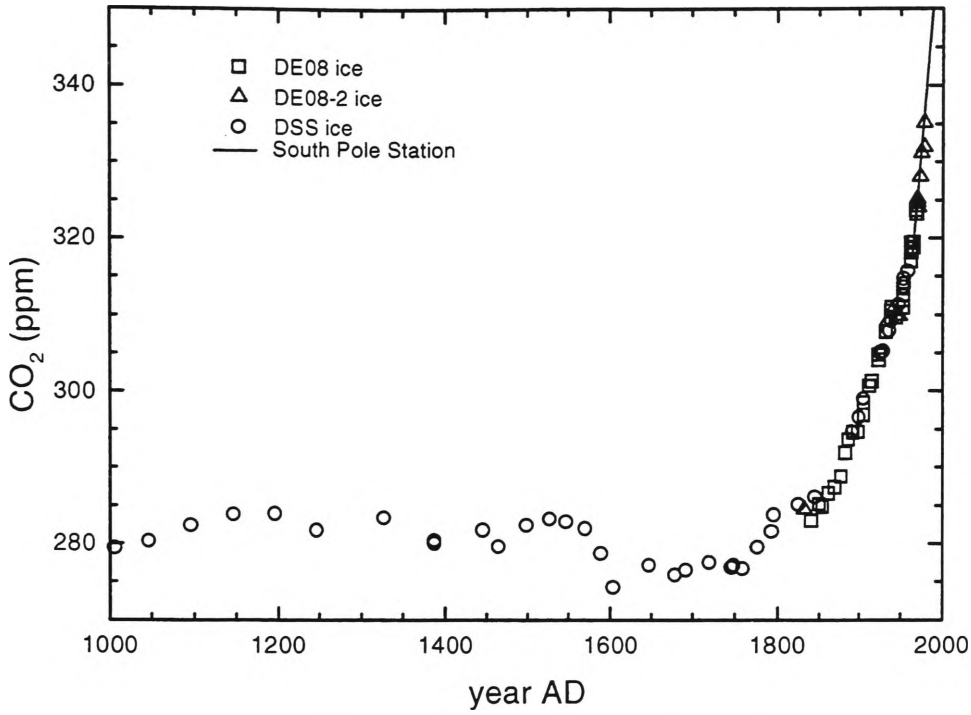

Figure 1.8. Record of CO_2 mixing ratios since 1000AD from Law Dome, Antarctica DE08, DE08-2 and DSS ice cores; and the modern atmospheric CO_2 record from south pole [*Etheridge et al.*, 1996].

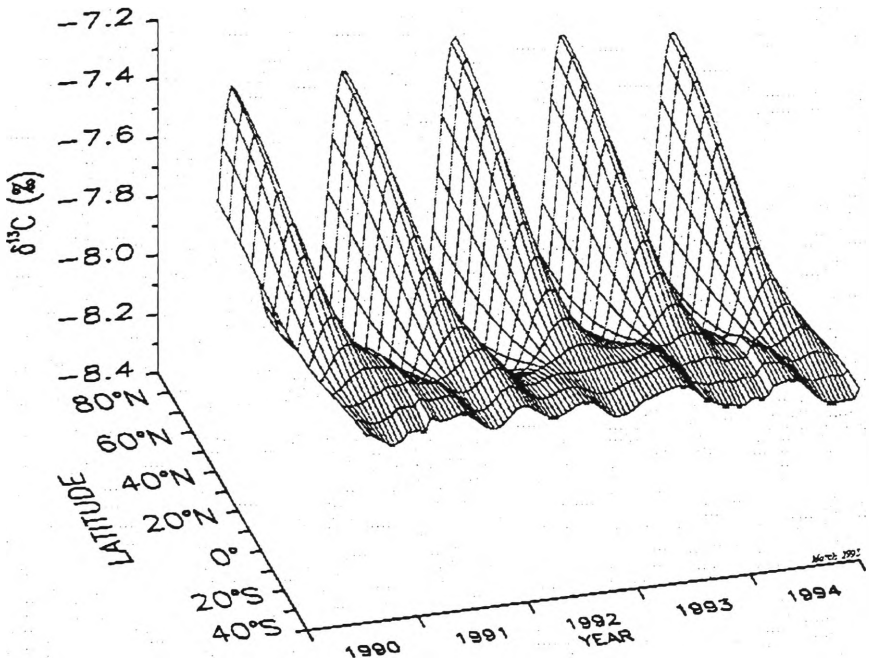

Figure 1.9. Three dimensional representation of the global distribution of the carbon isotopic composition of atmospheric carbon dioxide in the marine boundary layer for the period July 1990 through 1994 assuming no variation with longitude. The measurements of stable isotope ratios were made at the University of Colorado-INSTAAR, using air samples provided bythe NOAA/CMDL Global Cooperative Air Sampling Network. The surface represents data smoothed in time and latitude. (From Carbon Cycle Group, NOAA/CMDL website: http://ccg1.cmdl.noaa.gov)

The global average atmospheric mixing ratio of CO_2 persisted at approximately 280ppm for the 10,000 period before the beginning of the Industrial Revolution. Since then it has grown by 30% to 360ppm in 1997 as illustrated in Figures 1.7 and 1.8. The CO_2 mixing ratio is currently growing at about 1.5ppm/yr or 0.4%/yr [*IPCC*, 1996]. Figure 1.7 shows the northern and southern hemisphere seasonal trend as well as the asymmetry between the hemispheres. This is due to the northern hemisphere having significantly greater CO_2 emissions related to larger human population and greater land mass. Figure 1.9 illustrates the global distribution of carbon isotopic composition, $\delta^{13}CO_2$, showing the same north-south asymmetry (see section 1.4 below).

1.3.4 Orthodox Measurement Techniques

The most common analytical technique for determination of CO_2 mixing ratios in air is non-dispersive infrared (NDIR) spectroscopy. This method was first used to measure ambient CO_2 by Keeling [*Keeling*, 1958], the beginning of his now classic record of CO_2 mixing ratios at Mauna Loa in Hawaii from 1958 to the present, the longest continuous direct record of any atmospheric species. Since the 1970's additional NDIR CO_2 analysers have been installed in a global network of remote atmospheric monitoring. Instruments are used for continuous *in situ* analysis of ambient air as well as for analysis of flask samples collected from a much wider network of observation points, including ocean-going vessels (e.g. [*Conway et al.*, 1994]).

Infrared spectroscopy exploits the fact that molecules have well defined absorption features corresponding to infrared radiation at energies resonant with vibrational and rotational transitions of the molecule. There are a variety of NDIR (non-dispersive infrared) spectroscopic techniques. In being described as non-dispersive these techniques are distinguished from dispersive infrared techniques such as those based on grating spectrometers or interferometry where the infrared radiation is dispersed over a

broad range of the infrared spectrum. The output of a dispersive spectrometer is a spectrum of absorption versus wavelength, represented as a trace on paper or more usually converted into a two dimensional array of data points ($wavelength_i$, $absorption_i$). What the NDIR techniques have in common is their measurement of the infrared radiation absorption by a sample, integrated over a selected region of the spectrum. The bandwidth of this integration region may be selected by a bandpass filter or by some other means. The output of an NDIR instrument is a single number indicating the integrated absorption by the sample. Typically the strongly absorbing CO_2 band at 2350cm^{-1} (~4.3μm) is used (see Figure 2.2). An NDIR spectrometer is not normally capable of resolving the two main CO_2 isotopomers $^{12}CO_2$ and $^{13}CO_2$. A voltage (or current) proportional to the integrated intensity of the incident infrared radiation is generated by the detector. NDIR analysers are capable of measuring atmospheric CO_2 concentrations with a precision of about ±0.07ppm in 360ppm, or ±0.02%. The method described by *Komhyr et al.*, [1989] still prevails for background atmospheric CO_2 monitoring [*Steele et al.*, 1996a], however at least one significantly revised NDIR CO_2 analyser is being developed [*Da Costa and Steele*, 1996].

Another very precise analytical technique is gas chromatography for the separation of CO_2, followed by its reduction to CH_4 over a heated (400°C) nickel catalyst (a methaniser), and then detection by a flame ionisation detector (FID). This has been abbreviated as GC-FID with methaniser. A precision level of ±0.02%, or about ±0.07ppm in 360ppm, can be achieved [*Francey et al.*, 1996].

Accuracy is a far more challenging issue than precision. It is important that determinations of CO_2 mixing ratios made using a variety of instruments based on a

number of different possible techniques at different places and times be amenable to intercomparison and combination to provide a global CO_2 record. That is, to be useful, all measurements must be on the same scale as far as is possible. This is a continuing and quite non-trivial challenge and is addressed in Sections 3.3 and 3.7.3.

1.4 The Stable Carbon Isotope Ratio: $\delta^{13}C$ in CO_2

Isotope	Natural Abundance, %
^{12}C	98.89
^{13}C	1.11
^{14}C	$< 10^{-10}$
^{16}O	99.76
^{17}O	0.038
^{18}O	0.204

Table 1.3. The naturally occurring isotope abundances of carbon and oxygen.

There are three principal naturally occurring isotopes each of carbon and oxygen, with the natural abundances as listed in Table 1.3. The result is that the single molecular species CO_2, exists in eighteen isotopomeric forms, varying in molecular weight from 44 to 50Da. The ^{14}C isotope undergoes radioactive decay (half-life ~5730 yr), and is termed a radioisotope. The ^{12}C, ^{13}C, ^{16}O, ^{17}O, ^{18}O isotopes do not, and are termed stable isotopes. More than 99.98% of CO_2 is accounted for by the four most abundant species $^{12}C^{16}O_2$ (98.42%), $^{13}C^{16}O_2$ (1.09%), $^{12}C^{16}O^{18}O$ (0.40%), $^{12}C^{16}O^{17}O$ (0.075%).

There is a standard notation used to describe the ratios of isotopic species.

$$R^{13} = {}^{13}C/{}^{12}C \tag{1.9}$$

where ^{13}C is the concentration of $^{13}C^{16}O^{16}O$, ^{12}C the concentration of $^{12}C^{16}O^{16}O$. R^{13} is often expressed in the δ ("del") notation which is used to describe the isotopic ratio in a

sample relative to a certain accepted standard.

$$\delta^{13}C = \left(\frac{R^{13}_{sample}}{R^{13}_{standard}} - 1 \right) \times 1000 \qquad (1.10)$$

δ values are expressed in units of ‰ (per mil). For $\delta^{13}C$ in CO_2 the usual reference standard is the V-PDB scale('Vienna Peedee Belemnite', maintained by the International Atomic Energy Agency), originally derived from a piece of Peedee Belemnite, a $CaCO_3$ fossil deposit, whose C and O isotopic ratios have been well characterised [*Craig*, 1957]. These ratios define the zero point on the V-PDB scale, and $\delta_{V\text{-}PDB}$ values of a material describe how far the isotope ratio in that material differs from the ratios in V-PDB standard. The original reference material no longer exists but standard reference materials with δ values defined on the V-PDB scale are available. Material with a $\delta^{13}C_{VPDB}<0$ is said to be isotopically "light" relative to the V-PDB standard.

1.4.1 Geophysical Significance

Analysis of the ratios of the isotopomeric forms of an individual atmospheric trace gas has the potential to provide information that is not accessible by analysis of the molecular species' mixing ratio alone. This is because various physical and biological processes fractionate between the different isotopomers in distinct ways.

The most well known example of such a process is photosynthesis. During the day plants extract CO_2 from the air to synthesise carbohydrates for their growth. There is a carboxylation step in the photosynthetic process for which the rate of reaction is faster for $^{12}CO_2$ than for $^{13}CO_2$. As a result, plant photosynthesis discriminates against the heavier $^{13}CO_2$ isotope to a significant degree. While the ambient troposphere which

surrounds the plant has a $\delta^{13}CO_2$ of ~-7.9‰ (in 1997, by extrapolation from [*Allison et al.*, 1996]), the carbon incorporated into the plant tissue through photosynthesis typically has a $\delta^{13}C$ of approximately -13‰ or -28‰, depending on the type of plant. In advanced plants, there are two main groupings, the C3 plants and the C4 plants, so called because the carboxylation step proceed through either a 3-carbon or 4-carbon intermediate, respectively. Most plants are of the C3 type. Examples of the rarer C4 plants include sugar cane, corn and many grasses. C3 plants fractionate CO_2 by about -18 to -20‰ on average resulting in plant tissue with $\delta^{13}C$ of -26‰ to -28‰. C4 plants fractionate only by about -5‰ resulting in plant tissue with $\delta^{13}C$ of about -13‰. (See, for example, *Lloyd and Farquhar* [1994].)

The large isotopic fractionation that occurs in plant photosynthesis has extremely important ramifications for research into the greenhouse effect and global warming. In Section 1.3.2 the unresolved question of the relative importance of terrestrial and oceanic sinks for anthropogenic CO_2 emissions was discussed. $\delta^{13}CO_2$ values provide information which should help to answer this question.

Fossil fuels, are largely derived from plant matter and are correspondingly depleted in ^{13}C. The $\delta^{13}C$ of coal, for example, is typically similar to that of living plant tissue, ~-28‰. The CO_2 released into the air when the coal is burnt will also bear this isotopic ratio as there is negligible fractionation in the combustion process. The atmosphere itself currently has a $\delta^{13}CO_2$ of ~-7.9‰ and is becoming more negative due to the ^{13}C depleted CO_2 resulting from fossil fuel combustion entering the atmosphere. We have said that about half of this extra atmospheric burden of CO_2, due mainly to fossil fuel combustion,

is taken up by the terrestrial biosphere, through plant photosynthesis, and by the ocean through deep water storage of HCO_3^- and CO_3^{2-}. Terrestrial storage of CO_2 through photosynthesis proceeds with a large discrimination against $^{13}CO_2$, whereas dissolution in the ocean proceeds with a quite small isotopic fractionation. The CO_2 remaining in the atmosphere should have an $^{13}C/^{12}C$ ratio which reflects the relative scale of the terrestrial and oceanic sinks. A larger terrestrial sink will result in an enrichment in ^{13}C of the remaining atmospheric CO_2. Several recent publications attempt to exploit this route [*Ciais et al.*, 1995a; *Ciais et al.*, 1995b; *Francey et al.*, 1995b; *Tans et al.*, 1993]. The main limitation of this technique is one of analytical precision. The isotopic imprint of terrestrial sink processes on the atmosphere is very small. Ciais and coworkers [*Ciais et al.*, 1995b] estimate that a variation of ~0.025‰ in the mean atmospheric $\delta^{13}CO_2$ corresponds to a global net terrestrial transfer of ~1GtC. This is comparable to the best currently available analytical precision for $\delta^{13}C$ measurements of ± 0.01‰ using Isotope Ratio Mass Spectrometry [*Francey et al.*, 1996].

1.4.2 Orthodox Measurement Techniques

The major technique employed in measurements of the stable isotopes is mass spectrometry. This technique exploits the difference in mass between distinct isotopomers of the one molecular species, e.g. $^{12}C^{16}O_2$ and $^{13}C^{16}O_2$ at 44Da (Da=Dalton, atomic mass unit) and 45Da, respectively. Isotope Ratio Mass Spectrometry (IRMS) relies on ions accelerated through an electric field being deflected by a magnetic field. For two isotopomers with the same charge state, the heavier one will be deflected less than the lighter one. Downstream of the magnetic field, detectors are arranged so that each one collects ions of a specific mass/charge (m/z) ratio. The current generated by the ion striking the detector is converted to a voltage which is proportional to the

abundance of ions at that m/z ratio. A mass spectrometer designed for CO_2 isotope analysis will usually have detectors for m/z ratios of 44 ($^{12}C^{16}O_2$), 45 ($^{13}C^{16}O_2$ and $^{12}C^{16}O^{17}O$) and 46 ($^{12}C^{16}O^{18}O$ and the much less abundant multiply substituted $^{13}C^{16}O^{17}O$, $^{12}C^{17}O_2$). The existence of two CO_2 isotopomers of mass 45Da, which cannot be resolved directly by mass spectrometry is potentially a limitation of the technique. Current practice is to assume a certain $^{12}C^{16}O^{18}O$:$^{12}C^{16}O^{17}O$ ratio based on equilibrium isotopic fractionation considerations and to correct the m/z 45 detector signal accordingly [*Allison et al.*, 1994; *Craig*, 1957]. This is potentially a source of error in determinations of $\delta^{13}C$ if either the sample gas or the reference gas does not have a $^{12}C^{16}O^{18}O$:$^{12}C^{16}O^{17}O$ ratio typical of isotopic equilibrium. Another possible limitation is due to $^{14}N_2{}^{16}O$, the main isotopomer of atmospheric N_2O, having mass 44Da, the same as $^{12}C^{16}O_2$. CO_2 samples derived from the atmosphere will usually contain N_2O as an impurity, depending on the extraction technique. A correction to the m/z 44 detector signal is required based on the amount of N_2O present in the sample, usually independently determined by GC analysis, and on the efficiency with which N_2O is ionised in the mass spectrometer [*Allison et al.*, 1994; *Craig and Keeling*, 1963]. Protonated species may also cause problems in mass spectrometry, e.g. $^{12}C^{16}O_2H$ has mass 45Da and may mimic $^{13}C^{16}O_2$. Hard vacuums ($<10^{-5}$ Torr) and low impurity levels, especially of water vapour, must be scrupulously maintained.

The typical configuration for isotope analysis is dual-inlet IRMS. This type of analysis switches rapidly between two sources of CO_2, one being the sample of CO_2 which has been cryogenically extracted from an air sample, the other being a well characterised reference CO_2 gas used for calibration of all that instrument's measurements. Sample analyses are sandwiched between reference analyses to give the highest precision. With

care dual-inlet IRMS can deliver precision levels of ± 0.01‰ for $\delta^{13}C$ and ± 0.02‰ for $\delta^{18}O$ [*Francey et al.*, 1996]. IRMS is also routinely used for the measurement of $^{2}H/^{1}H$ and $^{15}N/^{14}N$ in atmospheric species by analysis of H_2 gas and detection of ions with m/z ratio of 2 and 3; or of N_2 gas and detection of m/z 28 and 29 ions.

While IRMS exploits the mass differences between isotopomers, spectroscopic techniques have been used that exploit the fact that isotopic substitution will affect the distribution of vibrational and rotational energy states of a molecule. For example, the ^{13}C-^{16}O covalent bond in $^{13}C^{16}O_2$ behaves differently from the ^{12}C-^{16}O covalent bond in $^{12}C^{16}O_2$ because of the significantly different masses of the two carbon isotopes. The $^{12}C^{16}O_2$ isotopomer in its electronic groundstate will undergo a transition to a higher vibrational energy state (ν_3, symmetric stretch) on absorption of a photon of infrared energy of about 2350cm^{-1}. The $^{13}C^{16}O_2$ isotopomer will undergo the equivalent vibrational transition at the lower energy of about 2280 cm^{-1}. The rotational constant, B, will also be slightly different for the two isotopomers. Thus, each distinct isotopomer of CO_2 has its own rotational-vibrational infrared spectrum. Analysis of carefully chosen features in the infrared spectrum of a sample containing a mixture of isotopomers can in principle be used to determine isotope ratios.

This has usually been achieved using tunable diode laser (TDL) spectroscopy. A TDL spectrometer operates on the principle of a laser frequency being tuned over a small range in the infrared region containing one or more rotational absorption lines of the species of interest. *Becker et al.*, [1992] have measured $\delta^{13}C$ in samples of CO_2 gas with a precision of ±4‰ by tuning a laser over a small region around 2291cm^{-1} which included two rotational lines, one each due to $^{12}C^{16}O_2$ and $^{13}C^{16}O_2$. Using a different

laser based technique (laser optogalvanic spectroscopy), *Murnick and Peer,* [1994] have determined $\delta^{13}CO_2$ in 5%CO_2-in-N_2 samples to a precision of ±0.2‰.

Recently isotope-selective NDIR spectrometers have been reported [*Haisch et al.*, 1994; *Koletzko et al.*, 1995]. One such instrument has been designed primarily for analysis of CO_2 in exhaled breath for diagnostic purposes based on ingestion and metabolism of a ^{13}C-labelled substrate. For 500ml breath samples, typically containing ~4% CO_2, $\delta^{13}CO_2$ is determined with a precision of ±0.4‰ [*Koletzko et al.*, 1995]

There are two recent accounts of measurement of $\delta^{13}CO_2$ using FTIR, both by *Kindness and Marr* [1996; 1997]. Their first technique employs 0.25 cm^{-1} resolution spectroscopy to analyse pure CO_2 samples at subambient pressures. The areas of several $^{12}C^{16}O_2$ and $^{13}C^{16}O_2$ rotational lines around the ν_3 transition are measured to perform the isotopic analysis. The level of precision reported for analysis of pure CO_2 samples was ±12‰. The second method employed 1cm^{-1} resolution spectroscopy and elevated sample pressures, ~10bar to provide a $\delta^{13}C$ precision of ±8‰.

1.5 Methane

Methane is the second most important anthropogenic greenhouse gas. It is also intimately connected with the oxidative state of the atmosphere through reaction with the hydroxyl radical in the troposphere. The following sections review the geophysical significance of atmospheric methane, the global methane budget, the historical record of its atmospheric mixing ratio, and current methods for its analysis.

1.5.1 Geophysical Significance

After water vapour and CO_2, methane is the most abundant greenhouse gas in the troposphere, accounting for approximately 20% of the added radiative forcing since pre-industrial times [*IPCC*, 1995]. It is a greenhouse gas because it absorbs terrestrial infrared radiation near 1300cm^{-1} (see Figure 1.3). It has a GWP many times larger than CO_2, ranging from 62 for a 20 year horizon to 7.5 for a 500 year horizon (see Table 1.1). The sources and sink terms for CO_2 were mainly biological and physical. The behaviour of methane is significantly different in that important methane chemistry occurs in both the troposphere and the stratosphere.

The most important atmospheric methane reaction is its oxidation by the hydroxyl radical ·OH. This reaction is the main cause of methane destruction, which occurs in the background atmosphere at low NO levels via the following overall reaction:

$$\cdot OH + CH_4 + O_2 \xrightarrow{net} CH_3O_2\cdot + H_2O \qquad (1.11)$$

Subsequent oxidation of the peroxy radical CH_3O_2· proceeds through a cycle in which ·OH radicals are regenerated via HO_2·. The ·OH and HO_2· cycle terminates in the formation of H_2O or peroxides such as H_2O_2 or CH_3OOH which are subsequently rained out. In regions of the troposphere where NO_x is present above ~10ppt, the oxidation of methane can proceed via a path catalysed by NO and NO_2 resulting in the formation of ozone (e.g. [*Graedel and Crutzen*, 1993]).

The hydroxyl radical, even though it is present at mixing ratios of only ~10^{-14} compared to 21% for O_2, is the main 'detergent' in the atmosphere, initiating the oxidation of a vast range of natural and anthropogenic pollutants. Increasing levels of methane may have

the net effect of changing the spatial distribution of the hydroxyl radical and reducing its overall tropospheric concentration. The main product of methane oxidation is CO which itself relies on oxidation by hydroxyl for its removal from the troposphere. Thus, increasing levels of methane and carbon monoxide in the troposphere will tend to depletion of available hydroxyl, leading to further increases in the levels of methane, carbon monoxide and other pollutants and greenhouse gases, constituting a positive feedback loop.

In the stratosphere, methane destruction leads to increased O_3 abundance through suppression of the O_3 destroying chlorine and nitrogen cycles. It also leads to increased levels of stratospheric water vapour, which acts as a greenhouse gas.

In summary, the existence of methane, a reduced species in an oxidising atmosphere, at a relatively high tropospheric mixing ratio of ~1.7 ppmv, gives it a crucial role. Methane chemistry is closely coupled with hydroxyl and CO chemistry and so is a central determinant of the oxidative state of the atmosphere as well as being the second most important anthropogenic greenhouse gas.

1.5.2 Sources and Sinks: The Methane Budget

Table 1.4 summarises the estimated sources and sinks in the methane budget. About 30% of methane is generated by natural processes and 70% is due to anthropogenic contributions. Of the total anthropogenic contribution, ~27% is identified as being fossil fuel related. This term mostly concerns leakage of methane into the atmosphere directly from coal, oil and gas mining as well as during the transport and processing of the raw materials and their eventual combustion in most cases as fuel. The coal combustion term

is as yet very uncertain and refers to methane generated by inefficient combustion. The remaining ~ 73% of anthropogenic emissions comes from agricultural practices, biomass burning and waste disposal practices. The two single largest components identified are enteric fermentation in ruminant animals, and anaerobic production in rice paddies, accounting for 23% and 16% respectively, or ~40% altogether of the total anthropogenic methane source term. The biomass burning component of the anthropogenic biospheric contribution is due to incomplete combustion. The remainder of the anthropogenic biospheric component as well as the wetlands and termite component of natural emissions are all due to basically the same process, i.e. the bacterial degradation of organic matter in anaerobic environments whether that be in sediments, swamps, rice paddies, landfills, termite digestive tracts or the rumen of cattle, sheep and other ruminant livestock.

On the sink side of the ledger, tropospheric oxidation of CH_4 by OH accounts for ~88 % of the total sink term, stratospheric destruction removing ~7%, and the remaining 5% is due to microbial uptake of methane in soils. About 6% of the total annual CH_4 emission remains in the atmosphere and accounts for the average annual rise of 10ppb in the CH_4 mixing ratio seen over the last decade.

(a)	Individual Estimate $TgCH_4/yr$	Total $TgCH_4/yr$
Atmospheric increase	**37** (35-40)	**37** (35-40)
Sinks of atmospheric CH_4		
tropospheric OH	**490** (405-575)	
stratosphere	**40** (32-48)	
soils	**30** (15-45)	
Total atmospheric sinks		**560** (460-660)
Implied sources (atmospheric increase + sinks)		**597** (495-700)

(b)	Individual estimate $TgCH_4/yr$	Total $TgCH_4/yr$
Natural sources		
Wetlands	**115** (55-150)	
Termites	**20** (10-50)	
Oceans	**10** (5-50)	
Other	**15** (10-40)	
Total identified natural sources		**160** (110-210)
Anthropogenic		
Total fossil fuel related		**100** (70-120)
Individual fossil fuel related sources		
Natural gas	**40** (25-50)	
Coal mines	**30** (15-45)	
Petroleum industry	**15** (5-30)	
Coal combustion	**?** (1-30)	
Biospheric carbon		
Enteric fermentation	**85** (65-100)	
Rice paddies	**60** (20-100)	
Biomass burning	**40** (20-80)	
Landfills	**40** (20-70)	
Animal waste	**25** (20-30)	
Domestic sewage	**25** (15-80)	
Total biospheric		**275** (200-350)
Total identified anthropogenic sources		**375** (300-450)
Total identified sources		**535** (410-660)

Table 1.4. (a) Observed atmospheric increase, estimated sinks and sources derived to balance the budget, $Tg(CH_4)/yr$; (b)Inventory of identified sources, $Tg(CH_4)/yr$ [*Prather et al.*, 1995; *Schimel et al.*, 1996]

1.5.3 Historical Record

In a similar manner to CO_2, the mixing ratio of CH_4 was stable at around 700ppb for the 10,000 period before the Industrial Revolution. Since 1800 it has increased by145% to a global average of 1720ppb in 1994, as illustrated in Figures 1.10 and 1.11. CH_4 is currently increasing at the rate of 10ppb/yr, or 0.6%/yr [*IPCC*, 1996]. The asymmetry between the northern and southern hemispheres reflects population and landmass differences.

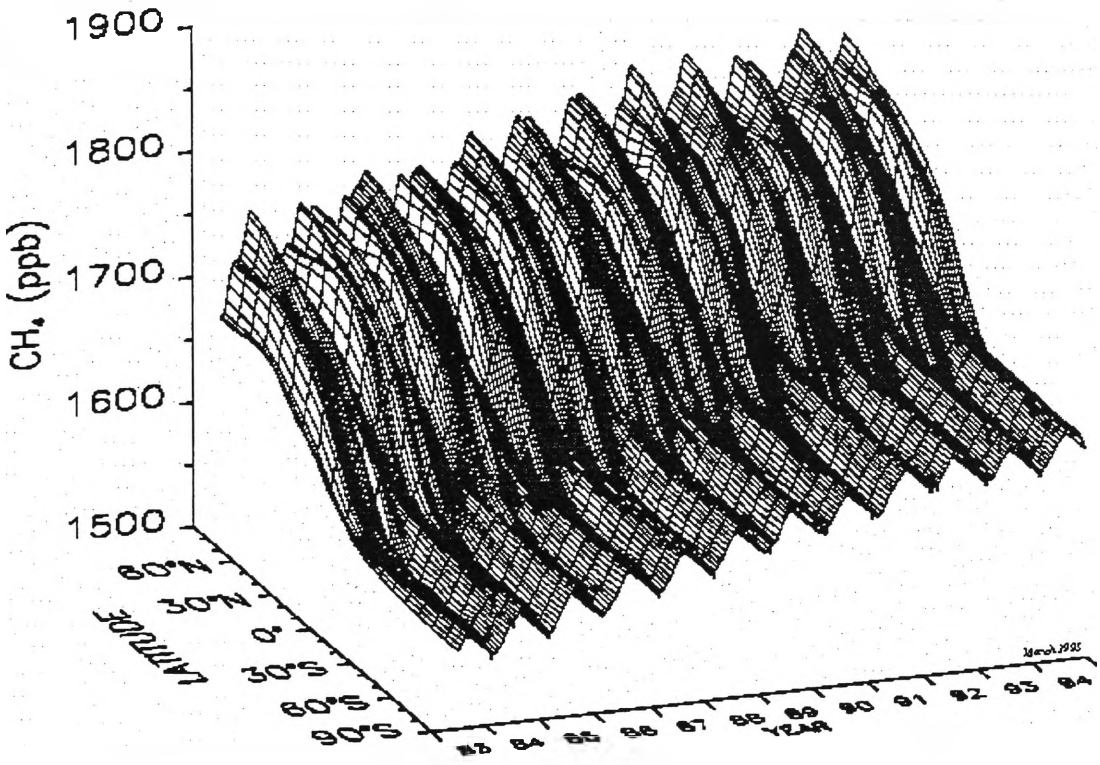

Figure 1.10. Three dimensional representation of the global distribution of atmospheric methane in the marine boundary layer for the period May 1983 through 1994 assuming no variation with longitude. Data from the NOAA/CMDL Global Cooperative Air Sampling Network were used. The surface represents data smoothed in time and latitude. (From Carbon Cycle Group, NOAA/CMDL website: http://ccg1.cmdl.noaa.gov)

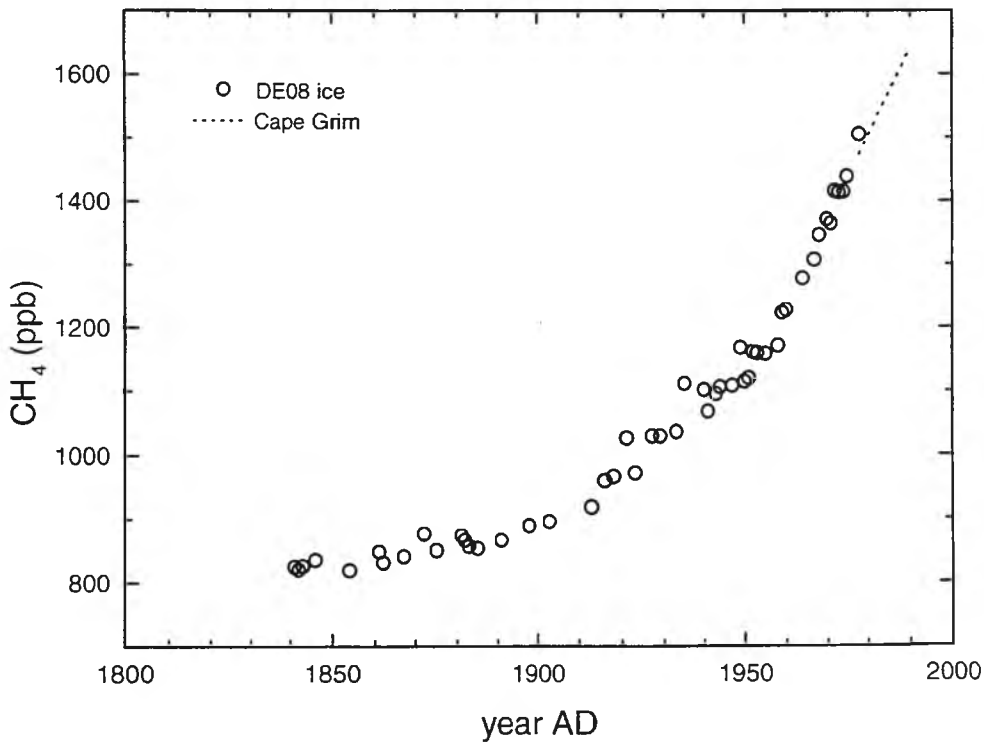

Figure 1.11. record of CH_4 mixing ratios since 1841 from Law Dome, Antarctica DE08 ice core; and the modern atmospheric CH_4 record at Cape Grim [*Etheridge et al.*, 1992].

1.5.4 Orthodox Measurement Techniques

Migeotte was the first to observe methane in the atmosphere. In 1948 he estimated a mixing ratio of 1.5ppm based on solar FTIR measurements of total column abundance at Jungfraujoch in Switzerland [*Migeotte*, 1948]. Solar FTIR spectroscopy is still used to determine total column abundances, [*Crill et al.*, 1995]. In recent decades methane concentrations (as distinct from total column abundances) have begun to be measured by chromatographic methods. Methane lends itself readily to analysis by gas chromatography with detection by flame ionisation detector (GC-FID). It is much less prone than some other trace species to sticking to or reacting with the surfaces of storage containers or plumbing, so sample handling is relatively straightforward [*Langenfelds et al.*, 1996]. It is well resolved from other species usually on a packed column and is sensitively and very linearly determined by FID. The method described by *Steele et al.*, [1987] still prevails in background tropospheric monitoring applications [*Steele et al.*, 1996b]. The level of precision achievable is around ±0.15% (1σ) , or ±2.5ppb CH_4 at background tropospheric levels of ~1720ppb [*Dlugokencky et al.*, 1995; *Francey et al.*, 1996]. Methane-in-air calibration standards are available from the Carbon Cycle Group at NOAA/CMDL (US Dept of Commerce, National Oceanographic and Atmospheric Administration/Climate Monitoring and Diagnostic Laboratory) and most measurements are now referred to the measurement scale maintained there (see Sections 3.3 and 3.7.3).

Spectroscopic techniques have been used for *in situ* analysis where rapid measurement was required, in the order of seconds rather than the minutes which GC-FID requires. Harriss and coworkers have developed an aircraft-mounted TDL instrument for

simultaneous determination of CH_4 and CO vertical profiles [*Harriss et al.*, 1992]. The instrument has a response time of a few seconds and a precision of ± 0.1 % (1σ) for CH_4 and ± 1 % (1σ) for CO. This type of instrument, while well suited for intensive field campaigns, is not appropriate for routine long term measurements because of its high maintenance demands and rate of cryogen and calibration gas consumption. An NDIR gas filter correlation (GFC) CH_4 instrument has been described [*Sebacher and Harriss*, 1982] but the method is not commonly applied in clean air studies.

Atmospheric CH_4 may be subject to stable isotope and radioisotope analysis in the same way CO_2 is, to provide information complementary to that obtained from mixing ratio analysis. There are both mass spectrometric and infrared spectroscopic techniques for measuring isotope ratios in methane. Accelerator mass spectrometry (AMS) analysis for the $^{14}C/^{12}C$ ratio provides information on the relative size of the fossil fuel source term [*Conny and Currie*, 1996]. Since ^{14}C is a radioisotope with a half life of ~5730 years fossil fuel carbon is entirely depleted in ^{14}C where modern biogenic carbon is not. $^{13}CH_4$ analysis provides complementary information, mainly about the wetland sources of methane as the $^{13}C/^{12}C$ of atmospheric CH_4 is influenced by the relative size of bacterial and non-bacterial sources [*Conny and Currie*, 1996; *Quay et al.*, 1995].

To determine $\delta^{13}CH_4$ by conventional dual inlet mass spectrometry the methane must first be extracted from a 15-30L air sample and converted to CO_2, usually by combustion. The large sample is required because CH_4 is about 200 times less abundant than CO_2 in the atmosphere. Normal analysis of CO_2 for $\delta^{13}C$ follows. The precision of this overall procedure is about ±0.1‰ [*Quay et al.*, 1995]. If the H_2O produced from the methane combustion step can be quantitatively collected and then converted to H_2, it

may be analysed by mass spectrometry for the $^{12}CH_3D/^{12}CH_4$ ratio which carries additional geophysical information about methane sources [*Conny and Currie*, 1996].

Merritt et al., [1995] have reported the isotopic analysis of atmospheric CH_4 by isotope-ratio-monitoring gas chromatography-mass spectrometry (IRM-GC-MS). An air sample of only 5 mL is required for a 15-minute analysis involving chromatographic separation followed by on-line combustion and mass spectrometric isotope measurement. The $\delta^{13}CH_4$ precision achievable is ±0.2‰ (1σ). *Rudolph et al.*, [1997] have recently reported an extension to this technique involving cryogenic preconcentration of VOCs (volatile organic compounds) from 0.5-8L of air. The method is capable of determining $\delta^{13}C$ in specific VOCs present at sub-ppb levels in ambient air with a precision of ±0.5‰.

Bergamaschi et al., [1994; 1995] have employed TDL absorption spectrometry for the measurement of both $\delta^{13}C$ and δD isotope ratios in CH_4. For repeated measurements of the same sample the precision is reported as $\sigma(\delta^{13}C) = \pm 0.5‰$ and $\sigma(\delta D) = \pm 2.5‰$.

There are no reports of the use of FTIR spectroscopy for the direct isotopic analysis of methane. In Chapter 6, it is proposed that the methods developed for low resolution FTIR spectroscopy in this work may be applied to high resolution FTIR spectroscopy for direct determination of $\delta^{13}C$ and δD in methane, and by extension, to the stable isotope ratios of other gases.

1.6 Carbon Monoxide

While not directly a significant greenhouse gas, carbon monoxide like methane is closely related to the oxidative state of the atmosphere through the CH_4-CO-OH cycle, and may affect the level of other pollutants in the atmosphere including greenhouse gases and stratospheric ozone depleting species. The following sections review the geophysical significance of atmospheric carbon monoxide, the global CO budget, the historical record of its atmospheric mixing ratio, and current methods for its analysis.

1.6.1 Geophysical Significance

Unlike the other species which are the subject of this work, CO is not considered a significant greenhouse gas as it has little direct radiative impact [*Evans and Puckrin*, 1995]. This is because apart from having a low abundance in the troposphere, ~100ppb globally averaged, CO absorbs infrared radiation at ~2200cm^{-1}, which is well outside the terrestrial blackbody emission range (see Figure 1.3). Its indirect impact on global climate may be large, however, due to its relationship with OH and O_3 concentrations. As already mentioned in Section 1.5, the atmospheric chemistry of CO is closely coupled with that of hydroxyl and methane. Just as methane is oxidised to CO by ·OH, the resulting CO is in turn oxidised to CO_2 by ·OH. The CO directly emitted from fossil fuel combustion, the other major source, is also removed by this mechanism.

$$CO + \cdot OH \rightarrow CO_2 + H\cdot \qquad (1.12)$$

Oxidation by ·OH is the single largest route for the removal of CO from the atmosphere and accounts for about 70% of atmospheric hydroxyl destruction (through chain terminating radical recombination reactions). Thus CH_4 and CO are the primary determinants of the oxidative state of the atmosphere.

CO chemistry is also closely linked to tropospheric levels of ozone and NO_x. In the background troposphere, where low levels of the pollutants NO and NO_2 may be expected, CO oxidation proceeds through reactions leading to ozone destruction via reaction of HO_2 with O_3 [*Graedel and Crutzen*, 1993].

$$CO + O_3 \xrightarrow{net} CO_2 + O_2 \qquad (1.13)$$

If the mixing ratio of NO in the lower troposphere exceeds ~10ppt, CO oxidation combined with NO_x photochemistry leads to tropospheric ozone production.

$$CO + 2O_2 + h\nu \xrightarrow{net} CO_2 + O_3 \qquad (1.14)$$

The oxidation of one methane molecule to CO and then to CO_2 in an NO-rich environment can lead to the net production of up to 4 ozone molecules. In and near urban areas NO_x levels can be as high as several tens of ppb, much higher than is necessary to catalyse this process.

1.6.2 Sources and Sinks: The Carbon Monoxide Budget

All of the terms in the carbon monoxide budget have large uncertainties (see Table 1.5). Analysis for CO is relatively difficult and the global record is not very extensive, either in terms of timespan or of the number of remote monitoring sites. About two-thirds of CO emissions currently result from anthropogenic activities. This includes transport, fossil fuel and wood fuel combustion, industry, waste incineration, anthropogenic biomass burning and oxidation of anthropogenic methane emissions. The remaining third is due to CO production by plants, possibly a photosynthetic byproduct, oxidation of natural plant-produced terpenes and oxidation of organic matter near the ocean surface. Apart from the major sink term of oxidation by OH, a small amount of CO removal is by soil

uptake and stratospheric removal (e.g. [*Warneck*, 1988]).

Sources	Range (Tg(CO)/year)
Technological (industry, transport, energy)	300-550
Biomass burning	300-700
Biogenics	60-160
Oceans	20-200
Methane oxidation	400-1000
NMHC oxidation	200-600
Total sources	1800-2700
Sinks	
OH reaction	1400-2600
Soil uptake	250-640
Stratospheric loss	~100
Total sinks	2100-3000

Table 1.5. Estimated sources and sinks of CO typical of the last decade, Tg(CO)/yr [*Prather et al.*, 1995].

1.6.3 Historical Record

Data for the global distribution of carbon monoxide does not generally exist before 1990, as illustrated in Figure 1.11, and there is no reliable CO data at all prior to 1950. Because CO is a relatively reactive species there is no record for it preserved in ice cores. The general trend since 1950 has been for growth in CO at about 0.85%/yr. Figure 1.11 shows the very strong interhemispheric asymmetry in CO mixing ratio. This reflects both landmass and population differences and the fact that CO has a short atmospheric lifetime allowing for little net transport between the hemispheres. However, the long term trend of CO mixing ratio is not monotonic, even showing periods of significant decline in the last decade, and is not well understood [*Khalil*, 1995; *Khalil and Rasmussen*, 1994; *Novelli et al.*, 1994].

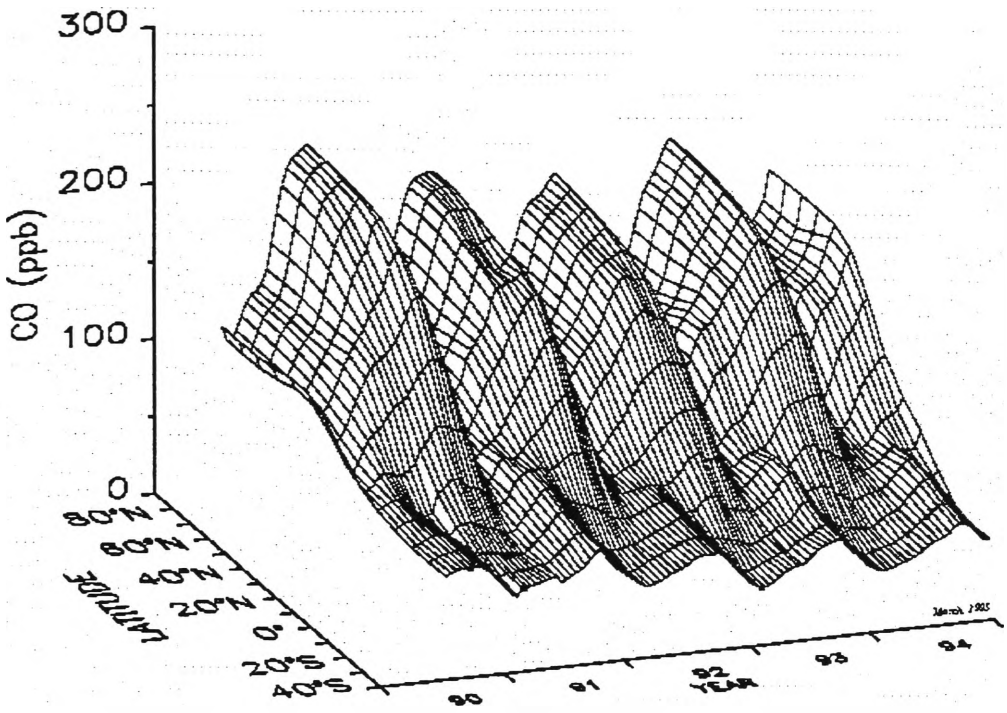

Figure 1.12. Three dimensional representation of the global distribution of atmospheric carbon monoxide in the marine boundary layer for the period July 1990 through 1994 assuming no variation with longitude. Data from the NOAA/CMDL Global Cooperative Air Sampling Network were used. The surface represents data smoothed in time and latitude. (From Carbon Cycle Group, NOAA/CMDL website: http://ccg1.cmdl.noaa.gov)

1.6.4 Orthodox Measurement Techniques

The first measurements of CO in the atmosphere were reported by *Migeotte and Neven* [1952] at the alpine Jungfraujoch observatory in Switzerland. An atmospheric total column abundance of CO was determined by analysis of the infrared solar absorption spectrum. Similar spectroscopic total column measurements still made at Jungfraujoch and other observatories provide the longest record of atmospheric CO, dating back to Migeotte's first measurement [*Dianov-Klokov et al.*, 1989; *Zander et al.*, 1989]. This spectroscopic technique provides only total column averaged mixing ratios and is relatively imprecise at ±6-10% [*Crill et al.*, 1995].

CO mixing ratio analysis is now usually performed by gas chromatographic methods. The current method of choice for background atmospheric flask sample and *in situ* analysis involves separation of CO on a packed GC column followed by reaction with HgO at temperatures greater than 210 °C [*Crill et al.*, 1995; *Francey et al.*, 1996; *Novelli et al.*, 1991].

$$CO + HgO_{(s)} \rightarrow CO_2 + Hg_{(g)} \qquad (1.15)$$

The HgO is reduced to elemental Hg which is vaporised at the high temperature. The Hg is swept by carrier gas into an optical cell where it is detected by resonance UV absorption at 254nm from a Hg lamp. This ensemble is known as a mercuric oxide reduction gas detector (RGD). The technique is sufficiently sensitive for air analysis at and below southern hemisphere baseline CO mixing ratios of ~50ppb. With thorough attention to linearisation and calibration a precision level of ~1% at 100ppbv can be attained [*Francey et al.*, 1996; *Novelli et al.*, 1992]. There are a few long term records of background tropospheric CO since the 1970's based on this technique [*Brunke et al.*, 1990; *Fraser et al.*, 1994]. Unfortunately, the RGD method exhibits significant nonlinear behaviour especially at low CO mixing ratios [*Crill et al.*, 1995; *Derwent et al.*, 1994]. Even more problematic, the nonlinear behaviour has been observed to change during the lifetime of the RGD detector as the HgO bed ages, and individual RGDs, even of the same model, are observed to have markedly different absolute response functions and linearity characteristics (P. Steele, personal communication). The main stimulus for the present FTIR spectroscopic work was the troublesome limitations in GC-RGD CO analysis in clean air.

Methods of CO analysis based on GC followed by methanisation and FID detection have been used in atmospheric monitoring [*Khalil and Rasmussen*, 1994]. This approach has

the advantage of the large dynamic range characteristic of FIDs and so is a very linear measurement. However at background levels, precision is only about 10%, which is no longer competitive with RGD detection. Spectroscopic methods have been described including TDL and NDIR gas filter correlation. TDL as mentioned already for CH_4 is a very fast response instrument, ~1s or faster, and offers excellent precision of ~1% for background CO levels [*Harriss et al.*, 1992; *Sachse et al.*, 1987]. Its use is restricted to intensive airborne and field campaigns due to the high degree of technical support required for this type of instrument. NDIR gas filter correlation analysis is relatively imprecise at ±10% for the CO mixing ratio range 100-1500ppb and a one minute average [*Fried et al.*, 1991].

As with the other trace gases, constraint of the global CO budget requires that temporally and geographically diverse measurements by a variety of groups be related to the one mixing ratio scale. For CO in particular this challenge has only recently received attention, and is far from being satisfactorily achieved (P. Steele, personal communication). This is discussed further in Sections 3.3 and 3.7.3.

1.7 Nitrous Oxide

Nitrous oxide is the third most important anthropogenic greenhouse gas. It is chemically inert in the troposphere but contributes to ozone destruction in the stratosphere. The following sections review the geophysical significance of atmospheric nitrous oxide, the global N_2O budget, the historical record of its atmospheric mixing ratio, and current methods for its analysis.

1.7.1 Geophysical Significance

N_2O is the only non-carbon gas dealt with in this work. It is a difficult gas to measure and because of its low atmospheric mixing ratio (~310ppb in 1997) and inertness, attracted little interest from atmospheric scientists until the 1970's when Crutzen [*Crutzen*, 1970] proposed that it was involved in stratospheric ozone depletion. The destruction of N_2O in the stratosphere is its only significant sink and proceeds either by photolysis

$$N_2O \xrightarrow{h\nu} N_2 + O(^1D) \tag{1.16}$$

or by reaction with excited oxygen, $O(^1D)$

$$N_2O + O(^1D) \rightarrow NO + NO \tag{1.17}$$

$$N_2O + O(^1D) \rightarrow N_2 + O_2. \tag{1.18}$$

Equation 1.34 is particularly important as this is the primary source of nitric oxide, which participates catalytically in ozone destruction according to equations 1.4-1.6, in Section 1.2.1. Thus, increased emissions of N_2O are expected to result in increased stratospheric ozone destruction.

Nitrous oxide is also the most significant greenhouse gas after CO_2 and CH_4. It is estimated that N_2O is responsible for about 6% of the radiative forcing due to greenhouse gases since the Industrial Revolution, as illustrated in Figure 1.4. Its inertness in the troposphere leads to a long atmospheric lifetime of ~120 years. Over a 100 year horizon, the GWP of N_2O is more than 300 times that of CO_2 and more than 12 times that of methane, (Table 1.1). In the very long term, based on current emission rates, the radiative forcing due to N_2O is likely to be of the same order as that due to methane, but still significantly less than that of CO_2. Thus, increased emissions of N_2O

are expected to result in increased global warming due to radiative forcing.

1.7.2 Sources and Sinks: The Nitrous Oxide Budget

	Estimate	Total
Atmospheric increase	**3.9** (3.1-4.7)	**3.9** (3.1-4.7)
Sinks		
stratosphere	**12.3** (9-16)	
soils	**?**	
Total sinks		**12.3** (9-16)
Implied total sources (atmospheric increase + total sinks)		**16.2** (13-20)
Identified sources		
Natural		
oceans	**3** (1-5)	
tropical soils		
wet forests	**3** (2.2-3.7)	
dry savannas	**1** (0.5-2.0)	
temperate soils		
forests	**1** (0.1-2.0)	
grasslands	**1** (0.5-2.0)	
Total identified natural sources		**9** (6-12)
Anthropogenic		
cultivated soils	**3.5** (1.8-5.3)	
biomass burning	**0.5** (0.2-1.0)	
industrial sources	**1.3** (0.7-1.8)	
cattle and feed lots	**0.4** (0.2-0.5)	
Total identified anthropogenic		**5.7** (3.7-7.7)
Total identified sources		**14.7** (10-17)

Table 1.6. Estimated sources and sinks of N_2O typical of the last decade (Tg(N)/yr [*Prather et al.*, 1995].

While N_2O removal from the atmosphere is now reasonably well understood, the quantification and global distribution of N_2O sources is still problematic since there are

many possible sources (see, for example, [*Bouwman et al.*, 1995]). The main source of N_2O is from the activity of anaerobic and nitrogen fixing bacteria in soils of arable land. N_2O soil flux is quite sensitive to pasture age, young pasture emitting far more than old pasture [*Keller et al.*, 1993]. Flux is greatly magnified by the application of natural or synthetic fertilisers [*Hargreaves et al.*, 1994]. Global estimates extrapolated mainly from chamber soil flux measurements are prone to great uncertainty due to spatial inhomogeneity and extrapolation [*Livingston and Hutchinson*, 1995]. In some instances it is even suggested that soil uptake of N_2O may occur, hence the unknown soil sink term in Table 1.6. During fossil fuel combustion and biomass burning, nitrogen present as either fuel impurities or as atmospheric N_2 may be oxidised to N_2O. Small oceanic sources have also been proposed [*Nevison et al.*, 1995]. At least 40% of N_2O emissions are thought to be anthropogenic in origin. Agricultural practices, especially in tropical latitudes, may see this increase.

1.7.3 Historical Record

The ice core record indicates that N_2O mixing ratios were stable at ~275ppb in pre-industrial times and have been monotonically increasing since then. The current global average mixing ratio is ~310ppb, 13% higher than in 1850, and is increasing at about 0.8ppb/yr, or 0.25%/yr [*IPCC*, 1996]. The global distribution of N_2O indicates very little evidence of interhemispheric asymmetry or of a seasonal cycle. This may reflect the very long atmospheric lifetime of N_2O (~120yr) and the current limitations of methods for its analysis.

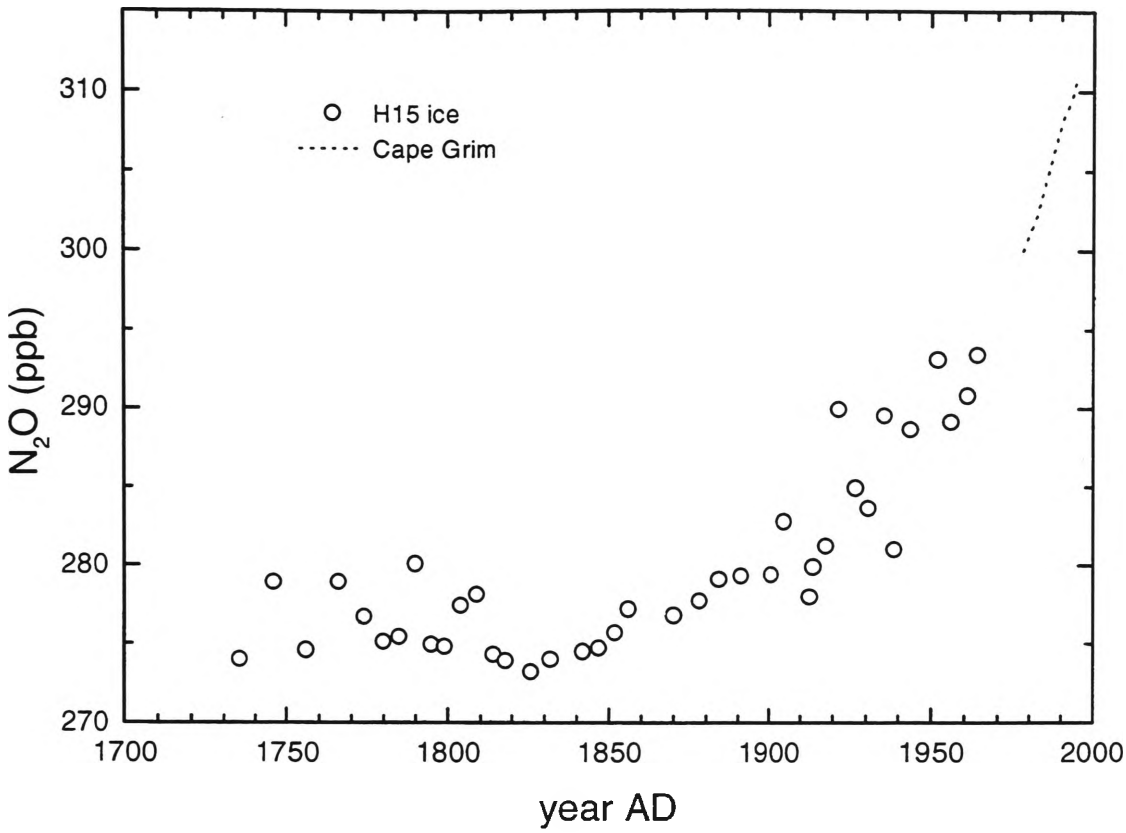

Figure 1.13. Record of N_2O mixing ratios since 1735 from Antarctic ice core H15; and the modern atmospheric N_2O record at Cape Grim [*Machida et al.*, 1995; *Langenfelds et al.*, 1996].

1.7.4 Orthodox Measurement Techniques

Just as Migeotte discovered CO and CH_4 in the atmosphere, so *Adel* [1938] discovered atmospheric N_2O in 1938 by the same approach, infrared solar spectroscopy. Little further N_2O analysis was performed by any method until the invention of the electron capture detector (ECD) by *Lovelock* [1960]. Refinement of the GC-ECD technique provided the sensitivity and precision required for useful analysis of N_2O in small air samples. GC-ECD remains the standard technique and precision levels of ±0.1%, (±0.3 ppb in 310 ppb), are attainable [*Francey et al.*, 1996; *Prinn et al.*, 1990]. An ECD does not always respond linearly to N_2O, so regular characterisation of the nonlinear response is necessary. Also ECD response may drift during use so very frequent analysis of

calibration standards is required. In a monitoring application analysis of reference standards are usually alternated with analysis of samples [*Prinn et al.*, 1990]. As with CO_2, CH_4 and CO, NOAA/CMDL maintains a suite of reference N_2O-in-air mixtures [*Elkins et al.*, 1996]. This is essential for absolute accuracy. Just as for the other trace gases, there are still unresolved interlaboratory calibration scale discrepancies (P. Steele, personal communication).

Spectroscopic techniques for N_2O analysis have been employed, usually in short duration field campaigns. Both TDL and FTIR instruments in combination with micrometeorological instrumentation have been used to study soil-air N_2O fluxes [*Hargreaves et al.*, 1994; *Smith et al.*, 1994a; *Smith et al.*, 1994b; *Wienhold et al.*, 1994]. Long open path spectroscopic techniques are considered to suffer less than small area chamber techniques from spatial inhomogeneity. However, none of the spectroscopic techniques is analytically more precise than GC-ECD.

There are very few reports of N_2O stable isotope studies. However *Wahlen and Yoshinari* [1985; *Yoshinari and Wahlen*, 1985] have determined $\delta^{18}O$ in N_2O samples using TDL spectroscopy to a precision of around ±1‰. They were able to distinguish between several N_2O sources based on their characteristic isotopic signatures.

1.8 Introduction to This Work

It is necessary to increase both the total number and quality (i.e. precision and accuracy) of trace gas measurements if the still large uncertainties in their global budgets are to be reduced. Typically, each of the trace gas species CO_2, CH_4, CO, N_2O and the isotope ratio $\delta^{13}CO_2$ currently requires a devoted instrument for high precision analysis in clean

air. In background monitoring situations a suite of GCs (for CH_4, CO and N_2O) with three different types of detectors, an NDIR (for CO_2) and an IRMS ($\delta^{13}CO_2$) instrument are required. The acquisition and commissioning of such a suite of instrumentation (even excluding IRMS) is a major capital investment and its ongoing operation and maintenance a significant expense. In practical terms this constitutes a limitation on the number of high quality trace gas measurements which can be made. If the same range of high precision measurements could be made with fewer instruments which were also less expensive, it should be possible to make far more such measurements with the same limited economic resources. In addition, limitations in GC techniques presently used for CO in particular, warrant investigation of alternative methods of analysis.

Fourier Transform Infrared Spectroscopy is a candidate for consideration as an alternative technique of high precision trace gas analysis. The instrumentation (for low to medium resolution spectrometers) is relatively inexpensive. In principle, any trace gas that absorbs in the infrared part of the spectrum, and several species simultaneously, may be analysed. Since it is an optical method based on the Beer-Lambert law, FTIR spectroscopy is arguably closer to being an absolute analytical technique than detection by FID, ECD or RGD associated with GC methods.

The chapters following investigate the utility of FTIR spectroscopy at $1cm^{-1}$ resolution for the high precision analysis of the trace gas species CO_2, CH_4, CO, N_2O and the stable isotope ratio $\delta^{13}CO_2$:

- Chapter 2:

  - reviews FTIR spectroscopy;

  - describes the optimal instrumental configuration for trace gas analysis;

  - develops a method of calibration and quantitative analysis based on the use of synthetic spectra and chemometrics;

  - verifies the method experimentally for CO_2, CH_4, CO and N_2O mixing ratio analysis and $\delta^{13}CO_2$ stable isotope analysis of air.

- Chapter 3:

  - applies the FTIR method to analysis of a suite tanks containing air already well characterised by the best available GC methods;

  - compares the FTIR and GC results;

  - assesses the stability of the FTIR in the context of calibration suite maintenance.

- Chapter 4:

  - applies the FTIR method to automated half hourly *in situ* monitoring of CO_2, CH_4, CO and N_2O mixing ratios at the Cape Grim Baseline Atmospheric Pollution Station over 5 weeks;

  - compares the 5-week FTIR trace gas record with the parallel NDIR record for CO_2 and AGAGE-GC record for CH_4, CO and N_2O.

  - demonstrates half-hourly *in situ* monitoring of $\delta^{13}CO_2$ by FTIR.

- Chapter 5:

  - introduces trace gas flux measurement techniques and the OASIS field campaign;

- applies the FTIR method to determination of trace gas vertical gradients in the atmospheric boundary layer;

- applies the FTIR method to determination of CO_2 and CH_4 biosphere-atmosphere fluxes in the boundary layer;

- applies the FTIR method to determination of $\delta^{13}CO_2$ vertical gradient in the nocturnal boundary layer;

- compares FTIR results with those of orthodox techniques.

- Chapter 6:

  - reviews preceding chapters;

  - considers the strengths and weaknesses of the FTIR method developed in the present work;

  - proposes further development and new applications of the FTIR method.

Chapter 2: Experimental Method and Quantitative Analysis

In this chapter is found a description of the FTIR-spectroscopic technique of trace gas analysis which is subsequently applied in various laboratory and field studies as described in Chapters 3-5. After a brief introduction to the principles of FTIR spectroscopy and its past application to trace gas analysis (Section 2.1), there follows a description of the configuration of the FTIR instrument used in the present work (Section 2.2). This includes a discussion of issues related to the configuration of the instrument and the experimental design. Section 2.3 deals with quantitative analysis of spectra and Section 2.4 with some second-order spectroscopic effects which must be considered to achieve the maximum analytical precision. Finally, tests of the integrated method involving both experimental and modelling exercises are described (Section 2.5).

2.1 FTIR Absorption Spectroscopy

2.1.1 The Michelson Interferometer

All commercially available FTIR instruments are based on the Michelson interferometer, invented late last century [*Michelson*, 1891]. The basic principles underlying FTIR spectroscopy can be outlined by consideration of the idealised case where an infinitely narrow, perfectly collimated beam of monochromatic light passes through a Michelson interferometer. This consists of a beamsplitter and two mirrors, one stationary and one moving, as illustrated below in Figure 2.1.

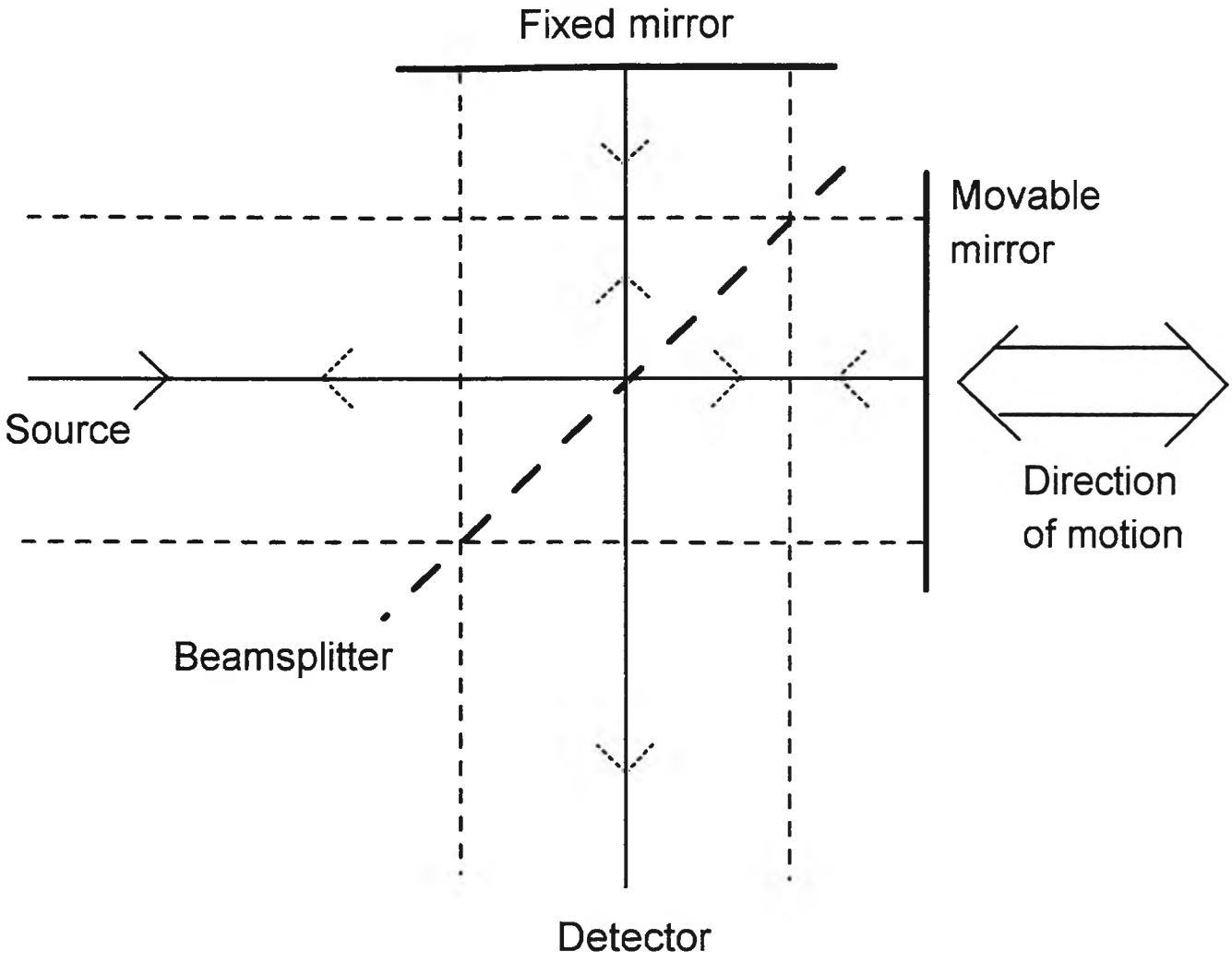

Figure 2.1. Schematic representation of a Michelson interferometer. The median ray is shown by the solid line, and the extremes of the collimated beam are shown by the broken lines.
(From *Griffiths and de Haseth*, [1986])

The beamsplitter reflects half of the light beam incident upon it to the fixed mirror and transmits half of the beam to the moving mirror. The beams are reflected back from the respective mirrors and return to the beamsplitter where each is in turn partially reflected and partially transmitted. The two reflected beams will interfere with each other at the beamsplitter. The two resultant recombined beams will be directed one back to the source, where it is effectively lost, and the other perpendicularly, to the detector by which its intensity is measured. Because of the effect of interference, the intensity of the beam passing to the detector (as well as that of the lost beam), depends on the difference in path of the beams in the two arms of the interferometer. Let the wavelength of the monochromatic light be λ (in centimetres). When the fixed and movable mirrors are equidistant from the beamsplitter, the two beams will be in phase on recombination at the beamsplitter and will interfere constructively. The intensity of the beam passing to the detector is then the sum of the intensities of the beams passing to the fixed and movable mirrors, and none of the light returns to the source. If the movable mirror is displaced a distance $\frac{1}{4}\lambda$, then the path difference in the two arms is $\frac{1}{2}\lambda$ and the beams recombining at the beamsplitter will be out of phase by exactly $\frac{1}{2}\lambda$ and will interfere destructively. All of the light will return to the source and none will reach the detector.

If the mirror is moved at constant velocity the beam intensity monitored by the detector will be seen to vary sinusoidally, as the path difference causes alternating constructive and destructive interference. This interference pattern, of changing intensity with mirror displacement is called the interferogram. Michelson recognised that it was possible to obtain spectra from the interferogram. The interferogram is the single beam intensity as a function of mirror displacement (in cm). The spectrum is the single beam intensity as a function of its wavenumber $\tilde{\nu}$ (in cm^{-1}, which is the inverse of the displacement unit).

Alternatively, the interferogram may be considered a function of time if the mirror is travelling at a constant velocity, and the spectrum a function of the wavenumber of the radiation. The interferogram and the spectrum are two closely related functions which exist in mathematical spaces which are inverse to each other. The simplest equation representing the relationship between the interferogram and the single beam spectral intensity is

$$I(\delta) = \frac{1}{2} H(\tilde{\nu}) I(\tilde{\nu})(1 + \cos 2\pi\tilde{\nu}\delta) \qquad (2.1)$$

where $I(\delta)$ is intensity of the beam striking the detector as a function of path difference δ, $I(\tilde{\nu})$ is the intensity of the source at wavenumber $\tilde{\nu}$ and $H(\tilde{\nu})$ is a wavenumber dependent correction factor to account for instrumental effects on the intensity. $H(\tilde{\nu})I(\tilde{\nu})$ is the single beam intensity spectrum. Mathematically, $I(\delta)$ is the cosine Fourier transform of $H(\tilde{\nu})I(\tilde{\nu})$. The single beam spectrum is calculated from the interferogram by computing the cosine Fourier transform of $I(\delta)$; hence the name "Fourier Transform" Infrared Spectrometry.

The reality is far more complex than the idealised case described above but the same principles hold. In a real FTIR spectrometer, the source is not monochromatic but typically continuous over a range of the infrared wavenumbers. Nor will the incident light beam be infinitely narrow or perfectly collimated, the beamsplitter perfectly efficient, the mirrors perfectly aligned nor the detector similarly responsive to all wavenumbers of incident light. These complications are well understood and documented, for example by *Griffiths and de Haseth* [1986]. When radiation of more than one wavenumber is emitted by a source, the measured interferogram is the arithmetic sum of the interferograms corresponding to each wavenumber. In other

words the interferogram simultaneously carries information about all spectral intensities of all the radiation incident on the detector. This simultaneous use of all the available source radiation is known as the multiplex or Felgett's advantage. It results in FTIR spectrometers making far more efficient use of the source radiation than, for example, a scanning monochromator instrument, in which most of the emitted radiation is discarded most of the time. It follows that the Fourier transform of such an interferogram will yield a single beam intensity spectrum across the wavenumber range of radiation emitted by the source. These interferograms, or more usually the single beam spectra into which they are immediately transformed, constitute the primary data for the analyses described in the following section and chapters.

2.1.2 Absorbance Spectra and the Beer-Lambert Law

Consider a single beam spectrum, $I_0(\tilde{\nu})$, and a second single beam spectrum, $I_{\text{sample}}(\tilde{\nu})$ collected on the same instrument under the same circumstances except that in the second case the intensity of the recombined beam leaving the interferometer is attenuated by then passing through a sample before reaching the detector. Both spectra contain information about the radiation source, the interferometer and the detector behaviour and the second spectrum, in addition, contains information about the sample. The transmittance spectrum is obtained from the ratio of the two

$$t(\tilde{\nu}) = \frac{I_{\text{sample}}}{I_0}, \tag{2.2}$$

and contains primarily information about the sample, the other contributions having largely cancelled out. According to the Beer-Lambert Law for monochromatic light the resulting transmittance t at a given $\tilde{\nu}$ is related to the absorption coefficient $\alpha(\tilde{\nu})$ of the

sample at that $\tilde{\nu}$, the thickness of (or pathlength through) the sample l, and the concentration of the absorbing species C, by an exponential function:

$$t(\tilde{\nu}) = \exp^{-\alpha(\tilde{\nu})Cl} \quad . \tag{2.3}$$

Combining equations 2.2 and 2.3 gives

$$A(\tilde{\nu}) = -\log_{10}\left(\frac{I_{\text{sample}}}{I_0}\right) = \alpha(\tilde{\nu})Cl \tag{2.4}$$

the equation for the absorbance $A(\tilde{\nu})$ at a given wavenumber. Absorbance is the negative log of the transmittance, and is directly proportional to the sample concentration provided the Beer-Lambert law is obeyed. This is the case for a single absorbing species. For a mixture of N components which are not interacting chemically with each other (usually the case with gas phase samples), absorbance is additive and the Beer-Lambert law may be expressed as

$$A(\tilde{\nu}) = \sum_{i=1}^{N} \alpha_i(\tilde{\nu}) C_i l \, . \tag{2.5}$$

In principle, when the Beer-Lambert law applies, it is possible to determine the concentrations of all the infrared absorbing species in a mixture from a single absorbance spectrum of the sample. Strictly, the Beer-Lambert Law holds only at infinite resolution, but is a good approximation at many finite resolutions. (The cases where the Beer-Lambert law is not a good approximation, even for mixtures of non-interacting gases, are briefly discussed in Section 2.4.1, below). Figure 2.2 illustrates how an absorbance spectrum of clean dry air is obtained from two interferograms.

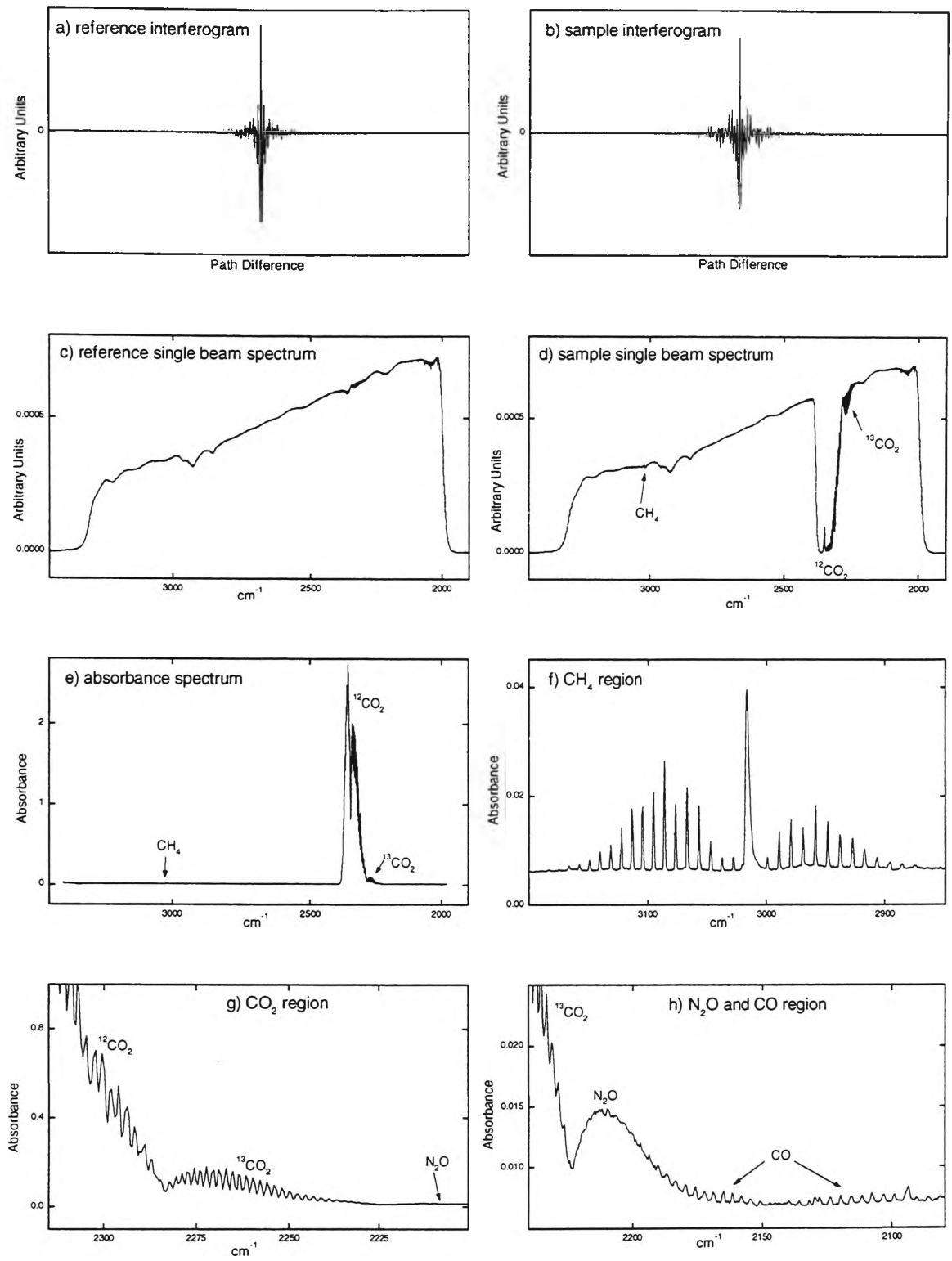

Figure 2.2. The process of obtaining an absorbance spectrum from interferometry. (a) interferogram of empty White cell; (b) interferogram of White cell containing sample; (c), (d) single beam spectra of empty White cell and White cell with sample, respectively, obtained from the Fourier transform of the interferograms; (e) whole absorbance spectrum obtained by applying equation 2.4 to the two single beam spectra; (f) region of absorbance spectrum showing CH_4 absorption features; (g) region showing $^{12}CO_2$, $^{13}CO_2$ and N_2O absorption features; (h) region showing $^{13}CO_2$, N_2O and CO absorption features.

2.1.3 FTIR Spectroscopy and Trace Gas Measurements

Gas phase FTIR spectroscopy, although probably not traditionally considered a routine technique for high precision quantitative analysis, is increasingly being used for such. Many of the atmospheric trace gases and pollutants have well resolved rotational-vibrational spectra in the mid infrared region, even at the relatively low resolution of $1cm^{-1}$, attainable with benchtop or field-deployable instruments. The review by *Hanst and Hanst* [1994] provides a detailed survey of FTIR analysis of many trace gases and pollutants in air. They discuss in detail LP-FTIR (long path - FTIR). This involves increasing the absorbance of a trace gas by increasing the pathlength, l, through the air sample (see equation 2.4). This results in lower detection limits, a higher absorbance-to-noise ratio, ANR, in the spectrum and therefore greater analytical precision. By placing the sample in a closed White cell [*White*, 1942; *White*, 1976] (see Section 2.2.1 below) pathlengths of up to 100m may be obtained. Using a particular instrumental configuration Hanst and Hanst estimate the Minimum Detection Limit (MDL) of a range of trace species in air (see Table 2.1). The configuration is $0.5cm^{-1}$ resolution, optical path 100m in a closed White cell, HgCdTe detector, spectrum noise level is 10^{-4} abs_{10} (absorbance units in the base-10 scale). MDL is taken to be when the height of a line or band is equal to the peak-peak noise level in the spectrum. Hanst and Hanst do not offer an explicit estimate of analytical precision but do speak of the MDL in terms of the smallest detectable change in the mixing ratio of a trace species, as summarised in Table 2.1. At these levels the FTIR-based technique would appear to approach the measurement precision offered by more traditional techniques, such as NDIR spectroscopy and gas chromatography (cf. Section 1.3.4, 1.5.4, 1.6.4, 1.7.4).

Species	Region	MDL
	cm^{-1}	(Hanst and Hanst)
CO_2	2363	0.05 ppm
CH_4	3018	2 ppb
N_2O	2210	1 ppb
CO	2200-2100	2 ppb

Table 2.1 Minimum Detection Limits as determined by *Hanst and Hanst* [1994]

There is an alternative approach to trace gas analysis by closed White cell LP-FTIR, known as LOP-FTIR (long open path - FTIR). The long open path can be achieved in several different ways. Firstly a pathlength of up to one kilometre can be achieved by constructing an open White cell, (with mirrors at either end but no walls) in the ambient atmosphere. *Galle et al* [1994] and *Griffith* [1996] report on a study of the exchange of atmospheric trace gases with soils in a rural environment using an open White cell. Spectra of $1cm^{-1}$ resolution were collected using an InSb detector and a total pathlength in the ambient atmosphere of 1000m (a base pathlength of 25m traversed 40 times). Analytical precision of the retrieved trace gas mixing ratios is estimated at 1 ppb N_2O and 2 ppb CH_4 for four minute averaging times.

Secondly, an infrared beam can be collimated, transmitted and collected with a telescope to minimize beam divergence over the long path. If the source and detector are located at the two ends of the base path then that distance is traversed only once. The placement of a retro-reflector at one end of the base path allows the distance to be traversed twice and for the source and detector to be located together at the other end (e.g. [*Grant et al.*, 1992]). *Hanst and Hanst* ([1994]; and references therein) provide many further examples where LOP-FTIR techniques have been applied in the study of emissions in a polluted urban or industrial environment.

The immediate stimulus for the present work, however, were studies by the Wollongong FTIR group of trace gas emissions from biomass burning in Australian tropical savannas [*Hurst et al.*, 1994a; *Hurst et al.*, 1994b]. Savanna fire smoke samples were collected and later analysed by high resolution FTIR spectroscopy for CO_2, CO and CH_4 to determine their emission ratios. Extrapolation from these results suggested that these species should be amenable to high precision analysis using a spectrometer of resolution as low as $1cm^{-1}$, even in ambient clean air samples.

Building on the work of the investigators cited above, it is one aim of the present work to investigate the limits of trace gas analytical precision attainable by closed-cell FTIR spectroscopy using a relatively low resolution instrument, $1cm^{-1}$. The following sections describe in detail the experimental and analytical factors considered in attempting to maximise precision.

2.2 Optimal Instrument Configuration for Trace Gas Analysis

The configuration of the instrument used in this work is illustrated schematically in Figure 2.3 and described below. Briefly, a commercial Bomem MB100 FTIR spectrometer, with resolution $1cm^{-1}$, and a liquid nitrogen cooled InSb infrared detector were used throughout this work. Air and gas samples were introduced to a White cell for analysis. The instrument, consisting of spectrometer, detector and White cell was enclosed in a sealed, thermostatted and purged box. The reasons for the configuration described here and the operation of the instrument are discussed more fully in sections 2.2 and 2.3.

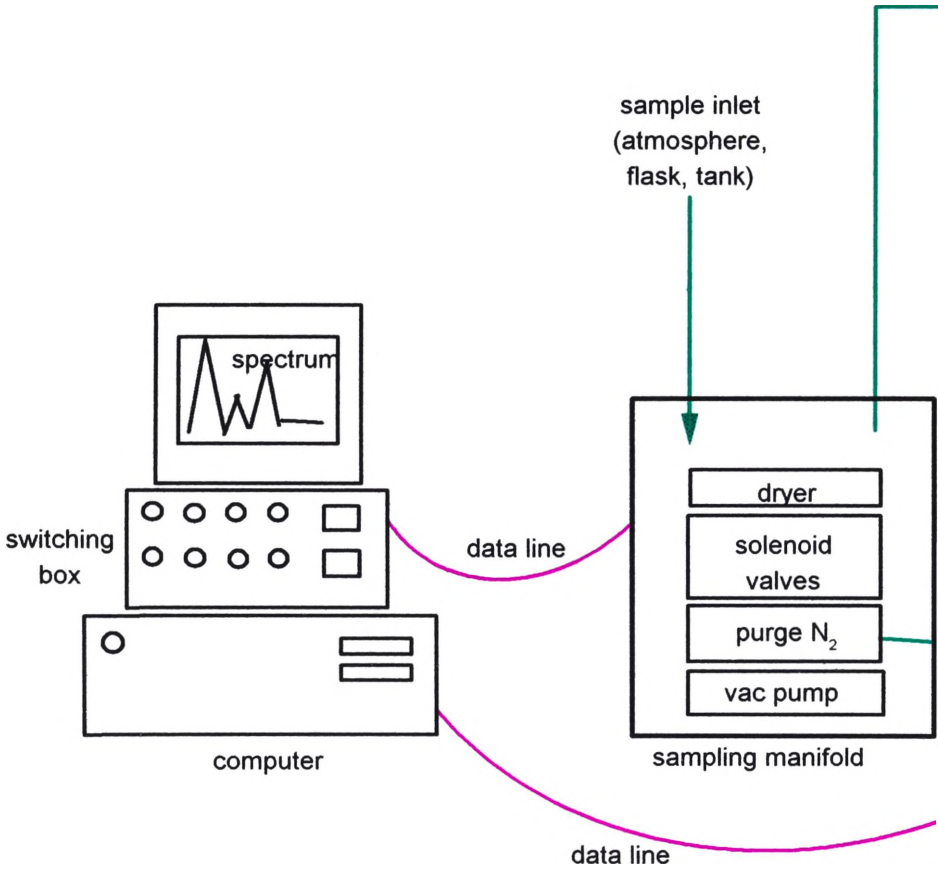

Figure 2.3. schematic diagram of FTIR instrument for trace gas analysis

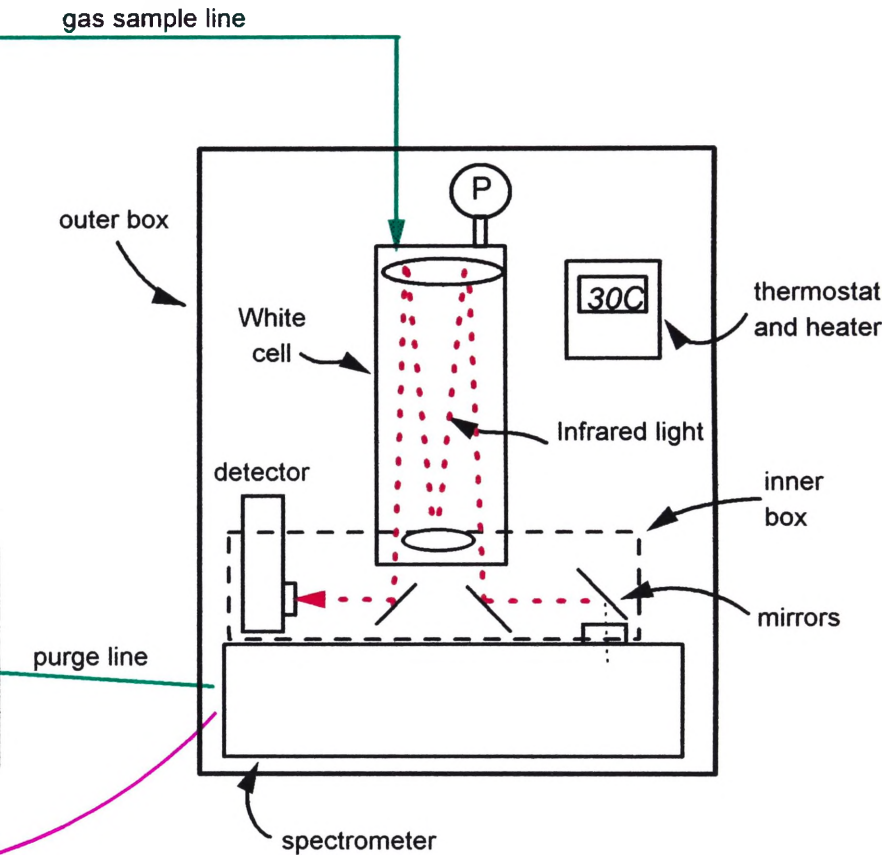
gas sample line
outer box
P
30C
thermostat
and heater
White
cell
Infrared light
detector
inner
box
mirrors
purge line
spectrometer

Spectrometer: Bomem (Canada) MB100 FTIR spectrometer with maximum resolution $1cm^{-1}$. Michelson type interferometer using permanently aligned "wish-bone" design. KBr beamsplitter.

Detector: InSb (Indium Antimonide) liquid nitrogen cooled infrared detector with range 1800 to 7000 cm^{-1} and $D^*=1.9\times10^{11}cm\ Hz^{½}\ W^{-1}$. The liquid nitrogen dewar had a boil-off time of >24h. Supplier: Cincinnatti Electronics (USA).

White cell: Two White cells were used. i) Model 22PA, 22m total pathlength (20 × 1.1m), 8L volume; ii) Model G-2-4.8-PA-X2-BA-AG, 9.8m total pathlength (40 × 0.25m), 0.5L volume. Supplier Infrared Analysis (USA).

Capacitance Manometer: MKS (USA) Baratron Model 122A, 1000 Torr, 0-10VDC. Fitted to White cell endplate. Pressure monitored by computer through data acquisition and control card.

Thermostat and Heater: Eurotherm model 91e PID control thermostat unit. Connected to small air circulating fan with resistive heating element. Maintains constant temperature ~35 ± 0.1°C.

Inner Box: Perspex with rubber gaskets. Encloses optical path external to White cell to enable efficient purging with UHP N_2.

Outer Box: Perspex and PVC and rubber gaskets. Isolates spectrometer, White cell, manometer and thermostat unit from laboratory environment to facilitate efficient temperature stability as well as purging.

Sampling Manifold: This consisted of ¼" O.D. copper and teflon tubing, Bürkert 240VAC vacuum tight oil-free solenoid valves, a glass cartridge of anhydrous magnesium perchlorate desiccant, an Edwards Pirani pressure gauge (10^{-3} to 1 Torr). Valves were controlled automatically from a computer program or manually from the switching box. Samples could be drawn from the ambient atmosphere, flasks or high pressure cylinders. An oil rotary vacuum pump was connected to the manifold. Swagelok and Cajon vacuum fittings were used.

Computer: A Compaq 33Mhz 486DX-PC computer was used. A spectrometer interface board allowed control of the spectrometer and storage and manipulation of collected spectra. The GRAMS spectroscopic software package was used (with significant customisation). A Strawberry Tree Mini-16 16-bit data acquisition and control card was installed in the computer. This allowed computer control of the sampling manifold solenoid valves, and computer monitoring of pressure and temperature sensors on the White cell and elsewhere.

Temperature Sensors: Platinum RTD's (resistance temperature detector) are used to monitor room, sample and instrument temperatures.

Purge Gas: BOC ultra high purity N_2, further scrubbed of CO and dried.

Table 2.2. Description of the main components of the FTIR instrument.

2.2.1 Signal-to-Noise Ratio Considerations

There are two necessary processes to maximise the precision of an FTIR trace gas analysis. Firstly, as good quality, information rich, spectra as possible must be obtained and secondly, as much information as possible must be extracted from these spectra in an efficient manner. Sections 2.2.1 and 2.2.2 address only the first of these issues, obtaining good quality spectra. Section 2.2.1 focuses on measures which maximise both the linearity and the signal-noise-ratio (SNR) of the measured spectra. Section 2.2.2 addresses issues related to reproducibility such as instrumental stability and sample handling. Optimal quantitative analysis of measured spectra is developed in Section 2.3.

There is a trade-off between resolution, $\Delta\tilde{\nu}$, averaging time, t, and signal-to-noise ratio, SNR, in FTIR spectroscopy described by the equation

$$\mathrm{SNR} = \frac{U_{\tilde{\nu}}(T)\cdot\Theta\cdot\Delta\tilde{\nu}\cdot t^{1/2}\cdot\xi}{\mathrm{NEP}} \quad . \tag{2.6}$$

where $U_{\tilde{\nu}}(T)$, a property of the source, is the spectral energy density at wavenumber $\tilde{\nu}$ from a blackbody source at temperature T; Θ and ξ, properties of the interferometer, are its throughput and efficiency respectively; and NEP is the noise-equivalent-power of the detector. (See *Griffiths and de Haseth* [1986] for an exhaustive account of FTIR trading rules).

In going from $1\mathrm{cm}^{-1}$ to $0.5\mathrm{cm}^{-1}$ the SNR is halved for the same averaging time (assuming constant throughput, Θ, as is the case for the MB100). To obtain the same noise level using $0.5\mathrm{cm}^{-1}$ resolution as for $1\mathrm{cm}^{-1}$, it is necessary to quadruple the averaging time at constant throughput. This, however, reduces the rate of sample processing and also increases the likelihood of introducing errors due to instrument instability in time (see

Section 2.2.2). Of the four molecular species of interest in this work, some of the rotational structure of three of them is quite well resolved at a resolution of $1cm^{-1}$. Only for N_2O are the rotational transitions separated by less than $1cm^{-1}$, and so remain unresolved. (The approximate rotational separations in the most intense absorption features are: CO_2 ~1.8, CH_4 ~9.0, CO ~3.4, and N_2O ~0.98 cm^{-1}). For the three less abundant trace gases, CH_4, CO and N_2O, with the correspondingly weak absorption features, it has been determined that spectroscopic SNR was the limiting factor in the analytical precision achieved, whereas for CO_2, this was not the case (see Section 2.5.1). Thus, the convenient compromise in attempting to measure all species simultaneously was to collect $1cm^{-1}$ resolution spectra. This also happened to be the highest resolution of the only instrument available to the project.

The White cell serves to improve the absorbance-to-noise ratio, ANR, of the absorbance spectrum by increasing the absorbance. The infrared beam is folded so that it traverses the sample many times (see Figure 2.3). There is no loss due to divergence of the beam as it is repeatedly refocussed onto one of the White cell mirrors. (SNR refers to the relationship between the intensity of a single beam spectrum and the noise level in the 100% transmission line, whereas ANR refers to the relationship between the intensity of an absorbance feature and the level of noise in the absorbance spectrum baseline). Judicious choice of total pathlength allows control of the peak absorbance so that the ANR is high but the absorbance is not so high as to deviate from Beer-Lambert linearity. Two different White cells were used in this work, as described in Table 2.3. Both were supplied by Infrared Analysis, Inc.

There is another SNR trade-off relating to the use of White cells. Reflective losses by the mirrors results in a 5-fold and 8-fold diminution of the signal for the 22m and 9.8m cell respectively. However, absorbance is increased by factors of approximately 100 and 50, respectively, due to the increased pathlength. The net ANR improvement is a factor of ~20 for the 22m cell and ~6 for the 9.8m cell. Consideration of calibration air consumption will favour the smaller volume cell for many applications, particularly for CO_2 analysis, where precision is not limited predominantly by ANR. This cell has the added advantages of being quicker to fill and pump out and, being smaller, is more easily incorporated in a field deployable instrument than the 22m cell.

	22m Cell	9.8m Cell
Model No.	22PA	G-2-4.8-PA-X2-BA-BG
Base pathlength	0.55m	0.25m
Total pathlength	22.1m	9.8m
No. of passes	20	40
Volume	8L	0.5L
Transmitted Energy	~20%	~12%

Table 2.3. Specifications of the two multipass White cells used in this work.

The primary and unavoidable source of noise in a spectrum measured on an FTIR instrument is detector noise. (In the mid infrared detector noise will normally be greater than shot noise [*Griffiths and Haseth*, 1986]). This can be minimised by appropriate detector selection. Those most commonly used currently are DTGS, MCT and InSb. DTGS (deuterated triglycine sulfate) detectors are pyroelectric, operate at room temperature and are relatively insensitive, with a typical D^* of 2×10^8 cm $Hz^{½}$ W^{-1}. (D^*, "specific detectivity", is a measure of the sensitivity of a given detector). They rely on a

capacitance element that varies with temperature changes due to incident infrared radiation. MCT (mercury-cadmium-telluride, or HgCdTe) and InSb (indium-antimonide) detectors are quantum detectors with a typical D^* of 10^{10} and 10^{11} cm $Hz^{½}$ W^{-1}, respectively, in the region around 2000cm^{-1} [*Griffiths and Haseth*, 1986]. Quantum detectors rely on incident infrared photons to excite electrons from the semiconductor ground state to its ionisation continuum with a quantum efficiency approaching unity. It is necessary to maintain the temperature of a quantum detector at liquid nitrogen levels (77K). For the present work, the obvious choice is the liquid nitrogen cooled InSb detector, as it provides access to the region of the spectrum where CO_2, CH_4, CO and N_2O have strong absorption features.

If the infrared radiation incident on an InSb detector is too great, the detector will no longer respond linearly with intensity and is said to be saturated. Neutral density filters may be required to reduce the amount of infrared light reaching the detector. This reduces the intensity of all incident wavenumbers by the same proportion. Normally, the only photons of interest to the analyst are those at wavenumbers corresponding to ro-vibrational transitions in the analyte species. For the present work a bandpass filter (OCLI, serial number W03999-4) was used to select only the region containing the main CO_2, CH_4, CO and N_2O transitions, i.e. 2000-3200cm^{-1}, see Figure 2.3. this measure removed the risk of detector saturation, obviated the need for neutral density filters and thereby increased the intensity of the infrared radiation at the wavenumbers of most interest. This enabled an improvement in SNR by a factor of about 2.

As already mentioned, there is a trade-off between spectrum averaging time and SNR (see equation 2.6). To double the SNR the averaging time, (or the number of coadded

scans, in effect), must be quadrupled. With the systems used in this work this relationship was observed to hold only up to averaging times of about 8 minutes (256 coadded scans). There was little evidence of improvement in averaging for longer than that time. In reality this is a trade-off between SNR, averaging time and instrument stability. While the statistical advantage in coadding many spectra is the prevailing determinant of SNR for times < 8 minutes, beyond that the predominant influence is instrument drift. When the SNR sensitive CO, CH_4 and N_2O were the subject of analysis, about 256-scans, or 8-minutes, was found to be optimal. This was sufficient to provide spectra with noise levels of the order of 10^{-5} abs_{10}. For some of the CO_2 only analyses, particularly the isotope studies, coadding more than 64 scans gave no improvement in precision. The experimentally determined relationship between between precision and averaging time is illustrated and discussed in detail in Section 2.5.

2.2.2 Reproducibility Considerations

2.2.2.1 Temperature & Pressure Control

The Beer-Lambert law relates absorbance to analyte concentration. To convert concentration to mixing ratio requires the measurement of the sample density, achieved by measuring temperature and pressure; the White cell pathlength is assumed to be constant. The sample pressure was determined with a capacitance manometer mounted on the White cell, its 0-10V output monitored with a 16-bit data acquisition card, and sample temperature was measured by platinum RTD's (see Table 2.2). Sample pressure was typically in the range 720-760 Torr. The precision of the pressure measurement in this range was of the order of 0.1 Torr, or 0.01 % at 760 Torr, and is therefore not considered to limit the precision of the method.

The temperature was measured at the top and bottom of the cell immediately before and after collection of each sample or calibrant spectrum. Sample temperature was calculated as the mean of the four, and this was used in the density correction by applying the ideal gas law, n=pV/*R*T. The measurements were made with platinum RTD's, all of which were calibrated against a thermometer which in turn was calibrated by the Commonwealth Bureau of Meteorology against a standard temperature scale. The RTD output was monitored using the 16-bit data acquisition card. The precision of the RTD's was better than ±0.03 K, or ±0.01% in 300K, and is not considered to significantly limit the precision of the method.

2.2.2.2 Purging and Enclosure

The portion of the optical path lying outside the White cell is swept clear of absorbing species by a combination of enclosure and purging of the instrument. Intrusions of laboratory air into this part of the optical path may cause errors in retrieved mixing ratios of the order of 5ppm CO_2, 5ppb CO and 20 ppb CH_4, and of 0.3‰ in $\delta^{13}CO_2$, even when using a 22m pathlength White cell.

Enclosure of the instrument in a box did not completely solve this problem as carbon monoxide was observed to build up within the enclosure, due either to some combustion process occurring at the globar source or to some material degassing process as has been observed to occur with nylon tubing in our laboratory previously. The enclosure was then routinely purged with ultra-high-purity nitrogen (BOC gases UHP N_2). When the purge gas was found to contain relatively high (~500 ppb) and variable levels of CO, it

was scrubbed online using Sofnocat™, a room temperature catalyst which quantitatively oxidises CO to CO_2 [*Foulger and Simmonds*, 1993].

The combination of enclosure and purging with CO-scrubbed and dried UHP N_2 at about 500-1000 mL $minute^{-1}$ effectively kept the optical path free of absorbing molecules except for those in the White cell. It was found that the most efficient means of combining purging and thermostatic control of the purged enclosure was to construct an inner and outer enclosure, see Figure 2.3. The purge gas first enters the outer box and travels through about 1m of ¼-inch copper tubing to bring it into temperature equilibrium with the instrument. It then passes into the spectrometer itself, purging the volume containing the source and interferometer, and then into the inner enclosure which is the volume containing the White cell transfer optics and detector. The slight overpressure allows the purge gas to diffuse from the inner box to the outer box and ultimately the laboratory. It is only the inner box and the instrument that need to be purged, not the outer box which is more important for temperature control.

2.2.2.3 Drying

Figure 2.4 illustrates the difference between the spectra of ambient air, dewpoint ~7°C, containing about 1% H_2O, and dried air. Strong H_2O absorption features occur in the same region as CH_4, N_2O and CO. In principle, the quantitative spectrum analysis algorithm employed in this work (described below, Section 2.3) is capable of resolving individual species contributions to a spectrum of their mixture, even when the absorption lines obscure and overlap each other seriously as in Figure 2.4. However in practice, significantly greater reproducibility is obtained for CH_4, N_2O and CO mixing ratio retrievals if the samples are well dried first. The H_2O absorption lines, as well as

obscuring the usually much weaker CH_4, N_2O and CO features, are sufficiently strong to behave in a non-linear Beer-Lambert manner. This can introduce serious "analytical crosstalk" into the fitting procedure, where the apparent mixing ratios of CH_4, N_2O and CO will be slightly dependent on the level of H_2O present. In ambient air, moisture levels are typically in the range 0.5% - 2.5% and are quite variable with time. If undried air samples are to be analysed, these various H_2O crosstalk artefacts must be characterised and corrected for. If it is at all practical to do so, a far simpler approach is to dry all samples to very low dewpoints. Typically, anhydrous magnesium perchlorate is used to dry ambient air samples to levels of <10 ppm H_2O, (-70°C dewpoint) without perturbing the concentrations of the components $^{12}CO_2$, $^{13}CO_2$, CH_4, N_2O and CO [*Francey et al.*, 1996]. Some alternative desiccants, eg. Drierite™ or some molecular sieves, have been observed to perturb either trace gas concentrations or the isotope ratio $\delta^{13}CO_2$ when used to dry air samples [*Meieraugenstein et al.*, 1994]. If very large quantities of moist air are to be analysed the disadvantages of using magnesium perchlorate are its expense and the inconvenience of keeping the drying unit charged with fresh desiccant. Some workers have successfully employed Nafion™ dryers (Permapure Industries, Inc.) in series with magnesium perchlorate to reduce desiccant consumption [*Francey et al.*, 1996]. The Nafion dryer consists of a number of parallel tubes made of a polymer membrane which is selectively permeable, allowing H_2O but not CO_2, CH_4, N_2O or CO to pass through it. The sample is passed in one direction through a set of Nafion tubes which are surrounded by a counterflow of dry air/nitrogen. The moisture gradient across the polymer membrane causes H_2O to move through it where it is swept away by the counterflow, leaving a much drier sample to pass to the magnesium perchlorate dryer where the remaining moisture is removed by the desiccant. While preliminary results from the course of this work indicate that this use of Nafion is

appropriate, the experiments described in the following chapters all relied on drying by magnesium perchlorate alone.

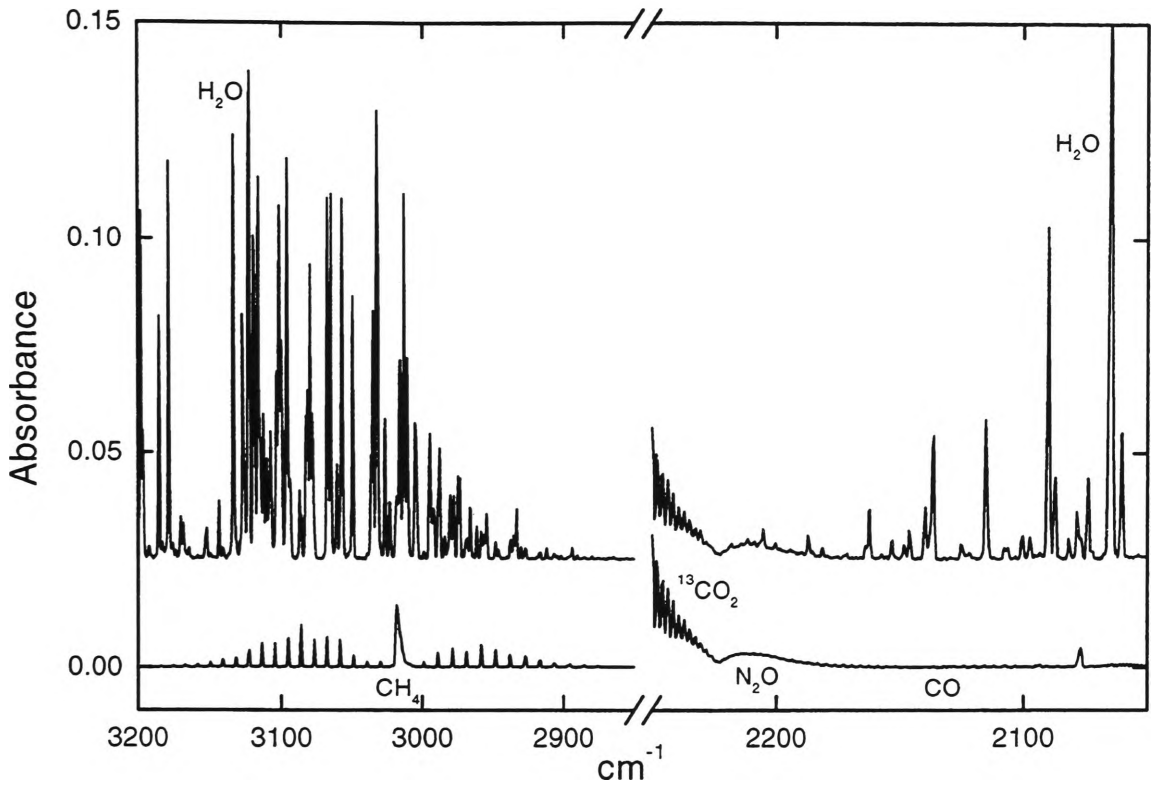

Figure 2.4. Absorbance spectra of wet (top) and dried (bottom) air, at 740 Torr and 305 K. The wet air contains about 1% H_2O, and the dried air contains < 10 ppm H_2O.

2.2.2.4 Sample Handling

The focus of this work is on developing a high-precision technique of trace gas analysis. There are a number of factors regarding sample handling which can mitigate against this. If a precision level of say 1% is the objective, the number of these factors is relatively small. When better than 0.1% precision is the objective, as in this work, there are potentially many more. What is considered here are those factors which cause an error in the retrieved trace gas mixing ratios due to either contamination of the sample by addition of material, or chemical alteration of the sample by reactions involving the trace gases.

As already noted, nylon tubing is a rich source of CO, and so cannot be used anywhere in the sampling manifold. Other polymers and elastomers have shown evidence of perturbing CO concentrations. Degassing of hydrocarbons from these substances is also implicated in perturbing the apparent CH_4 concentration of samples. As far as possible, the sampling manifold is constructed of materials which are believed to be trace gas inert. These include glass, copper, stainless steel, PTFE (Teflon) and Viton. PTFE tubing, while chemically inert, is slightly porous and so not suitable for plumbing where a good vacuum must be sustained. Copper or stainless steel is more appropriate in these circumstances. Viton, an elastomer used in most of the o-rings in the solenoid valves, plumbing connections and the White cell, has been implicated in causing CO growth in stored air samples [*Novelli et al.*, 1991]. This was a problem over a time scale of days and weeks and is not considered a problem in applications where the air is only in contact with a small area of viton for minutes. The system was kept as free as possible of hydrocarbons. The moving components in the solenoid valves had to be cleaned of lubricants. An activated alumina hydrocarbon trap was fitted to the rotary oil pump to prevent backstreaming of oil vapours to the manifold and White cell. Samples were always moved using vacuum pumping to avoid direct contact with pumps. Even oil free diaphragm pumps may be a ready source of CO [*Mak and Brenninkmeijer*, 1994] and probably of other contaminants.

The solenoid valves were powered by 240V AC rather than by, say, 24V DC since direct current leads potentially to much higher temperatures in the valves than does alternating current. Higher temperatures are more likely to drive reactions involving the trace gases which may lead to measurable changes in their concentrations. There was some slight evidence of production of CO within the White cell when it was exposed to sunlight.

Covering the cell with dark cardboard appeared to remove this effect, suggesting that it was due to photolysis. Similarly, there was apparent destruction of CO_2 occurring within the White cell. This was sufficient to cause the mixing ratio of the sample to change at about the rate of -1ppm CO_2 $hour^{-1}$. The internal surfaces of the White cell consist mainly of glass, anodised aluminium, and a small area of viton o-ring. There are significant surface areas of mirror (ceramic coated silver) on glass, which are held in place by an epoxy resin. The most likely candidate for the consumption of CO_2 is the epoxy resin. It may be selectively absorbing CO_2 into its slightly porous matrix, or it may be reacting directly with the CO_2. There seems to be no corresponding change in either CO, CH_4 or N_2O mixing ratios. The small effect on CO_2, whatever its cause, is quite consistent and reproducible. As long as sample handling of both calibration gas and analyte gas is consistent, this effect is unlikely to compromise CO_2 or $\delta^{13}CO_2$ measurement precision.

2.2.2.5 Automation

A further source of random error in analysis is the inconsistency of the human operator. An effective way to remove this inconsistency is by automating the analysis using a computer program. Appendix B contains several Array Basic programs used in this work to automate the FTIR analysis of trace gases. The program controls sample handling by opening and closing the solenoid valves as required. A Strawberry Tree Mini-16 data acquisition and control card was used to achieve this. The Mini-16 card had 12 digital output channels, each of which could be used to control one solenoid valve. Pressure and temperature were logged by the program using some of the 8 analog input channels on the card, and its 16-bit analog to digital converter (ADC). A 16-bit ADC was used to ensure that measurement precision was not limited by the ADC. A

program command initiated and concluded collection of spectra. In each cycle of the program, single beam spectra were collected, saved to disk for archiving, ratioed with reference spectra to produce absorbance spectra, and these were fitted as described in Section 2.3 below, the parameters of the fit directly providing the concentration of the trace gas constituents. These are combined with pressure and temperature data to provide mixing ratios. The program writes all results to a formatted text file. The files of the archived spectra and the data file may be downloaded and analysed on another computer while the automated FTIR analysis continues.

2.3 Quantitative Analysis

Where Section 2.2 described how to obtain high quality spectra, this section deals only with how to best analyse those spectra. This may be considered as a three phase process, as outlined below in Figure 2.5. In the first phase, the MALT (Multiple Atmospheric Layer Transmission) program is used to calculate a set of absorbance spectra, **A,** that closely simulate the spectra obtained on the actual instrument. In the second phase, this set of spectra, **A**, and a matrix, **C**, containing the trace gas concentration information for the calculated spectra are used as the training set input to the multivariate calibration algorithm, in this case CLS (classical least squares) [*Haaland et al.*, 1985]. In practice the entire spectrum is not used for calibration. Rather, particular regions within the spectrum with a high density of information for particular species are chosen. For example, the region 2050-2200 cm^{-1} is rich in CO spectroscopic information but poor in information for other species. This window may be used to determine the calibration for CO, and other windows will be optimised for the other species. This procedure of window selection is detailed in Section 2.3.4. The CLS calibration step produces as its output a matrix, $\hat{\mathbf{K}}$, the calibration matrix, which

describes the relationship between species concentration and absorbance strength for all species and regions of the spectrum included in the calibration. Absorbance is assumed to be proportional to concentration at all wavenumbers $\tilde{\nu}$. The third phase is the prediction CLS step, in a sense the inverse of the calibration CLS step. The calibration matrix, $\hat{\mathbf{K}}$, is used to perform a least squares fit of a synthetic spectrum to a real experimental spectrum, A^s. The parameters of the fit, the vector C, directly give the concentrations of the trace gas components of the real sample.

Normally, the first step, MALT simulation, and the second step, CLS calibration need to be performed once for a given type of analysis. The resulting calibration matrix is stored in the computer. The CLS prediction step is performed every time a spectrum is fitted to derive its concentrations. The first and second steps can be completed in a few minutes. The third step takes less than a second of computer time and so may be performed on-line in real time.

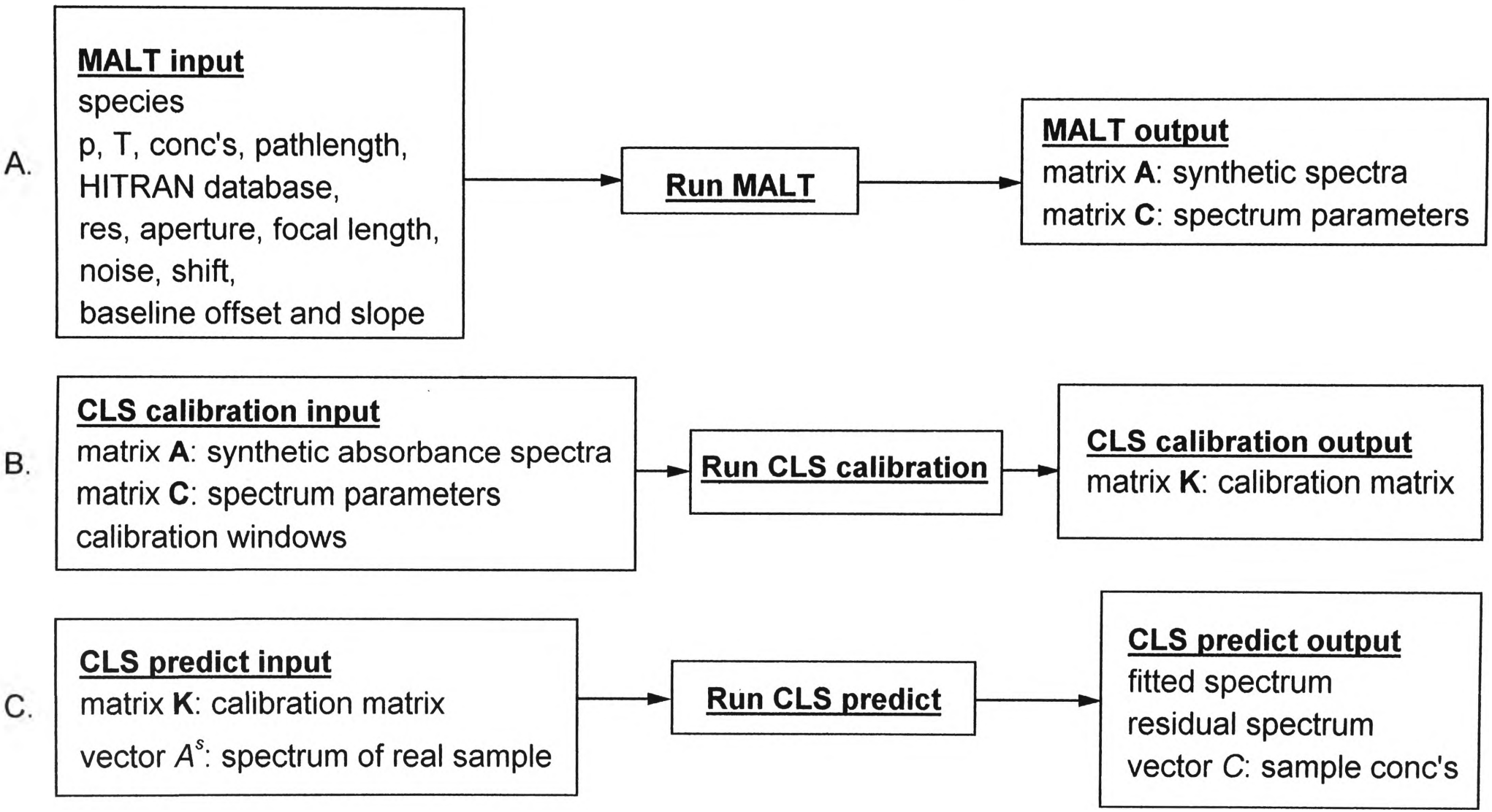

Figure 2.5. Flowchart of calibration and prediction process using MALT and CLS

2.3.1 CLS - Multivariate Calibration and Prediction

CLS analysis is one of several chemometric techniques developed in the last decade or so and ideally suited to the retrieval of quantitative information from spectra. Similar techniques are PLS (partial least squares), ILS (inverse least squares) and PCR (principal component regression) [*Haaland*, 1990; *Haaland and Thomas*, 1988]. There are a number of commercial software packages which incorporate one or several of these approaches. This work used a package originating from Galactic Industries Inc which has been significantly customised for this type of application. The basic algorithm is unchanged however.

CLS is a whole spectrum technique. Prior to the development of these chemometric techniques, analysis for a particular species in a spectrum would focus on a single absorption peak known to be associated with that species. Using a set of calibration spectra, a relationship would have been derived between the height of the peak (or sometimes the area under it), and the amount of the species present in the sample. Measuring the height (or area) of the peak in the unknown spectrum would thus provide a direct measure of the unknown's concentration. CLS differs from this approach in that it enables the simultaneous analysis of many absorption features across one or several regions of the spectrum. Many spectroscopic peaks rather than just one are exploited. This is a far more efficient use of the information in the spectrum. Also the technique allows much more robust analysis of molecules that may have overlapping features in the spectrum. The result is the possibility of very precise measurements of several species simultaneously in the one sample, e.g. the trace gases CO, N_2O, CH_4, CO_2 in air.

Calibration. The description of CLS theory that follows is basically that of *Haaland* [1990]. The calibration step analysis begins with the assumption of the Beer-Lambert law and a restating of equation 2.5

$$A_i = \sum_{j=1}^{l} a_{ij} b c_j \tag{2.7}$$

where A_i is the absorbance of a multicomponent sample or reference at a wavenumber i, a_{ij} is the absorptivity of component j at wavenumber i, b is the pathlength, and c_j is the concentration of the jth component (of a mixture containing l components). Defining k_{ij} as the product $a_{ij}b$ and adding random error (e_i) in the spectrum at each wavenumber i yields

$$A_i = \sum_{j=1}^{l} k_{ij} c_j + e_i \tag{2.8}$$

Usually a set of accurately known real mixtures is used as the training set for the calibration phase of the analysis. In this work, a set of spectra, typically 40 in number, calculated using the MALT program serves this purpose. A set of simultaneous equations like 2.8, one for each spectrum, can be used to describe the calculated spectra. In matrix notation (denoted by bold typeface) these equations are

$$\mathbf{A} = \mathbf{KC} + \mathbf{E} \tag{2.9}$$

where

A = the $n \times m$ matrix whose columns represent the spectrum of each of the m MALT-calculated standard spectra,

K = the $n \times l$ matrix whose columns represent the l pure-component spectra at unit concentration and unit relative path length,

C = the $l \times m$ matrix of the known component concentrations ($m \geq l$), and

E = the $n \times m$ matrix of random measurement errors in the spectra.

Provided $m>l$ the equations are overdetermined and the least-squares solution is

$$\hat{\mathbf{K}} = \mathbf{AC}'(\mathbf{CC}')^{-1} \tag{2.10}$$

where the primes indicate the transposed matrices and $\hat{\mathbf{K}}$ denotes the least-squares estimate of **K**. Equation 2.10 shows that the estimate of **K** is accomplished with a series of matrix multiplications and one matrix inversion. The matrix to be inverted **CC′** is an $l \times l$ matrix where l is the number of components. Since this is usually a relatively small number, $l < 8$, the inversion is quickly accomplished with the computer.

Prediction. In the analysis of an unknown sample, a least-squares fit of the sample spectrum is performed using the least-squares estimates of the pure-component spectra which were generated in the calibration phase. The absorbance spectrum of the unknown sample can be expressed by

$$A^s = \hat{\mathbf{K}}C + E \tag{2.11}$$

where the A^s vector represents the unknown sample spectrum, the $\hat{\mathbf{K}}$-matrix is determined from equation 2.12 and the C-vector is composed of the unknown sample component concentrations. The least-squares solution for C is given by

$$\hat{\mathbf{C}} = (\hat{\mathbf{K}}'\hat{\mathbf{K}})^{-1}\hat{\mathbf{K}}'A^s \tag{2.12}$$

Again the matrix to be inverted is $l \times l$, and independent of the number of wavenumbers, n, included in the analysis.

The CLS calibration and prediction algorithm described here is for the simplest case where it is assumed that Beer-Lambert linearity applies, and that the spectrum baselines

are flat and not offset from zero. The algorithm is trivially extended as described in Section 2.4.2 to allow for non-zero and sloping baselines. It was in this form that the CLS algorithm was applied in the present work.

PLS. A general disadvantage of the CLS method is that all interfering chemical components in the spectral region of interest need to be known and included in the calibration. If there is an unknown absorbing component present in the analysed sample, the method will give erroneous results. In many analytical situations this renders CLS an inappropriate chemometric technique. Often, the conceptually similar but more complex Partial Least Squares (PLS) technique is applied. Whereas in CLS one single-component spectrum is determined for each absorbing species, in PLS a set of factors is determined for each absorbing species These factors are pseudo-spectra in that they do not usually correspond to the actual spectrum of any one component, but rather to linear combination of several components. In CLS the coordinate system is single-component spectra and component concentrations, in PLS the coordinate system is factors and factor scores. The factor scores can be modelled as being linearly related to concentrations. *Haaland and Thomas* [1988] provide a full account of the comparison of the CLS and PLS algorithms.

The significant advantage of PLS over CLS is that PLS does not require that all absorbing components of the system be known or included in the calibration. Where CLS is appropriate for analysis of mixtures where all the components of the mixture are known, PLS can be used for mixtures where some components are known and others are not.

The disadvantage of PLS is that, being a higher dimensional technique than CLS, much of the transparency of the latter and the valuable qualitative information it provides is lost. In this project the sample, being air, is nearly always known to consist of the main absorbing components H_2O, CO_2, CH_4, CO and N_2O in the 2000-3000 cm^{-1} region of the spectrum. Except for the rare contamination event due to non-methane hydrocarbons, the absorbance due to other trace gas species is less than the noise level of the recorded spectra. This enables the system to be fully characterised, i.e. calibrated in all absorbing species present, as required when employing the CLS technique. In the developmental stage of this project, a parallel study, where both CLS and PLS techniques were applied analysis of the same samples, indicated that there was nothing to be gained in using PLS rather than CLS. Indeed, while it was observed that PLS typically gave better fits to experimental spectra (i.e. smaller residuals), this did not translate into higher analytical precision for trace gas analysis. On the other hand, it is anticipated that the much greater flexibility of PLS may prove more useful than CLS in further studies incorporating variable sample temperature into the analytical scheme.

2.3.2 MALT/HITRAN (First Calibration)

The central element of software that has made high quality measurements of trace gases and isotope ratios feasible as described in the later chapters of this work is the program MALT (Multiple Atmospheric Layer Transmission). What follows is a summary of the full description of MALT given by *Griffith* [1996].

The calculation of synthetic spectra is based on a compilation of absorption line parameters, which includes, for each absorption line of each molecule, the line wavenumber $\tilde{\nu}_0$, integrated line strength S, lower state energy level E_0 and pressure and temperature dependent Lorentzian halfwidth α_L. One suitable line parameter set is the commonly used HITRAN [*Rothman et al.*, 1992], which includes line parameters for 31 individual common atmospheric gases, and in many cases, their isotopomers. Table 2.4 lists the species covered in the HITRAN set of line parameters.

No.	Molecule	Isotopes	No.	Molecule	Isotopes
1	H_2O	H, D, ^{16}O, ^{17}O, ^{18}O	17	HI	
2	CO_2	^{12}C, ^{13}C, ^{16}O, ^{17}O, ^{18}O	18	ClO	^{35}Cl, ^{37}Cl
3	O_3	^{16}O, ^{17}O, ^{18}O	19	OCS	^{12}C, ^{13}C, ^{16}O, ^{18}O, ^{32}S, ^{34}S
4	N_2O	^{14}N, ^{15}N, ^{16}O, ^{17}O, ^{18}O	20	H_2CO	^{12}C, ^{13}C, ^{16}O, ^{18}O
5	CO	^{12}C, ^{13}C, ^{16}O, ^{17}O, ^{18}O	21	HOCl	^{35}Cl, ^{37}Cl
6	CH_4	H, D, ^{12}C, ^{13}C	22	N_2	
7	O_2	^{16}O, ^{17}O, ^{18}O	23	HCN	^{12}C, ^{13}C, ^{14}N, ^{15}N
8	NO	^{14}N, ^{15}N, ^{16}O, ^{18}O	24	CH_3Cl	^{35}Cl, ^{37}Cl
9	SO_2	^{32}S, ^{34}S	25	H_2O_2	
10	NO_2		26	C_2H_2	^{12}C, ^{13}C
11	NH_3	^{14}N, ^{15}N	27	C_2H_6	
12	HNO_3		28	PH_3	
13	OH	H, D, ^{16}O, ^{18}O	29	COF_2	
14	HF		30	SF_6	
15	HCl	^{35}Cl, ^{37}Cl	31	H_2S	^{32}S, ^{33}S, ^{34}S
16	HBr	^{79}Br, ^{81}Br			

Table 2.4. List of molecular and isotopomeric species included in the HITRAN database.

Each absorption line of each molecule will contribute to the total optical depth of a sample at each wavenumber. For each absorption line k of molecule i the contribution to the monochromatic optical depth τ at wavenumber $\tilde{\nu}$ is given by

$$\tau_i^k(\tilde{\nu}) = \sigma_i^k(\tilde{\nu}) a_i \tag{2.13}$$

where $\sigma_i^k(\tilde{\nu})$ is the absorption coefficient or cross-section at $\tilde{\nu}$ and a_i is the amount of component i, equal to the pathlength times the concentration. In common practice $\sigma_i^k(\tilde{\nu})$ has units of cm^2 $molec^{-1}$ and a_i has units of $molec.cm^{-2}$. The absorption coefficient is calculated from the integrated line strength by convolution with the true lineshape. There are two main broadening mechanisms contributing to the lineshape. Doppler broadening is due to random molecular motion and leads to a Gaussian lineshape

$$f_G(\tilde{\nu}) = \frac{1}{\alpha_G \sqrt{\pi}} \exp\left(-\frac{(\tilde{\nu} - \tilde{\nu}_0)^2}{\alpha_G^2} \right) \tag{2.14}$$

where α_G is the Gaussian half width at 1/e height

$$\alpha_G = \frac{\tilde{\nu}_0}{c} \sqrt{\frac{2kT}{m}} \tag{2.15}$$

where m is the molecular mass, k is Boltzmann's constant, T is absolute temperature and c is the speed of light. Pressure broadening is due to collisions perturbing the molecular energy levels and leads to a Lorentzian lineshape contribution

$$f_L(\tilde{\nu}) = \frac{\alpha_L / \pi}{(\tilde{\nu} - \tilde{\nu}_0)^2 + \alpha_L^2} \tag{2.16}$$

where α_L is the Lorentzian half-width at half-height and is proportional to the total pressure. The Lorentzian half-width at 1 atmosphere and its temperature dependence are tabulated for each absorption line in the HITRAN database. The Gaussian halfwidth is

calculated from the temperature and molecular weight. Typical values are around 0.7 cm^{-1} atm^{-1} for α_L and 0.003 cm^{-1} for α_G for medium sized molecules at room temperature. Thus the Lorentz contribution dominates except at low pressures. The convolved lineshape is known as the Voigt profile.

The absorption coefficient for each absorption line $\sigma_i^k(\tilde{\nu})$ is the convolution of the integrated line strength and the two lineshape contributions:

$$\sigma_i^k(\tilde{\nu}) = S_i^k \otimes [f_L(\tilde{\nu})]_i^k \otimes [f_G(\tilde{\nu})]_i^k \tag{2.17}$$

where $\otimes$ represents convolution. The integrated linestrengths are tabulated in the HITRAN database at 296K and must be corrected to the temperature of the calculation. The temperature correction due to the temperature dependence of the population of the lower state energy level and the (small) contribution from spontaneous emission is given by

$$S(T) = S(296) \cdot \frac{Q(296)}{Q(T)} \cdot \frac{\exp\left(-\frac{c_2 E_0}{T}\right)}{\exp\left(-\frac{c_2 E_0}{296}\right)} \cdot \frac{\left(1-\exp\left(\frac{c_2 \tilde{\nu}_0}{T}\right)\right)}{\left(1-\exp\left(\frac{c_2 \tilde{\nu}_0}{296}\right)\right)} \tag{2.18}$$

where the Q's are the partition functions and c_2 is the second radiation constant (= hc/k = 1.439 cm K).

The total monochromatic optical depth at wavenumber $\tilde{\nu}$ for a homogeneous sample is then the sum of the $\tau_i^k(\tilde{\nu})$ over all absorption lines of all molecules:

$$\tau(\tilde{\nu}) = \sum_i \sum_k \tau_i^k(\tilde{\nu}) \tag{2.19}$$

The transmission spectrum of the sample without instrumental effects is then given by

$$T(\tilde{\nu}) = \frac{I(\tilde{\nu})}{I_0(\tilde{\nu})} = \exp[-\tau(\tilde{\nu})] \tag{2.20}$$

where $I_0(\tilde{\nu})$ and $I(\tilde{\nu})$ are the intensities before and after traversal of the absorbing sample. The corresponding absorbance spectrum, $A(\tilde{\nu})$ is simply equal to $\tau(\tilde{\nu})$. However any spectrometer convolves the true intensity

$$I = I_0 \exp[-\tau(\tilde{\nu})] \tag{2.21}$$

with an instrument lineshape function to produce the observed or measured spectrum. If the width of the instrument lineshape function is much narrower than the true monochromatic lineshape then the above relations for T and A will be good approximations, but this is often not the case. The instrument lineshape for a perfectly aligned spectrometer is itself a convolution of an apodization lineshape, which depends on a weighting (apodization) applied to the interferogram as a function of optical path difference, and a rectangular lineshape whose width depends on the divergence of the collimated beam in the interferometer due to the finite input aperture. The width of the rectangular divergence or field-of-view (FOV) contribution is equal to $\tilde{\nu}\alpha^2/2$ where α is the divergence half-angle, and $\alpha=\phi/2f$ where ϕ is the entrance aperture (collimator field stop) diameter in the spectrometer and f the focal length of the collimator. The maximum acceptable divergence angle is determined by the resolution and the maximum wavenumber in the spectrum. For an optimally chosen aperture $\tilde{\nu}\alpha^2 = 1/L$, where L is the maximum optical path difference in the interferometer, so that

$$\phi = 2f\sqrt{\frac{1}{\tilde{\nu}_{\max} \cdot L}} \ . \tag{2.22}$$

The consequent FOV rectangular contribution to the lineshape, 0.5/*L*, is somewhat narrower than the width of the narrowest apodizing function (boxcar, 0.603/*L*).

If $f_I(\tilde{\nu})$ represents the instrument line shape, the measured spectrum is given by

$$I'(\tilde{\nu}) = I(\tilde{\nu}) \otimes f_I(\tilde{\nu}) \tag{2.23}$$

and the measured absorbance spectrum is

$$A'(\tilde{\nu}) = -\log\left(\frac{I(\tilde{\nu}) \otimes f_I(\tilde{\nu})}{I_0(\tilde{\nu}) \otimes f_I(\tilde{\nu})}\right). \tag{2.24}$$

Spectra I' or A' calculated as above should be identical to those obtained by an ideal FTIR spectrometer. In practice, this is usually achievable in that good fits of measured spectra can be obtained such that the residual spectrum after fitting (= fitted spectrum - real spectrum) is close to the real spectrum noise level. Any non-ideality in the FTIR spectrometer performance will appear in the residuals and provides valuable information on the possible errors in spectrometer performance.

The HITRAN line parameters are temperature-corrected in accordance with equation 2.18. The vibrational contributions to the partition functions are evaluated in the harmonic approximation and the rotational contributions are proportional to T for linear molecules and $T^{1.5}$ for non-linear molecules. The exponent for the temperature dependence of Lorentzian halfwidths is taken from the HITRAN line parameters. The line positions and intensities form a "stick" spectrum of δ-functions which is convolved with the aforementioned Lorentzian and Gaussian lineshape functions to obtain the monochromatic optical depth, $\tau_i(\tilde{\nu})$. The algorithms for the convolution are described by *Griffith* [1996]. The single component optical depth spectrum for each gas or

isotopomer is stored for later re-use. The optical depth is then summed over all absorbing molecules and the monochromatic transmission calculated as:

$$T(\tilde{\nu}) = \exp(-\tau(\tilde{\nu})). \tag{2.25}$$

Finally, the monochromatic transmission spectrum is convolved with the instrument lineshape function (apodization and FOV) and converted to the required y-axis units (transmittance or absorbance). This step matches the monochromatic spectrum to the instrumentally degraded spectrum, including matching the point spacing to that of the real spectrum.. The spectrum is saved for analysis in the standard GRAMS binary format.

For a set of calibration spectra, the number of spectra required and the range of concentrations for each absorber are input and a set of spectra with random concentrations within the given ranges are calculated. A variable baseline can be optionally included in the set by treating the baseline offset and slope as additional pseudo-components, which allows the fitting of non-zero baselines in real spectra. Finally, the calibration set calculation also produces a list file of all calibration spectra and their species concentrations in a format suitable for direct input to the CLS software.

In operational terms, one full run of the synthetic spectrum calculating program, MALT, is substantially equivalent to the generation of a full set of calibration spectra. Typically 40 spectra were calculated. The number of calibration spectra required depends in part on deviations from the ideal Beer-Lambert law; in an ideal Beer-Lambert case, if there are N components and no noise only N spectra are required. However as the spectra are

generated synthetically on a computer within reasonable time limits, the cost in time of generating large calibration sets is negligible.

Figure 2.6 illustrates an example of the CLS best fit to two regions of a real spectrum, based on a set of calibration spectra calculated by MALT/HITRAN. The real spectrum is that associated with a clean air sample. The residual spectrum is useful as a diagnostic indicator of the quality of the fit.

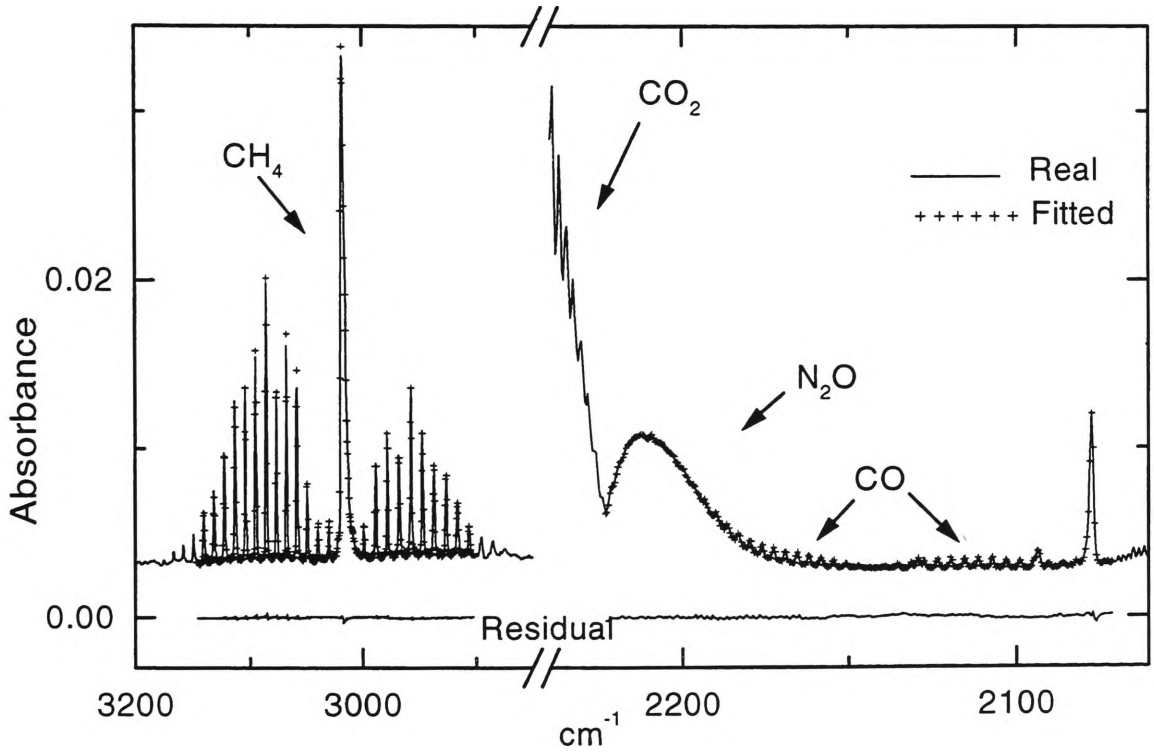

Figure 2.6. Example of two regions of a real spectrum of clean air, a MALT/CLS fit to the real spectrum, and the residual spectrum, the difference between fitted and real spectra.

2.3.3 Second Calibration

The process described in Sections 2.3.1 and 2.3.2, of utilising the MALT-calculated spectra derived from the HITRAN database and CLS analysis serves to carry out a first order, or working, calibration of the instrument. The calibration reference standard in

this case may be considered as the HITRAN database. A subsequent, more absolute calibration can be carried out by analysing real samples from a suite of calibration tanks containing air which has been well characterised by independent techniques and determining their apparent composition using the MALT/CLS technique. In the present work the concentrations of the trace gases in these tanks were referenced to the best available international calibration scale, (maintained by NOAA/CMDL, US Dept of Commerce). It was found that there can be a systematic difference of up to 5% between the FTIR MALT/HITRAN calibrated concentrations and the concentrations on the international scale. This is thought to be due to limitations in some of the assumptions needed to be made in using MALT and HITRAN to calibrate the instrument. For many applications, systematic errors of less than 5% will not be a serious problem. However, for use of the instrument in other applications, e.g. monitoring of trace gas concentrations at clean air monitoring stations, or measurement of isotope ratios, a further level of calibration is often necessary. It was found that usually, a simple linear equation is sufficient to transform the raw FTIR retrieved concentrations into concentrations on the international scale. For example, when the instrument was used to analyse samples of air from the ambient atmosphere at half-hourly intervals continuously for several weeks (see Chapter 4), a sample of well characterised calibration gas was analysed under the same conditions every six hours. This enabled not only precise trace gas concentration retrievals, but also a level of accuracy of the order of 0.1%. Chapter 3 describes the intercomparison with international standards in detail.

2.3.4 *Optimal Window Selection*

In utilising the CLS prediction procedure, it is necessary to fit the synthetically derived single component spectra to a real experimental spectrum of a mixture and hence a decision must be made as to precisely which region(s) of the spectrum to fit. For example, Figure 2.7 illustrates a spectrum of a sample of air which includes 310 ppb N_2O. The calculated spectrum for N_2O is also illustrated, offset in the y-axis for clarity. Virtually all the infrared absorption features for the species N_2O occur in the region 2170-2270 cm^{-1}. Intuition would suggest that, in attempting to retrieve quantitative information about N_2O from the spectrum, the optimal CLS calibration window will lie somewhere in the region 2170-2270 cm^{-1}.

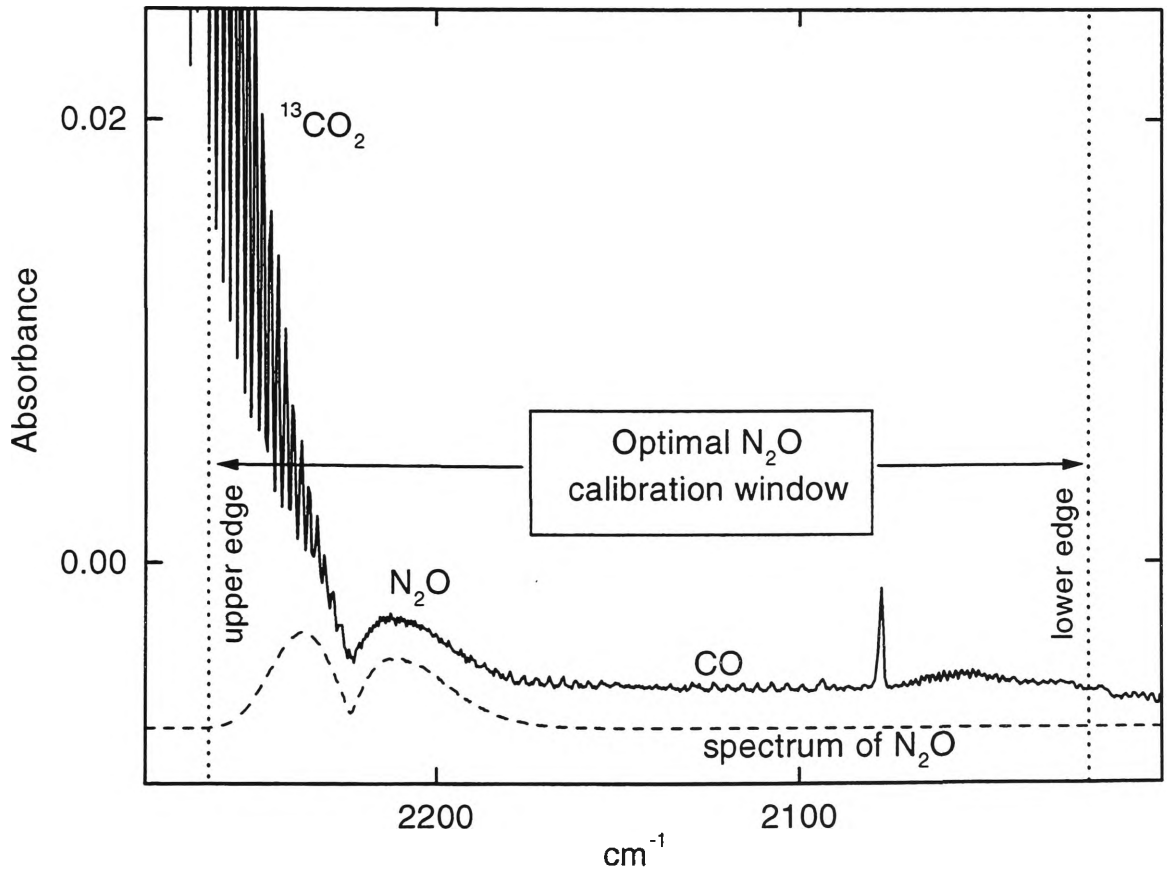

Figure 2.7. Spectrum of air sample and of the N_2O component of the air, showing the optimal spectroscopic window for N_2O analysis.

However there are significant gains to be made in precision by systematically rather than intuitively determining the ideal left and right edges of the calibration window for each individual species. Note that for N_2O in air, half of the N_2O band, the P-branch (2170-2225 cm^{-1}), lies relatively clear of other absorption bands with just a few weak CO line overlapping with it. The other half, the R-branch (2225-2270 cm^{-1}), lies under considerably stronger absorption lines due mainly to $^{13}CO_2$. If a decision is made to fit N_2O only in the region not obscured by $^{13}CO_2$, then this may effectively discard as much as half of the N_2O information which could potentially have made the measurement more precise. If, on the other hand, all of the N_2O information under $^{13}CO_2$ is included, the risk of having the N_2O measurement perturbed by interference from the much stronger $^{13}CO_2$ absorption features is much higher. The N_2O information may be diluted by the strong $^{13}CO_2$ information.

For ideal spectra, the optimal CLS window for a species can be systematically determined solely by use of MALT calculated spectra and the CLS calibration procedure. The first step is to generate a set of spectra using MALT which closely simulates the lineshape and range of concentrations of the instrumentally obtained spectra to be analysed, including realistic levels of noise. The wavenumber region of the MALT spectra should extend beyond the range of wavenumber regions to be considered for the optimal calibration window. First a guess at the best left and right edges of the calibration window is made. Using these, along with the MALT calculated spectra as input, the CLS calibration step is undertaken. As well as producing a calibration, the CLS algorithm produces as output a statistical estimate of the precision of that

calibration. Either the Standard Error of Prediction (SEP) or the statistically similar Root Mean Squared Deviation (RMSD) of the calibration line can be used:

$$SEP = \sqrt{\frac{\sum_{n} \left(y_{actual} - y_{predicted} \right)^2}{n}} \tag{2.26}$$

$$RMSD = \sqrt{\frac{\sum_{n} \left(y_{actual} - y_{predicted} \right)^2}{n-1}} \tag{2.27}$$

There are n spectra in the calibration training set, and y_{actual} and $y_{predicted}$ are the actual and CLS-predicted concentrations, respectively, of a given species in a particular training spectrum. In this work, n=40 typically, so SEP and RMSD are very similar, differing by less than 1.3%.

That is, for a given set of input spectra and a given calibration window specified by its upper and lower edges, the CLS calibration step estimates how precisely it can retrieve each species concentration from the spectroscopic information provided in that window. To systematically determine the optimal window for a given species, the CLS calibration step is performed many times, but each time with a different choice of calibration window. Then a three-dimensional (x,y,z) plot of the Standard Error of Prediction (in this case) versus upper and lower window edges is constructed. This will generate a three-dimensional "precision surface", the minimum point on which specifies the calibration window which will produce most precise retrievals of that species concentration from MALT spectra. The assumption is then made that the same surface will give a good indication of achievable precision for real spectra.

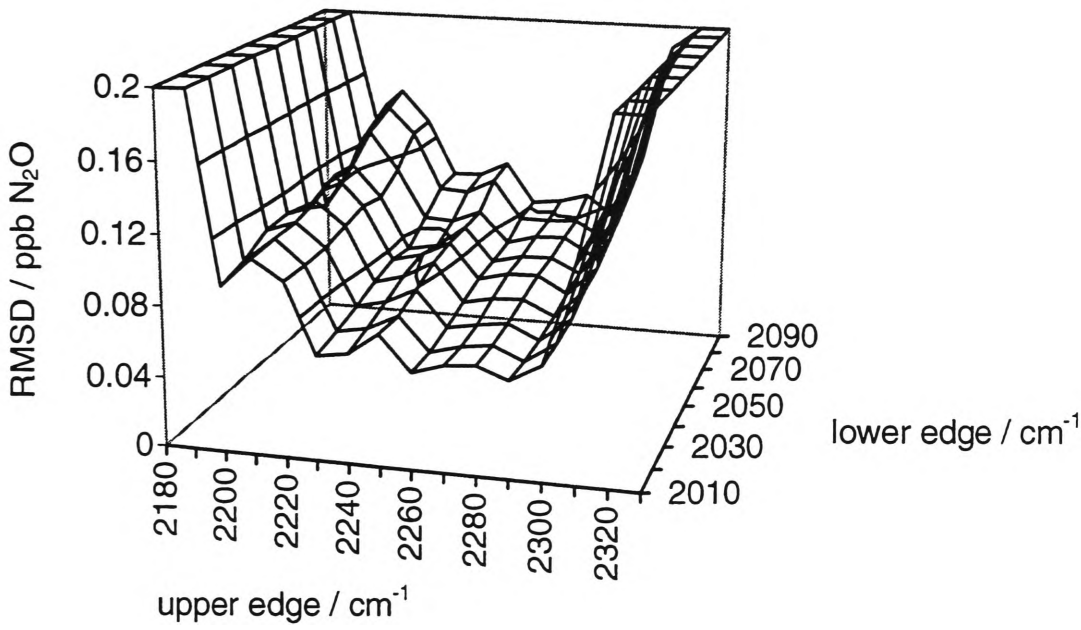

Figure 2.8. Precision surface for N_2O. RMSD of calibration vs left and right edge of spectrum region used in calibration.

Figure 2.8 illustrates such a precision surface for calibration of N_2O measurements in the region of the spectrum bounded by 2010 cm^{-1} and 2320 cm^{-1}. The position of the minimum on this surface suggests that an optimal choice for an N_2O calibration window would be the region 2020-2260 cm^{-1}. This optimal window is illustrated in Fig 2.7. Choosing a left edge much higher than 2260 cm^{-1} leads to a loss of measurement precision due to the inclusion in the window of too much strong $^{13}CO_2$ information which obscures or dilutes the N_2O information content. Somewhat counterintuitively, the optimal right edge for the N_2O window is 2020 cm^{-1}, resulting in the inclusion of a large region where there is very little absorption, by N_2O or any other species. It is believed that the inclusion of such baseline regions in optimal calibration windows is precisely because these regions serve to characterise the baseline. Only when the baseline is well characterised are the non-baseline absorption features well constrained by reference to it, thus leading to improved measurement precision. This is particularly

important for a broad "featureless" spectrum like N_2O. Similar precision surfaces for the molecules CO_2, CH_4, and CO can be found in Appendix A.

2.4 Further Precision Considerations

The main physical determinants of analytical precision of the FTIR method were discussed above in section 2.2. There are, however, a few second order effects which need to be considered if precision is to be maximised. These include departures from Beer-Lambert law linearity due to limited resolution, and spectrum lineshape effects due to temperature and pressure variation.

2.4.1 The Beer-Lambert Law, Linearity and Resolution

If the maximum path difference of an interferometer is Δ_{max}, the best resolution obtainable, $\Delta\tilde{\nu}$, is given approximately by

$$\Delta\tilde{\nu} \approx (\Delta_{max})^{-1}. \tag{2.28}$$

In FTIR spectroscopy the main deviation from Beer-Lambert law behaviour is due to the effect of insufficient spectral resolution, i.e. where the absorption features are narrower than can be resolved using the available resolution. This will result in the apparent peak absorbance, A^a_{peak}, being less than the true peak absorbance, A^t_{peak}. This is not a problem for quantitative analysis as long as A^a_{peak} continues to vary linearly with A^t_{peak}. However this will only be true for values of A^a_{peak} below a certain threshold. Above this threshold A^a_{peak} tends to vary as a function of $(A^t_{peak})^{1/2}$. *Anderson and Griffiths* [1975] have quantified the expected deviations from Beer-Lambert linearity when resolution is limited in this way. In the case of interest the actual absorbance linewidth (FWHH) of gas phase

molecules at ambient pressure and temperature is about $0.15cm^{-1}$ and the instrument resolution $1cm^{-1}$. According to Anderson and Griffiths' study, A^a_{peak} will change linearly with A^t_{peak} (and therefore with concentration) only for $A^a_{peak} < 0.1$ abs_{10}. For stronger absorbances, $A^a_{peak} > 0.1$ abs_{10}, the relationship between concentration and A^a_{peak} tends to become nonlinear, and A^a_{peak} will vary with the square-root of concentration.

In the present work, the strength of the peak absorbance features due to CO, N_2O, CH_4 and $^{13}CO_2$ were generally well within this region of linearity. Some of the $^{12}CO_2$ lines used for analysis were somewhat stronger and potentially nonlinear. However, it was found experimentally that the degree of nonlinearity was not a source of systematic error for peak absorbances up to $A^a_{peak} \approx 0.4$ abs_{10}. (See CO_2 linearity study, Section 4.6.1). There may be several reasons for this. Firstly, there is a distinction to be made between the linearity of A^a_{peak} and the linearity of a CLS fit to a region of the spectrum. Even if the fitted region contains a few strong absorption features where $A^a_{peak} > 0.1$, the fit will be determined mainly by the majority of wavenumbers, for which $A^a_{peak} < 0.1$ abs_{10}, and are thus behaving linearly. Secondly, the $^{12}CO_2$ mixing ratio calibration ranges required in the present work were relatively small, corresponding at most to a 15% change in A^a_{peak}. The assumption of linearity when calibrating over a very small segment of a non-linear instrument response function is often justified as the errors introduced are likely to be very small. The MALT program [*Griffith*, 1996] described below, by which the spectrometer is calibrated, accurately models this source of Beer-Lambert nonlinearity, and was used to minimise its contribution to systematic error. Considering all of the

above, we are justified in exploiting the directly linear relationship between trace gas concentration and apparent absorbance, A^{a}_{peak}.

2.4.2 Second-Order Pressure Effect

Pressure differences were found to contribute a source of systematic error in mixing ratio determination. In the Cape Grim experiment (see Chapter 4), the cell was routinely filled with the sample to ambient pressure which varied from 730-765 Torr, while the calibrant was analysed at a fixed pressure of 760 Torr. All spectra were analysed using CLS and a calibration set of synthetic spectra calculated to model a pressure and temperature of 760 Torr and 305 K respectively. The retrieved sample concentrations were corrected to 760 Torr and 305 K using measured pressure and temperature and assuming ideal gas law behaviour. However there was a small second order correction required to the resulting mixing ratios, which was made empirically. The source of this effect is illustrated in Figure 2.9 which illustrates the slight difference in absorbance peak width of a $^{13}CO_2/N_2$ mixture due to a pressure change from 760 Torr to 720 Torr. The difference spectrum is shown expanded by a factor of 20. This second order pressure effect on retrieved concentration has been both modelled using MALT and CLS as well as measured empirically from real sample spectra (see section 2.3 for description of MALT and CLS). The results are listed in Table 2.5.

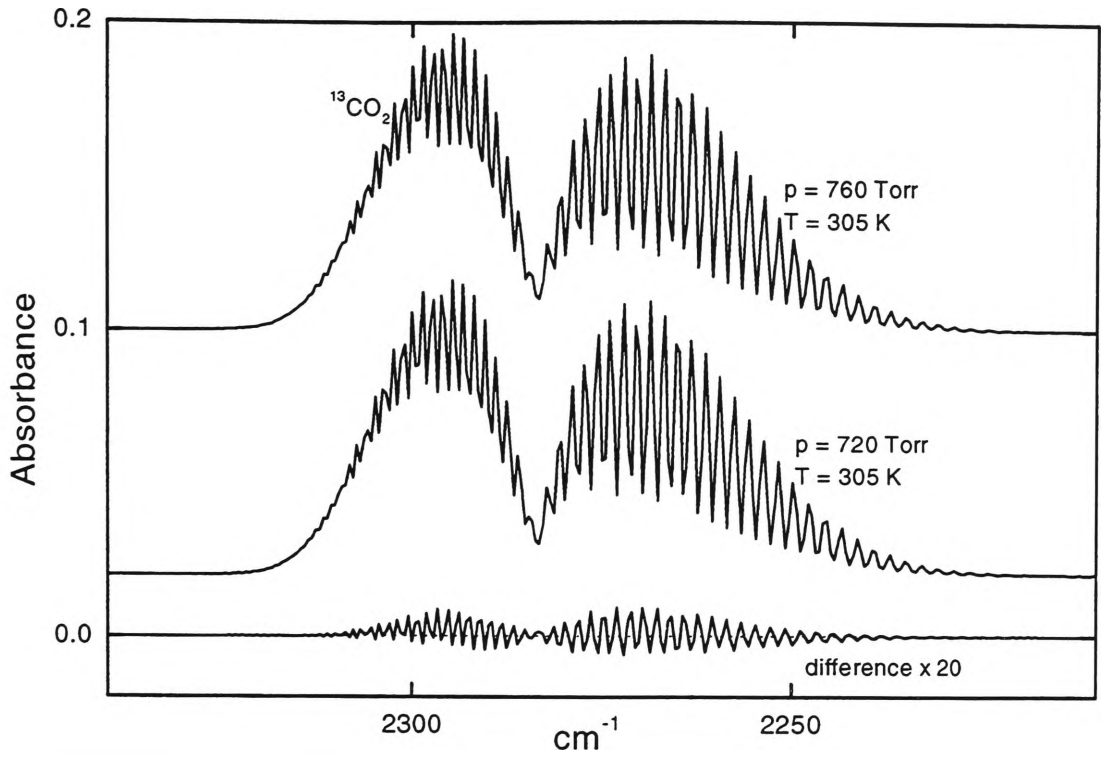

Figure 2.9. MALT spectra of $^{13}CO_2$ in N_2 calculated for different pressures. The amount of $^{13}CO_2$ analysed, temperature and pathlength is the same in both cases. The difference spectrum illustrates the line broadening effect of pressure.

The correlation in both magnitude and direction between the empirical and modelled results in Table 2.5 gives confidence that this systematic effect can be well characterised by consideration of pressure broadening effects. That the empirical result is larger than the modelled result suggests that there may be additional (so far unidentified) contributions to this effect. The result is a relationship between retrieved mixing ratio and sample pressure which depends primarily on a simple density effect and to a lesser extent on a line broadening effect. In subsequent experiments all samples and calibrants were analysed at the same (to within ±0.3 Torr) fixed, slightly subambient pressure to remove this source of error from the method. It is possible that the analysis of $^{12}CO_2$, which showed the largest second order pressure effect, may still be limited in precision by this effect. It should be insignificant for the other species, including $^{13}CO_2$.

	Region Fitted	Modelled $\Delta\mu/\Delta p$		Observed $\Delta\mu/\Delta p$	
$^{12}CO_2$	2050-2310 cm^{-1}	+0.07 ppm $Torr^{-1}$	(+0.02 %)	+0.18 ppm $Torr^{-1}$	(+0.051 %)
$^{13}CO_2$	2050-2265 cm^{-1}	~0		+0.0001 ppm $Torr^{-1}$	(+0.003%)
$\delta^{13}CO_2$	as above	-0.21 ‰ $Torr^{-1}$		-0.41 ‰ $Torr^{-1}$	
N_2O	2050-2250 cm^{-1}	-0.013 ppb $Torr^{-1}$	(-0.004 %)	-0.09 ppb $Torr^{-1}$	(-0.03 %)
CO	2050-2223 cm^{-1}	-0.017 ppb $Torr^{-1}$	(-0.017 %)	~0	
CH_4	2810-3190 cm^{-1}	-0.088 ppb $Torr^{-1}$	(-0.005%)	-0.15 ppb $Torr^{-1}$	(-0.009 %)

Table 2.5. Dependence of retrieved mixing ratio on the difference between the MALT calibration pressure and the sample pressure. $\Delta\mu$ is change in retrieved mixing (or isotope) ratio and Δp = (calibration pressure - experimental pressure). Gas mixing ratio in model calculation is 350 ppm $^{12}CO_2$, 3.9 ppm $^{13}CO_2$, 310 ppb N_2O, 100ppb CO, 1700 ppb CH_4. The modelled results are determined from two sets of calculated spectra with pressures and 720 Torr and 760 Torr respectively but similar in all other ways. The experimental results are taken from five weeks of baseline air measurements at Cape Grim where the observed range of pressures is 730-765 Torr.

2.4.3 Second-Order Temperature Effect

In an analogous manner to pressure, as described above, instability in the temperature is a source of systematic error. Figure 2.10 illustrates this. The two calculated MALT spectra are of an identical sample except that the temperature is different by 2K. They have been corrected for the density difference which results from a 2K temperature difference at constant pressure. Also illustrated is the difference spectrum (× 20) between the two. A 2K temperature difference results in the two spectra being significantly different, due to the greater probability at elevated temperatures of the high J-number rotational states being populated. The resulting error in the retrieved mixing ratio when a spectrum is predicted using calibrant spectra calculated for a temperature different from the experimental temperature will depend on which part of the band is used for the spectral fit. This systematic error due to temperature differences has been

quantified for a typical set of regions used in the present work in Table 2.6. In particular note that $^{12}CO_2$ is very temperature sensitive, to the extent that even small temperature instabilities will cause significant changes in the retrieved $^{12}CO_2$ concentration, resulting from the use of only high J-number absorption features with strong temperature dependence. The lower J-number lines of $^{12}CO_2$ are far too intense and will not obey the Beer-Lambert law.

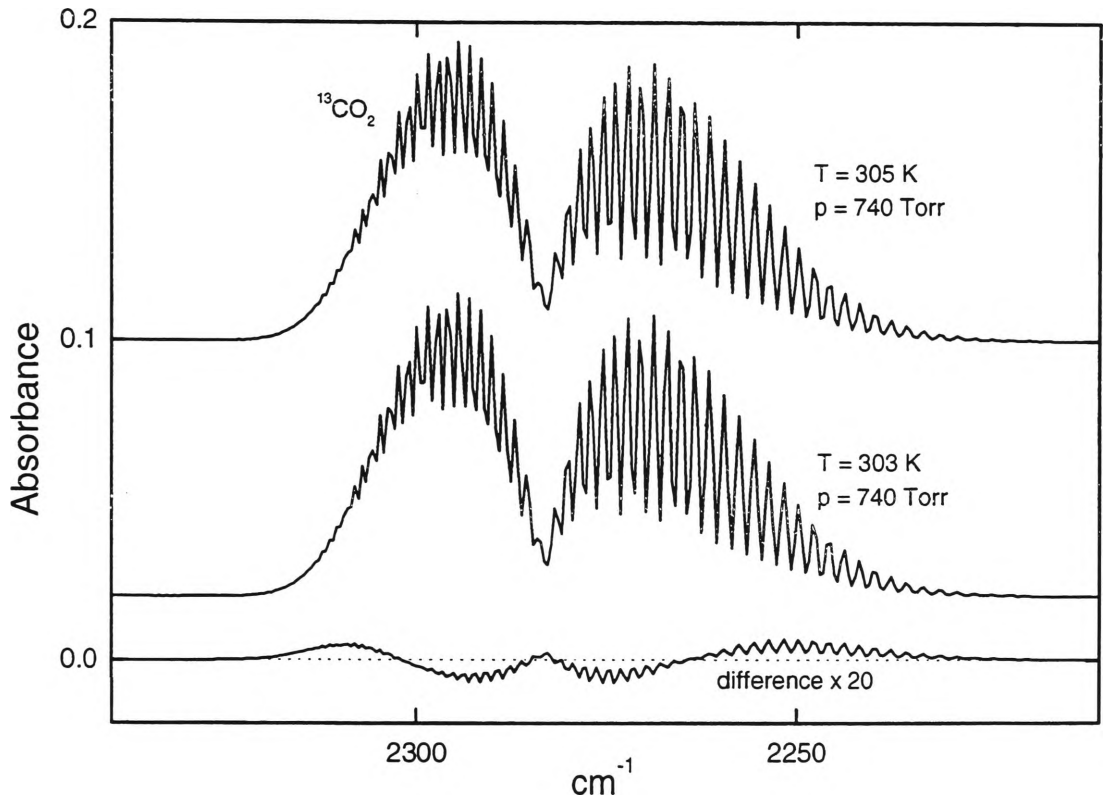

Figure 2.10. MALT spectra of $^{13}CO_2$ in N_2 calculated for different temperatures. The amount of $^{13}CO_2$ analysed, pressure and pathlength is the same in both cases. The difference spectrum illustrates the effect of temperature on bandshape.

The temperature effect is of more concern than the pressure effect described above. The second order pressure effect is rendered insignificant with the introduction of relatively straightforward sample pressure control measures. However, even with temperature control to much better than ±1K, the second-order temperature effect is significant for $^{12}CO_2$ and $\delta^{13}CO_2$ analyses but not for the other species. For the highest precision

measurements, the temperature effect will need to be characterised and the appropriate correction made.

	Region Fitted	Modelled $\Delta\mu/\Delta T$		Observed $\Delta\mu/\Delta T$	
$^{12}CO_2$	2050-2310 cm-1	+4.5 ppm K^{-1}	(+1.3 %)	+1.2 ppm K^{-1}	(+0.33 %)
$^{13}CO_2$	2050-2290 cm-1	+0.0143 ppm K^{-1}	(+0.37 %)	+0.0023 ppm K^{-1}	(+0.06 %)
$\delta^{13}CO_2$	as above	-10.5‰ K^{-1}		-1.9 ‰ K^{-1}	
N_2O	2050-2250 cm-1	-0.39 ppb K^{-1}	(-0.13 %)	-0.47 ppb K^{-1}	(-0.15 %)
CO	2050-2223 cm-1	+0.08 ppb K^{-1}	(+0.08 %)	~0	
CH_4	2810-3190 cm-1	-2.4 ppb K^{-1}	(-0.14 %)	-1.5 ppb K^{-1}	(-0.087 %)

Table 2.6. Dependence of retrieved mixing ratio on the difference between the MALT calibration temperature and the sample temperature. $\Delta\mu$ is change in retrieved mixing (or isotope) ratio and ΔT = (calibration temperature - experimental temperature). Gas mixing ratio in both modelled and experimental is 350 ppm $^{12}CO_2$, 3.9 ppm $^{13}CO_2$, 310 ppb N_2O, 100 ppb CO, 1700 ppb CH_4. The modelled results are determined from two sets of calculated spectra with temperatures 303K and 305K respectively but similar in all other ways. The experimental results were taken from repeated sampling from a reference tank when the temperature was changing slowly, over a total range of 0.4K

2.5 Verification Of Method

A series of instrumental and modelling experiments was performed in an attempt to verify the validity of the approach described in the preceding sections of this chapter. Section 2.5.1 describes two different instrumental approaches in estimating the analytical precision which can be achieved in practice when FTIR spectroscopy is applied to trace gas analysis of air samples. In the first experiment a sample of air was introduced to the White cell, then analysed repeatedly over a period of several hours. This provides an estimate of the method's precision when there is no sample handling involved. In the second experiment, many separate aliquots of well characterised air from the same source were introduced to the White cell over a period of several hours; each sample was

analysed only once. This provides an estimate of the precision of the method when sample handling as well as spectroscopy is involved.

Section 2.5.2 describes a purely modelling experiment where the MALT program is used as the virtual experimental platform, recalling that MALT simulates the behaviour of an ideal FTIR spectrometer. The aim of this experiment was to determine the relationship between analytical precision and the level of random noise in the sample spectra. In particular, such an experiment should indicate what ultimate level of precision of trace gas analysis may be achieved using FTIR spectroscopy.

2.5.1 Experimental Precision

Spectroscopy only experiment. A sample of air was introduced to the 9.8m pathlength White cell from a calibration tank. This air was known from independent gas chromatographic analysis by CSIRO's GASLAB to have the following approximate trace gas mixing ratios: 354 ppm $^{12}CO_2$, 4 ppm $^{13}CO_2$, 1700 ppb CH_4, 90 ppb CO, 310 ppb N_2O. The pressure and temperature of the sample were 740 Torr and 305 K respectively. A set of 30 single-beam spectra of this sample was collected over a four hour period, each spectrum consisting of 256 coadded scans and taking 8 minutes to collect . These were converted to absorbance spectra with reference to a 256-scan spectrum of the evacuated White cell. In a similar manner, four further sets of 30 absorbance spectra were collected, consisting of 128-scan, 64-scan, 32-scan and 16-scan spectra, respectively. All of these spectra were analysed using the CLS prediction procedure. Thus, each set of spectra provided five sets of 30 trace gas concentrations, one set each for $^{12}CO_2$, $^{13}CO_2$, CH_4, CO and N_2O.

As an example, Figure 2.11 illustrates the results for the 256-scan and 16-scan experiments, with retrieved concentration plotted against time. There were two types of variation observed in the data sets. Firstly there was random variation in the retrieved concentrations, reflecting the precision limits of the technique. Secondly, there was a monotonic variation due to slow changes in the laboratory (and instrument) temperature with time. A simple linear regression algorithm (MS Excel, LINEST function) was used to measure the level of scatter about the regression line fitted to a 10 data-point section of this data set, as indicated on Figure 2.11. This is the standard error of prediction, SEP, calculated according to equation 2.26, where the independent variable is in this case the time of analysis, and the dependent variable the retrieved concentration of the trace gas. This standard error of prediction is taken to be an estimate of the precision of the FTIR analysis. The slow drift due to laboratory temperature change is not included in the calculation of precision by this method, since it is the random variation which is primary interest here. The results of this experiment are plotted as solid squares separately for the five species concentrations and the isotope ratio $\delta^{13}CO_2$ in Fig 2.12 and 2.13. Figure 2.12 illustrates analytical precision in both absolute and percentage terms as a function of the number of coadded scans in the spectra. Figure 2.13 illustrates the same data as a function of $1/\sqrt{\text{Scans}}$, since ANR is expected to vary linearly with $1/\sqrt{\text{Scans}}$. If ANR is the main determinant of analytical precision then the plot of precision vs $1/\sqrt{\text{Scans}}$ is also expected to be linear.

Spectroscopy + automated sample handling experiment. An experiment analogous to that described immediately above was performed on the same instrument. This

experiment, however, included automated sample handling as well as spectroscopy. The same tank of calibrated well characterised air was used. Sample pressure and temperature were maintained at 760 Torr and 306 K respectively. After each analysis, the White cell was evacuated and then refilled from the tank via the sampling manifold, the whole process automated by a computer program. A set of 32 consecutive 256-scan spectra were collected in this way, as well as a set of 40 consecutive 64-scan spectra and a set of 12 32-scan spectra. There were no 128-scan or 16-scan spectra collected. These were analysed in the same manner as described above. The results of this experiment are illustrated in Fig 2.12 and 2.13 as open triangles. Note that in this data set, normal density corrections were made using White cell pressure and temperature measurements. In the previous experiment this was not necessary as the sample, and therefore its density, was not changing.

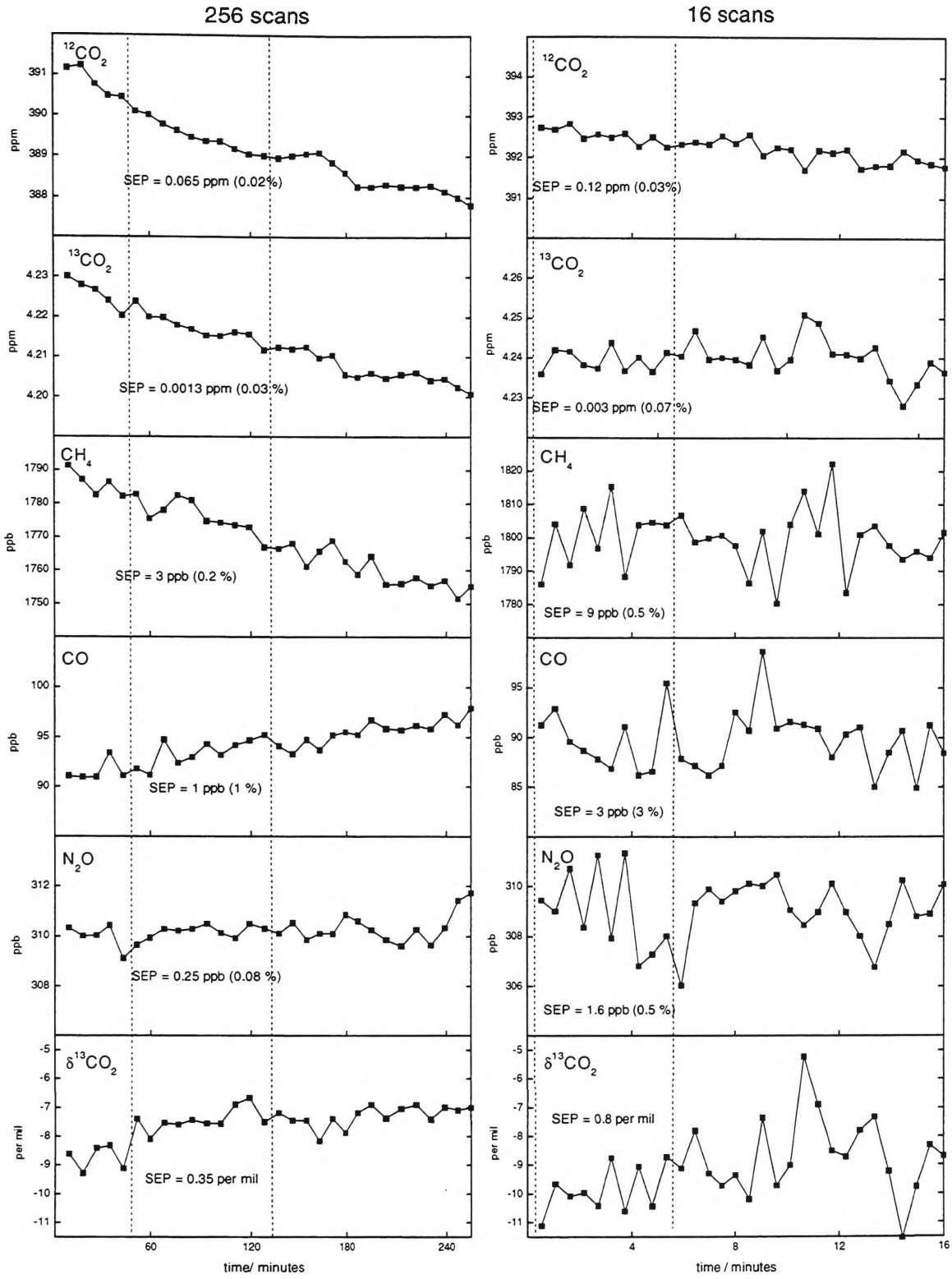

Figure 2.11. Results of repeat FTIR analysis of a single air sample with no sample handling involved. Retrieved concentrations for $^{12}CO_2$, $^{13}CO_2$, CH_4, CO, N_2O and the isotope ratio $\delta^{13}CO_2$ are plotted as a function of time. The 256-scan and 16-scan experiments only are illustrated. A single scan takes about 2 seconds. The dashed lines illustrate which data were used in calculating the SEP (Standard Error of prediction) values indicated on the plots. (The sample handling experiment was conducted under more favourable SNR conditions than was the non-sample handling experiment - see text).

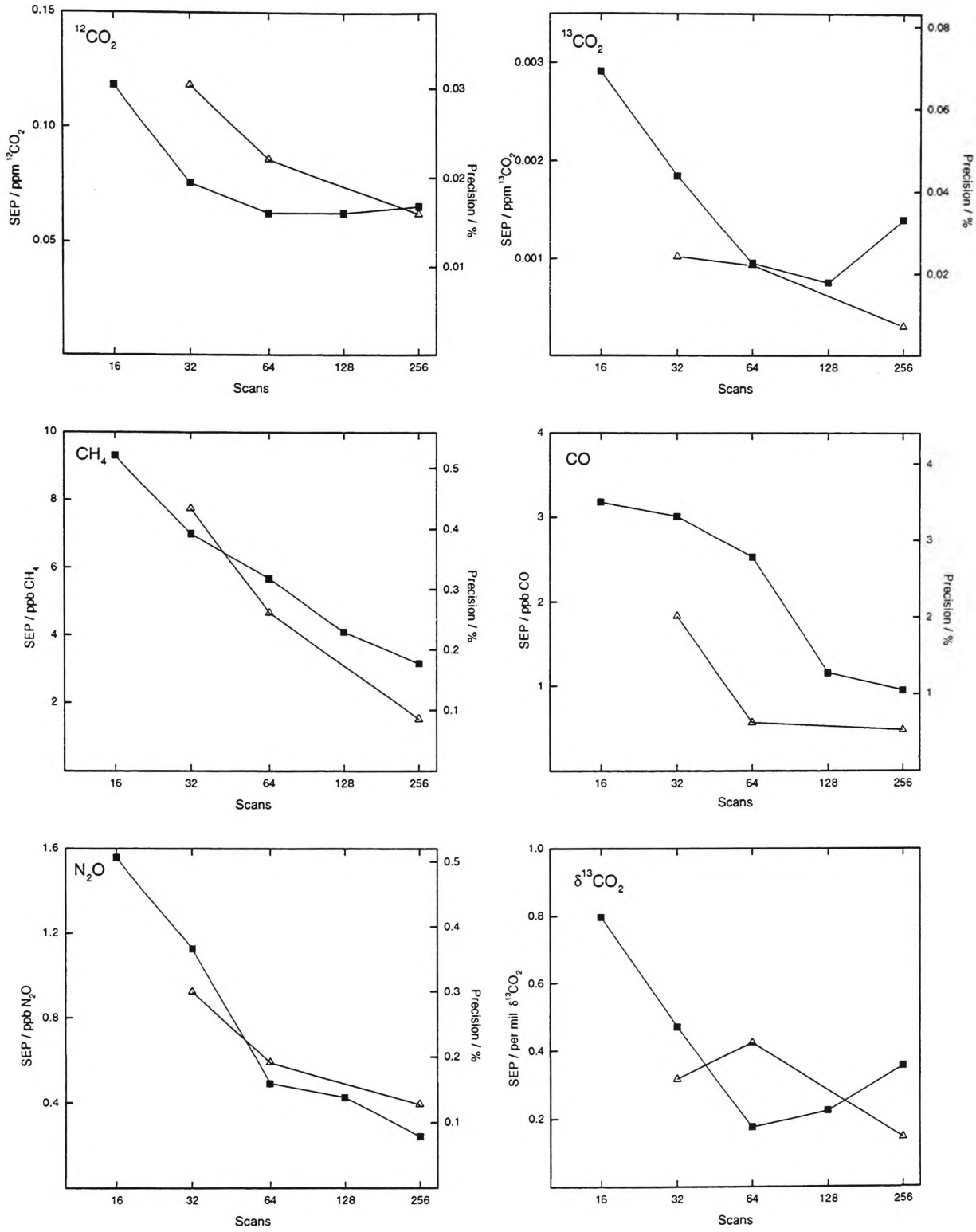

Figure 2.12. SEP (Standard Error of Prediction) vs number of co-added scans for $^{12}CO_2$, $^{13}CO_2$, CH_4, CO, N_2O and $\delta^{13}CO_2$. Filled squares indicates the no-sample-handling experiment results, and open triangles are the spectroscopy + sample handling results. (MALT parameters: resolution 1cm^{-1}, 740 Torr, 305 K, pathlength 9.8m, 0<H_2O<10ppm, 340<CO_2<380ppm, 1680<CH_4<1750ppb, 300<N_2O<320ppb, 50<CO<100ppb. CLS calibration windows: $^{12}CO_2$ 2020-2306 cm^{-1}; $^{13}CO_2$ 2020-2290 cm^{-1}; CH_4 2805-3195 cm^{-1}; CO 2020-2200 cm^{-1}; N_2O 2020-2250 cm^{-1}.)

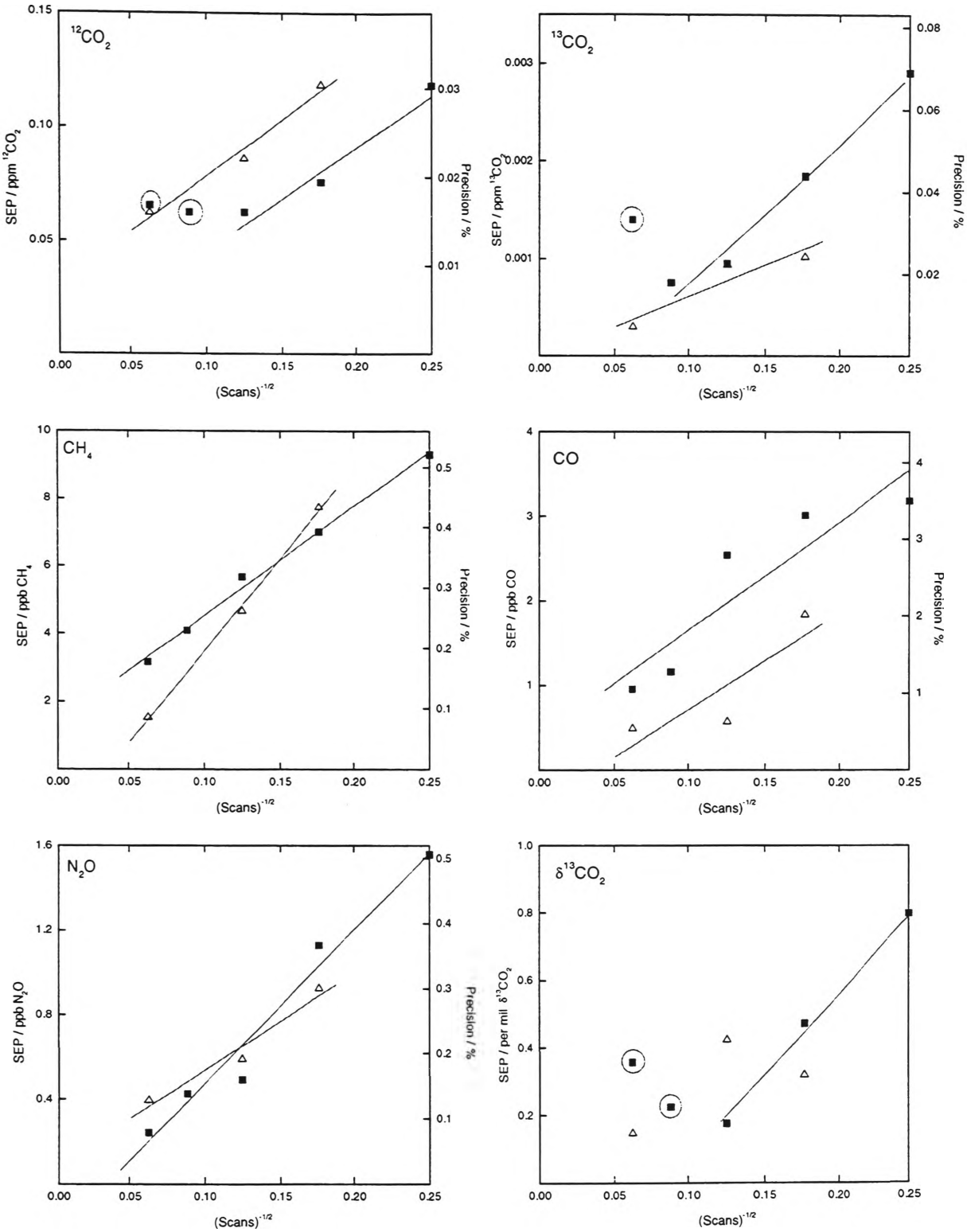

Figure 2.13. SEP (Standard Error of Prediction) vs (Scans)$^{-½}$ for $^{12}CO_2$, $^{13}CO_2$, CH_4, CO, N_2O and $\delta^{13}CO_2$. Filled squares indicates the no-sample-handling experiment results, and open triangles are the spectroscopy + sample handling results. Lines of best fit are shown where the data is consistent with the expected linear relationship between precision and $1/\sqrt{\text{Scans}}$. (MALT and CLS parameters same as Figure 2.12)

Discussion. With reference to Figures 2.12 and 2.13, the results of both experiments illustrate that the normal square-root relationship between analytical precision and number of coadded scans is obeyed approximately. Surprisingly, the results suggest at first glance that marginally better precision is achieved with sample handling rather than without it, for the species $^{13}CO_2$, CH_4, CO. This is actually an artefact of the single-beam signal strength declining by about 25% between the time of the sample-handling experiment and the later non-sample-handling experiment. Thus the sample-handling experiment was performed under more favourable SNR conditions than the non-sample-handling experiment. Bearing this in mind, for the species, $^{13}CO_2$, CH_4, CO and N_2O, there is no significant difference between the level of precision obtained with and without sample handling. This confirms that the precision is not currently limited by perturbations due to automated sample handling and vindicates the level of caution exercised in this regard as described in Section 2.3.2.

In contrast, the precision of $^{12}CO_2$ analysis appears to be significantly degraded by sample handling. This is difficult to reconcile with the apparent insensitivity of the other species to sample handling, unless temperature effects are considered. In section 2.4.3 above, it was seen that the retrieval of $^{12}CO_2$ concentrations was much more temperature sensitive than that of the other species due to the $^{12}CO_2$ analysis being dependent on the behaviour of high J-number absorption features. It follows that any uncertainty in temperature measurement will have more effect on the analysis of $^{12}CO_2$ than on the other species. It is only in the sample-handling experiment that sample temperature is incorporated into the analysis because of the need to make the density correction when changing samples.

The $\delta^{13}CO_2$ results illustrated in Figure 2.12 and 2.13 probe the precision with which the ratio $^{13}CO_2/^{12}CO_2$ can be determined. As is usual for many isotope ratios, the relative precision is reported in units of ‰ (per mil, i.e. per 1000). In the sample-handling experiment, the contributions of pressure and temperature measurements to $^{13}CO_2$ and $^{12}CO_2$ concentrations will cancel when the ratio is calculated. In principle this allows the determination of $\delta^{13}CO_2$ to a greater level of precision than the individual precisions of $^{13}CO_2$ and $^{12}CO_2$ would suggest, because of the cancellation of potentially perturbing factors. Note that in figures 2.12 and 2.13, there is little or no improvement in $\delta^{13}CO_2$ precision in going from 64-scans to 256-scans. This suggests that, for the regime beyond about 64-scans, the limiting factor in $\delta^{13}CO_2$ precision is something other than ANR. One possible candidate for such a limiting factor is a slight Beer-Lambert nonlinearity. Since the $^{12}CO_2$ absorption spectroscopic features are the most intense used in this work, that species is likely to be the source of such a nonlinear absorbance behaviour. Another candidate is some second order $^{12}CO_2$ temperature sensitivity which is not completely cancelled in taking the ratio of the two CO_2 isotopomers. In this case, $\delta^{13}CO_2$ precision will depend ultimately on the temperature stability of the instrument. A third possibility is that we are approaching the limitations of the CLS algorithm itself. Only a relatively few $^{12}CO_2$ absorption features are available to the analysis because apart from these few they are too strong and will certainly behave nonlinearly. There is a finite limit to the level of precision which can be extracted from a finite amount of information. Finally, a combination of more than one of these factors may be at work. The optimal solution may involve a trade-off between Beer-Lambert linearity, temperature effects and the limited number of suitable $^{12}CO_2$ absorption lines.

2.5.2 MALT Modelling Of Precision vs Noise

The MALT program was used to calculate sets of spectra of air containing the trace gases in the mixing ratio ranges and spectrum regions below:

$340 < CO_2 < 380$ ppm,	2020 - 2310 cm^{-1}
$1680 < CH_4 < 1750$ ppb,	2810 - 3150 cm^{-1}
$40 < CO < 100$ ppb,	2050 - 2220 cm^{-1}
$310 < N_2O < 320$ ppb,	2020 - 2265 cm^{-1}.

The MALT model also specified 1 cm^{-1} resolution, pressure of 760 Torr, temperature of 300 K and a pathlength of 22m. The 22m cell was the one in use at the time of these calculations, rather than the 9.8m White cell which was used for the results presented in Section 2.5.1. This means a direct comparison of the results below with those of Section 2.5.1 is not straightforward as the spectra obtained from the 22m cell generally had a SNR which was more than twice that of spectra obtained from the 9.8m cell.

In the first instance the MALT spectra were calculated with a peak-to-peak noise level of 3.5×10^{-5} abs_{10} in the region of the spectrum where CO_2, CO and N_2O are analysed and about 7×10^{-5} abs_{10} in the CH_4 region. This is the noise level observed in a 256-scan spectrum of air under the conditions described above. A CLS calibration was generated with this set of spectra. For each species the CLS calibration procedure provides two measures of the precision of the calibration, as mentioned in section 2.3.4, equations 2.26 and 2.27. For these purposes the values of these statistics are very close. In this case RMSD was more conveniently retrieved.

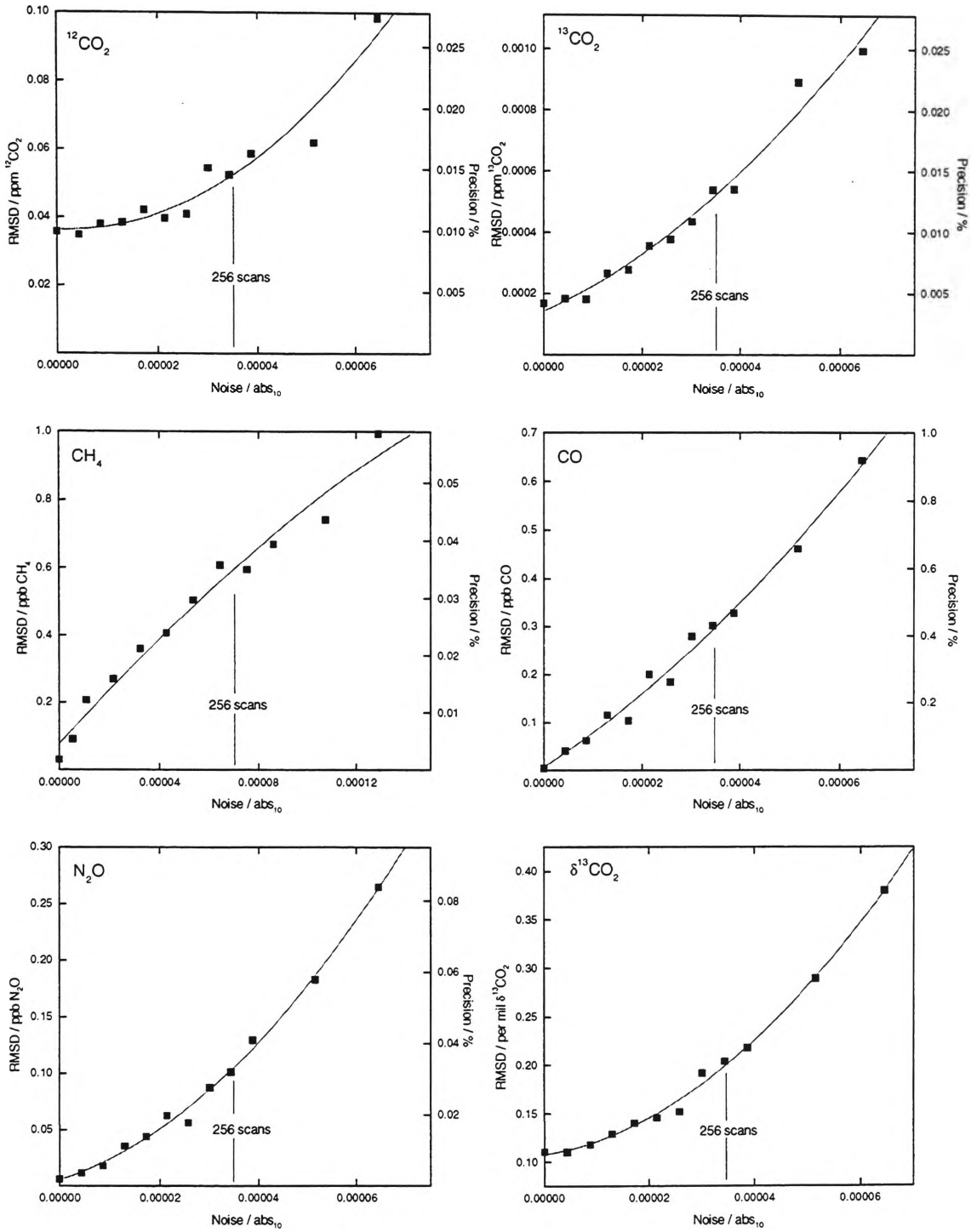

Figure 2.14. MALT model of analytical precision vs noise for the trace gases species $^{12}CO_2$, $^{13}CO_2$, CH_4, CO and N_2O. Left axis is absolute precision, right axis is relative precision. Y-intercept indicates ultimate precision achievable as number of co-added scans → ∞ and noise → 0. In each case the modelled data points have been fitted with a quadratic line of best fit. Precision was calculated as RMSD of species calibration line. Typical noise level at 256-scans indicated. (MALT parameters: resolution 1 cm^{-1}, 760 Torr, 300 K, pathlength 22.1m, -5<H_2O<5ppm, 340<CO_2<380ppm, 1680<CH_4<1750ppb, 40<CO<100ppb, 300<N_2O<320ppb. CLS calibration windows: $^{12}CO_2$ 2020-2310 cm^{-1}; $^{13}CO_2$ 2020-2265 cm^{-1}; CH_4 2810-3150 cm^{-1}; CO 2050-2220 cm^{-1}; N_2O 2020-2265 cm^{-1}.)

The whole process was repeated with nothing changed except the random noise level, which was varied from zero (equivalent to a number of scans approaching infinite), to twice the noise level observed in a 256-scan spectrum (approximately equivalent to a 64-scan spectrum). Even if random noise is set to zero in the MALT calculation there will still be residual "noise-like structure" in the resulting absorbance spectrum due to apodization of the interferogram and its subsequent Fourier transform. Inspection of such a calculated spectrum suggests that this type of "noise-like structure" is of the order of 10^{-5} abs_{10} peak-to-peak. For each species and for the isotope ratio $\delta^{13}CO_2$, the results are plotted in Figure 2.14 as precision (RMSD) as a function of MALT calculated peak-to-peak noise.

For the species CH_4 and CO, the relationship between precision and noise is almost directly linear and a near-zero y-intercept is observed, indicating that, at least theoretically, extremely high levels of analytical precision may be achieved with a sufficiently large number of scans. This is the classical and simplest relationship between precision and SNR, and seems to be obeyed by CH_4 and CO. It is interesting to note that in the regions of the spectrum used for the analysis of these two molecules, there are very few absorption features due to other species, providing an almost single component calibration scenario in each case. The N_2O precision vs noise function also tends towards a near-zero intercept, however its shape flattens with decreasing noise to a non-zero intercept. The origin of the curvature might be related to N_2O being in a much more complicated region of the spectrum than either CO or CH_4; N_2O overlaps significantly with both $^{13}CO_2$ and CO absorption features. Also, unlike all of the other

species considered here, the rotational structure of the N_2O spectrum is not resolved at 1 cm^{-1} resolution, appearing as a broad absorption band.

The results for both $^{12}CO_2$ and $^{13}CO_2$ (and hence $\delta^{13}CO_2$ also) show considerable curvature with decreasing noise, resulting in y-intercepts significantly greater than zero. Particularly for $^{12}CO_2$ and to lesser extent for $^{13}CO_2$, there is little additional precision to be achieved in going to very high numbers of coadded scans. The ultimate achievable precision is apparently driven in these cases by something other than SNR. The fact that the flattening out is more serious for $^{12}CO_2$ and $^{13}CO_2$ is strongly suggestive, once again, that the limiting factor here is either non-linear Beer-Lambert behaviour due to the strength of the absorption features in $^{12}CO_2$ in the vicinity of 2310 cm^{-1}, or that the precision is limited by the fact of there being relatively few $^{12}CO_2$ lines which are sufficiently weak to be included in the calibration window. While there is an enormous amount of $^{12}CO_2$ information in the spectrum, there is a relative paucity of accessible linear information. Temperature sensitivity effects can be excluded from consideration in this case because the model is of an ideal spectrometer with perfectly stable temperature and pressure.

The MALT-modelled results determined in this section and the experimental results of section 2.5.1 are summarised in Table 2.7. Comparing the modelled and experimental results it is generally the case that the model is a good guide to what can be achieved in practice. The only slight exception to this is for N_2O, where the experimental precision was never better than a third of the model's. It is suspected that this is due to the CLS prediction algorithm not being entirely successful in distinguishing between the broad

featureless N_2O band and low frequency baseline fluctuations in the N_2O region which are a feature of experimental spectra but not of MALT spectra.

SEP or RMSD	Modelled Precision ∞-scans, 22m cell ±σ (±σ%)	Modelled Precision 256-scans, 22m cell ±σ (±σ%)	Experimental Precision 256-scans, 22m cell ±σ (±σ%)	Experimental Precision ≤256-scans, 9.8m cell ±σ (±σ%)
$^{12}CO_2$ (ppm)	0.036 (0.01%)	0.05 (0.014%)	0.15 (0.04%)	0.06 (0.015%)
$^{13}CO_2$ (ppm)	0.00017 (0.0004%)	0.0005 (0.014%)	- -	0.0005 (0.01%)
CH_4 (ppb)	0.03 (0.002%)	0.6 (0.04%)	0.9 (0.05%)	2 (0.1%)
CO (ppb)	0.005 (0.01%)	0.3 (0.6%)	0.27 (0.5%)	0.5 (0.5%)
N_2O (ppb)	0.006 (0.002%)	0.1 (0.03%)	0.28 (0.1%)	0.3 (0.1%)
$\delta^{13}CO_2$ (‰)	0.11	0.2	-	0.2

Table 2.7. Summary of the modelled results and a comparison with actual experimentally achieved precision. The Table lists for each species, the ultimate precision as modelled here, the modelled precision for spectroscopic noise levels equivalent to a 256-scan spectrum, the experimental precision levels attained using 256-scans and the 22m cell at Cape Grim, and the experimental precision levels obtained using 256-scans and the 9.8m cell as described in Section 2.5.1.

The implications of this predictive capability of the MALT/CLS model are important. The MALT program combined with the CLS calibration and prediction processes as described above can serve as a virtual experimental platform, allowing systematic optimisation of the many experimental parameters and trade-offs to be performed without actually needing to prepare or analyse any samples on a spectrometer.

The levels of precision achieved in this work, as summarised in Table 2.7, may be compared with the minimum detection limits (MDL) estimated by Hanst and Hanst, in Table 2.1. The present work employed instrumentation with only half the spectral

resolution, and 10-20% of the pathlength used by Hanst and Hanst, and therefore required shorter averaging times and a smaller sample. Despite these potential limitations, the method described here delivered levels of precision at least competitive with current FTIR techniques, such as that of Hanst and Hanst. The present work additionally provides a method of $\delta^{13}CO_2$ isotope ratio analysis of air samples with natural isotopic abundances at useful levels of precision without the need for sample separation or preconcentration.

2.6 Summary

This chapter describes a novel method of precise and accurate trace gas analysis using FTIR spectroscopy. The method is applied to whole air samples, the only pretreatment usually required being drying. Simultaneous analyses of CO_2, CH_4, CO and N_2O mixing ratios in air as well as the isotope ratio $\delta^{13}CO_2$ are achieved. The precision of the mixing ratio retrievals is of the order of 0.01% for $^{12}CO_2$ and $^{13}CO_2$, 0.1% for CH_4 and N_2O, 0.5% for CO and 0.2 ‰ for the isotope ratio $\delta^{13}CO_2$. The analysis is carried out on a benchtop, $1cm^{-1}$ instrument which is deployable in field studies.

It has been demonstrated that the MALT program allows the modelling an FTIR experiment without having to perform it. The influence of various experimental parameters may be investigated and the experiment optimised first on a virtual platform, offering economies in both time and resources. The results returned by the modelling exercise offer realistic estimates as to what may be achieved by actual experiment.

Chapter 3: Results I: Study of CSIRO-GASLAB Calibration Tanks

3.1 Introduction to GASLAB

The Global Atmospheric Sampling LABoratory, (GASLAB), is a facility of the CSIRO Division of Atmospheric Research, Aspendale, Victoria. Its role is to study global changes in atmospheric trace gas composition. GASLAB is very closely linked to the trace gas monitoring program at Cape Grim. This involvement includes supply, installation and maintenance of *in situ* trace gas monitoring instrumentation at the station. GASLAB further fulfils the support role of provision of calibration standards for several Cape Grim programs. Where it is not possible to perform *in situ* monitoring at Cape Grim, e.g. of the stable isotope ratios $^{13}C/^{12}C$ and $^{18}O/^{16}O$ in CO_2, GASLAB provides the alternative of mass spectrometric analysis of flask samples of Cape Grim air.

GASLAB's involvement in trace gas analysis is not geographically restricted to the Cape Grim station. It analyses samples from an aircraft based Cape Grim overflight program and from routine Southern Ocean shipboard sampling. There is a GASLAB global air sampling network comprising about a dozen sites located in Antarctica, Australia, New Zealand, India, Hawaii, Canada and the UK. As well as providing valuable trace gas and stable isotope information for a range of latitudes and longitudes, the network assists in the determination of the spatial representativeness of the high precision record at Cape Grim. GASLAB has also been involved in the provision of calibration standards to, and analysis of samples from, relevant experimental field campaigns, e.g. OASIS '95 (see Chapter 5).

ICELAB (Ice Core Extraction LABoratory), developed in association with GASLAB, is a facility for the extraction of air samples from Antarctic ice cores and the overlying firn ice. Subsequent analysis of these samples by GASLAB extends the accessible atmospheric trace gas record backwards in time to the preindustial era and beyond. Where the ice core record overlaps with the Cape Grim instrumental record, they are seen to agree [*Etheridge et al.*, 1992; *Etheridge et al.*, 1996].

3.2 GASLAB Instrumentation

The central activities in GASLAB are the automated analyses of air from flasks by gas chromatography (GC) and mass spectrometry (IRMS) using the instruments listed in Table 3.1. These consist of an array of GC's employing several different principles of detection used for the trace gas mixing ratio analysis and a high precision dual-inlet isotope-ratio mass spectrometer for stable isotope analysis, usually of CO_2.

After GC separation CH_4 is detected directly by FID (flame ionisation detector). CO_2 is first quantitatively converted to CH_4 on a hot nickel catalyst before FID detection. N_2O is detected directly by ECD, (electron capture detector). H_2 and CO are detected by their reduction of HgO to Hg vapour which is then measured by UV absorption. Other than the FID, the GC detectors characteristically possess a non-linear response function and are calibrated only in the range indicated in Table 3.1

Instrument	Detector	Species	Sample ml STP	Precision %	Precision in clean air	Calibrated range
Carle-3	GC-Ni cat.-FID	CO_2	30	± 0.02 %	± 0.07 ppm	200-380 ppm
		CH_4		± 0.15 %	± 2.5 ppb	300-1850+ ppb
Trace Analytical RGA3-1	GC-HgO RGD	CO		± 1 %	± 0.5 ppb	20-400 ppb
		H_2		± 0.5 %	± 2.5 ppb	200-1600 ppb
Shimadzu-1	GC-ECD	N_2O	30	± 0.1 %	± 0.3 ppb	263-344 ppb
Finnigan MAT 252	dual-inlet IRMS	$\delta^{13}C$ in CO_2	50	± 0.01 ‰	-	
		$\delta^{18}O$ in CO_2		± 0.02 ‰		

Table 3.1. Specifications for routine flask analysis at GASLAB for mixing ratios. Calibrated range refers to the concentration range over which the instrument response has been characterised and the quoted % precision verified. STP (standard temperature and pressure) is 25°C and 760 Torr. (Adapted from *Francey et al.* [1996]).

3.3 GASLAB: Calibration Issues

The GC protocol used at GASLAB typically requires that each analysis of an unknown air sample be sandwiched between analyses of a calibrated reference air sample. Thus analysis alternates between unknown sample and reference sample. This maximises precision by minimising the effect of temporal instrumental instabilities. Precision is initially established with respect to internal laboratory *working* reference air. High pressure cylinders are filled for this purpose at Cape Schanck, which is about 70 km south of Aspendale and experiences extended air trajectories coming from over the southern ocean. These tanks of working standards are calibrated with reference to a suite of other high pressure tanks containing *calibration* standards. These calibration standards have in turn been precisely calibrated against a suite of higher level standards and ultimately back to a set of primary standards which have been gravimetrically or manometrically prepared. Tanks are assigned values with reference to more primary

standards on the basis of interpolation. This requires an assumption of only local linearity, or of a smooth sensitivity vs concentration dependence. It would not be unusual for a working standard to be 4 or 5 levels removed from the primary standard in the hierarchy of standards.

The GC measurement programs at GASLAB are linked directly to the NOAA/CMDL (US National Oceanic and Atmospheric Administration / Climate Monitoring and Diagnostics Laboratory) trace gas measurement scales for CO_2, CH_4, CO and N_2O. The working and calibration standards at GASLAB and at NOAA/CMDL are traceable to the same primary standards. In most cases these primary standards originated from NOAA/CMDL itself. *Dlugokencky et al.* [1994] have described the CMDL methane calibration scale and *Novelli et al.* [1991] give an account of the development of CMDL's gravimetric reference scale for carbon monoxide. For CO_2, CMDL employs a manometric technique for primary calibrations and an NDIR analyser for lower level calibrations [*Tans et al.*, 1996]. *Elkins et al.* [1996] describe the preparation of N_2O in air standards by a gravimetric method, and also give details of a new unified program whereby CMDL gravimetric standards are being prepared for CH_4, CO, CO_2, N_2O and a number of the halocompounds.

The related issues of calibration scale maintenance, and intercalibration of different instruments and datasets which may be both geographically and temporally removed from each other, is considered further in section 3.7.3.

3.4 FTIR Experimental Details

The 25 tanks listed in Table 3.2 were analysed by FTIR using the experimental and quantitative techniques described in Chapter 2. The equipment was located in GASLAB for these experiments. For each tank two consecutive analyses were made on separate aliquots. Two of the tanks, ALTH8459 and CC113591, were chosen for repeated analysis throughout the experiment as a probe of instrument stability. Generally the other tanks were analysed (twice) on the one occasion only.

Suite	Tank #	CO_2 ppm	CH_4 ppb	CO ppb	N_2O ppb	Fill & Initial Calibration Details
'ICE'	CC106602	318.51	1269.18	36.2	(120)	CMDL 1992
	CC106596	290.49	677.58	26.88	(112)	"
	CC106591	326.83	1429.58	41.59	(61)	"
	CC106604	305.88	880	29.36	(106)	"
	CC106605	197.93	289.19	27.98	(118)	"
	CC106592	377.17	1850.77	195.96	(99)	"
'N_2O'	CLM6681	364.02			290.8	CMDL 1993
	CLM6647	409.47			328.3	"
	CLM6652	382.87			306.4	"
	CLM6689	331.09			263.7	"
	CLM6670	368.83			294.8	"
	CLM6644	428.53			344.1	"
'NIWOT'	CC64041	346.1	1670.84	200.59	300.56	CMDL 1987-8
'CO_2'	2176616	358.49		442.08		French CO_2 stds
	2176465	371.65		438.84		"
Various	ALTH8459	363.71	1707.11	415.84	311.59	Aspendale 1993
	CC113591	358.17	1694.87	90.82	311.01	Cape Schanck 1994
	CC99530	358.74	1694.31	98.25	311.06	Cape Schanck 1994
	ALVZ864	352.32	1652.37	62.19	308.97	Cape Grim 1990
	ALVT567	353.33	1626.87	47.26	308.32	Cape Grim 1990
	S35L-CO7	289.68	2094.44	60.95	270.55	Enriched Cape Grim
	CC113587					"Zero Air"
	ALVW538		22971.6	194.06		CH_4 enriched
	CAL8341		3844.24	154.97	469.1	CH_4 enr. + C_3H_8
	ALTH8454	363.64	1879.7	401.74	309.9	Sydney Plume

Table 3.2. The 25 tanks that were analysed by FTIR at GASLAB. The mixing ratios listed are those assigned by GASLAB to the tanks. The collection consists of two main suites, 'ICE' and 'N_2O' supplied by CMDL in 1992 and 1993. Several additional members of the 'ICE' suite were unavailable as they were being analysed by another laboratory as part of an intercalibration program. Various supplementary tanks, mostly filled at Cape Grim or Cape Schanck by GASLAB, or representing extreme samples, were also analysed. Where there is no mixing ratio listed, GASLAB has not analysed for that species. N_2O values in parentheses are GASLAB GC estimates based on extrapolation beyond the instrument's calibration range.

The instrument was configured basically as described in Section 2.3: Bomem MB100 spectrometer operating at $1cm^{-1}$ resolution, liquid N_2 cooled InSb detector, 22m pathlength White cell (volume 8L), enclosed in a box thermostatted at 28±0.1°C, purged with dry UHP N_2. At the time of this experiment, the FTIR sample handling manifold had not been fully automated. The samples were introduced manually and analysed using the following protocol:

1. Each tank analysed had its own devoted regulator (Air Products). The tank regulators were pressurised and vented at least three times before analysis, according to standard GASLAB procedure.
2. After attaching the tank to the evacuated FTIR manifold including the White cell, the cell was filled to ~50 Torr from the tank and then this air was pumped away to <0.1Torr. This was repeated. There was no drying agent, scrubbing agent or filter in the sampling line. The sample came into contact with copper, stainless steel and glass surfaces, and small areas of teflon and viton. (o-rings).
3. The White cell was filled to ~760±1Torr from the tank and then both the cell and the tank were closed.
4. After a minimum of two minutes, sufficient time to allow for pressure and temperature equilibration, the pressure of the sample and the temperature of the cell were measured.
5. A 256-scan single beam spectrum of the sample was recorded, taking about 8 minutes. This was ratioed against a 256-scan single beam spectrum of the evacuated cell which had been collected immediately before the sample was introduced to the cell, providing an absorbance spectrum.
6. The absorbance spectrum was saved to disk for subsequent analysis for CO_2, CH_4, CO and N_2O mixing ratios.

7. The cell was pumped out to a pressure of <0.1Torr in preparation for the next analysis and a new empty cell reference spectrum recorded.

The spectra were analysed using the infrared regions and the MALT calibration ranges listed in Table 3.3

Species	IR Region Analysed	MALT Calibration Range
CO_2 ($^{12}CO_2$ lines)	2060 - 2304 cm^{-1}	350 - 380 ppm
CO_2 ($^{13}CO_2$ lines)	2060 - 2304 cm^{-1}	350 - 380 ppm
CH_4	2900 - 3150 cm^{-1}	1680 - 1750 ppb
CO	2060 - 2223 cm^{-1}	40 - 100 ppb
N_2O	2060 - 2260 cm^{-1}	310 - 320 ppb

Table 3.3. The regions of the infrared spectrum which were used in the trace gas analyses and the mixing ratio ranges over which the FTIR instrument was calibrated using MALT spectra.

3.5 Results: FTIR and GASLAB Tank Analyses

The results of the FTIR analyses are recorded in Table 3.4, alongside the GASLAB assigned mixing ratios determined by GC. In total, 102 samples of air, originating from 25 different tanks were analysed. The FTIR data reported is in the form of raw mixing ratios in that they have not been calibrated against any other standard gas. The FTIR nominal mixing ratio scale is determined solely by synthetic spectra calculated from the HITRAN database using the MALT program. The GC values are for the most recent analysis of the tank by GASLAB at the time of the FTIR analysis. Where there is no value given for a GC determined concentration, no GC analysis had been performed for that species. N_2O mixing ratios in parentheses are estimates based on extrapolation beyond the calibration range of the GC analysis. Except where it is indicated in Table 3.4, the analysis that follows includes the FTIR results for all four species in all tanks.

Spectrum	Tank	Analysis Date	CO_2/ppm (FTIR)	CH_4/ppb (FTIR)	CO/ppb (FTIR)	N_2O/ppb (FTIR)	CO_2/ppm (GC)
fe089601	ALTH8459	29/9/94	359.72	1804.25	394.13	317.75	363.71
fe089602	ALTH8459	29/9/94	359.72	1804.25	394.13	317.75	363.71
fe089603	ALTH8459	29/9/94	357.92	1803.26	394.40	317.62	363.71
fe089604	ALTH8459	29/9/94	358.07	1803.09	394.43	317.83	363.71
fe089605	ALTH8459	29/9/94	359.59	1804.06	394.33	317.22	363.71
fe089606	ALTH8459	29/9/94	358.75	1803.83	394.61	317.25	363.71
fe089607	ALTH8459	29/9/94	358.11	1804.53	394.23	317.18	363.71
fe089608	ALTH8459	29/9/94	358.09	1802.66	394.58	317.11	363.71
fe089609	ALTH8459	29/9/94	358.08	1804.33	394.62	317.26	363.71
fe089610	ALTH8459	29/9/94	360.59	1807.94	394.91	317.96	363.71
fe089611	ALTH8459	29/9/94	359.78	1812.72	394.66	317.81	363.71
fe089612	ALTH8459	29/9/94	359.18	1805.84	394.65	318.58	363.71
fe089613	ALTH8459	29/9/94	358.80	1812.60	395.09	318.73	363.71
fe089614	ALTH8459	29/9/94	359.83	1808.15	395.50	319.66	363.71
fe089615	ALTH8459	29/9/94	358.92	1812.15	395.38	319.61	363.71
fe089616	ALTH8459	29/9/94	359.65	1809.75	394.88	318.58	363.71
fe089617	ALTH8459	29/9/94	359.16	1813.02	395.32	318.85	363.71
fe089618	ALTH8459	29/9/94	359.93	1806.11	393.84	318.76	363.71
fe089619	ALTH8459	29/9/94	359.17	1808.39	393.91	318.75	363.71
fe089620	ALTH8459	30/9/94	359.83	1804.23	394.88	318.81	363.71
fe089621	ALTH8459	30/9/94	358.45	1808.80	395.67	319.39	363.71
fe089622	ALTH8459	30/9/94	360.01	1803.95	393.63	318.55	363.71
fe089623	ALTH8459	30/9/94	359.16	1808.45	393.58	318.74	363.71

CH_4/ppb (GC)	CO/ppb (GC-ht)	CO/ppb (GC-area)	N_2O/ppb (GC)	Remarks
1707.11	415.84		311.59	
1707.11	415.84		311.59	
1707.11	415.84		311.59	
1707.11	415.84		311.59	
1707.11	415.84		311.59	
1707.11	415.84		311.59	
1707.11	415.84		311.59	
1707.11	415.84		311.59	
1707.11	415.84		311.59	
1707.11	415.84		311.59	
1707.11	415.84		311.59	
1707.11	415.84		311.59	
1707.11	415.84		311.59	
1707.11	415.84		311.59	
1707.11	415.84		311.59	
1707.11	415.84		311.59	
1707.11	415.84		311.59	
1707.11	415.84		311.59	
1707.11	415.84		311.59	
1707.11	415.84		311.59	
1707.11	415.84		311.59	
1707.11	415.84		311.59	
1707.11	415.84		311.59	
1707.11	415.84		311.59	
1707.11	415.84		311.59	

Spectrum	Tank	Analysis Date	CO_2/ppm (FTIR)	CH_4/ppb (FTIR)	CO/ppb (FTIR)	N_2O/ppb (FTIR)	CO_2/ppm (GC)
fe089624	ALVZ864	30/9/94	348.82	1741.41	61.26	315.60	352.32
fe089625	ALVZ864	30/9/94	348.00	1743.99	61.65	315.93	352.32
fe089626	ALTH8459	30/9/94	360.15	1798.47	393.30	318.36	363.71
fe089627	ALTH8459	30/9/94	359.48	1800.14	393.18	318.63	363.71
fe089628	ALVZ864	30/9/94	348.46	1748.98	61.93	315.75	352.32
fe089629	ALVZ864	30/9/94	348.10	1749.31	62.41	316.03	352.32
fe089630	CC113591	30/9/94	353.41	1787.68	89.97	318.03	358.17
fe089631	CC113591	30/9/94	353.41	1791.38	90.24	318.35	358.17
fe089632	CC113591	4/10/94	357.10	1798.64	90.37	320.89	358.17
fe089633	CC113591	4/10/94	355.95	1799.42	89.66	321.02	358.17
fe089634	ALTH8459	4/10/94	361.83	1814.94	395.69	319.77	363.71
fe089635	ALTH8459	4/10/94	360.85	1815.96	395.00	319.55	363.71
fe089636	CC106602	4/10/94	317.67	1353.59	35.72	121.87	318.51
fe089637	CC106602	4/10/94	316.91	1353.22	35.80	122.04	318.51
fe089638	CC106596	4/10/94	288.68	728.55	22.70	112.93	290.49
fe089639	CC106596	4/10/94	288.08	729.71	22.86	113.06	290.49
fe089640	CLM6681	4/10/94	362.62	13.20	1128.17	295.92	364.02
fe089641	CLM6681	4/10/94	362.00	13.02	1128.19	296.11	364.02
fe089642	CC113591	4/10/94	355.68	1789.90	90.52	318.77	358.17
fe089643	CC113591	4/10/94	355.22	1789.41	90.39	318.96	358.17
fe089644	CC106591	4/10/94	325.24	1521.62	43.60	59.62	326.83
fe089645	CC106591	4/10/94	324.71	1522.42	43.41	59.93	326.83
fe089646	CC113591	5/10/94	354.40	1786.97	90.34	318.63	358.17
fe089647	CC113591	5/10/94	353.68	1789.48	90.75	318.92	358.17
fe089648	CLM6647	5/10/94	404.74	16.73	810.38	334.65	409.47

CH_4/ppb (GC)	CO/ppb (GC-ht)	CO/ppb (GC-area)	N_2O/ppb (GC)	Remarks
1652.37	62.19	61.87	308.97	
1652.37	62.19	61.87	308.97	
1707.11	415.84		311.59	
1707.11	415.84		311.59	
1652.37	62.19	61.87	308.97	
1652.37	62.19	61.87	308.97	
1694.87	90.82	89.38	311.01	
1694.87	90.82	89.38	311.01	
1694.87	90.82	89.38	311.01	concentration outlier[1]
1694.87	90.82	89.38	311.01	concentration outlier
1707.11	415.84		311.59	
1707.11	415.84		311.59	
1269.18	36.2	33.96	(120)	
1269.18	36.2	33.96	(120)	
677.58	26.88	22.86	(112)	
677.58	26.88	22.86	(112)	
			290.8	very high CO
			290.8	very high CO
1694.87	90.82	89.38	311.01	
1694.87	90.82	89.38	311.01	
1429.58	41.59	40.33	(61)	concentration outlier [2]
1429.58	41.59	40.33	(61)	concentration outlier
1694.87	90.82	89.38	311.01	
1694.87	90.82	89.38	311.01	
			328.3	very high CO

Spectrum	Tank	Analysis Date	CO_2/ppm (FTIR)	CH_4/ppb (FTIR)	CO/ppb (FTIR)	N_2O/ppb (FTIR)
fe089649	CLM6647	5/10/94	404.00	16.66	811.21	334.91
fe089650	CC106604	5/10/94	303.31	943.24	27.60	106.06
fe089651	CC106604	5/10/94	303.07	945.46	27.51	106.07
fe089652	CLM6652	5/10/94	379.58	15.31	815.96	311.91
fe089653	CLM6652	5/10/94	378.64	14.54	816.64	312.22
fe089654	CC106605	5/10/94	192.45	320.76	23.04	120.46
fe089655	CC106605	5/10/94	191.80	319.64	22.77	120.71
fe089656	CC113591	5/10/94	354.73	1793.59	90.63	319.12
fe089657	CC113591	5/10/94	354.07	1793.11	90.43	319.05
fe089658	ALTH8459	5/10/94	360.23	1811.66	394.33	318.66
fe089659	ALTH8459	5/10/94	359.71	1810.17	394.23	318.77
fe089660	CC113591	7/10/94	354.15	1784.86	90.15	316.97
fe089661	CC113591	7/10/94	354.01	1788.43	90.05	317.49
fe089662	CC99530	7/10/94	355.06	1787.74	97.22	317.15
fe089663	CC99530	7/10/94	354.12	1786.41	97.07	317.18
fe089664	CLM6689	7/10/94	328.54	8.06	863.99	267.56
fe089665	CLM6689	7/10/94	328.10	8.06	864.50	267.78
fe089666	CC106592	7/10/94	373.77	1960.80	189.01	99.15
fe089667	CC106592	7/10/94	372.81	1961.57	189.38	99.20
fe089668	CLM6670	7/10/94	366.18	13.72	1433.02	296.77
fe089669	CLM6670	7/10/94	365.14	15.49	1433.06	297.01
fe089670	CC113587	7/10/94	4.34	10.95	4.19	107.40
fe089671	CC113587	7/10/94	4.36	10.55	4.35	107.37
fe089672	CC113591	7/10/94	355.08	1791.50	90.73	317.95
fe089673	CC113591	7/10/94	354.23	1791.98	90.64	317.88

CO_2/ppm (GC)	CH_4/ppb (GC)	CO/ppb (GC-ht)	CO/ppb (GC-area)	N_2O/ppb (GC)	Remarks
409.47				328.3	very high CO
305.88	880	29.36	26.06	(106)	
305.88	880	29.36	26.06	(106)	
382.87				306.4	very high CO
382.87				306.4	very high CO
197.93	289.19	27.98	24.26	(118)	
197.93	289.19	27.98	24.26	(118)	
358.17	1694.87	90.82	89.38	311.01	
358.17	1694.87	90.82	89.38	311.01	
363.71	1707.11	415.84		311.59	
363.71	1707.11	415.84		311.59	
358.17	1694.87	90.82	89.38	311.01	
358.17	1694.87	90.82	89.38	311.01	
358.74	1694.31	98.25	97.51	311.06	
358.74	1694.31	98.25	97.51	311.06	
331.09				263.7	very high CO
331.09				263.7	very high CO
377.17	1850.77	195.96	195.47	(99)	
377.17	1850.77	195.96	195.47	(99)	
368.83				294.8	very high CO [3]
368.83				294.8	very high CO
358.17	1694.87	90.82	89.38	311.01	
358.17	1694.87	90.82	89.38	311.01	

Spectrum	Tank	Analysis Date	CO_2/ppm (FTIR)	CH_4/ppb (FTIR)	CO/ppb (FTIR)	N_2O/ppb (FTIR)
fe089674	CC113591	10/10/94	354.05	1788.10	89.72	316.55
fe089675	CLM6644	10/10/94	422.27	15.38	1110.40	348.15
fe089676	CLM6644	10/10/94	421.25	14.71	1110.56	347.92
fe089677	ALVW538	10/10/94	0.36	22814.65	185.37	5.78
fe089678	ALVW538	10/10/94	0.34	22827.40	185.06	5.71
fe089679	S35L-CO7	10/10/94	286.39	2283.11	59.89	289.11
fe089680	S35L-CO7	10/10/94	286.17	2298.90	59.26	277.90
fe089681	CC64041	10/10/94	342.01	1773.14	191.70	306.21
fe089682	CC64041	10/10/94	341.77	1772.31	191.64	306.60
fe089683	CAL8341	10/10/94	351.68	3996.26	148.72	476.46
fe089684	CAL8341	10/10/94	350.89	4011.25	149.30	476.50
fe089685	CC113591	10/10/94	354.21	1720.64	89.59	318.13
fe089686	CC113591	10/10/94	353.38	1739.88	89.73	317.99
fe089687	CC113591	11/10/94	353.75	1775.28	89.91	316.85
fe089688	CC113591	11/10/94	353.12	1779.68	89.87	317.30
fe089689	ALTH8454	11/10/94	358.11	1987.86	382.58	315.36
fe089690	ALTH8454	11/10/94	358.25	1989.29	382.57	315.69
fe089691	2176616	11/10/94	355.29	11.73	443.15	0.09
fe089692	2176616	11/10/94	354.71	12.11	443.24	0.25
fe089693	2176465	11/10/94	368.62	15.99	438.37	-0.39
fe089694	2176465	11/10/94	367.96	15.06	438.17	-0.45
fe089695	CC113591	12/10/94	353.94	1783.06	89.90	316.83
fe089696	CC113591	12/10/94	353.35	1783.85	89.88	317.08
fe089697	CC106591	12/10/94	323.87	1518.74	41.40	57.76

CO_2/ppm (GC)	CH_4/ppb (GC)	CO/ppb (GC-ht)	CO/ppb (GC-area)	N_2O/ppb (GC)	Remarks
358.17	1694.87	90.82	89.38	311.01	
428.53				344.1	very high CO
428.53				344.1	very high CO
	22971.56	194.06	193.76		very high CH_4 [4]
	22971.56	194.06	193.76		very high CH_4
289.68	2094.44	60.95	60.11	270.55	wet, ~300 ppm H_2O [5]
289.68	2094.44	60.95	60.11	270.55	wet, ~300 ppm H_2O
346.1	1670.84	200.59	200.21	300.56	
346.1	1670.84	200.59	200.21	300.56	
	3844.24	154.97	154.74	469.1	high CH_4 & C_3H_8 [6]
	3844.24	154.97	154.74	469.1	high CH_4 & C_3H_8
358.17	1694.87	90.82	89.38	311.01	NMHC contamination [7]
358.17	1694.87	90.82	89.38	311.01	NMHC contamination
358.17	1694.87	90.82	89.38	311.01	concentration outlier [8]
358.17	1694.87	90.82	89.38	311.01	concentration outlier
363.64	1879.7	401.74		309.9	
363.64	1879.7	401.74		309.9	
358.49			442.08		
358.49			442.08		
371.65			438.84		
371.65			438.84		
358.17	1694.87	90.82	89.38	311.01	
358.17	1694.87	90.82	89.38	311.01	
326.83	1429.58	41.59	40.33	(61)	

Spectrum	Tank	Analysis Date	CO_2/ppm (FTIR)	CH_4/ppb (FTIR)	CO/ppb (FTIR)	N_2O/ppb (FTIR)	CO_2/ppm (GC)	CH_4/ppb (GC)	CO/ppb (GC-ht)	CO/ppb (GC-area)	N_2O/ppb (GC)	Remarks
fe089698	CC106591	12/10/94	323.52	1519.94	41.67	58.11	326.83	1429.58	41.59	40.33	(61)	
fe099601	ALTH8459	12/10/94	359.78	1804.05	393.50	316.69	363.71	1707.11	415.84		311.59	
fe099602	ALTH8459	12/10/94	359.04	1804.05	393.28	316.76	363.71	1707.11	415.84		311.59	
fe099603	ALVT567	12/10/94	349.79	1804.92	47.57	315.03	353.33	1626.87	47.26	45.91	308.32	spectroscopic outlier [9]
fe099604	ALVT567	12/10/94	348.76	1783.88	47.72	313.44	353.33	1626.87	47.26	45.91	308.32	spectroscopic outlier

Table 3.4. Composition of air in 102 samples drawn from 25 different reference tanks as determined by FTIR. The FTIR data reported is in the form of raw mixing ratios in that they have not been calibrated against any other standard gases. The FTIR nominal mixing ratio scale is determined solely by synthetic spectra calculated from the HITRAN data base. GC values are for the most recent analysis of the tank by GASLAB at the time of the FTIR analysis. Where there is no value given for a GC determined concentration, no GC analysis had been performed for that species. N_2O mixing ratios in parentheses are estimates based on extrapolation beyond the calibration range of the GC analysis.

[1] Spectra fe089632-33 were excluded from further analysis because of outlier concentration values obtained.

[2] This pair had concentration outliers in several species. These data were not used and the tank was reanalysed, fe099697-98.

[3] All tanks with the prefix CLM- have very high CO mixing ratios, 800-1400 ppb, and very low CH_4 content. They were included in the analysis of CO_2 and N_2O instrument response only. In the case of tank CLM6670, the high CO level, ~1400 ppb, caused perturbation to the retrieved N_2O mixing ratios. Only the CO_2 data from this tank was used.

[4] This tank contained only ~23 ppm CH4 and ~190 ppb CO with almost no CO_2 and N_2O. It was used only in the analysis of instrument response to methane.

[5] This pair of samples was quite wet, ~300 ppm H_2O, which resulted in FTIR mixing ratio outliers in CO, N_2O and CH_4. It was retained in the CO_2 analysis. All other samples were relatively dry, at less than 5 ppm H_2O by FTIR analysis.

[6] This tank contained high methane, ~4 ppm CH_4, and an unknown but significant amount of propane. It was included in the instrument response analyses for CH_4, CO and N_2O.

[7] This pair of spectra showed evidence of propane contamination and was not included in any further analyses.

[8] This pair of spectra had concentration outliers in CH_4 only. They was retained for use in CO_2, CO and N_2O analysis.

[9] This pair of spectra had anomalous features in the CH_4 region of the spectrum. They was retained for use in CO_2, CO and N_2O analysis.

3.6 Comparison of FTIR and GASLAB Data

In the following sections the relationship between FTIR and GC measurements are considered for each species in turn. The FTIR data are plotted against corresponding GC data. The shape of the resulting regression line provides information on the relative linearity and dynamic range of the two techniques; its slope and offset from the 1:1 line provide further information on the relationship between the GASLAB GC and FTIR scales, the former being referenced to real standards and the latter calibrated only against the HITRAN database. The scatter in the regression data provides some indication of the relative precision of the two techniques.

All the analyses were performed over a two week period. Where a tank was considered unsuitable for inclusion into the analysis for a particular species, the reason for this will be found in Table 3.4. Typically this was because there was no known GASLAB value for that species or the concentration was extremely high or low.

3.6.1 CO_2: FTIR vs GASLAB GC

Twenty-two different tanks were suitable for CO_2 analysis. Each suitable tank was analysed on only one occasion, two aliquots being analysed consecutively; except that two tanks were each analysed in this manner on two separate occasions, making forty-eight aliquots in all. The results are summarised in Figure 3.1.

Figure 3.1a illustrates that over the broad CO_2 mixing ratio range 150-450ppm, the relationship between the two sets of data is well characterised by a shallow quadratic function. Note that this range is larger than that for which the FTIR CO_2 analysis is

explicitly calibrated, 350-380ppm (see Table 3.3). Over the near ambient range, Figure 3.1b, 320-390ppm, the relationship is linear with a slope=0.995, within 0.5% of unity, and a related offset from the 1:1 line of about -4ppm. (The y-intercept of the regression, -2.3 ± 4.9 ppm, is not statistically different from zero). Thus, for near ambient mixing ratios, the FTIR (uncalibrated) scale differs from the GASLAB GC (calibrated) scale by about -1%. The linearity of the relationship between FTIR and GC may mean two things: either (a) that both instruments behave nonlinearly in precisely the same way; or (b) that both instruments behave linearly. The former requires an improbable degree of coincidence so that the latter conclusion is more likely to be the case.

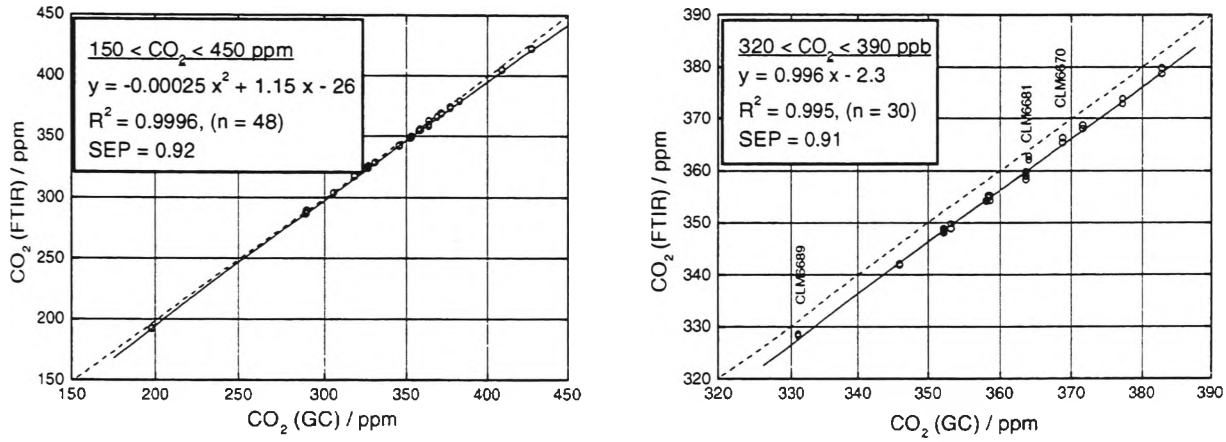

Figure 3.1. Regression plots of FTIR vs GASLAB-GC mixing ratios of CO_2. Regression line is solid and 1:1 line is dotted.

The regression line when all tanks are included in the analysis has SEP_{all}=0.9ppm CO_2. Most of this apparent scatter is, on closer examination, due to the three tanks CLM6689, CLM6681 and CLM6670. These three tanks have in common unusually high CO mixing ratios, in the range 800-1500ppb. This result is consistent with the existence of some 'crosstalk' between CO and CO_2 in the analysis of the FTIR spectrum. The effect of heightened CO levels on perceived CO_2 mixing ratios seems to be of the order of +1ppm CO_2/ppm CO. It is not entirely unexpected that extreme mixing ratios of one species

may affect the apparent mixing ratio of a species which is nearby in the infrared spectrum, as is the case with CO and CO_2. It should be noted however that the CO levels in these three tanks are far beyond the range for which the analysis is calibrated. Possibly, the strong CO absorption features are not being well fitted and there is a compensating overestimation of CO_2 mixing ratio as the least squares fitting algorithm converges on the mixing ratio prediction which results in the smallest spectroscopic residual. Alternatively, the analytical crosstalk may be in the CMDL procedure by which these extreme-CO tanks were assigned their CO_2 values. The issue cannot be resolved here.

If the three extreme-CO tanks are excluded from the analysis, then the apparent scatter in the regression from the remaining 19 tanks is significantly reduced, $SEP_{selected}$=0.64 ppm CO_2, equivalent to 0.18% prediction precision if CO_2 is at ambient concentrations. Possible reasons for this still large degree of scatter are considered in section 3.6.5.

3.6.2 CH_4: FTIR vs GASLAB GC

Fourteen different tanks were suitable for CH_4 analysis. Each suitable tank was analysed on only one occasion, two aliquots being analysed consecutively; except that two tanks were each analysed in this manner on two separate occasions, making a total of thirty-two aliquots. The results are summarised in Figure 3.2.

Figure 3.2 illustrates that the relationship between the two sets of data was linear over the three mixing ratio ranges shown, even out to the extreme of ~25ppm CH_4. Again, this is well beyond the FTIR instrument's explicit CH_4 calibration range of 1680-1750ppb. For the range around ambient atmospheric mixing ratios, 1650-1800ppb the

regression slope is about 7% greater than unity and the FTIR value is consequently offset from the 1:1 line by about +100ppb CH_4. (The y-intercept of the regression, -22±25ppb, is not statistically different from zero). This represents an offset difference between the FTIR and GC scales of about +6% at ambient CH_4 concentrations. Such a systematic difference between the uncalibrated FTIR data and the GASLAB GC scale is understandable and the possible reasons for it are discussed in section 3.6.5, below. No evidence of analytical 'crosstalk' between CH_4 and any other species is apparent. This is as expected since the CH_4 absorption features used in the FTIR analysis are far removed from those of CO_2, CO and N_2O, overlapping only with H_2O features which are absent in this case because the samples are of dried air (see Table 3.3 and Figure 2.6).

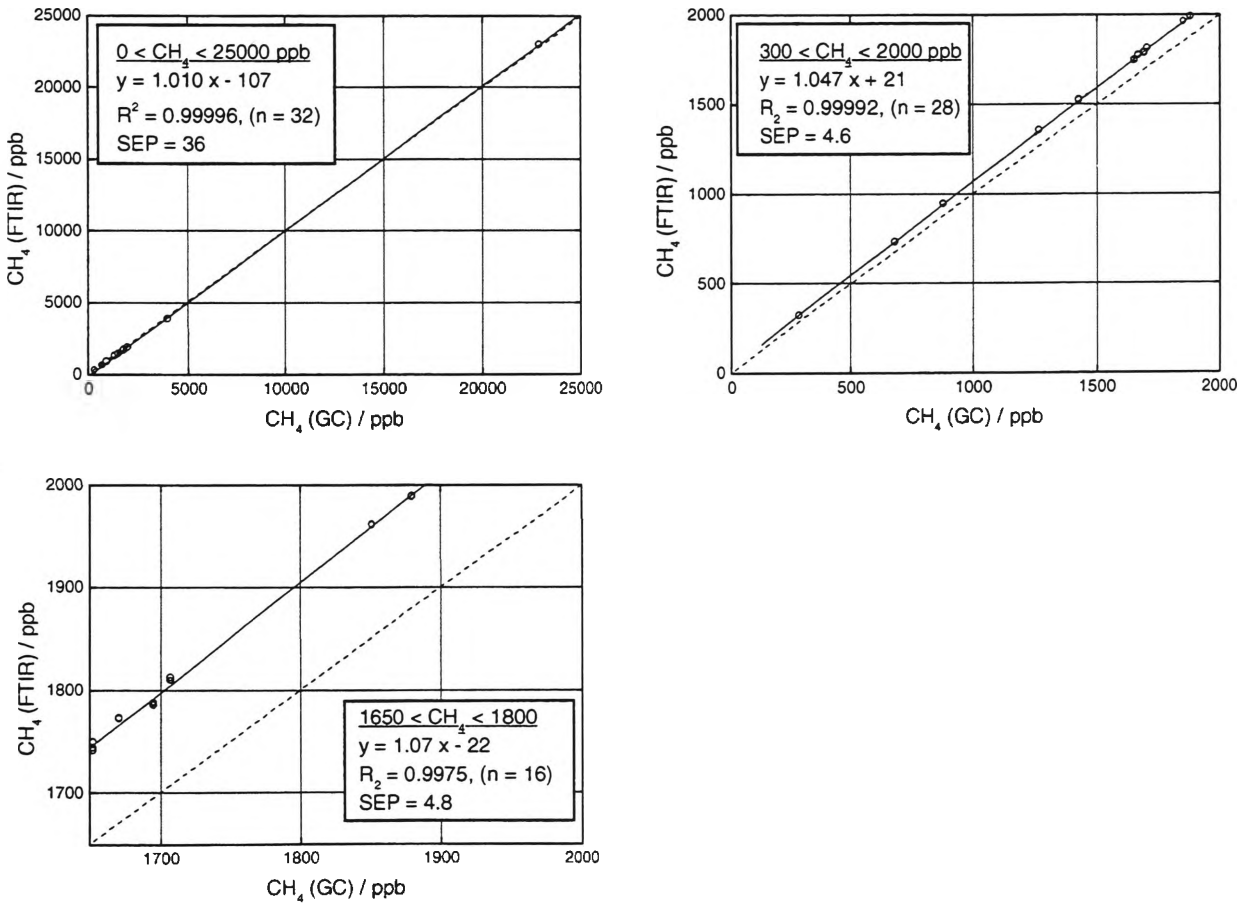

Figure 3.2. Regression plots of FTIR vs GASLAB-GC mixing ratios of CH_4. Regression line is solid and 1:1 line is dotted.

The degree of scatter in the regression lines for both the broad range, 300-2000ppb, and the near-ambient range, 1650-1800ppb CH_4, is similar, having an SEP≈4.7 ppb CH_4. This is equivalent to a prediction precision of 0.28% for CH_4 at ambient concentrations.

3.6.3 CO: FTIR vs GASLAB GC

Fourteen different tanks were suitable for CO analysis. Each suitable tank was analysed on only one occasion, two aliquots being analysed consecutively; except that one tank was analysed in this manner on two separate occasions making a total of thirty aliquots. The results are summarised in Figure 3.3. A comparison is made with both peak-height and peak-area GC analysis as either GC approach may be employed.

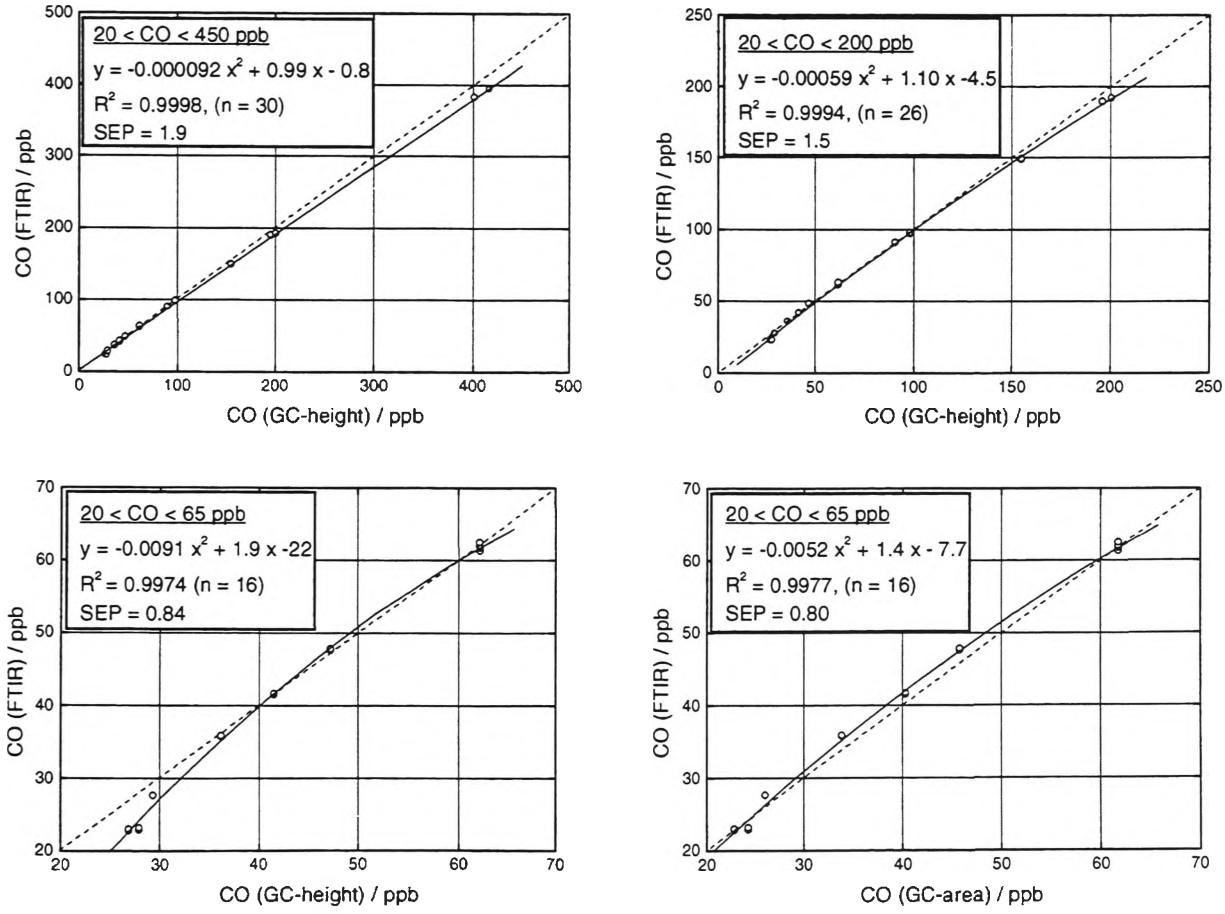

Figure 3.3. Regression plots of FTIR vs GASLAB-GC mixing ratios of CO. Regression line is solid and 1:1 line is dotted.

The relationship between the FTIR data and the GC data derived from peak-height analysis are characterised by quadratic functions over the three ranges shown here, Figure 3.3a-c. Over the low CO range, 20-65ppb, GC peak-area is also considered for comparison, Figure 3.3d. The FTIR vs GC peak-area regression shows less curvature than the FTIR vs GC peak-height regression. The reasons for greater linearity of integrated peak-area over peak-height analysis is well understood in gas chromatography and related to the changing shape of the chromatogram peak. In the case of CO, peak-height analysis has usually been the approach taken by GASLAB because of evidence of somewhat higher precision than with peak-areas, despite the greater nonlinearity. FTIR, as an independent technique, is able to probe the different linear response characterising the two chromatogram analysis approaches. There is not sufficient evidence here to conclusively determine that FTIR analysis of CO is linear and that GC analysis is not. We can only conclude definitely that the two approaches are non-linear with respect to each other. There is, however, some circumstantial evidence suggesting that FTIR is the more linear of the two methods. The HgO reduction gas analyser involved in the GC analysis of CO has been observed to behave nonlinearly by several workers [*Crill et al.*, 1995; *Derwent et al.*, 1994]. FTIR, on the other hand, is observed in sections 3.6.1, 3.6.2 above and in section 3.6.4 below, to behave in a very linear fashion with respect to GC analyses of CO_2, CH_4 and N_2O. At first it would seem unlikely that the FTIR response function would be linear for these three molecules and yet nonlinear for CO. As discussed in Chapter 2, the FTIR analysis has been explicitly designed to exploit Beer-Lambert linearity in the absorbance spectra of CO as well as the other species. However, FTIR measurement of CO concentration involves quantitative analysis of absorption features which are far weaker than those available for analysis of the other three species. Furthermore, CO analysis is necessarily performed over a much greater

range of concentrations than for the other three species because of its large natural variability. The matter of FTIR vs GC linearity for CO analysis is not yet resolved.

Figure 4.3 shows that the regression line for CO has a slope very close to unity, and that the offset from the 1:1 line, although variable because of nonlinearity, is rarely more than ±2ppb CO, and then only for extreme CO values, well outside the explicit FTIR calibrated range of 40-100ppb CO. This represents a typical offset of the uncalibrated FTIR scale from the calibrated GASLAB GC scale of ~2% at ambient CO levels.

The degree of scatter in the regression lines over the near clean-air range 20-65ppb is SEP=0.8ppb CO, and about SEP=1.5ppb for the broader 20-200ppb range. This represents a prediction precision of ~1.5%.

3.6.4 N_2O: FTIR vs GASLAB GC

Nineteen different tanks were analysed for N_2O. Each suitable tank was analysed on only one occasion, two aliquots being analysed consecutively; except that one tank was analysed in this manner on two separate occasions, making a total of forty aliquots. The results are summarised in Figure 3.4.

The relationship between FTIR data and GC data is found to be linear at near ambient mixing ratios and over the entire range tested, 50-500ppb. For the near-ambient range, 250-350ppb N_2O, the regression line has a slope different from unity by about +1% and consequently the FTIR concentration value is systematically offset from the 1:1 line by about +5ppb N_2O. (The y-intercept of the regression, 2.3±3.5ppb, is not statistically

different from zero). This represents an offset of the uncalibrated FTIR scale from the calibrated GASLAB GC scale of about +1.9% at ambient N_2O concentrations.

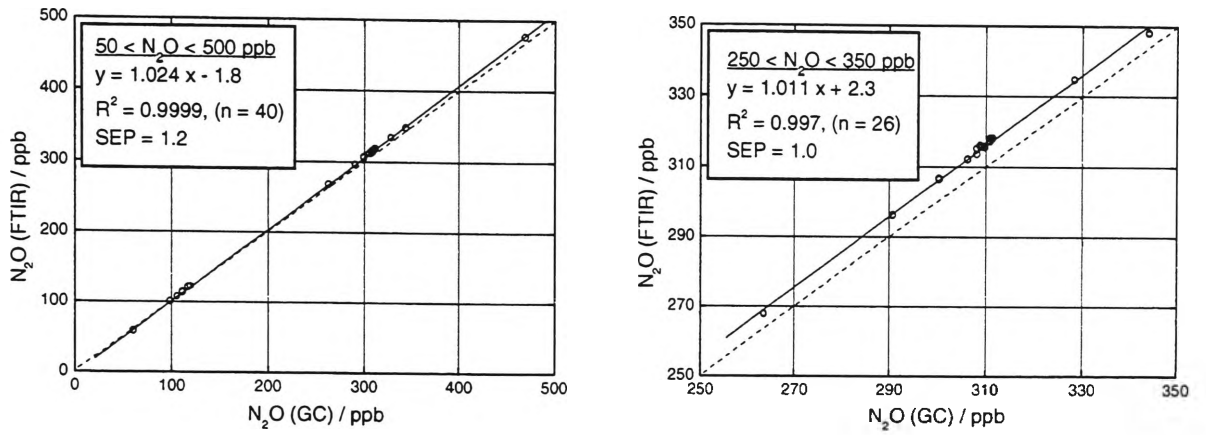

Figure 3.4. Regression plots of FTIR vs GASLAB-GC mixing ratios of N_2O. Regression line is solid and 1:1 line is dotted.

The degree of scatter in the regression lines is SEP=1ppb N_2O. This represents a prediction precision of 0.3%. There is no conclusive evidence of 'crosstalk' between CO and N_2O in the FTIR analysis even though several tanks with very high CO levels were included and CO and N_2O absorption features partially overlap in the infrared region analysed.

3.6.5 Discussion

Linearity. For CO_2, CH_4 and N_2O the FTIR vs GC regression lines indicate that the FTIR response function is linear both within and well beyond the mixing ratio ranges for which the analyses were explicitly calibrated (assuming the GASLAB GC scale is correct). The situation for CO is less clear and was discussed above.

Precision. Regression plots of the FTIR determined uncalibrated mixing ratio against the GASLAB GC determined mixing ratio have been determined for each of the four species. The regression has been performed over several ranges of mixing ratio for each

species. In each case either a linear or a quadratic function was fitted to the data and the regression statistics determined. These are summarised in Table 3.5.

Ideally, an ODR (orthogonal distance regression) algorithm should have been used [*Boggs and Rogers*, 1990], as there was uncertainty in both the FTIR mixing ratio (y-axis) and the GASLAB mixing ratio (x-axis). Despite significant programming efforts by personnel both at Wollongong University and at GASLAB, the ODR algorithm was not successfully implemented. Instead, a simple linear regression algorithm has been used which implicitly assumes all the uncertainty in the data points to reside in the dependent (*y*-axis) variable, in this case the FTIR mixing ratio. The SEP value determined for each regression is then a measure of the vertical scatter about the line of best fit. While this ought not be seen as a measure of the precision of the FTIR analysis of that species, it may be seen as an upper limit (i.e. conservative estimate) of the uncertainty in the FTIR analysis. SEP values of 4.7ppb CH_4, 1.5ppb CO and 1 ppb N_2O were retrieved. For these three species, the SEP of the regression is of a similar magnitude to the typical analytical precision achieved using GASLAB GC instrumentation (see Table 3.5).

It seems reasonable to conclude from this experiment that analysis of these three species by FTIR is able to deliver a similar degree of precision to that achievable by GC. The relative precision of the two techniques is explored more thoroughly in Chapter 4, where GC and FTIR instruments were run in parallel for an extended period. The conservative estimates of FTIR analytical precision presented here for CH_4, CO and N_2O are somewhat larger than, but consistent with, those estimates of precision determined in Chapter 2 (see table 2.6). One difference between the two sets of results is that those of Chapter 2 reflect short term internal precision over a period of minutes to hours, whereas

the results in the present Chapter are derived from an experiment performed over a two week period, for which no drift correction was made in the analysis, and were referenced to an independent analytical technique, GC, which is itself of limited precision. In the light of these differences, the present results suggest that the FTIR response function was very stable throughout the two week period of the tanks' analysis for the species CH_4, CO and N_2O. Stability of the instrument is investigated further in Section 3.7 below.

For CO_2, however, the two-week SEP value of 0.64ppm is significantly larger than the short term precision estimate of Chapter 2, ~0.1 ppm. This may again reflect the greater sensitivity of $^{12}CO_2$ analysis to temperature fluctuations than for the other species.

Species	slope	y-intercept	local offset from 1:1	SEP	GC precision
CO_2	0.996 ± 0.01	-2.3 ± 4.9 ppm	-4 ppm	± 0.64 ppm	± 0.07 ppm
CH_4	1.07 ± 0.01	-22 ± 25 ppb	+100 ppb	± 4.7 ppb	± 2.5 ppb
CO	~1	-	-	± 1.5 ppb	± 0.5 ppb
N_2O	1.01 ± 0.01	+2.3 ± 3.5 ppb	+5 ppb	± 1.0 ppb	± 0.3

Table 3.5. Linear regression parameters from FTIR vs GASLAB GC data plots. Also listed is the analytical precision achieved by GASLAB GC instrumentation.

Uncalibrated Accuracy. In each of the comparisons of FTIR and GC data there are systematic differences between the instruments' measurement scales. This is seen in regression lines with slopes which differ from unity, and the resulting offset of the regression lines from the 1:1 line. For CO_2, CH_4 and N_2O the regression parameters are summarised in Table 3.5. CO is not discussed here because the complicating element of nonlinear behaviour.

None of the y-intercepts of the regressions differ significantly from zero when the statistical uncertainty in their determination is considered. This is because the intercept is at x=0, a long way from the measured range. The local offset from the 1:1 line is a more useful parameter and is quite significant. Similarly, for CO_2 and N_2O, the slope of the regression line is not significantly different from unity. At ambient mixing ratio levels, if the GASLAB GC measurement scale is assumed to be correct, then the uncalibrated FTIR measurement scale for CO_2 and N_2O is seen to be accurate to within about -1% and +1.6% respectively, as indicated by the local offset from the 1:1 line. For CH_4, however, the regression line slope differs from unity by about +7%, a statistically significant degree. Correspondingly, the offset from the 1:1 line at ambient CH_4 mixing ratios indicates a systematic inaccuracy of about +6% with respect to the GASLAB GC scale.

It must be stressed that the FTIR data being discussed here are essentially uncalibrated data in that the FTIR mixing ratios are the direct output from the CLS calibrations for each species based only on a training set of MALT calculated spectra. At no stage have these raw mixing ratios been 'calibrated' with reference to a real gas sample analysed on this instrument. In Chapter 2 there was a description of a two step calibration process, with initial calibration against a MALT training set via a CLS algorithm, and subsequent "absolute" calibration against real calibration gas standards. While the FTIR data discussed in Chapters 4 and 5 have undergone both processes of calibration, the data presented in this chapter have only undergone the first. Indeed, the rigorous determination of a simple relationship between the calibrated GC scale and the uncalibrated FTIR scale for trace gas species, as derived in this chapter, justifies the two

step calibration process applied in Chapters 4 and 5. In many potential applications of the FTIR technique, for example combustion studies or urban pollution monitoring, an absolute accuracy of ±5% is satisfactory and further calibration would not be necessary. Even a single calibration measurement with some working standard would usually provide FTIR accuracy of better than 1%.

There are several possible reasons for systematic differences between the uncalibrated FTIR mixing ratios and an absolute mixing ratio scale:

1. The difference between real and synthetic spectra lineshape. There will always be some small difference between the real lineshape of the experimental spectra and our best attempt at modelling it using the MALT program which assumes 'perfect' spectra. For example, MALT does not yet model asymmetry in lineshapes which may occur in real spectra due to the spectrometer being imperfectly aligned. Such differences between real and synthetic lineshape may have different effects on different species, resulting in either overestimation or underestimation.
2. The strength of the absorption lines from the HITRAN-92 line parameters. Rothman et al estimates that these are accurate to about 2%, with the uncertainty for some species being better constrained than for others [*Chackerian and Tipping*, 1983; *Johns*, 1987; *Rothman et al.*, 1992; *Toth*, 1993].
3. The absolute calibration of the cell's pressure manometer. The specified nominal accuracy is 0.3% for a single measurement. This would tend to give a slope which differed from unity to the same extent for all species.

4. The pathlength of the cell. This is given as 22m by the manufacturer with an implied precision of 2%. This also would result in a consistently non-unity slope for all species. This factor could be accounted for with a single calibration of the White cell.

3.7 Stability of FTIR Instrument

The experiment described below was an attempt to quantify to some extent the stability of the FTIR instrument over a two week period. Instrumental stability is examined firstly in terms of mixing ratios, and secondly, in terms of ratios of mixing ratios. The results have implications for the maintenance of calibration scales in time, and for intecalibration of instruments and of datasets which may be geographically and/or temporally remote.

3.7.1 Repeat Analyses of Tank CC113591

The tank CC113591 containing relatively unpolluted ambient Cape Schanck air was sampled a total of 21 times over the two week period of the calibration tank study. Figure 3.5 shows the raw mixing ratios retrieved by 17 of these analyses. The results of the other four analyses were discarded as concentration outliers, apparently due to sample contamination. For this experiment, absorption features due to $^{13}CO_2$ as well as $^{12}CO_2$ were used and are treated separately in the analysis below. Figure 3.5 illustrates that the FTIR measurement stability over the two week period varies according to the species concerned.

Mixing Ratios. Analysis of $^{13}CO_2$ is apparently the most reliable the measurements having a standard deviation, $\sigma = 0.07\%$, and CO the least reliable with $\sigma = 0.37\%$, over the two weeks (see Figure 3.5 and Table 3.6). It is observed that the degree of scatter

for the species CH_4, CO and N_2O is somewhat smaller than the SEP results of FTIR vs GASLAB GC regressions for those species reported in Section 3.6. This is consistent with the earlier SEP results being due in significant part to the analytical uncertainty in the GASLAB GC procedure as well as to the FTIR procedure. The standard deviations listed in Figure 3.5 may be considered a more reliable indication of the precision of uncalibrated FTIR analysis over a two week period. It is not surprising that $^{13}CO_2$ analysis is more stable in time than that of $^{12}CO_2$ in the light of the latter species' much greater sensitivity to temperature change (see Section 2.3.2.1). Similarly, it is understandable that analysis of CH_4 is performed with greater precision than that of either CO or N_2O. CH_4 is present in much greater abundance than CO or N_2O, and its spectrum is much better rotationally resolved than that of N_2O.

The level of precision achieved over the two week period (Figure 3.5) may be compared with the short-term experimental precision determined in Chapter 2 (see Table 2.6), corresponding to several hours at most. For CH_4, CO and N_2O the results are quite similar in the two cases, i.e. ~2ppb CH_4, ~0.3ppb CO and ~0.5ppb N_2O. However, for $^{12}CO_2$ and $^{13}CO_2$, the two-week level of precision is about an order of magnitude inferior to the short term precision achieved. This is consistent with CH_4, CO and N_2O analytical precision being limited mainly by spectroscopic SNR in both the short and long term. For $^{12}CO_2$ and $^{13}CO_2$, it is suggested that instrument stability may be the limitation in both the short and long term. Another possible difference between the short-term experiments of Chapter 2 and the two-week experiments described here is that the latter-mentioned was actually conducted much earlier in the course of the overall project, before sample handling was fully automated. If the experiment was repeated with

automated sample handling, there may be a significant improvement in $^{12}CO_2$ and $^{13}CO_2$ analysis.

Ratios of Mixing Ratios. The mixing ratios obtained for five different species may be combined in a total of ten different ways to form 'ratios of mixing ratios'. Ratios of mixing ratios are considered in an attempt to eliminate random noise due to sample handling. The extent to which the observed level of scatter in the ratios of mixing ratios is less than what would have been calculated given the level of scatter in the original mixing ratios is a measure of how important the sampling handling error was in each case. The record of these is illustrated in Figure 3.6 for the repeated analysis of tank CC113591.

The important result is that these ratios of ratios are in each case determined with significantly greater precision than what would be predicted to be the case from the precision with which the individual species mixing ratios are determined. Table 3.6 lists the observed precision for each ratio, calculated as the standard deviation of the set of retrieved ratios. Also listed are the expected precision levels calculated from the mixing ratio precisions according to,

$$\sigma(a/b) = \sqrt{\sigma(a)^2 + \sigma(b)^2} \qquad (3.1)$$

where $\sigma(a)$ and $\sigma(b)$ are the standard deviations of the set of analyses of species a and b respectively. Note that in calculating the expected precision of the ratio of two mixing ratios we assume that the two are totally uncorrelated. The fact that the corresponding observed precision is in every case better than what is predicted suggests strongly that this assumption is false. Presumably the source of correlation is small errors in the

measurement of pressure and temperature. While these will degrade the precision of an individual mixing ratio they will cancel when the ratio of simultaneously determined mixing ratios is determined.

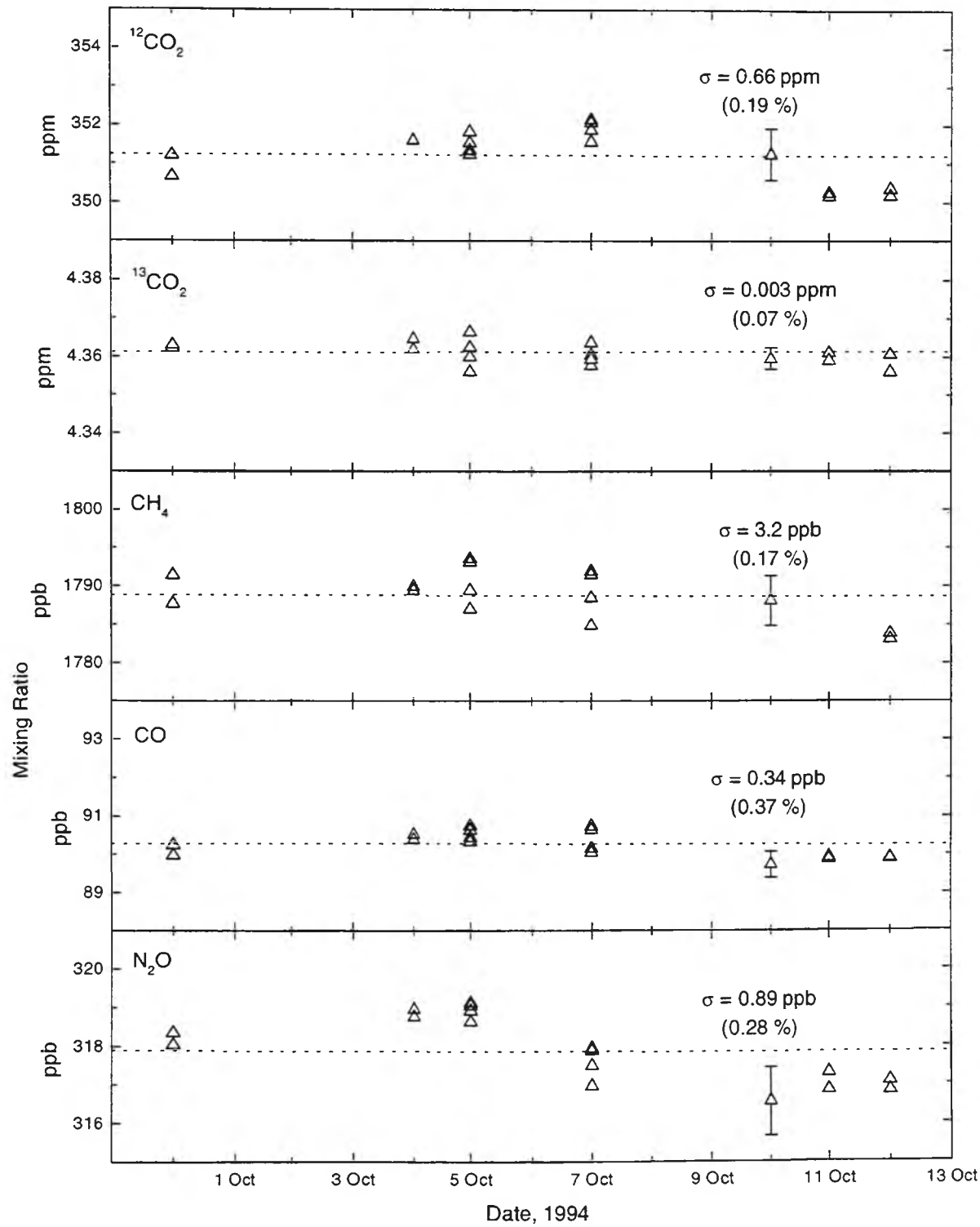

Figure 3.5. Uncalibrated trace gas mixing ratios determined by FTIR analysis of tank CC113591. Seventeen individual aliquots analysed on seven different days spanning a thirteen day period. Dotted line is mean mixing ratio over period. Precision reported as ± 1 standard deviation (σ). Samples fe089687-88 were excluded as outliers in CH_4 only, due to C_3H_8 contamination distorting that region of the spectrum.

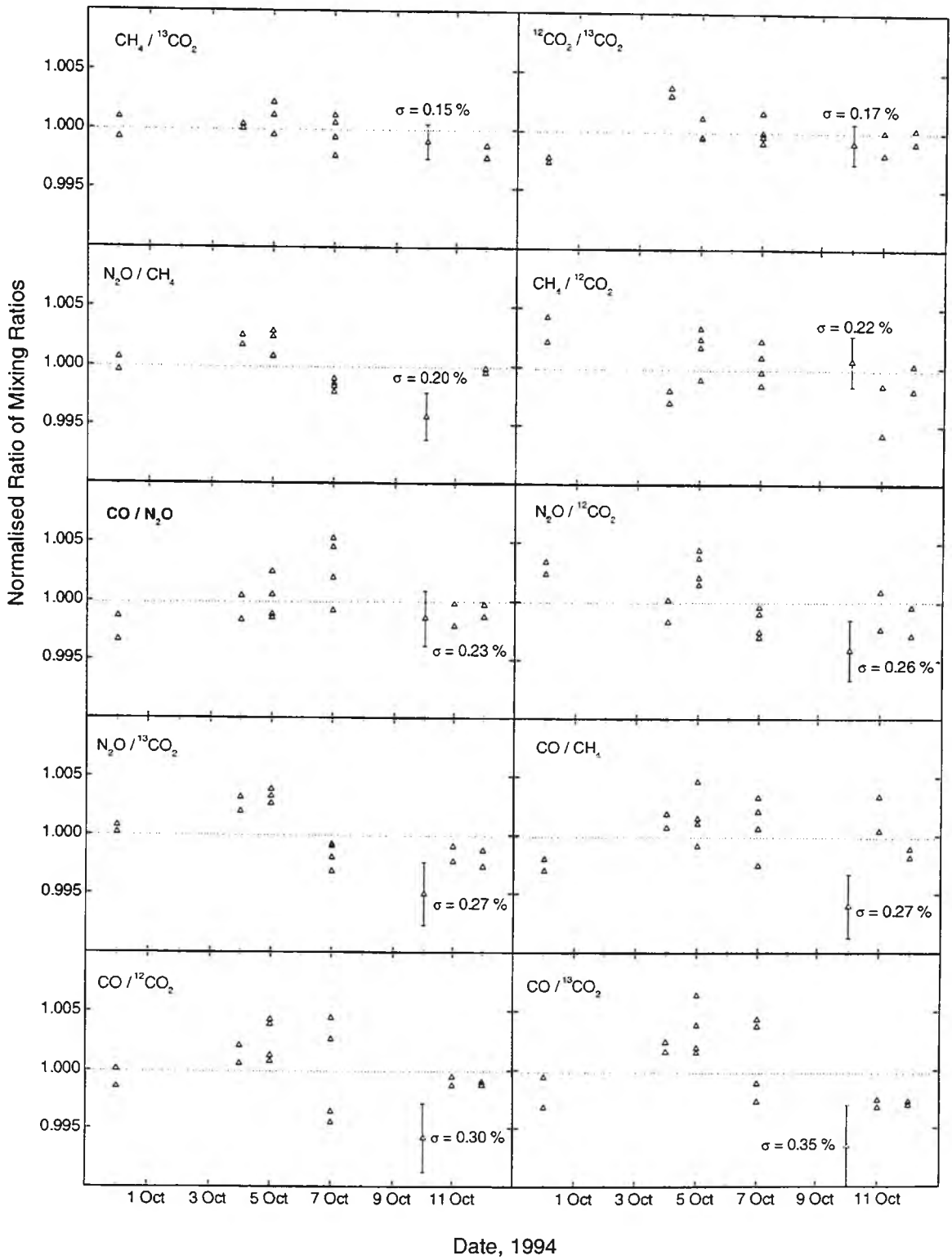

Figure 3.6. Ratios of trace gas mixing ratios in the analyses of tank CC113591. Each set of ratios has been normalised to unity by dividing by its mean value, to make comparison easier. Precision of ratio determination is reported as ± 1 standard deviation (σ) %.

Species *a*	σ(*a*) %	Species *b*	σ(*b*) %	Observed σ(*a*/*b*) %	Calculated σ(*a*/*b*) %
CH_4	0.17	$^{13}CO_2$	0.07	0.15	0.18
$^{12}CO_2$	0.19	$^{13}CO_2$	0.07	0.17	0.20
N_2O	0.28	CH_4	0.17	0.20	0.33
CH_4	0.17	$^{12}CO_2$	0.19	0.22	0.25
CO	0.37	N_2O	0.28	0.23	0.46
N_2O	0.28	$^{12}CO_2$	0.19	0.26	0.34
N_2O	0.28	$^{13}CO_2$	0.07	0.27	0.29
CO	0.37	CH_4	0.17	0.27	0.41
CO	0.37	$^{12}CO_2$	0.19	0.30	0.42
CO	0.37	$^{13}CO_2$	0.07	0.35	0.38

Table 3.6. The precision (as ± 1 std dev.) of ratios of mixing ratios for repeated analysis of tank CC113591, as observed and as calculated. The calculation is $\sigma(a/b) = [(\sigma(a))^2 + (\sigma(b))^2]^{1/2}$.

This result may have implications for calibration suite maintenance. For example in monitoring the CO mixing ratio in the one tank over two weeks, the precision with which the mixing ratio is determined is 0.37%, or 0.34ppb. Using CH_4 as an effective internal standard by using the CO/CH_4 ratio to monitor the CO mixing ratio yields a precision of 0.27%, or 0.24ppb, from a single measurement. If the same advantage applies over significantly longer timescales this multi-species ratio approach may characterise the relationships between calibration tanks better than is currently possible using gas chromatography.

One other potentially important result to note here is that the $^{12}CO_2/^{13}CO_2$ ratio is determined to a precision of about 0.17% for a single measurement, over a two week period, with no calibration or correction made for instrumental drift. This is equivalent to a $\delta^{13}CO_2$ precision of 1.7‰, without reference to calibration gas. It has already been

shown in Chapter 2 that this level of precision can be improved by an order of magnitude if measurements only over the short term are considered. From the short term precision and the longer term stability characteristic of the FTIR technique described here, it follows that with only moderately frequent calibration, FTIR spectroscopy should provide a means of long term monitoring of the stable isotope ratio $\delta^{13}CO_2$ at useful levels of precision.

3.7.2 Repeat Analyses of Tank ALTH8459

The tank ALTH8459, containing somewhat polluted ambient Aspendale air was subject to a similar analysis as CC113591 above. The main difference between tanks CC113591 and ALTH8459 is in their CO mixing ratios, ~90ppb and ~390ppb respectively. CO_2 and CH_4 mixing ratios in ALTH8459 were not determined with quite the same precision as for CC113591. The reason for this is unknown. Once again the observed ratios of mixing ratios are determined with greater precision than the mixing ratios themselves would suggest, assuming no correlation. The observed and expected precisions are listed in Table 3.6.

Consider again the case of CO mixing ratios over the two week period. This time the CO mixing ratio itself is determined to a high degree of precision, 0.18% or 0.69ppb. There is no apparent precision gain in considering the ratio of mixing ratios where one of them is CO. However for the other species the same benefits can be seen as with CC113591. Again, $^{12}CO_2/^{13}CO_2$ is determined with greater precision than is $^{12}CO_2$ alone.

Species *a*	σ(*a*) %	Species *b*	σ(*b*) %	Observed σ(*a*/*b*) %	Calculated σ(*a*/*b*) %
CO	0.18	CH_4	0.24	0.19	0.30
$^{12}CO_2$	0.25	$^{13}CO_2$	0.13	0.19	0.28
N_2O	0.28	$^{13}CO_2$	0.13	0.22	0.31
CO	0.18	$^{13}CO_2$	0.13	0.23	0.22
N_2O	0.28	CH_4	0.24	0.23	0.37
CH_4	0.24	$^{13}CO_2$	0.13	0.24	0.27
CO	0.18	N_2O	0.28	0.24	0.33
CH_4	0.24	$^{12}CO_2$	0.25	0.27	0.35
N_2O	0.28	$^{12}CO_2$	0.25	0.28	0.38
CO	0.18	$^{12}CO_2$	0.25	0.30	0.31

Table 3.6. The precision (as ± 1 std dev.) of ratios of mixing ratios for repeated analysis of tank ALTH8459, as observed and as calculated. The calculation is $\sigma(a/b) = [(\sigma(a))^2 + (\sigma(b))^2]^{1/2}$.

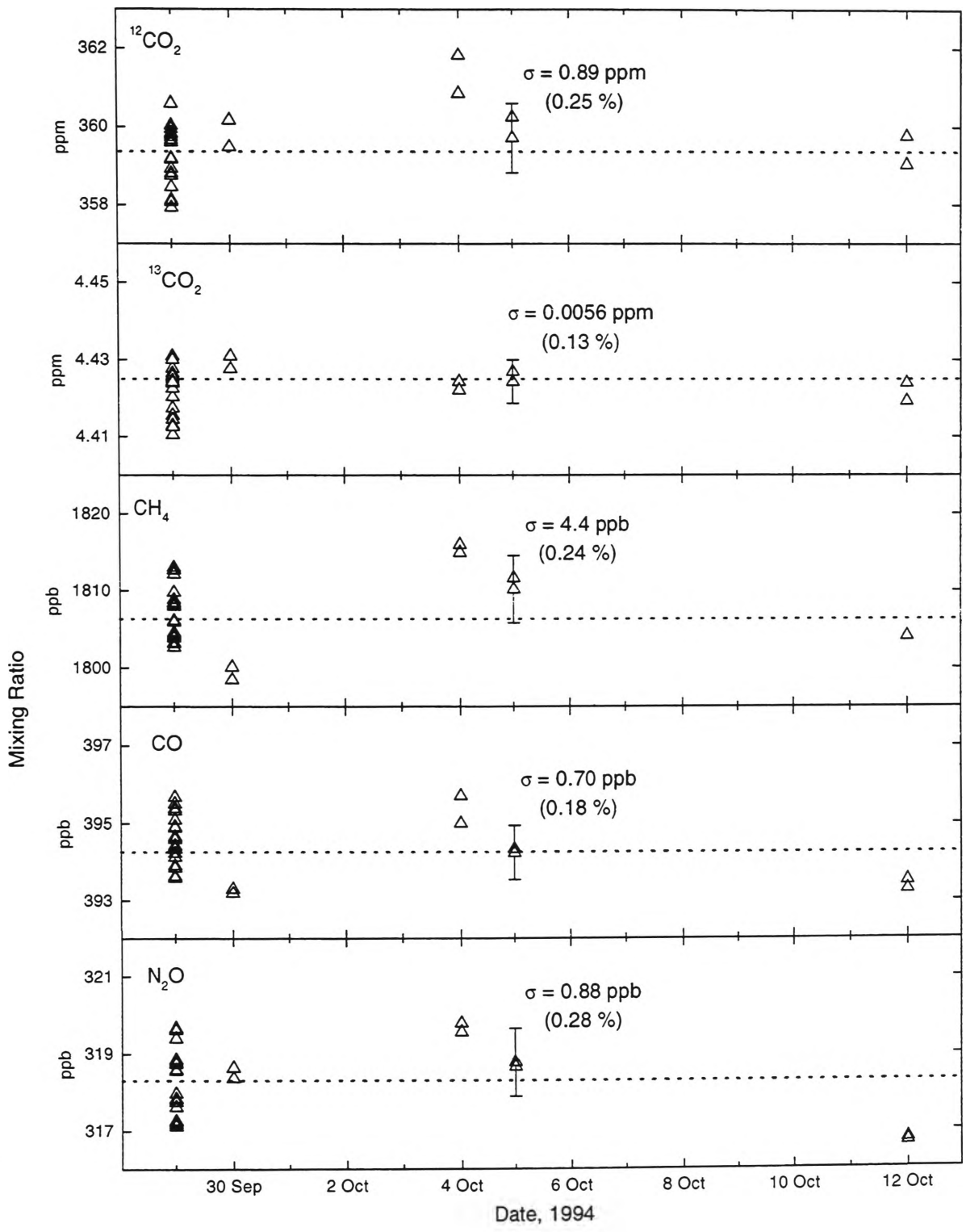

Figure 3.7. Uncalibrated trace gas mixing ratios determined by FTIR analysis of tank ALTH8459. Thirty-one individual aliquots analysed on five different days spanning a fouteen day period. Dotted line is mean mixing ratio over period. Precision reported as ± 1 standard deviation (σ). Note that the first nineteen analyses occurred on the one day, 29/9/94.

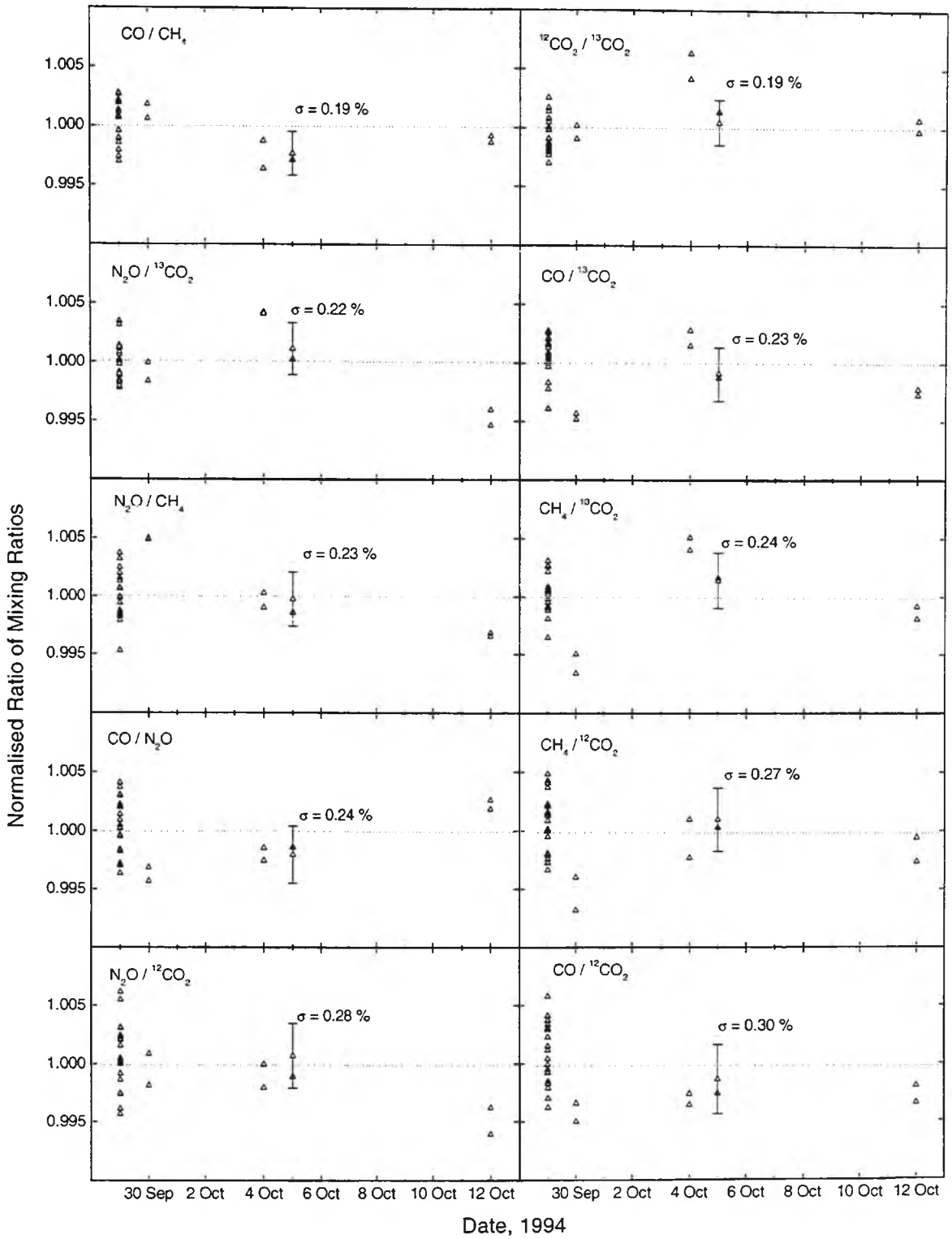

Figure 3.8. Ratios of trace gas mixing ratios in the analyses of tank ALTH8459. Each set of ratios has been normalised to unity by dividing by its mean value, to make comparison clearer. Precision of ratio determination is reported as ±1 standard deviation (σ) %.

3.7.3 Calibration Maintenance and Intercalibration Issues

Both precision and absolute accuracy are important in GASLAB trace gas analyses. The primary scientific goal of establishing spatial and temporal changes in the atmospheric trace gases would be satisfied by concentrating on maximising precision. However, to maintain the high precision of a trace gas record over inter-annual timescales issues of accuracy necessarily arise. When the aim is to ensure intercomparibility of data from different times, perhaps measured using different procedures and instrumentation in different laboratories, accuracy concerns are unavoidable. For intercomparibility of two data sets to be legitimate, it is necessary that both sets of analyses be referenced to standards which are traceable to the same primary standards. Furthermore, since reference standards may drift with respect to other standards, it is necessary to monitor and characterise the relationship between all the standards. This simply stated principle is often overlooked and its execution is quite non-trivial.

For example, beginning in 1993, NOAA/CMDL conducted an intercomparison [*Tans et al.*, 1996] for CO. Four gravimetrically prepared [*Novelli et al.*, 1991] CO in air standards were circulated through 11 laboratories in 8 countries over a 28 month period. The laboratories used their own 'standards', from a range of suppliers or created in-house, to assign CO mixing ratios to the four test tanks. Differences between participants were as large as 20%. Different calibration procedures and different instrument configurations in addition to differences in calibration gases are thought to account for the lack of consensus. CO in particular seems to be prone to this sort of uncertainty, as *Weeks et al.* [1989] had earlier observed a similar scale of discrepancy between two laboratories. Since CO is the least abundant of the main trace gases, and

therefore difficult to measure, as well as the most chemically reactive, these intercomparison results are somewhat understandable.

One of the important scientific objectives of GASLAB is the combination of the trace gas data from the Cape Grim baseline station and the GASLAB flask sampling network together with that from the NOAA/CMDL flask sampling and baseline station network. The successful combination of these two high quality data sets would provide a single large self consistent data set that can reliably be used for modelling and interpretive studies of global trace gas budgets. GASLAB and CMDL have several procedures in place to allow a 'seamless' integration. Initially there was the periodic (every few years) exchange of cylinders of standard gases. Greater frequency of intercalibration has been achieved by a degree of overlap of the GASLAB and CMDL networks. GASLAB flask sampling sites at South Pole, Mauna Loa (Hawaii) and Cape Grim are also part of the NOAA/CMDL network. However, even with this measure, the two laboratories are not actually analysing the same air sample. The most recent measure began in 1991 [*Steele et al.*, 1995]. In this (operational intercalibration), four pairs of flasks each month are filled at Cape Grim for analysis by the Carbon Cycle Group at NOAA/CMDL. These flasks are routed through GASLAB where one member of every second pair is analysed for CO_2, CH_4, CO, H_2 and ^{13}C and ^{18}O in CO_2 before being sent on to NOAA/CMDL for similar analysis. Preliminary results indicate a calibration offset between the two laboratories of some tenths of 1 ppm CO_2, ~0.1‰ $\delta^{13}CO_2$ and ~5ppb CO [*Francey*, 1996]. This is despite the fact that both labs use very similar instrumentation and procedures and both use reference standards traceable to the same primary standards. The causes of these systematic differences between GASLAB and CMDL trace gas

mixing ratio scales have not yet been identified. (The author is not aware whether or to what extent CH_4 and N_2O analyses are similarly affected).

It is likely that some of the remaining problems in establishing, propagating and maintaining an international calibration scale in each of the trace gases may be solved by improved methods of monitoring the behaviour of individual tanks of reference air over time. As already mentioned, standards drift, i.e the mixing ratio of one or several components of the mixture may increase or decrease in time. Not all species exhibit this behaviour to the same extent. Methane is considered to be a well behaved gas and is observed to drift only rarely in stored air; whereas carbon dioxide is somewhat less well behaved and may drift through physical and chemical interactions with the tank walls [*Langenfelds et al.*, 1996]. Carbon monoxide, being a more reactive gas, is less stable again. A significant minority of CO in air calibration standards are observed to drift in concentration (Paul Steele, personal communication). If some members of a suite of calibration standards are drifting, then all measurements calibrated against the drifting standards will be affected. It is important to be able to identify even small drifts and to characterise them accurately if the integrity of the calibration scale is to be maintained. Using the GC technology currently available for CO analysis for example, it is unlikely that a drift in a calibration standard of as much as 1ppb yr^{-1} would be detected, much less quantified (Paul Steele, personal communication).

Recent calibration standard monitoring strategies focus on exploiting multi-species measurements [*Francey et al.*, 1996; *Langenfelds et al.*, 1996]. Single species approaches used only analyses of the species of interest to monitor the behaviour of a suite of calibration standards. This probably has historical roots in the earlier common

practice of using simple binary mixtures for calibration. For example NDIRs for CO_2 measurement might be calibrated with synthetic CO_2-in-N_2 standards rather than the more natural CO_2-in-air mixtures. It would only have been possible to analyse for the one species of interest. Now, it is generally accepted that calibration standards for ambient air analysis should indeed consist of air, containing all the species that are naturally present in air, at close to their natural levels. Implementation of this principle at GASLAB means that most of their whole air standards may simultaneously serve as calibration standards for CO_2, CH_4, CO and N_2O. A multi-species approach to calibration suite maintenance exploits not only the measurements of the individual species but also the relationships between different species in a given tank. That is, the ratios of mixing ratios CO/CH_4, CO_2/CH_4, N_2O/CH_4, CO/CO_2, N_2O/CO_2, CO/N_2O will be monitored in addition to the mixing ratios of the individual compounds. This is somewhat akin to using an internal standard in an analytical procedure. Methane or CO_2, since they can both be measured very precisely and are usually well-behaved in standard tanks, may be used as an 'internal standard' in the detection of concentration-drifting behaviour by CO, for example. The ratios provide significant additional diagnostic information.

There is a limit to how far this 'internal standard' metaphor applies, however. It is still the case at GASLAB that CO_2, CH_4, CO, and N_2O are measured on three different GC instruments (effectively four since CO_2 passes through a methaniser before detection by FID, whereas the CH_4 does not). The time record of the ratios of mixing ratios will reflect not only any changes due to calibration tank drift, but also any changes in the response function of any of the instruments with respect to the other instruments. While

this may be useful information in itself, deconvolving the two possible contributions to the signal, i.e. tank drift and instrumental drift, will be nontrivial.

This is where FTIR spectroscopy may have a natural advantage. A single FTIR absorbance spectrum of one air sample simultaneously yields mixing ratio information on all four species of interest. The 'internal standard' metaphor applies far more literally in this circumstance. When FTIR spectroscopy is used to generate a record of ratios of mixing ratios for a suite of calibration standards, in the same way that tanks CC113591 and ALTH8459 were analysed in sections 3.7.1-2, it is likely that that record will be determined with significantly higher precision than can be determined either of the individual mixing ratios contributing to their ratio. This is because the two species' mixing ratios result from the one analysis on the one instrument. Uncertainties in the measurement of certain environmental parameters, such as sample temperature, pressure and pathlength, will contribute noise to mixing ratio analyses but will (at least partially) cancel out in the ratio of mixing ratios. The resulting time record of ratios of mixing ratios will have only one instrument response function convolved in it, and so should be relatively straightforward to interpret regarding the behaviour of calibration standard tanks. FTIR spectroscopy then may have a role in the maintenance of calibration integrity through its ability to analyse several species at once. The work described in this chapter has shown the potential usefulness of using FTIR techniques in the maintenance of calibration scales.

3.8 Summary and Conclusions

The FTIR method of trace gas measurement has been applied to the analysis of a set of calibration standards which have been well characterised independently by gas

chromatography. Comparison of the FTIR and GASLAB GC data sets provides information regarding the linearity, accuracy and precision of the FTIR method with respect to the GASLAB GC method.

The FTIR response function is observed to be linear for CO_2, CH_4 and N_2O over a large dynamic range, well beyond the explicit calibration range of the method and what would normally be encountered in ambient air analysis. For CO, the two techniques are nonlinear with respect to one another, and some evidence suggests that it is more likely to be the GASLAB GC than the FTIR instrument which is behaving with a nonlinear response function.

FTIR spectroscopy offers absolute trace gas analytical accuracy of the order of ±1-5% without the need to calibrate the instrument with reference standards. Analytical precision of the FTIR technique over a two week period, uncorrected for instrumental drift, is of the order of 0.1% for $^{13}CO_2$; 0.2% for $^{12}CO_2$ and CH_4; and 0.3% for CO and N_2O. The simultaneous retrieval of ratios of mixing ratios effectively eliminates some of the error due to instrumental drift and sample handling which currently limits the precision with which mixing ratios are determined. This potentially offers a technique to monitor the integrity of calibration standards more stringently than either normal mixing ratio analysis by FTIR or gas chromatographic techniques can provide.

Chapter 4: Results II: Cape Grim Trace Gas Monitoring By FTIR

4.1 Introduction to Cape Grim Baseline Air Pollution Station (CGBAPS) and Baseline Monitoring

In 1976 atmospheric monitoring began at Cape Grim with measurements of CO_2. Cape Grim lies near the northern extremity of the west coast of Tasmania, Australia's southern island state (40° 41′ S, 144° 41′ E), as shown in Figure 4.1. The prevailing wind is from the west-south-west, frequently bringing air from a long trajectory across the Southern Ocean. Such air, not having been recently perturbed by anthropogenic emissions, is considered to represent the global, or Southern Hemisphere, well-mixed background or "baseline" atmosphere. Baseline conditions are generally defined for Cape Grim to be those when the wind direction is between 190° and 280° and where there are less than 600 cm^{-3} condensation nuclei (CN). These conditions typically prevail about 30% of the time.

Today Cape Grim Baseline Air Pollution Station (CGBAPS) is host to a comprehensive program of automated analyses, and discrete sample collections for remote analyses. Trace gases analysed include CO_2, CH_4, CO, N_2O, O_3, H_2, CFCs, HFCs and HCFCs, dimethyl sulfide and radon. Air samples are collected for remote analysis for the carbon and oxygen stable isotope ratios $\delta^{13}C$ and $\delta^{18}O$, and for radiogenic carbon content, $\Delta^{14}C$. There are also analyses of air aerosol content, solar radiation, and a full suite of meteorological observations. During non-baseline conditions, much data is still

automatically collected and archived but does not contribute to the characterisation of the baseline atmosphere.

Cape Grim BAPS is administered by the Australian Bureau of Meteorology in close collaboration with the CSIRO's Division of Atmospheric Research. It is classified as a fully operational Baseline (global) station in the World Meteorological Organisation's Global Atmospheric Watch (WMO-GAW) program. Many of the scientific programs at Cape Grim are collaborative, involving other Australian and overseas research agencies and universities.

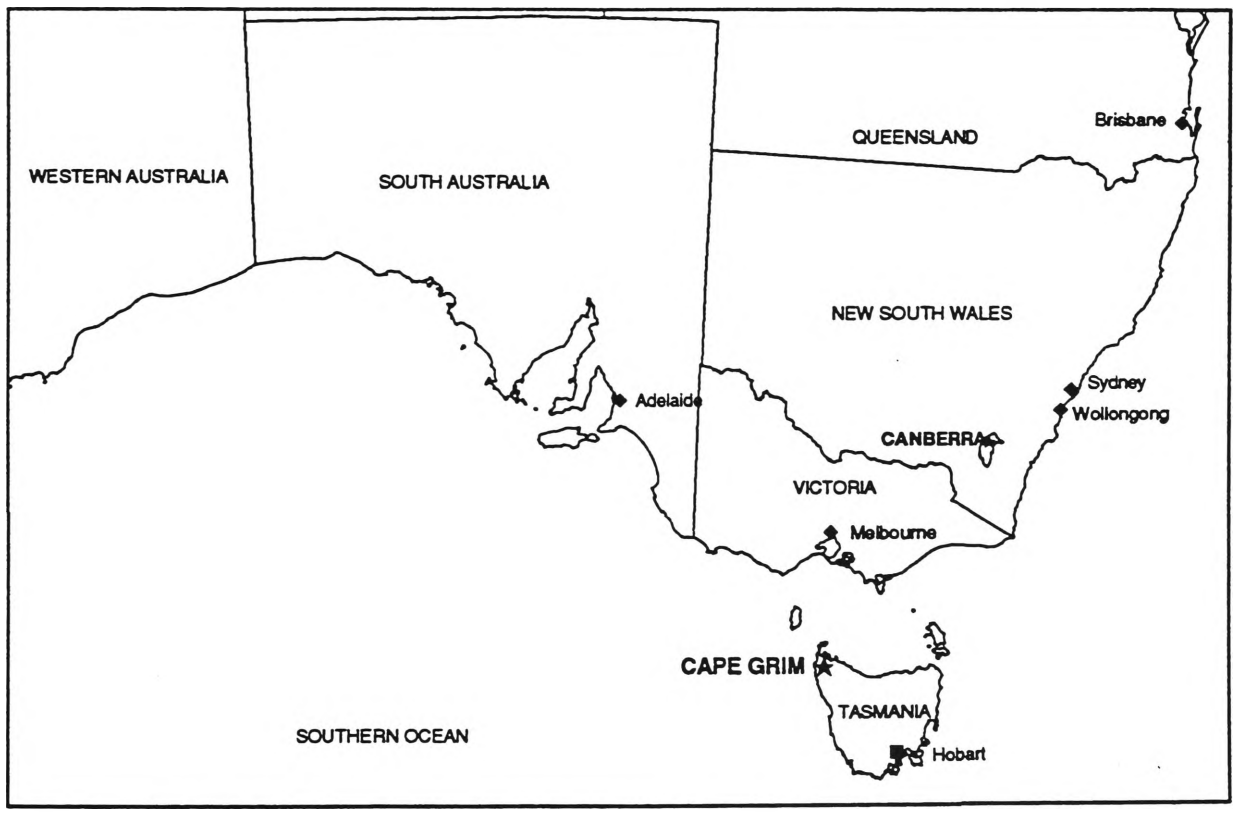

Figure 4.1. Map of southern Australia. Cape Grim is situated on the northernmost part of Tasmania's west coast.

4.2 The Cape Grim AGAGE-GC and NDIR Instruments

Carbon dioxide is continuously analysed at Cape Grim by a Siemens 'ULTRAMAT 5E' non-dispersive infra-red (NDIR) gas analyser [*Beardsmore et al.*, 1996]. The instrument is a continuous flow-through system. Every hour high and low range dry air calibration standards are analysed for 5 minutes each. Dried ambient air is analysed for the remaining 50 minutes. Raw data recorded includes one-minute average CO_2 mixing ratios which are then reduced to calibrated one-hour mean CO_2 mixing ratios. The NDIR data presented here were obtained from CGBAPS on 4 September 1995 and are not necessarily in their final calibrated form.

CH_4, CO and N_2O are all normally analysed at Cape Grim by gas chromatography on the Advanced Global Atmospheric Gases Experiment (AGAGE) instrument. This instrument, installed at Cape Grim in 1993, has been described elsewhere [*Fraser et al.*, 1996; *Prinn et al.*, 1996; *Steele et al.*, 1996c]. It consists of three coupled GCs and a Sun Unix workstation for controlling, processing and storing *in situ* observations of CH_4, CO, N_2O as well as H_2, CFC-11, CFC-12, CFC-113, $CHCl_3$, CH_3CCl_3 and CCl_4. Typically, an air sample is analysed for all species listed above every twenty minutes. However, every alternate sample is from a calibration standard tank, so the ambient air is sampled approximately every 40 minutes. After chromatographic separation on an appropriate column, CH_4 is detected by FID (flame ionisation detector), CO by RGD (reduction gas detector), and N_2O by ECD (electron capture detector) (as described in Sections 1.8.4, 1.9.4 and 1.10.4 respectively). The data are then adjusted for nonlinearities with reference to the best estimates of the calibration standards. The AGAGE data presented here were downloaded from the AGAGE instrument at CGBAPS on 29 June 1995 in the case of CO and N_2O. That data set may still be subject

to slight correction. In the case of CH_4 , the data were supplied by Paul Steele (GASLAB) on 2 April 1996. The CH_4 data set is in its final calibrated form.

4.3 The FTIR Monitoring Protocol

FTIR analysis of ambient air was performed on a 30 minute cycle. Each cycle contained the following elements.

1. Collect a 256-scan spectrum of the empty cell, evacuated to <0.1 Torr from the previous cycle, at $1cm^{-1}$ resolution, taking ~8 min. This single beam spectrum serves as the reference spectrum.
2. Open the White cell to the 10m inlet line containing ambient air. Allow air to flow into the cell for 60 seconds, allowing the pressure in the cell to equilibrate with the pressure in the 10m inlet line which is near ambient. Close the cell and let the sample stand for 2 minutes, sufficient time for it to reach temperature and pressure equilibrium with the instrument. Measure the pressure and temperature of the sample.
3. Collect a 256-scan spectrum of the filled cell at $1cm^{-1}$ resolution, taking ~8 min. Save this single beam spectrum as the sample spectrum. Re-measure the temperature and pressure of the sample.
4. Calculate the absorbance spectrum of the sample as log (I_0/I). Retrieve raw mixing ratios from this spectrum using the Classical Least Squares prediction algorithm. This algorithm, in addition to generating species mixing ratios, produces a number of fitting parameters.
5. Log all raw mixing ratios, spectroscopic parameters and temperature and pressure measurements to a file. The temperature and pressure

measurements are used to make density corrections to the retrieved mixing ratios.

6. Pump out the White cell to a pressure of <0.1 Torr in readiness for the next cycle.

Every six hours, a sample drawn from the calibration tank CC113591 was analysed. This whole process was automated and the instrument was capable of running unattended for 24 hours, limited by the need to manually fill the InSb detector with liquid nitrogen once a day. The Array Basic program, AUTOMATE.AB, written for this particular experiment is included in Appendix B for reference. The two calibration tanks used in this study, CC113591 (analysed 6-hourly) and ALTH8459 (analysed only on 28-29 June 1995) are described in Table 4.1.

Calibration tank:	CC113591	ALTH8459
CO_2 / ppm	358.17	363.71
CH_4 / ppb	1694.87	1707.11
CO / ppb	90.82	415.84
N_2O / ppb	311.01	311.59
$\delta^{13}CO_2$ / ‰	-7.88	-8.14

Table 4.1. Trace gas mixing ratios and stable isotope ratio $\delta^{13}CO_2$ for the two calibration tanks used in this study.

4.4 FTIR, AGAGE-GC and NDIR Records for CO_2, CH_4, CO and N_2O

Installation and calibration of the FTIR instrument at Cape Grim was commenced on 19 May, 1995. Half hourly data collection began at 15:00 22 May and continued for five weeks until 13:00 28 June. In the first week there were a few periods of data loss due to software problems.

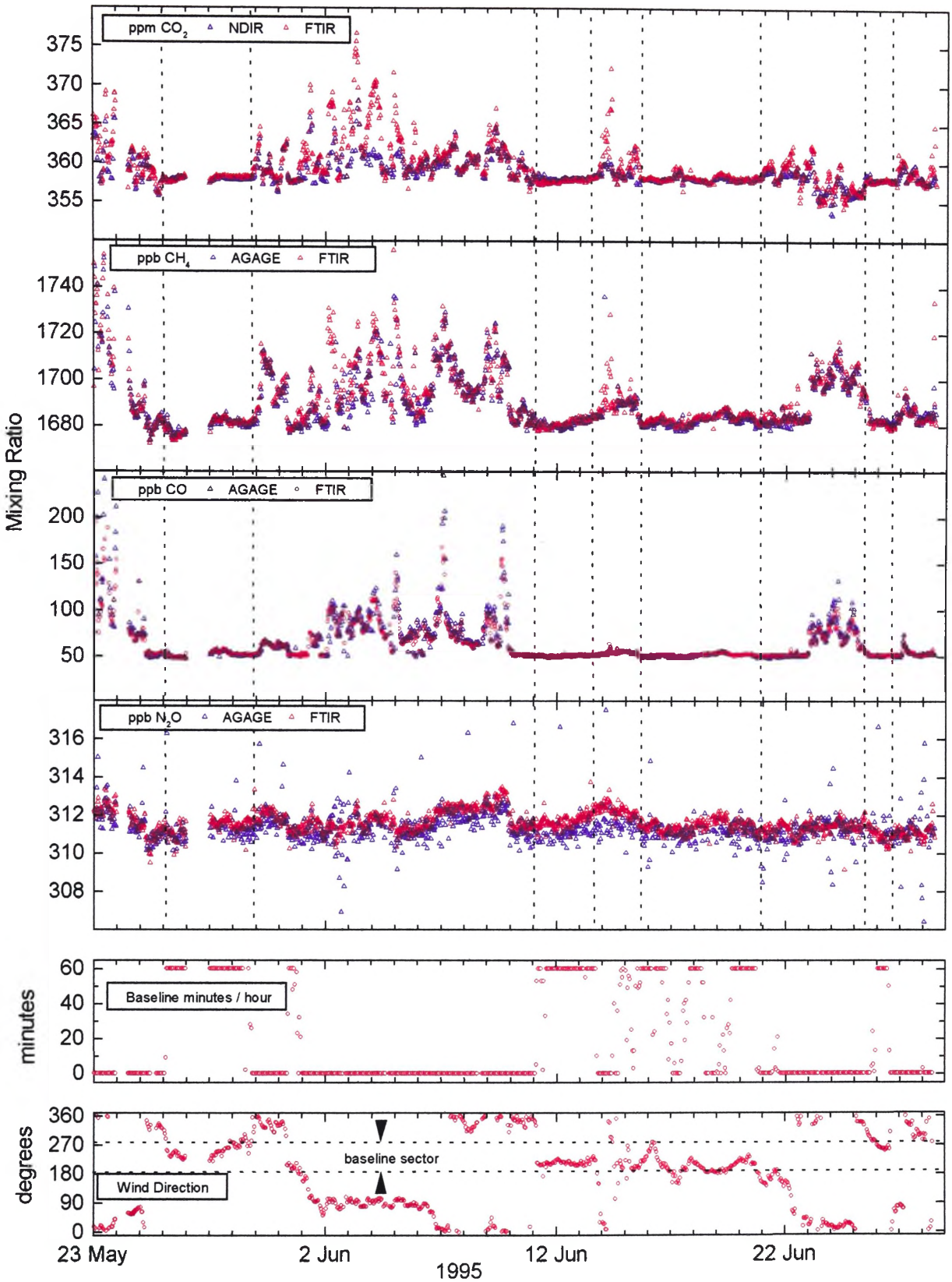

Figure 4.2. Parallel FTIR (CO_2, CH_4, CO and N_2O), NDIR (CO_2) and AGAGE-GC (CH_4, CO, N_2O) records of trace gas mixing ratios at Cape Grim during the period 23 May to 28 June, 1995. Pollution events are banded by dotted lines. Also minutes in the hour that baseline conditions prevailed and wind direction record for the same period.

For the period following 27 May the instrument was operational 98.5% of the time. The 1.5% down time corresponds to the 1-2 hours of maintenance required approximately every five days to recharge the $Mg(ClO_4)_2$ dryer. Apart from these periods there has been no loss, exclusion, selection or outlier-filtering of the FTIR data. All FTIR data are plotted in Figure 4.2.

There are several general features immediately apparent in the trace gas record at Cape Grim for the period illustrated in Figure 4.2. Firstly, there is close agreement between the AGAGE-GC record and the FTIR record of CH_4, CO and N_2O, and between the NDIR and FTIR records for CO_2. Secondly, the records for CO_2, CH_4 and CO show strong correlations in the timing of pollution episodes and baseline periods as shown on the figure. The N_2O record is much less influenced by pollution events and rarely departs more than +0.5ppb from baseline mixing ratio levels. However, even N_2O shows apparent elevation around the 23 May, 9 June and 14 June pollution peaks seen in the other species.

A correlation is observed in Figure 4.2 between trace gas mixing ratios on the one hand and wind direction and the Cape Grim defined baseline criterion on the other. The long, relatively intense pollution episode 30 May to 11 June coincides with wind direction almost continuously from the East (90°) and then the North (0°). Easterly winds are those most likely to bring air from the Tasmanian landmass and urban centres while northerlies tend to carry air directly from the strong pollution sources of Melbourne and the south-eastern Australian mainland. Wind direction and trace gas mixing ratio correlations are discussed below in Section 4.6.

The mixing ratio records of a single species retrieved by two different instruments are observed in Figure 4.2 to agree well during baseline periods when the mixing ratios are not changing. However, during pollution episodes the level of agreement between parallel instruments deteriorates. There are at least two reasons for this. Firstly, the parallel measurements are not strictly simultaneous. The AGAGE-GC record is initially recorded on a 40-minute time grid. To facilitate data handling and comparison with the 30-minute time grid FTIR record, each AGAGE-GC observation datum has been artificially shifted to coincide with the FTIR observation nearest in time. The FTIR and AGAGE-GC observations that are treated as simultaneous will, in fact, have been made a few minutes apart, rarely more than 10 minutes however. This will make little difference when stable well mixed conditions prevail. During pollution episodes the air mass is much less well mixed and the mixing ratios changing rapidly in time. The sampled air mass may change significantly between sampling by the FTIR and the AGAGE instruments. Similarly, for CO_2, the NDIR data represent not instantaneous sampled mixing ratios but hourly mean mixing ratios which may be somewhat different from the instantaneous CO_2 mixing ratio retrieved half-hourly by FTIR.

Secondly, there may be linearity and calibration differences between two instruments. Although the mixing ratio records retrieved by parallel analysis by FTIR and either AGAGE or NDIR show a high level of agreement, there has been no linking or shifting of one data set to facilitate apparent agreement. At no stage have the instruments been calibrated directly against each other, for example, by all sampling a common reference gas or set of reference gases. Each instrument's scale is determined by frequent calibration against different air reference tanks which have been individually calibrated by GASLAB. For the NDIR two tanks are used, a high reference and a low reference each

hour, with CO_2 values lying just either side of the normal baseline mixing ratio. The AGAGE-GC instrument is calibrated every 40 minutes from a single reference tank containing near baseline air. The FTIR instrument was calibrated by 6-hourly sampling from a single tank, CC113591, also containing near baseline air. A second reference tank, ALTH8459, containing relatively polluted air was analysed by FTIR several times on June 28 and 29 only, to better define a scale for both baseline and pollution measurements. All the reference tanks were assigned values by GASLAB by comparison with their suite of reference tanks. Thus, it is not so surprising that all instruments agree quite well when ambient conditions are very close to those for which they are optimally calibrated, i.e. baseline conditions. As conditions depart from baseline, the various instruments will be increasingly subject to systematic error depending on how well non-baseline mixing ratios can be quantified with reference to baseline calibration standards. It is clear in Figure 4.3 that during pollution episodes there is a systematic discrepancy between the mixing ratios retrieved by the alternative instruments for CO_2 and CO. The mixing ratio trend is $CO_{2(NDIR)}<CO_{2(FTIR)}$ and $CO_{AGAGE}>CO_{FTIR}$. The instrumental comparisons are discussed on a species by species basis in Section 4.5 below.

The predominantly baseline period illustrated in Figure 4.3 is useful in gauging the relative precision of the three instruments considered. Qualitatively, inspection of the degree of scatter in the parallel mixing ratio records reveals that for CO_2, half-hourly FTIR analyses are marginally less precise than the hourly mean of NDIR analyses. For CH_4 the precision of FTIR and AGAGE-GC analyses are virtually identical. For CO, the FTIR precision is perhaps marginally superior. FTIR is clearly more precise than AGAGE-GC for N_2O retrieval however it should be noted that the problem which was causing frequent N_2O outliers in the GC analysis has since been identified and remedied

[*Steele et al.*, 1996]. Even with N_2O outlier-removal FTIR precision is superior to that of AGAGE-GC.

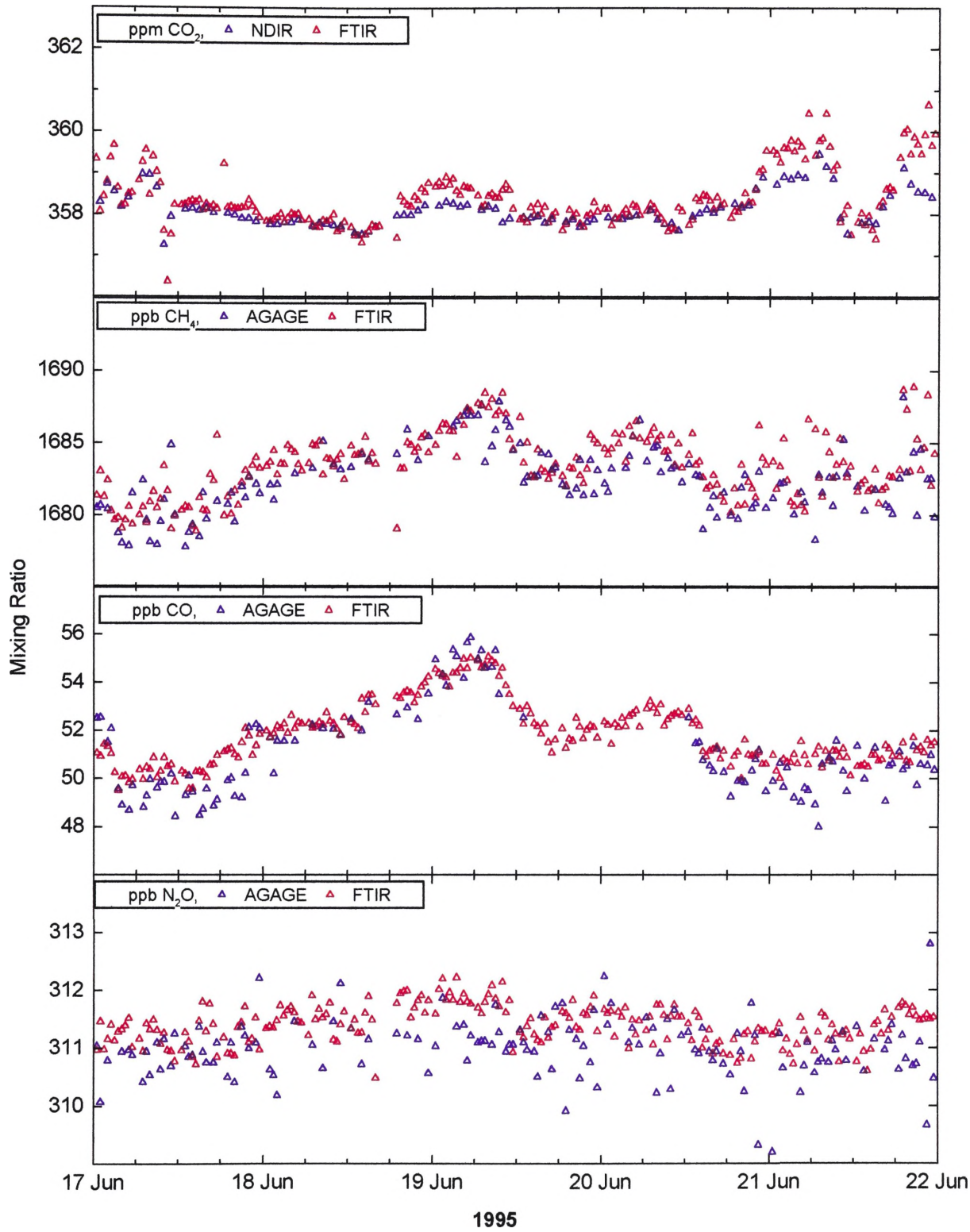

Figure 4.3. FTIR, AGAGE-GC and NDIR trace gas mixing ratios during the predominantly baseline period 17-21 June 1995 at Cape Grim.

Species	Baseline Mixing Ratio	Precision of FTIR		Precision of NDIR (CO_2) and AGAGE-GC (CH_4, CO, N_2O)	
		± σ	±σ%	± σ	±σ%
CO_2	358 ppm	0.15 ppm	0.04	-	-
		(0.11 ppm)	(0.03)	(0.07 ppm)	(0.02)
CH_4	1680 ppb	0.9 ppb	0.05	0.9 ppb	0.05
CO	50 ppb	0.27 ppb	0.5	0.35-0.95 ppb	0.7-1.9
N_2O	310 ppb	0.28 ppb	0.09	0.57 ppb	0.2

Table 4.2: Precision of analysis of trace gases by FTIR and NDIR and AGAGE-GC, as ± 1 s.d. and as percentage of southern hemisphere baseline mixing ratio. FTIR precision determined from repeated 6-hourly analysis of CC113591 reference tank during experiment. For the FTIR CO_2 analyses the precision is estimated in terms of half hour measurements (no brackets) and of hourly mean measurements (in brackets). The latter are more appropriately compared with the NDIR hourly mean CO_2 measurements.

Quantitatively, the precision (as ±1σ) of each measurement has been determined, here summarised in Table 4.2. For CH_4, CO and N_2O the FTIR precision was determined from repeated 6-hourly analyses of reference tank CC113591 during the experiment. Similarly the AGAGE-GC precision for the same species were determined from repeated (at 40 minute intervals) analysis of the reference tank G-035 throughout the period of the parallel experiment. The AGAGE-GC precisions reported here for CH_4 and N_2O were calculated after the application of an outlier filter to the data. This is particularly significant for N_2O where 14% of the reference gas analyses were flagged as outliers. No such filter was applied to the FTIR data, resulting in the precision estimates reported here being arguably more conservative than their corresponding AGAGE-GC estimates. For CO, the AGAGE-GC precision deteriorated during the course of the experiment due to instrumental problems which have since been rectified. The range of analytical precision observed for CO is indicated. Since the NDIR CO_2 precision is reported on the

basis of an hourly measurement, the corresponding FTIR precision is reported in terms of half-hourly analyses and then recalculated to provide an estimate of the precision of an hourly mean FTIR CO_2 measurement (in parentheses). Comparison of the hourly precision for the two techniques should be a meaningful one.

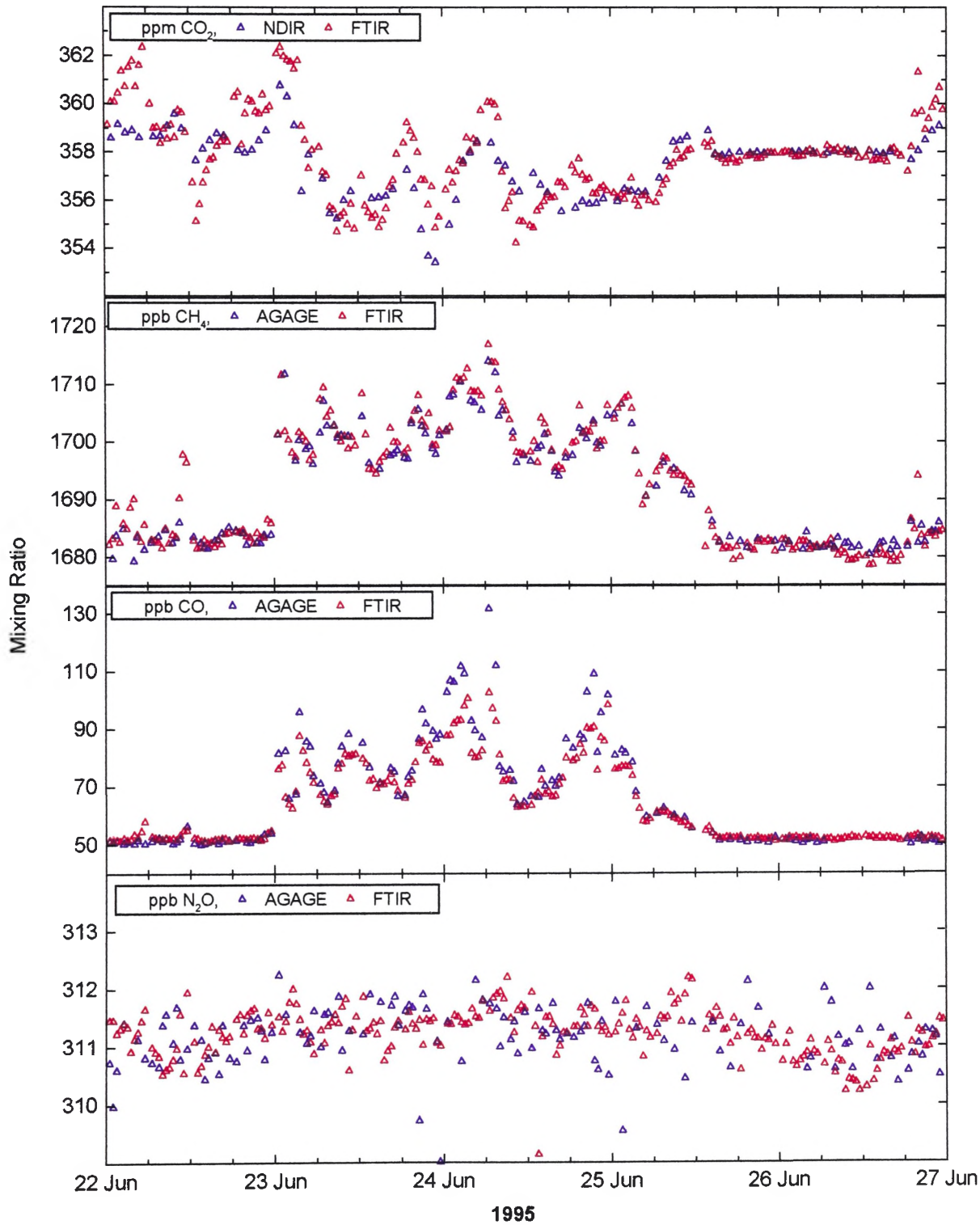

Figure 4.4. FTIR, AGAGE-GC and NDIR trace gas mixing ratios during the moderate pollution event 22-26 June 1995 at Cape Grim.

Figure 4.4 illustrates that during the pollution event occurring 23-25 June both CH_4 and CO mixing ratios are significantly elevated. The CO_2 mixing ratio, however, varies strongly and is for a considerable time below the baseline level of ~358 ppm according to both the FTIR and the NDIR instruments. According to Figure 4.2 the wind was predominantly northerly (340°-30°) during this period which is consistent with trajectories bringing polluted air from the Australian mainland. The subambient CO_2 mixing ratios is consistent with the continental air also being affected by photosynthetic drawdown.

4.5 Comparison of Parallel Records

This section compares the parallel FTIR and NDIR records of CO_2, and the parallel FTIR and AGAGE-GC records of CH_4, CO and N_2O. Analysis of the parallel data sets yields information about the extent to which different instruments analysing the same airmass will report different mixing ratio results. Both baseline and non-baseline conditions are considered. The latter has consequences for the exploitation of the non-baseline trace gas record of baseline stations like Cape Grim.

4.5.1 Results

Figure 4.5 shows the difference in mixing ratios between the parallel instruments for each species, for the term of the experiment. During pollution episodes significant differences are observed in the parallel records. If only the baseline difference data are selected, the mean and standard deviation of these data sets provide an indication of how well two instruments agree under baseline conditions. These parameters are listed in Table 4.3.

Mixing Ratio Differences, Baseline selected		Mean	± Std. Dev.	N
ΔCO_2	$(CO_{2[FTIR]} - CO_{2[NDIR]})$	0.023 ppm	± 0.24 ppm	138
ΔCH_4	$(CH_{4[FTIR]} - CH_{4[AGAGE]})$	0.46 ppb	± 1.42 ppb	176
ΔCO	$(CO_{[FTIR]} - CO_{[AGAGE]})$	0.63 ppb	± 0.85 ppb	145
ΔN_2O	$(N_2O_{[FTIR]} - N_2O_{[AGAGE]})$	0.37 ppb	± 0.64 ppb	169

Table 4.3. The mean and standard deviation of the differences between parallel measurements of the CO_2 mixing ratio by FTIR and NDIR; and for CH_4, CO and N_2O the mean and standard deviation of the differences between mixing ratios determined by FTIR and AGAGE-GC. Only data collected during baseline conditions as defined at Cape Grim are considered. N is size of data set.

Figure 4.6 illustrates the relationship between parallel records in terms of a regression of the FTIR–AGAGE (or FTIR–NDIR) mixing ratio difference versus the FTIR mixing ratio. For a sufficiently large data set, >600 data points for each species in this case, the regressions should reveal something of the average relationship between the data sets generated on different instruments, particularly under non-baseline conditions. The regression slope parameters are listed in Table 4.4.

Regression	Slope	Uncertainty in slope	N
$\Delta CO2$ vs $CO_{2[FTIR]}$	0.52	± 0.01	687
ΔCH_4 vs $CH_{4[FTIR]}$	0.16	± 0.01	952
ΔCO vs $CO_{[FTIR]}$	-0.21	± 0.02	947
ΔN_2O vs $N_2O_{[FTIR]}$	0.48	± 0.03	962

Table 4.4. Slope parameter of linear regression of mixing ratio measurement difference versus FTIR mixing ratio measurement, for parallel FTIR and NDIR analyses of CO_2, and parallel FTIR and AGAGE-GC analyses of CH_4, CO and N_2O. These are illustrated in Figure 4.6. Baseline and non-baseline data included in analysis. N is size of data set.

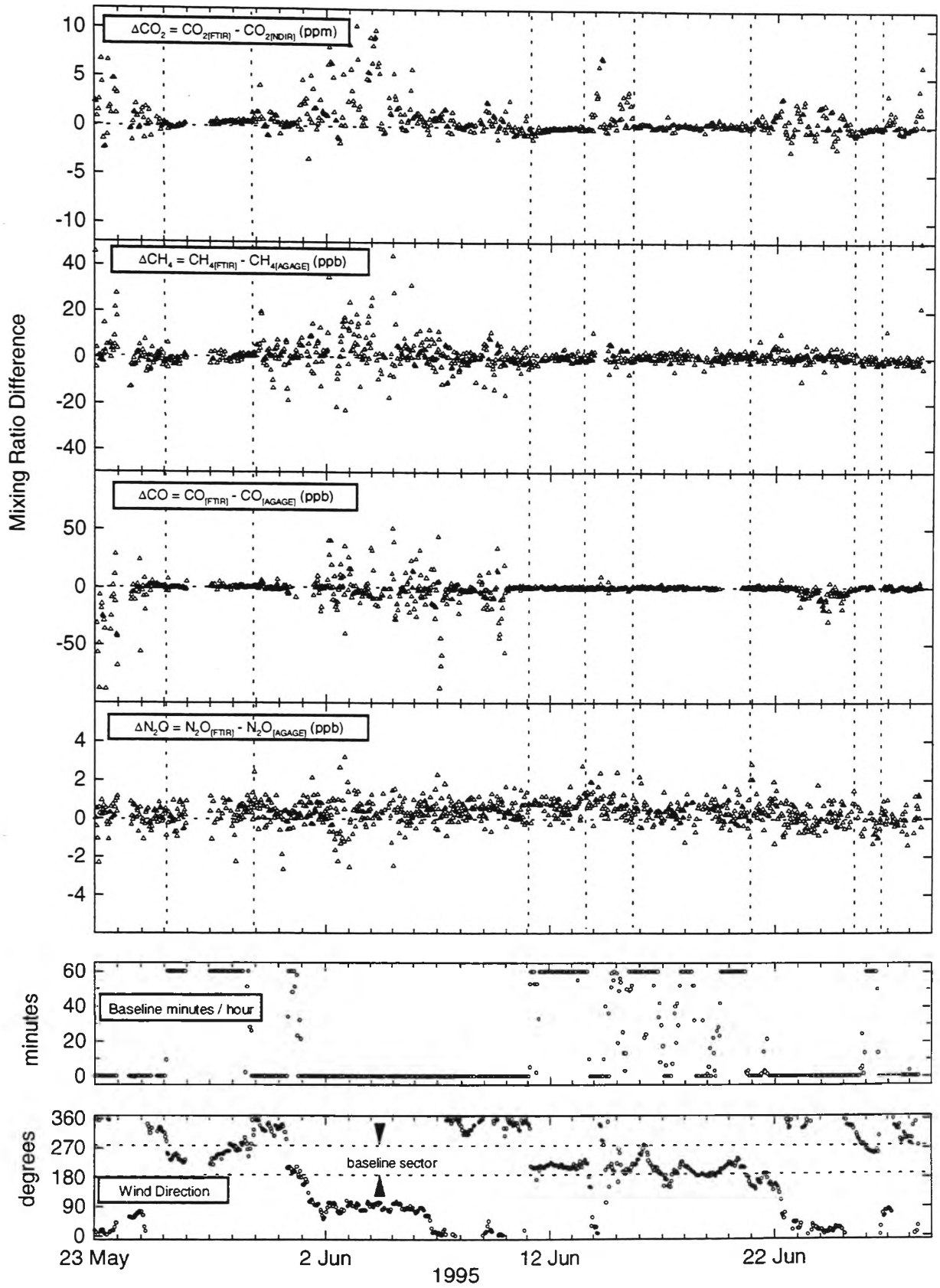

Figure 4.5. Record of the difference between parallel FTIR and NDIR measurements of CO_2 mixing ratio; and the difference between parallel FTIR and AGAGE-GC measurements of CH_4, CO and N_2O mixing ratios. Also, record of the number of minutes per hour that baseline conditions prevailed, and wind direction. Cape Grim 23 May to 28 June 1995.

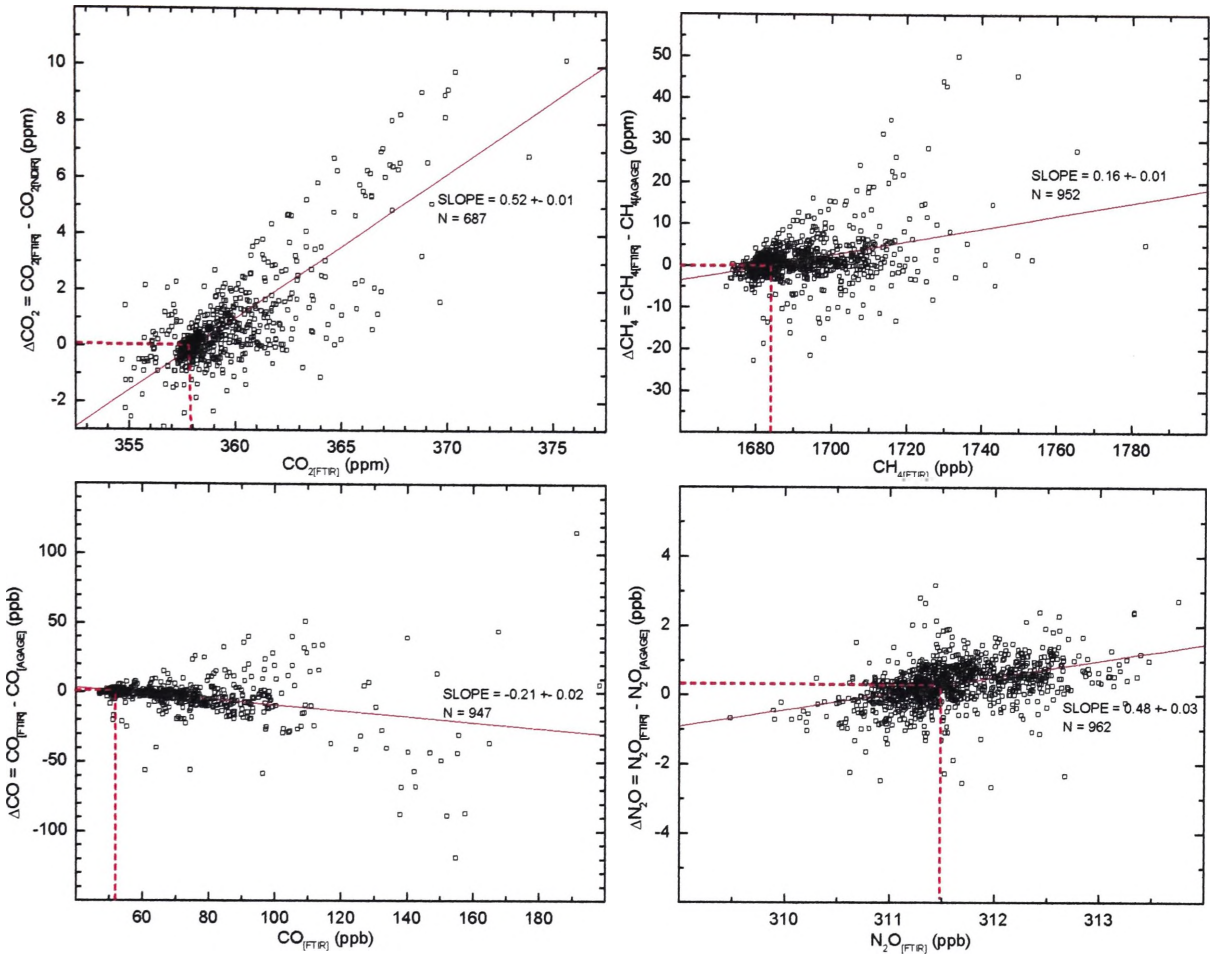

Figure 4.6. Linear regressions of mixing ratio measurement difference versus FTIR mixing ratio measurment. For parallel FTIR and NDIR analyses of CO_2 and for parallel FTIR and AGAGE-GC analyses of CH_4, CO and N_2O. Some extreme-value data points removed. Each regression line is labelled with its slope and uncertainty in slope. N is size of data set. Vertical dotted line illustrates mean mixing ratio during baseline conditions; and horizontal dotted line indicates mean mixing ratio difference between methods under baseline conditions (listed in Table 4.3).

4.5.2 FTIR and NDIR/AGAGE Differences Under Baseline Conditions

In Figure 4.5, if the parallel instrumental records agreed perfectly, all points would lie on the zero difference line and there would be no scatter about this line. The main reason for the scatter observed is that the "parallel" measurements are not quite simultaneous and that during pollution episodes a trace gas mixing ratio at the sampling inlet is usually changing rapidly. Air samples taken only a few minutes apart may have very different

mixing ratios. Conversely, baseline difference data exhibit very little variation from the zero line and minimal scatter.

Table 4.3 illustrates that for each of the four species there is a systematic difference between the data sets of two instruments, operating under baseline conditions, however in no case was this difference statistically significant. It is concluded that, under baseline conditions, the FTIR method shows very close agreement with the NDIR method for CO_2 analysis and with the AGAGE-GC analyses of CH_4, CO and N_2O.

4.5.3 FTIR and NDIR/AGAGE Differences Under Non-Baseline Conditions

There is a second reason for disagreement between instruments during pollution episodes, other than the rapid mixing ratio fluctuations mentioned above.. It is related to the measurement scales of the two instruments concerned. Although the FTIR, AGAGE-GC and NDIR instruments are all optimised and calibrated for baseline trace gas measurements, and show a high level of agreement there, as illustrated in Table 4.3, the instruments' calibrations for non-baseline analysis are not necessarily the same and larger disagreements may be apparent the further the air sample is from baseline constitution. In Figure 4.6, if the both instruments were reporting the mixing ratios on the same absolute scale, the regression line would necessarily have zero gradient. However, in each case the regression yields a statistically significant non-zero gradient, as listed in Table 4.4.

4.5.3.1 CO_2

For nonbaseline conditions, CO_2 > 358.5 ppm, it is apparent that $CO_{2[NDIR]}$ is systematically less than $CO_{2[FTIR]}$, hence the regression gradient of +0.52 listed in Table

4.4. When the FTIR instrument is reporting 365ppm CO_2, the NDIR will on average report a mixing ratio 3ppm lower. At levels so close to baseline conditions, this discrepancy is large and as yet unresolved. While the FTIR cannot be excluded as the source of some or all of this problem, there is evidence to suggest that it is not the main source. Firstly, the FTIR technique has demonstrated a large dynamic range and linear response in the analysis of CO_2 (and CH_4, CO and N_2O) in the calibration tank study described in Chapter 3. The NDIR, in contrast, is known to have a small dynamic range and a slightly nonlinear response and so is calibrated using calibration gases which span only a small mixing ratio interval, typically about 355-365ppm at present. Relying on this calibration when extrapolating to CO_2 mixing ratios beyond the range of the span gases is likely to result in large errors. Secondly, there is no evidence of such a serious discrepancy in the comparison of FTIR and AGAGE-GC analyses of CO or CH_4.

4.5.3.2 CH_4

For non-baseline CH_4 mixing ratios, the AGAGE instrument will, on average, report mixing ratios slightly lower than the FTIR, as illustrated in Figure 4.6. At 1710ppb CH_4 the difference between the two instruments is apparently of the order of 5ppb. The parameters of the linear regression listed in Table 4.4 confirm that the slope of the regression line is significantly greater than zero. The source of the discrepancy between the two instruments' CH_4 mixing ratio scales for non-baseline conditions has not yet been identified.

4.5.3.3 CO

The FTIR measurements were calibrated primarily against tank CC113591 containing air with the much greater than baseline CO mixing ratio, 91ppb. Baseline CO measurements

of ~50ppb therefore necessitated a large degree of extrapolation from the FTIR's optimal calibration conditions. Despite this, as listed in Table 4.3, there was no significant difference between the $CO_{[FTIR]}$ and $CO_{[AGAGE]}$ mixing ratios under baseline conditions.

Under non-baseline conditions, $CO_{[FTIR]}$ was systematically less than $CO_{[AGAGE]}$, as illustrated in Figure 4.6. When the former was reporting ~100ppb the latter on average was ~90ppb, a relatively large discrepancy of 10% in absolute terms, at only modest levels of CO pollution. There is the suggestion of nonlinearity in the ΔCO vs $CO_{[FTIR]}$ regression. This may reflect the behaviour of the AGAGE instrument's mercuric oxide reduction gas detector which is known to exhibit a nonlinear response (see Section 1.9.4). The degree and direction of the observed nonlinear behaviour are consistent with those observed in Chapter 3 when parallel FTIR and GC-RGD analyses of CO were examined in the calibration tank study.

4.5.3.4 N_2O

The ΔN_2O vs $N_2O_{[FTIR]}$ regression, having gradient 0.48±0.03, suggests a significant discrepancy between $N_2O_{[FTIR]}$ and $N_2O_{[AGAGE]}$ under non-baseline conditions. However, this conclusion must be somewhat speculative since the range of the N_2O measurements is of a similar magnitude to the degree of scatter in them, as illustrated in Figure 4.6.

4.5.4 Discussion

The Cape Grim CO_2 NDIR and AGAGE-GC instruments are optimised for baseline and near baseline measurements only. The possibility of errors due to extrapolation beyond the calibrated range have already been mentioned for the NDIR instrument. Similarly, the AGAGE-GC instrument is in general calibrated in the range of baseline ±25%. This

is achieved using a single calibration tank, but generating a three point calibration by making injections of the calibration gas at three different pressures, approximately atmospheric pressure and 25% above and 25% below atmospheric. This is considered equivalent to calibration over the approximate ranges 1300-2100ppb CH_4, 38-62ppb CO and 230-390ppb N_2O. For the period of this study, all CH_4 and N_2O data, whether collected during baseline or nonbaseline conditions, lie well within the AGAGE-GC calibration range. However, for CO, much of the nonbaseline data lies well outside the AGAGE-GC calibration range and is, like CO_2, susceptible to extrapolation errors.

It might be argued that for CO_2 and CO, there is no point in comparing the instrumental response functions under nonbaseline conditions since the CO AGAGE-GC and CO_2 NDIR instruments are explicitly not calibrated for such conditions. However, there is increasing interest in extracting information from the nonbaseline portion of the Cape Grim trace gas record. Until recently these data were collected but remained unprocessed as the scientific focus lay entirely on baseline studies. It is now recognised that the nonbaseline trace gas record may contain valuable information about pollutant emissions from the non-baseline sector. Two recent studies involving the Cape Grim nonbaseline record have provided estimates of mainland and Tasmanian N_2O flux densities [*Wilson et al.*, 1997], and of CFC emissions from Melbourne [*Dunse et al.*, 1996]. If the nonbaseline CO_2 and CO records are to be similarly exploited, knowledge of the AGAGE-CO and NDIR-CO_2 instrument response functions under nonbaseline conditions is essential. Comparison with an independent technique, FTIR spectroscopy, provides a suitable probe. Further, the large dynamic range and high degree of linearity characteristic of the FTIR technique, as demonstrated in Chapter 3, makes it an ideal standard by which to gauge other techniques which are calibrated over narrower ranges.

That the FTIR technique is characterised by a large dynamic range is further supported by its success in measuring baseline CO mixing ratios when calibrated using distinctly non-baseline air containing 91ppb CO.

4.6 Correlation of Mixing Ratio and Wind Direction

The FTIR mixing ratio data and the wind direction data, illustrated separately in Figure 4.2, can be combined to systematically investigate their correlation. This is illustrated in Figures 4.7 and 4.8.

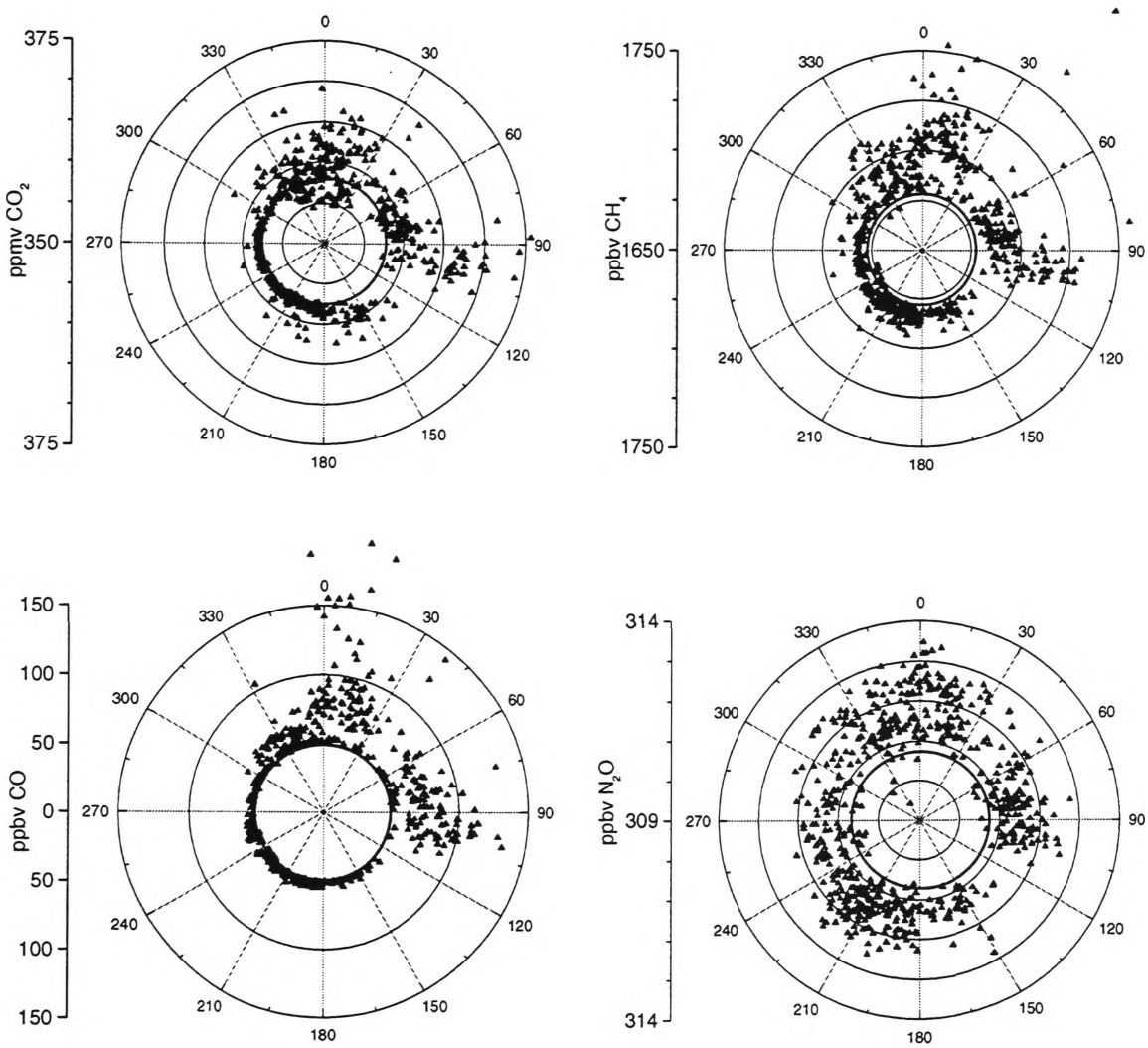

Figure 4.7. FTIR trace gas mixing ratio vs wind direction, 23 May-28 June 1995 Cape Grim. The solid circle in each plot represents the normal baseline mixing ratio. All CO_2 and N_2O data are shown. Several CH_4 data points in the northerly sector (maximum 1850 ppb) and many CO data points (max 600 ppb) in the northerly sector are not shown.

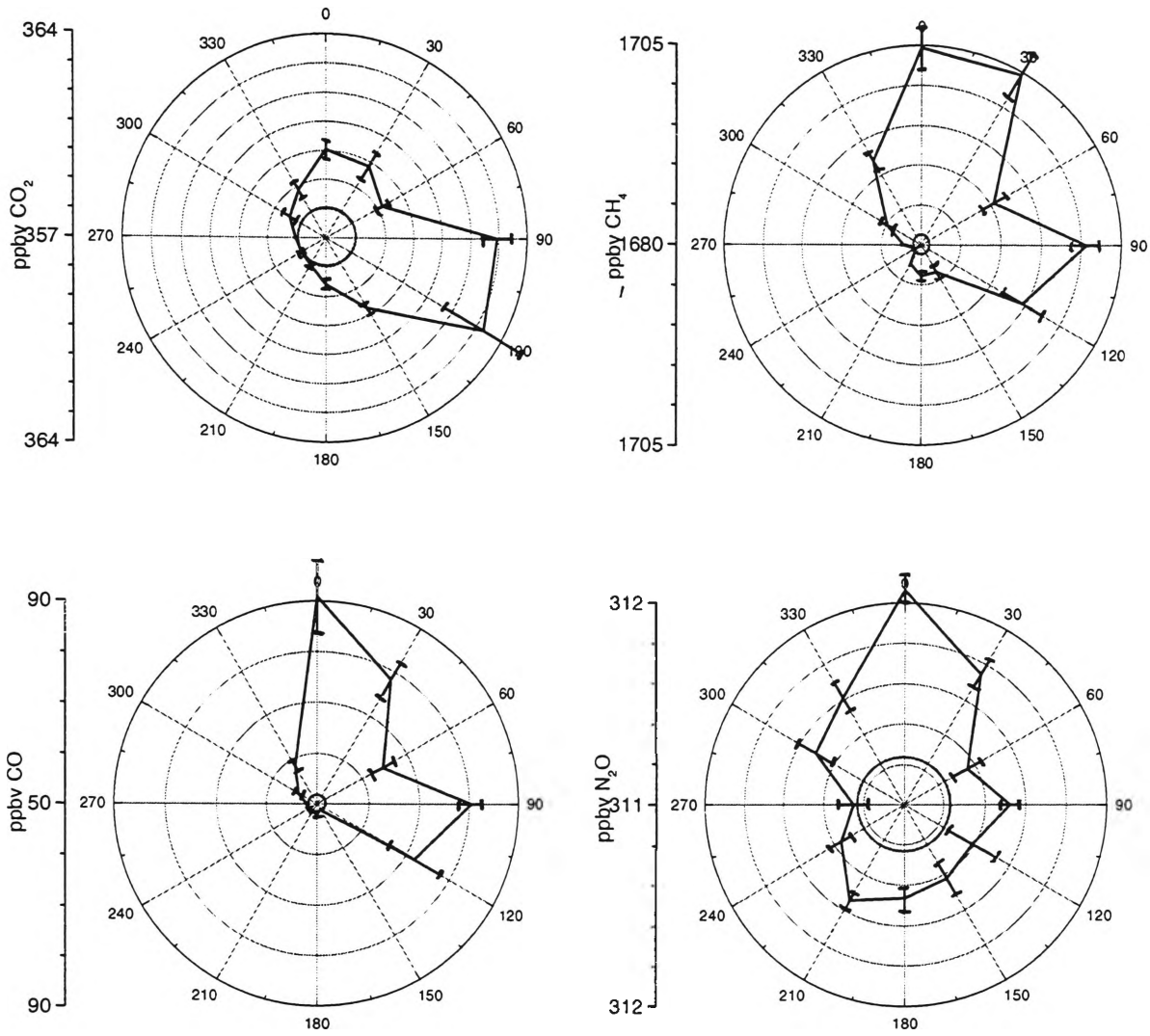

Figure 4.8. FTIR trace gas mixing ratio vs wind direction where data have been binned into 30° sectors. Solid circle represents normal baseline mixing ratio. Error bars represent standard deviation of the mean of the data in that sector.

Figure 4.7 confirms the suitability of 190°-280° as a baseline sector since that sector is very largely clear of significant enhancements in any of the trace species. The other general observation is that northerly (330°-30°) and easterly (60°-120°) trajectories are responsible for virtually all pollution episodes seen in the CO_2, CH_4 and CO records, even though the Tasmanian sector extends to 190°. However, during the five week period of FTIR monitoring, there was very little data from 115°-150° wind sector. Figure 4.7a indicates two different types of pollution episode involving CO_2. The

strongest sources of CO_2 are apparently Tasmanian, in the 60°-120° wind sector. There are no significant sub-baseline CO_2 mixing ratios recorded in this sector. This is consistent with there being little photosynthetic uptake. In June in Tasmania plants are largely dormant and little photosynthetic uptake is expected. The northerly wind sector, 330°-30°, however, is characterised by both elevated and sub-baseline mixing ratios. This may reflect a seasonal pattern where northerly trajectories will end to bring air from south eastern Australia where there is significant photosynthetic uptake even in June. Also coming from the mainland will be air enriched in CO_2 due mainly to fossil fuel emissions.

In Figure 4.8 the wind-mixing ratio data is binned into 30° sectors and the mean plotted. The error bars indicate the standard deviation of the mean of the data in that sector. The windroses for CH_4 and CO, illustrated in Figures 4.8b-c, are very close to the same shape, both indicating a strong northerly source and a somewhat less strong easterly source. This is consistent with the main sources of these two gases being landbased and anthropogenic. Likely sources are natural gas leakage and livestock enteric fermentation for CH_4, and fossil fuel and biomass combustion for CO. The CO_2 windrose indicates sources in the same two general directions but has their relative strength reversed. As observed above, this may reflect the effect of photosynthetic uptake on the mainland rather than the relative magnitude of the CO_2 sources, due mainly to fossil fuel combustion. There is little variation in the 30°-binned N_2O behaviour compared to the uncertainty in the standard deviation and any conclusions from Figure 4.8d must be speculative. However, there is an apparent northerly enrichment of ~0.8 ppb N_2O over baseline. There is also the evidence of a source to the east, suggesting that both mainland and Tasmanian sources of N_2O exist, just as for the other trace gases. The

fluxes of N_2O from the south-east Australian mainland and from Tasmania for the period 1985-1993 have been estimated by *Wilson et al.*, [1997] to be similar in magnitude, at 130 ± 30 kgN km^{-2} yr^{-1} and 160 ± 45 kgN km^{-2} yr^{-1} respectively.

There is the suggestion of an N_2O source to the south-west (210°), within the baseline sector. While there have been previous reports of the open ocean being a source of N_2O [*Bange et al.*, 1996; *Nevison et al.*, 1995], the estimated oceanic flux is much smaller than land based fluxes. An alternative scenario explaining the apparent oceanic N_2O source is that some of the air reaching Cape Grim from the ~210° sector had a back trajectory which had carried it across part of Tasmania, picking up N_2O emissions, then north-west out to sea a short distance, and finally north-eastl, passing over Cape Grim from a direction of about 210°. Data selected by wind direction alone may be misleading if the back trajectory of the air parcel is unknown.

4.7 Correlations Among CO_2, CO and CH_4

Cape Grim is a global baseline station and the collection and analysis of data during baseline conditions is the scientific priority. However, examining the FTIR mixing ratio data collected during non-baseline conditions may provide knowledge of relatively local pollution sources such as Tasmania to the east and the south-eastern Australian mainland to the north of Cape Grim. In particular, the way in which the mixing ratios of two different pollutant species are correlated can potentially reveal the nature of and relationship between their sources.

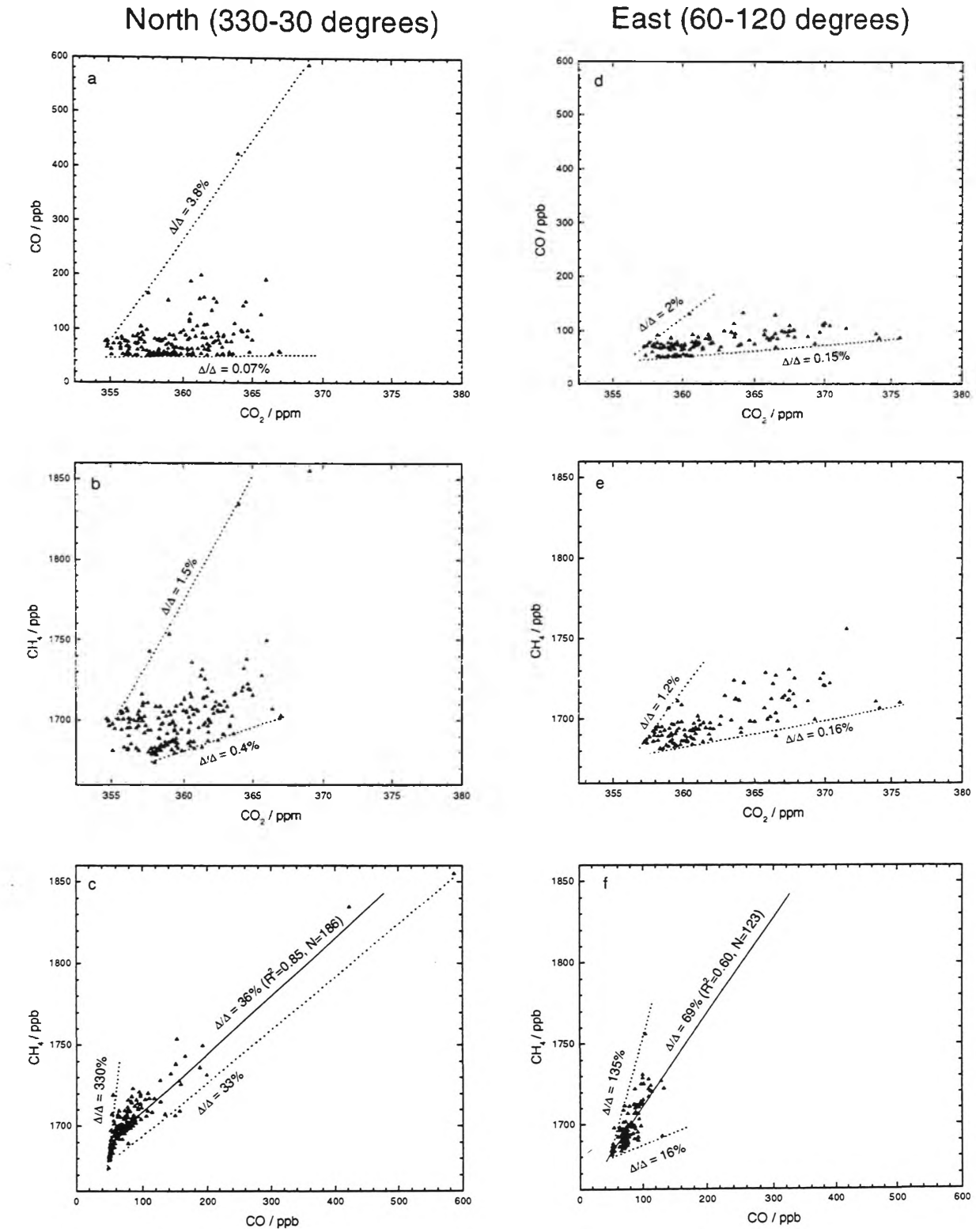

Figure 4.9. Linear regression plots illustrating the correlation between CO, CH_4 and CO_2 mixing ratios for the northerly (330°-30°) and easterly (60°-120°) wind sector FTIR data.

Figure 4.9 illustrates the mixing ratio correlations of CO with CO_2, CH_4 with CO_2 and of CH_4 with CO in the northerly (330°-30°) and easterly (60°-120°) wind sectors associated with pollution episodes observed at Cape Grim. The data are bracketed between two

lines indicating the maximum and minimum molar emission ratios observed. The molar emission ratio of CO with respect to CO_2, for example, is given by

$$E.R. = \frac{\Delta CO}{\Delta CO_2} \tag{4.1}$$

where ΔCO is the excess over baseline of the CO mixing ratio and ΔCO_2 is the excess over baseline CO_2. In Figure 4.9 the emission ratios are reported as percentages, normalised against either CO_2 or CO emissions.

Typical emission ratios for Australian sources of atmospheric pollution are available in the literature, notably the 1994 National Greenhouse Gas Inventory [*NGGIC*, 1996]. Table 4.5 lists the main identified sources of CO and CH_4 pollution and estimates of their respective emission ratios. The biomass burning emission ratios are from the south-east Australian forest fire study by *Hurst et al.*, [1997]. There is no separate $\Delta CO/\Delta CO_2$ emission ratio listed for agriculture in general as this is thought to be almost entirely due to biomass burning.

It is possible to draw some general conclusions from Figure 4.9 when it is studied in the light of Table 4.5. Firstly, neither CO nor CH_4 emissions appear to be particularly closely correlated with CO_2 emissions, as illustrated in Figure 4.9a,d. The observed $\Delta CO/\Delta CO_2$ emission ratio varies from 0.07% to 3.8%. While the high end of this range is more or less consistent with typical biomass burning (~5-10%) or fossil fuel combustion (~2.6%) emissions, the bulk of the data lie closer to the lower 0.07% $\Delta CO/\Delta CO_2$ emission ratio. Since this is not characteristic of any of the significant sources of CO, it is suggested that most of the CO_2 variation observed is not associated with CO emissions. Such would be the case if most of the CO_2 variation is due simply to

photosynthetic and respiration processes. Similarly, the $\Delta CH_4/\Delta CO_2$ emission ratio varies from 0.16% to 1.5% and there is very little correlation observed. The major source of CH_4 emissions in Australia is from agriculture, more specifically, from enteric fermentation in ruminant livestock. Unfortunately, NGGIC is unable to assign a meaningful $\Delta CH_4/\Delta CO_2$ to the agriculture sector since agriculture (but not land use change) is defined as being neither a net source nor sink of CO_2 for the purposes of the inventory. The observed lack of correlation of CH_4 with CO_2 emissions in Figure 4.9b,e, even though located in the same wind sectors, is consistent with their sources being independent. Such may be the case if CO_2 variation is predominantly photosynthesis/respiration driven and CH_4 emission is predominantly ruminant livestock driven. Indeed, if photosynthesis and respiration are causing most of the CO_2 variation observed at Cape Grim, then CO_2 is not the ideal tracer for the study of the other pollutant species.

The correlation of CH_4 and CO emissions illustrated in Figure 4.9c,f is somewhat stronger than for either of those species with CO_2 emissions. The $\Delta CH_4/\Delta CO$ emission ratio varies from about 16% to 330%. The high end of this range is consistent with a source of fugitive fossil fuel emissions, for example natural gas leakages during processing or pipeline delivery. The lower end of the range is more consistent with a mixture of agriculture (including enteric fermentation) and combustion activities (biomass burning, and fossil fuel combustion including transport). The regression line in Figure 4.9c has a slope of 36 ± 1% (R^2=0.85, N=186). The same regression for Figure 4.9f gives a slope of 69 ± 4% (R^2=0.60, N=123). These are both typical of agricultural regions. The northerly sector, however, is influenced by some episodes which are relatively high in both CH_4 and CO which are not apparent in the easterly sector. This

may indicate the greater influence of Melbourne and the south-eastern mainland on the northerly sector than on the easterly sector.

Source	Source Size as % of Nat. Total	Trace Gas Excess	Ratio Excess	typical emission ratio %
biomass burning	63	ΔCO	ΔCO_2	5-10
fossil fuel comb.	26	ΔCO	ΔCO_2	2.6
transport	21	ΔCO	ΔCO_2	8.8
fugitive emissions	0.05	ΔCO	ΔCO_2	0.28
biomass burned for energy	4.5	ΔCO	ΔCO_2	6.7
biomass burning	5	ΔCH_4	ΔCO_2	0.4
fossil fuel comb.	2	ΔCH_4	ΔCO_2	0.11
fugitive emissions	23	ΔCH_4	ΔCO_2	78
agriculture	59	ΔCH_4	ΔCO_2	N/A
transport	0.5	ΔCH_4	ΔCO_2	0.11
biomass burned for energy	1.6	ΔCH_4	ΔCO_2	1.3
biomass burning	5	ΔCH_4	ΔCO	5
fossil fuel comb.	2	ΔCH_4	ΔCO	4.4
fugitive emissions	23	ΔCH_4	ΔCO	277
agriculture	59	ΔCH_4	ΔCO	52
transport	0.5	ΔCH_4	ΔCO	1.3
biomass burned for energy	1.6	ΔCH_4	ΔCO	19

Table 4.5. Trace gas emission ratios $\Delta CO/\Delta CO_2$, $\Delta CH_4/\Delta CO_2$ and $\Delta CH_4/\Delta CO$ for a range of Australian emission sources. Biomass burning emission ratio from *Hurst et al.*, [1997] other emission ratios and source sizes from NGGIC [*NGGIC*, 1996].

In the northerly sector there are several measurements, associated with a single pollution event on 23 May during winds from the north (355°-10°), which are high in CO and CH_4. In each of Figure 4.9a,b,c these data define the maximum $\Delta CO/\Delta CO_2$ and $\Delta CH_4/\Delta CO_2$ and the minimum $\Delta CH_4/\Delta CO$ emission ratios at 3.8%, 1.5% and 33%, respectively. The high mixing ratios, the brevity of the event and the emission ratios are all consistent with the source being the combustion of biomass in the near vicinity of Cape Grim, possibly from burnoff activity on the adjacent Woolnorth station.

4.8 Isotope Ratio Measurements: $\delta^{13}CO_2$ at Cape Grim

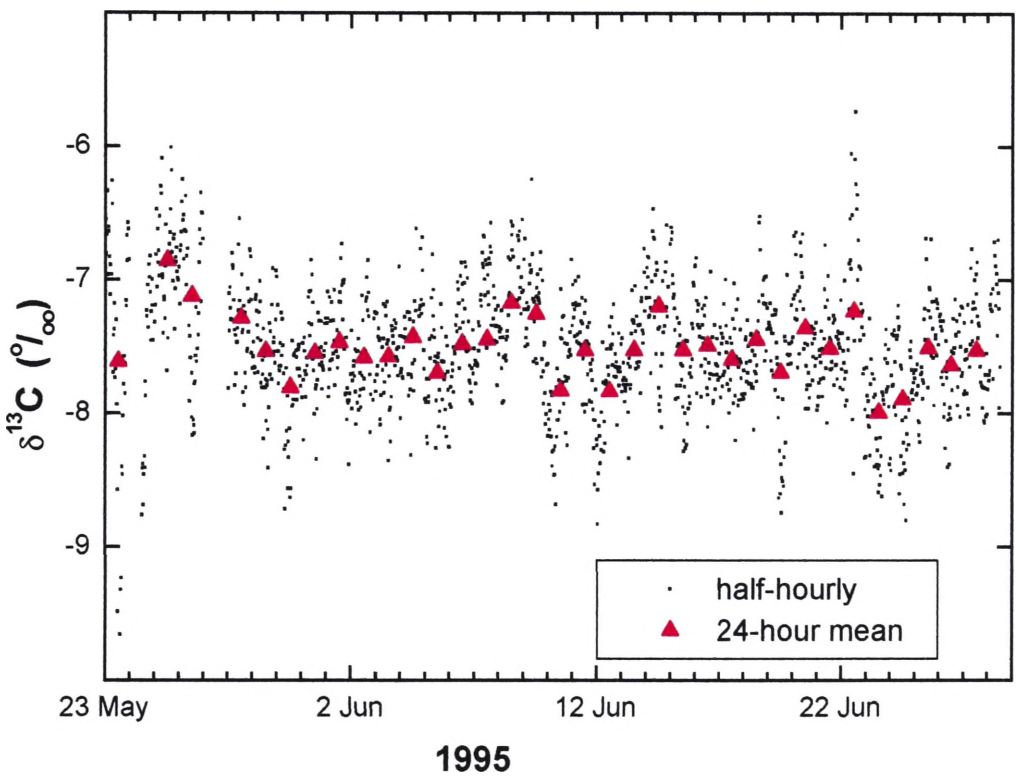

Figure 4.12. FTIR record of $\delta^{13}CO_2$ at Cape Grim, 23 May to 28 June 1995. Individual half-hourly measurements and 24-hour means.

During the Cape Grim experiment the first attempt was made in the present work to extract $^{13}CO_2$:$^{12}CO_2$ isotope ratio information from the $1cm^{-1}$ resolution spectra of ambient air samples which were being analysed primarily for trace gas mixing ratios. A

full account of our method of FTIR isotope analysis can be found in Chapter 2. It has already been demonstrated that, using MALT and CLS, we are able to determine mixing ratios of several trace molecular species independently and simultaneously. Extending this approach a little further, we are also able to determine mixing ratios of several isotopomeric species, e.g. $^{12}CO_2$ and $^{13}CO_2$, independently and simultaneously. One absorbance spectrum of a sample of air yields mixing ratios for $^{12}CO_2$, $^{13}CO_2$, (and therefore $\delta^{13}CO_2$), as well as for CH_4, CO and N_2O.

The $\delta^{13}CO_2$ measurements of ambient air were calibrated against two reference tanks, CC113591 and ALTH8459, provided by CSIRO's GASLAB. These tanks have been thoroughly analysed and values have been assigned for their trace gas mixing ratios and $\delta^{13}CO_2$ as listed in Table 4.1. The first tank, CC113591, was sampled every six hours throughout the experiment. This constitutes essentially a one point calibration for $\delta^{13}CO_2$. At the conclusion of the continuous sampling period, both tanks were repeatedly analysed on 28-29 June to fix a 2-point calibration for their $^{12}CO_2$ and $^{13}CO_2$ mixing ratios and hence for the $\delta^{13}CO_2$ scale. Since the second tank, ALTH8459, was analysed only after the continuous sampling period had finished, it was only possible to apply this "two-point" calibration in a *post hoc* manner.

Figure 4.10 shows the FTIR record of $\delta^{13}CO_2$ during the experimental period, as 30 minute measurements and as daily means. The mean and standard deviation ($\pm 1\sigma$) of all the half-hourly analyses from 1-28 June was calculated as -7.5 ± 0.4 ‰. This level of measurement precision is still about an order of magnitude inferior to what can be achieved using IRMS. Already, significant improvements over this result have been

reported in Chapter 2 resulting from experiments subsequent to the Cape Grim trial. To put these results in some context with respect to previous attempts at $\delta^{13}CO_2$ analysis of air using gas phase FTIR, the two methods of *Kindness and Marr*, [1996; 1997] reported recently, offer precision of only ± 8-12 ‰ at natural abundances There are a number of further observations to be made regarding the accuracy and precision of these FTIR $\delta^{13}CO_2$ analyses.

Firstly, the high precision mass-spectrometric isotope program conducted by GASLAB provides a $\delta^{13}CO_2$ value of -7.8 to -7.9‰ for baseline Cape Grim air in June 1995. This has been determined by extrapolating from the 11-year (1982-92) $\delta^{13}CO_2$ Cape Grim record reported by *Francey et al.*, [1995a]. The FTIR analysis has apparently overestimated $\delta^{13}CO_2$ by up to 0.4‰. One possible reason for this is that either the calibration gas or the sample gas has systematically experienced an isotopically fractionating process which the other has not, such as might be caused by a narrow orifice in a plumbing component of the sampling manifold. This experiment was designed without any consideration given to the possibility of isotope ratio measurements and unfortunately there were several points in the process where such a fractionation may have occurred. A second possibility relates to the manner in which the $\delta^{13}CO_2$ analyses were calibrated against the two reference tanks. The *post hoc* imposition of the two-point calibration scale determined on 28-29 June on the entire period of the experiment assumes that the conditions on those two days are representative of the whole period. This assumption is probably not justified, however there was no alternative at the time.

Secondly, there is a quasi-periodic behaviour evident in the half-hourly FTIR $\delta_{13}CO_2$ record. This is almost certainly an instrumental artefact caused by temperature variation. Determination of $\delta^{13}CO_2$ by FTIR is very sensitive to the instrument temperature, as discussed in Section 2.3.2.1. Six-hourly sampling from the calibration tank was not sufficiently frequent to characterise the diurnal temperature variation which the instrument experienced. This is thought to account for most of the apparently non-random variation in the half-hourly record, which contributes significantly to the standard deviation of ±0.4‰ in this data set. Subsequent measurements of $\delta^{13}CO_2$, reported in Chapters 2 and 5 have taken this into account by calibrating more frequently, and a smaller standard deviation is obtained in those data sets of replicate analyses.

The reference tank CC113591 was sampled repeatedly, 14 times in a 7 hour period, on June 29. The precision of a single $\delta^{13}CO_2$ analysis determined in this way was ± 0.19‰, (1σ). A similar repeat analysis of tank ALTH8459 yielded a precision of ± 0.25‰ (1σ). While still some way from matching the precision attainable with a research grade isotope ratio mass spectrometer, such as the Finnigan MAT 252, it is worth noting that the FTIR instrument described here is an order of magnitude less expensive than such an IRMS, and significantly more portable. A simple analysis suggests that an FTIR taking hourly samples with σ=±0.25‰ may be capable of providing daily mean $\delta^{13}CO_2$ readings with σ=±0.05‰ and monthly means with σ=±0.01‰. This would be contingent on successfully addressing issues affecting accuracy such as temperature sensitivity, frequency of calibration, and isotope fractionation. Nevertheless, the prospect of FTIR playing a role in routine baseline atmospheric stable isotope monitoring is realistic. Even more likely is that FTIR isotope analysis will be useful in non-baseline environments, e.g.

forest and agricultural ecosystems, where $\delta^{13}CO_2$ is more variable and frequent in situ measurement is necessary to characterise the dynamic system.

4.9 Conclusion: Long Term Trace Gas Monitoring by FTIR

Chapter 2 described a novel method of trace gas analysis using FTIR spectroscopy. In this chapter that method is applied to the continuous monitoring of air for a five week period at the Cape Grim Baseline Air Pollution Station, Tasmania. During this period the instrument was collecting data 98.5% of the time. The analytical precision achieved was of the order of 0.05% for CO_2 and CH_4, 0.1% for N_2O and 0.5% for CO at southern hemisphere baseline mixing ratios. For CH_4, CO and N_2O this was equal to or better than the precision achieved by the AGAGE-GC instrument during the same period. The Cape Grim NDIR instrument delivered higher precision CO_2 analyses than did the FTIR instrument, estimated at 0.03% and 0.02%, respectively for hourly mean data.

The greater dynamic range of the FTIR instrument compared to the AGAGE-GC and NDIR instruments enabled exploitation of the nonbaseline data in addition to the baseline data. This allowed some preliminary characterisation of trace gas emission ratios according to wind sector.

The FTIR method demonstrated for the first time its potential as a precise probe of the isotope ratio $\delta^{13}CO_2$ at levels of natural abundance in ambient air. While not yet competitive with mass spectrometric methods, the ease with which this measurement was accomplished in a routine monitoring application, simultaneously with trace gas mixing ratio analyses, by an inexpensive, mobile instrument suggests isotope ratio studies as a promising area for further development of the FTIR technique.

The Cape Grim monitoring experiment also identified several limitations of the FTIR technique as it was applied there. Firstly, the sample size of 8L results in reasonably high consumption rates of calibration gas. This was partly offset by the fact that the FTIR instrument sampled from the calibration tank only every six-hours whereas the AGAGE-GC instrument was calibrated with reference gas every forty minutes and the NDIR from two different calibration tanks every hour. In subsequent work, see Chapters 2 and 5, the sample size was reduced by a factor of sixteen with only a small loss in precision. Two other limitations of the Cape Grim experiment have since been addressed. Firstly, in all work subsequent to Cape Grim, precise pressure control was introduced to the experimental protocol so that all analyses, whether of samples or calibration gas, were conducted at the same slightly sub-ambient pressure, typically, 740±0.3Torr. Secondly, our laboratory has recently implemented a procedure where the detector dewar is kept filled with liquid N_2 automatically rather than manually. This has resulted in the instrument being able to run unattended for periods of several days (Ian Jamie, personal communication).

The FTIR technique has been shown here to be appropriate for the monitoring of trace gases over a five week period. A longer term, possibly permanent, installation at Cape Grim or a similar baseline monitoring station is envisaged. Another possible application, taking advantage in particular of the FTIR method's multi-species simultaneity and large dynamic range, is the characterisation of trace gas emission ratios for a variety of pollutant sources in urban, industrial or agricultural environments.

Chapter 5: Results III: Trace Gas Flux Measurements by FTIR in the Convective Boundary Layer

5.1 Introduction

This chapter describes the application of the FTIR analysis technique described in Chapter 2 to the study of biosphere-atmosphere fluxes of trace gases in an Australian agricultural ecosystem. The analysis of flask air samples collected variously from towers and aircraft allows the construction of vertical profiles in trace gas mixing ratios. From these and other meteorological measurements the fluxes of CO_2 and CH_4 have been estimated. Patch-scale fluxes are inferred from flux-gradient techniques. Regional scale fluxes are inferred from application of a convective boundary layer budget model.

5.1.1 The OASIS Experiment

The OASIS (Observations at Several Interacting Scales) experiment was a field campaign conducted in October 1994 and October 1995. Coordinated by the CSIRO Centre for Environmental Mechanics (CEM), Canberra, it involved the participation of Wollongong, Macquarie, Flinders and the Australian National Universities, the CSIRO Divisions of Atmospheric Research, Plant Industry and Wildlife and Ecology, HortResearch from New Zealand, and the University of Colorado. The groups contributing in some way to the present work are described in Table 5.1, below.

The experiment involved intensive experimental investigation of the biosphere-atmosphere exchange of energy, water, CO_2, CH_4, N_2O and stable isotopes in heterogeneous terrain. The site of the campaign was a 100×100 km^2 region near

Wagga Wagga, NSW, south-eastern Australia. The major land uses are grazing (60%) and cropping (30%) with a small amount of forest. The predominantly flat landscape is heterogeneous at two scales: the paddock scale (1km) because of variation in land use, and the regional scale (100km) because the mean annual rainfall, 550mm at Wagga, decreases westward by about 1mm per km. Several sites along an east-west transect of the region were selected for intensive automated groundbased observations while an aircraft made observations along the entire transect in and above the convective boundary layer (CBL) [*Raupach et al.*, 1994].

Chambers were used to study CO_2, N_2O and CH_4 flux at the scale of $1m^2$. (The convenient term "flux" will be used here to describe what are more correctly "flux densities" since the dimensions of this quantity are $mass.area^{-1}.time^{-1}$). Micrometeorological and trace gas sampling instrumentation at several points on a 22m tower were used to determine fluxes by eddy correlation and flux-gradient techniques. Airborne instrument platforms included helium-filled balloon sondes, kites and manned aircraft, all for investigation of fluxes at the scale of the atmospheric CBL. A significant degree of experimental redundancy was built into the campaign as one of its aims was to be able to reconcile and link observations made using different techniques and at overlapping scales ranging from small chamber ($0.3m^2$) to regional ($100km^2$). Most of what follows refers to the OASIS 95 campaign only.

Group	Main Personnel	Experiment/Instrument	Relevance to Present Work
UoW_{FLASK} (University of Wollongong)	Michael Esler	FTIR - flask instrument	analysis of flask samples for CO_2, CH_4, CO, N_2O, $\delta^{13}CO_2$. Samples collected by aircraft and from 22m and 4m tower.
UoW_{TOWER}	David Griffith Ian Jamie	FTIR - tower instrument	continuous half-hourly analysis of air from 22m tower for H_2O, CO_2, CH_4 and N_2O; flux-gradient calculations; UoW_{TOWER} and UoW_{FLASK} 22m tower profiles and fluxes compared.
$UoW_{CHAMBER}$	David Griffith Ian Jamie Paul Beasley	FTIR - chamber instrument	continuous analysis of chamber ($0.3m^2$) headspace air for H_2O, CO_2, CH_4, N_2O. $UoW_{CHAMBER}$ N_2O flux discussed.
CSIRO-CEM (CSIRO Centre for Environmental Mechanics)	Mike Raupach (coord.) Tom Denmead Ray Leuning Helen Cleugh	balloon sondes (H.C.); NDIR-CO_2 & H_2O (T.D.); Vaisala (H_2O), micrometeorology (flux-gradient and eddy correlation) (T.D., R.L.)	measured *h* (CBL depth) for UoW_{FLASK} CBL budget CO_2 and CH_4 calculations; micromet data used for flux-gradient calculation from UoW_{FLASK} and UoW_{TOWER} 22m tower samples; CEM, UoW_{FLASK} and UoW_{TOWER} profiles and fluxes compared.
FIAMS (Flinders University Institute of Air and Marine Science)	Jorg Hacker Peter Isaacs	"Grob" light aircraft equipped with gas and energy sensors	collected flask samples in and above CBL for FTIR analysis by UoW_{FLASK}
UC (University of Colorado, U.S.A.)	John Birks Ty Smith	Kite and balloon borne flask sampling system	collected flask samples in and above CBL for FTIR analysis by UoW_{FLASK}
RSBS (Research School of Biological Sciences, Australian National University)	Jon Lloyd	Air samples collected in and near crop and pasture canopies for remote stable isotope analysis by IRMS.	RSBS and UoW_{FLASK} plant respiration $\delta^{13}CO_2$ signatures compared.
CSIRO-DAR (CSIRO Division of Atmospheric Research)	Ian Galbally Mick Meyer Paul Steele Roger Francey	Chambers and GC's, CO_2; CH_4, N_2O fluxes (I.G., M.M.); supply of calibration gas suite (P.S); DAR-aircraft flask sampling (P.S., R.F); IRMS $\delta^{13}CO_2$ analysis of DAR flasks and RSBS samples.	UoW_{FLASK}, UoW_{TOWER}, $UoW_{CHAMBER}$, CEM calibrated against DAR suite. DAR flask, RSBS and UoW_{FLASK} $\delta^{13}CO_2$ results compared.

Table 5.1. Some of the groups participating in OASIS chosen by relevance to the work discussed here, their scientific/experimental focus, and connection with the present author's FTIR flask analysis program, UoW_{FLASK}.

5.1.2 FTIR Spectroscopy in OASIS

Three FTIR spectrometers were used in three different parts of the experiment as summarised in Table 5.1. The three, denoted UoW_{FLASK}, UoW_{TOWER} and $UoW_{CHAMBER}$ were deployed for studies in the three different scale regimes region ($100km^2$), patch ($1km^2$) and chamber ($1m^2$), respectively. The present work is concerned primarily with the first of these instruments, UoW_{FLASK}. Samples of air from different heights within and just above the tropospheric CBL, were collected in evacuated glass flasks variously by manned aircraft (FIAMS) and unmanned balloon (UC). These samples were analysed on-site using $1cm^{-1}$ resolution FTIR spectroscopy for the mixing ratios of the trace gases CO_2, CH_4, CO and N_2O. A set of 4-5 flasks collected within a short period (say <15 min) provided a vertical profile of trace gas mixing ratios within and just above the CBL. Together with the independently measured (by CSIRO-CEM) depth of the CBL, the trace gas mixing ratio data are used to infer estimates of the trace gas flux from the surface at the regional scale. This is achieved through application of the recently developed CBL budget method [*Denmead et al.*, 1996; *Raupach et al.*, 1992]. The UoW_{FLASK} FTIR instrument was also used on several occasions to analyse samples collected by flask from within the surface layer, at seven different heights on a 22m tower erected over lucerne pasture, and from four different heights on a 4m tower erected over a triticale crop. Vertical profiles in the surface layer may be combined with simultaneous micrometeorological observations to yield patch scale estimates of surface trace gas flux using the flux-gradient technique described below, Section 5.2.3.

A second FTIR instrument, UoW_{TOWER}, was programmed to analyse two samples of air from each of seven different heights on the 22m tower over a 10ha lucerne pasture in a

30-minute cycle to provide a trace gas concentration gradient in the surface layer. This instrument operated almost continuously, producing 30-minute-average profiles for CO_2, CH_4 and N_2O and H_2O throughout the period of the OASIS experiment. The mixing ratio gradients were combined with simultaneous micrometeorological measurements to derive fluxes (not generally reported here), again by the flux-gradient technique. When the UoW_{FLASK} 22m tower profiles coincide with the UoW_{TOWER} profiles the two independent FTIR results are compared along with flux-gradient and eddy correlation data obtained simultaneously by CSIRO-CEM investigators using NDIR and micrometeorological instrumentation.

$UoW_{CHAMBER}$, a third FTIR, was connected to chambers placed variously over patches of triticale grain crop and lucerne pasture to monitor the changes in concentration of CO_2, N_2O and CH_4 in the chamber headspace and hence the flux of these species to the atmosphere at the chamber scale. The results of this experiment will ultimately be compared (not in this work) with those obtained simultaneously using more orthodox GC methods of chamber gas analysis.

For the 4-week duration of the OASIS 95 campaign the three FTIR instruments were housed in an air-conditioned demountable cabin supplied with mains power. Other trace gas analysis instruments deployed in the field during OASIS included gas chromatographs, a tunable diode laser spectrometer and non-dispersive infrared spectrometers. In addition samples of air collected both at ground level and at altitudes up to 2000m by aircraft were taken to a remote laboratory (GASLAB) for analysis on gas chromatography and isotope-ratio mass spectrometry instruments.

5.2 Atmosphere-Biosphere Exchange Measurement Techniques

There are three main types of trace gas flux measurement technique. These vary in scale from chambers covering ~1 m^2, then micrometeorological methods covering 1000m^2 to 10km^2, and finally convective boundary layer (CBL) budget methods for regions of 100km^2 to 1000km^2. The different experimental approaches are based on several different theoretical considerations, exploit a range of different sensor technologies and, as already mentioned, apply to different spatial scales which may range over nine orders of magnitude. The approaches, although quite different in method and scale of application, are complementary as each is employed to provide a measurement of the flux of a trace gas from the ground or vegetation canopy to the atmosphere. The two methods employed in connection with the UoW_{FLASK} measurements of this work, CBL budget and flux-gradient techniques are described briefly below.

5.2.1 The Atmospheric Boundary Layer

The characteristics of the atmospheric boundary layer (ABL) have been the focus of much research in the last two decades. *Garratt* [1992], and *Kaimal and Finnigan* [1994], provide very detailed descriptions, *Lenschow* [1995], a useful but much briefer account. What follows is a simple outline only.

The ABL is that lower part of the atmosphere which interacts with the biosphere and is closely coupled to the earth's surface by turbulent exchange processes. At night this layer, then known as the nocturnal boundary layer (NBL), may be only a few tens of metres deep, and is a stably stratified structure where the ground is cooler than the air lying above it. At dawn the air and more effectively the ground are heated by the sun,

initiating convective mixing, and the NBL breaks up. During clear sunny conditions, in high atmospheric pressure systems the daytime ABL will be the particular case of a convective boundary layer (CBL), described below.

Ideal CBL description. The CBL is the result of surface heating by the sun. This produces a layer of buoyant convection. As the sun rises and the surface absorbs more heat the convective heating becomes stronger and a deepening layer of convective turbulence develops. As illustrated in Figure 5.1 there are three sublayers within the CBL. Nearest the ground is the "surface layer", typically about one tenth the depth of the CBL. In this region the atmosphere is flowing over a rough surface and the dominant transport mechanism is turbulent diffusion. Above this lies the "mixed layer" accounting for most of the remaining CBL depth. The dominant transport mechanism in the mixed layer is the convective turbulence already mentioned. Near the top of the surface layer upward-moving buoyant thermals form, extend through the mixed layer and dissipate near the top of the CBL. In this sublayer of the CBL mixing by convection is very efficient. Modelling suggests that the time required to mix a constituent released at the surface throughout the CBL is of the order of about an hour [*Lenschow*, 1995]. Potential temperature, and concentration of other scalar entities such as water vapour and trace gases are thought to be quite uniform through the mixed layer. (This is not at all the case in the thin surface layer). These are said to be conserved scalars in the mixed layer. While actual air temperature is not a conserved scalar quantity in the CBL budget model, potential temperature is. Potential temperature, $\Theta = T + \Gamma_z$, is the temperature of an air parcel brought adiabatically and without water phase changes from height z to the ground. T is actual temperature of the air parcel and Γ_z (≈ 0.010 K m^{-1}) is the dry adiabatic lapse rate. Above the CBL and separated from it by a sharp capping

temperature inversion is the free troposphere, not closely coupled to the land surface below. Its trace gas concentrations are close to those of the remote maritime surface layer, such as is observed at Cape Grim BAPS during baseline conditions (see Chapter 4). There is a zone between the top of the CBL mixed layer and the base of the free troposphere, called the "entrainment zone". Here some of the kinetic energy of the thermals in the mixed layer is dissipated in entraining warmer more buoyant air from the free troposphere into the CBL.

During the day, the CBL grows in depth by incorporating air into itself from the free troposphere above. When the sun sets, the solar heating and thus the convective mixing switches off. As the ground cools a temperature inversion is established and the new NBL is formed beneath the residual of the day's CBL.

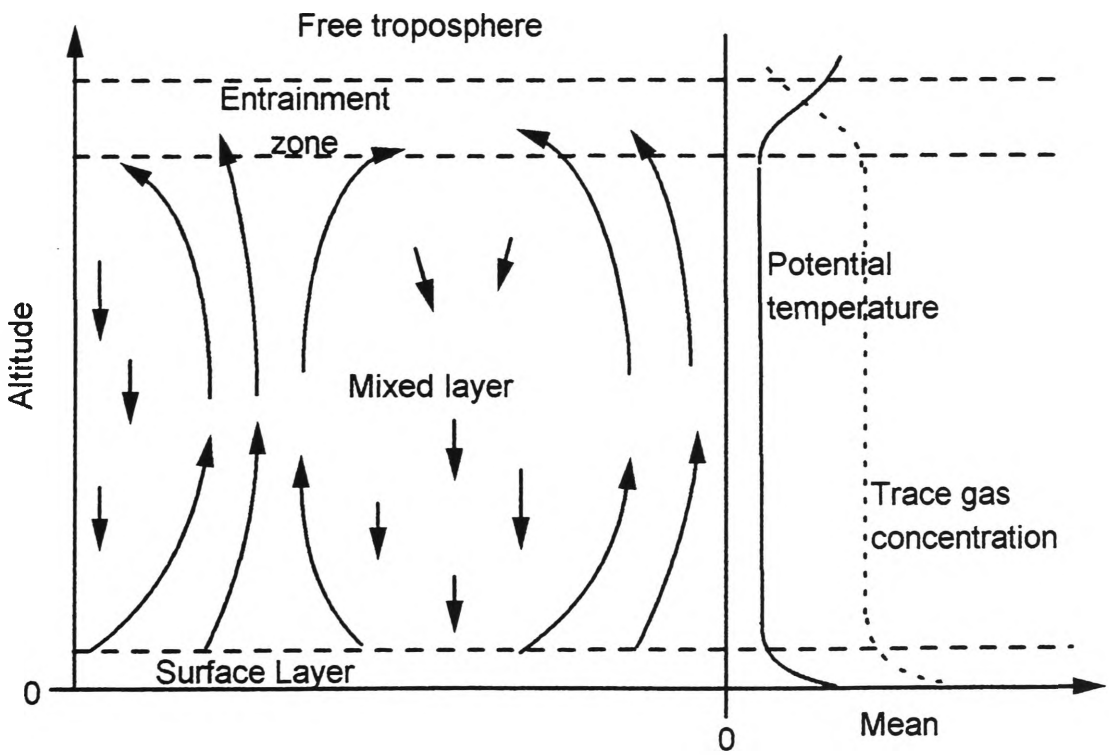

Figure 5.1. A convective boundary layer. The left panel shows the sublayers that make up the CBL, and the schematic of flow patterns. The right panel shows potential temperature and the concentration of a trace gas (in this case with a ground level source) as conserved variables within the mixed layer.

5.2.2 *Convective Boundary Layer Budget Method*

Denmead et al. [1996], and *Raupach et al.* [1992], have extended the range of trace gas flux measurement techniques available by the development of the CBL budget method, described briefly below. When applicable, this method infers regional trace gas surface fluxes integrated over a large footprint from only a few relatively straightforward trace gas concentration measurements and from the depth of the CBL.

A scalar conservation equation can be written for the well mixed CBL

$$\frac{dC_m}{dt} = \frac{F_C}{h} + \left(\frac{C_+ - C_m}{h}\right)\frac{dh}{dt} - \left(\frac{C_+ - C_m}{h}\right)W_+ \qquad (5.1)$$

where:

F_C = Flux of trace gas (or other scalar) at the surface

C_m = mean concentration of trace gas in the CBL

C_+ = free-troposphere concentration of trace gas just above the CBL

h = CBL depth,

W_+ = subsidence velocity at the top of the CBL.

The first term on the right hand side is the contribution of the surface flux to the change in the CBL trace gas concentration and the second is the contribution of entrainment. The third, subsidence, term is relatively small and is neglected from here on. All terms are implicitly dependent on time t. The equation describes the properties of a column of vertically well-mixed air extending throughout the depth of the CBL as it moves across the land surface in response to the mean wind field.

Equation 5.1 may be rearranged and integrated to:

$$I_C = h(C_m - C_+) - h_0(C_{m0} - C_{+0}) + \int_{C_{+0}}^{C_+} h dC_+ \qquad (5.2)$$

where $I_C = \int_0^t F_C dt$ is the integrated surface flux and h_0, C_{m0} and C_{+0} are the respective values at t=0. If C_+ is assumed to vary linearly with height, i.e. $C_+ = C_+' + \gamma h = C_{+0} + \gamma(h - h_0)$ then the third term can be explicitly integrated and equation 5.2 becomes:

$$I_C = h(C_m - C_+) - h_0(C_{m0} - C_{+0}) + \frac{\gamma}{2}(h - h_0) \qquad (5.3)$$

The CBL budget method then applies two restrictions:

1) choose t=0 to be a time such that C_{m0}=C_{+0} so that the second term is zero. This is usually taken as the time in the morning when the CBL is just forming, typically around 0800h.

2) assume $\gamma \approx 0$ (i.e. C_+ is constant) so that the third term is zero. This should be reasonable when the vertical concentration gradient just above the CBL is much smaller than the vertical concentration gradient across the top of the CBL $(C_+ - C_m)/h$.

The expression for cumulative flux is then simplified to:

$$I_C = h(C_m - C_+) \qquad (5.4)$$

with the dimension of length multiplied by the dimension of C. If C is a concentration (in g m^{-3}), of CO_2 for example, then $-I_C$ is the net cumulative CO_2 mass uptake by the surface (in g m^{-2}); "net" because the biosphere may be both a source and a sink of CO_2. All fluxes are defined with positive directed away from the surface. It is most reasonable

to apply this equation in the afternoon when both h and the uptake $C_m - C_+$ are close to their largest values for the day. The simple expression for the daily averaged trace gas flux (in g m^{-2} s^{-1}) is then,

$$F_C = I_C / t = h(C_m - C_+)/t \tag{5.5}$$

In a further development of the CBL budget method, *Raupach et al.* [1992], proceed to derive expressions for I_C where the concentration measurements are made in the surface layer only rather than in and above the mixed layer of the CBL, and where the CBL depth, h, is estimated rather than measured directly. This further degree of simplification will be distinguished from the full CBL budget method of equation 5.5 by denoting it as the "reduced CBL budget method". In the experiment described below, the full CBL budget method is applied. The trace gas fluxes estimated by applying equation 5.5 to the UoW_{FLASK} data may, therefore, later serve to assess the validity of the reduced CBL budget method. At the time of writing, the results of applying the reduced CBL budget method to infer regional fluxes from surface layer data were unavailable, so the comparison with UoW_{FLASK} results cannot yet be made.

5.2.3 Flux-Gradient Method

Micrometeorological methods for determining trace gas fluxes involve the measurement of the vertical transport of trace gases through the surface layer of the atmosphere. These methods include eddy correlation, eddy accumulation, mass balance and flux gradient techniques. Along with chamber techniques (reviewed also by *Livingston and Hutchinson* [1995]), these are well documented by, for example, *Denmead and Raupach* [1993].

Flux-gradient techniques rely on the assumption that in the surface boundary layer gas transport occurs by a process of turbulent diffusion along the gradient of mean concentration. The vertical flux of the gas is calculated as

$$F_g = \overline{\rho}_a K \frac{\partial \overline{s}}{\partial lnz} \tag{5.6}$$

where ρ_a is the density of dry air, K is an eddy diffusivity, $s(=\rho_g/\rho_a)$ is the mixing ratio of the gas with respect to dry air, z is height and the overbar denotes a time average. The eddy diffusivity depends on wind speed, surface roughness, height and atmospheric stability. It is usually not measured directly but inferred from the simultaneous measurement of heat or water vapour fluxes and concentration gradients or from eddy correlation measurements. For example, if the flux of water vapour has been determined by one technique, the flux of CO_2 can be derived from the $\partial CO_2/\partial H_2O$ gradient as follows:

If $$F_{H2O} = \overline{\rho}_a K \frac{\partial H_2O}{\partial lnz}, \tag{5.7}$$

and $$F_{CO2} = \overline{\rho}_a K \frac{\partial CO_2}{\partial lnz} \tag{5.8}$$

then, $$F_{CO2} = F_{H2O} \frac{\partial CO_2}{\partial H_2O} \tag{5.9}$$

The gradient approach has often been used successfully for CO_2 where an NDIR sensor has sufficient sensitivity and speed to measure a concentration gradient over a vertical separation of one or several metres [*Denmead and Raupach*, 1993]. For CH_4 and N_2O the situation is more problematic since the vertical concentration gradient for these species is much smaller relative to their background concentrations than is the case for

CO_2 (see Table 5.3). This places CH_4 and N_2O flux gradient measurements at the very limit of, or beyond, the precision available with current GC and NDIR technology. Some work has been done on the application of TDLs (tunable diode lasers; reviewed in [*Kolb et al.*, 1995]) to flux gradient methods.

5.2.4 Summary of Flux Measurement Techniques

Tables 5.2 and 5.3 summarise the characteristics of the various trace gas flux measurement techniques available. Only eddy correlation requires a very fast response sensor. This is probably the only technique of those listed where FTIR spectroscopy is unlikely to be useful. The most demanding, in terms of their requirement for trace gas mixing ratio analytical precision, are the micrometeorological techniques. The CBL method requires a level of precision which is intermediate between that required by micrometeorological methods and chambers. On the basis of these considerations it seems reasonable to apply FTIR spectroscopic trace gas sensor analysis to the CBL budget method. Note that there is a range of 4-5 orders of magnitude spanning the typical fluxes of CO_2 and N_2O, with CH_4 intermediate.

Method	Footprint	Required instrument response time
Chamber	1 m^2	100 s
Mass balance	10^3 m^2	100 s
Flux-Gradient	10^5 m^2 (10ha)	100 s
Eddy accumulation	10^5 m^2 (10ha)	100 s
Eddy correlation	10^5 m^2 (10ha)	0.1 s
Convective boundary layer	10^8 m^2 (100 km^2)	100 s

Table 5.2. Characteristics of various methods for measuring trace gas fluxes (from *Denmead* [1993])

Gas	Surface	Typical Flux $g\ m^{-2}\ s^{-1}$	Method	Required Sensor Precision ppb
CO_2	Forest	10^{-3}	Open chamber	150
	Forest	10^{-3}	Micromet.	30
	Wheat	10^{-3}	Micromet.	300
	Wheat	10^{-3}	CBL	3000
CH_4	Rice field	10^{-6}	Closed chamber	200
	Rice field	10^{-6}	Micromet.	2
	Rice field	10^{-6}	CBL	10
N_2O	Soil	10^{-7}	Closed chamber	10
	Grassland	10^{-8}	Open chamber	3
	Grassland	10^{-8}	Micromet.	0.02
	Grassland	10^{-8}	CBL	0.1

Table 5.3. Sensor precision required for measuring fluxes to within 10% (from *Denmead* [1993] and references)

5.3 Experimental: FTIR and Flask Sample Trace Gas Measurements

5.3.1 Flask Sample Collection

Three different methods of flask sample collection were used during the OASIS 95 experiment. Two of these were from airborne platforms used in retrieving trace gas vertical profiles in and above the CBL's mixed layer. The third method was used to retrieve trace gas vertical profiles within the surface layer by sampling from the 22m and 4m towers.

5.3.1.1 Balloon Flask Sampling

The UC group (see Table 5.1) used tethered helium-filled balloons to bear aloft a payload consisting of several evacuated 2L flasks and instrumentation to measure

humidity, ozone, temperature and altitude. The instruments relayed information to the ground base in real time by telemetry where the data were saved to file. Each flask could be opened and closed once only by telemetry, at any altitude required, so that a vertical profile of the trace gas mixing ratios in and above the CBL could be derived from later analysis of the flask samples. Some useful profile data were obtained in this way, although wind conditions were far from optimal. All balloon flask analyses are listed in Table C.2 and the vertical profiles illustrated in Figure C.1, Appendix C.

5.3.1.2 Aircraft Flask Sampling

A manually operated 5-flask air sampling apparatus was constructed and flown on the FIAMS (see Table 5.1) light aircraft, the Grob. An intake line facing into the wind carried air through a manifold past a series of five closed evacuated flasks before venting outside the cabin in the downwind direction. The pressure differential between intake and vent ensured sufficient flow through the manifold. The intake was well forward of the aircraft exhaust outlet but in the prop wash air. The pilot sampled the air in the CBL and above it by briefly opening the flasks in turn at required altitudes. Once this system was in place, profiling was performed each day at approximately 0900 and 1500 when weather conditions allowed flying. This provided two 5-point trace gas profiles per day, one as the CBL was developing in the morning and another when it was almost fully developed in the mid-afternoon. All Grob-sampled flask analyses are listed in Table C.1 and the vertical profiles illustrated in Figure C.1, Appendix C.

5.3.1.3 22m and 4m Tower Flask Sampling

Micrometeorological observations by CSIRO-CEM (see Table 5.1) in the surface layer were facilitated by the mounting of instruments at various heights on a 22m tower

erected in a field of lucerne pasture and on a 4m tower in the triticale crop of an adjacent field. An air sampling manifold connected to both towers allowed a centrally located array of trace gas analysers (UoW_{TOWER} FTIR for H_2O, CO_2, CH_4 and N_2O; CSIRO-CEM NDIR for CO_2 and H_2O, and TDL for CH_4) to analyse air in rotation from 7 different heights (0.5, 1, 2, 4, 8, 14 and 22m above the pasture) on the 22m tower and from four different heights on the 4m tower (0.5, 1, 2 and 4m above the crop; by NDIR and TDL only). The sampling heights were logarithmically distributed because in the ideal surface layer trace gas concentration gradients vary with the log of height. While the author's primary involvement in the OASIS campaign was in CBL rather than surface layer studies, it was decided to take advantage of the easy access to surface layer sampling which the towers presented. Using the CSIRO-CEM sampling manifold, it was possible to fill a set of flasks near-simultaneously from all sampling heights of a tower. This provided a surface layer trace gas profile for the time of sampling. Several daytime and one nocturnal profiles were collected in this way. The data are listed in Table C.3, Appendix C, the profiles illustrated in Figure 5.9, and discussed below in Section 5.5. One important objective in collecting these surface layer samples was to attempt the retrieval of a vertical gradient in the stable isotope ratio $\delta^{13}CO_2$ from analysis by FTIR. Such a gradient is likely to be more marked in the surface layer than in the mixed layer, particularly within the NBL when respired CO_2 is trapped under the capping inversion. The UoW_{FLASK} tower profiles provide another degree of mixing ratio intercalibration and redundancy through comparison with simultaneous analyses of almost the same airmass by the UoW_{TOWER} FTIR instrument as well as by the CEM NDIR (for CO_2) and TDL (for CH_4). At the time of writing, there was no data available from the CSIRO-CEM CH_4 TDL. The other comparisons are made in Section 5.5 below.

5.3.2 *FTIR Flask Analysis Protocol*

The measurements of the UoW_{FLASK} FTIR instrument are the subject of the remainder of this chapter. This instrument was configured essentially as described in Chapter 2, inside a temperature controlled enclosure which was in addition purged with dry nitrogen. A 0.5L, 9.8m White cell was used in place of the 8L, 22m cell used in the work described in Chapters 3 and 4, resulting in a significant improvement in the pathlength:volume ratio. This was necessary as the instrument was used to analyse air samples retrieved by airborne sampling platforms which limited the maximum practical sample size to 2L at ambient pressure and temperature. The reduced White cell volume also leads to significant reductions in calibration gas consumption. Unfortunately, the reduced optical throughput and reduced total pathlength also leads to a reduction in the spectroscopic SNR and ANR, and in turn of the analytical precision of the instrument, as discussed below (Section 5.4.1).

Samples were collected in pyrex-glass flasks of about 2L volume as described above. The flasks were fitted with manually operated glass valves sealed with Teflon O-rings (Glass Expansion Pty Ltd, Melbourne). The only materials in contact with the air sample were glass and Teflon. Typically, samples were analysed within 12 hours of collection so that the flasks could be reused for further sampling. A sample handling manifold with a capacity of 8×2L-flasks was constructed. The instrument was automated so that a batch of up to 8 flasks, once connected to the manifold, could be processed unattended. At the end of the batch analysis, all the flasks were pumped down to a pressure of <0.1 Torr in readiness for further sample collection. The Array Basic program, "flask.ab" (see Appendix B) automated the analysis according to the scheme set out here:

1. White cell is empty, pumped down to ~0.1 Torr. Collect a 256-scan spectrum of the empty cell at 1cm^{-1} resolution, (~8 min). This single beam spectrum serves as the reference spectrum for all the samples in this batch.
2. Fill the White cell to 450.0 Torr with air from either one of the flasks (or the calibration standard tank CC113591). Close the White cell and let the sample stand for 1 minute to approach temperature and pressure equilibrium with the instrument. Measure the pressure and temperature of the sample.
3. Collect a 256-scan spectrum of the filled cell at 1cm^{-1} resolution, (~8min). Save this single beam spectrum as the sample spectrum. Measure the temperature and pressure of the sample again.
4. Ratio the sample spectrum to the reference spectrum, producing the absorbance spectrum of the sample. Retrieve raw mixing ratios and spectral diagnostic parameters (baseline offset, baseline slope and RMS residual) from this spectrum using the Classical Least Squares prediction algorithm.
5. Log CO_2, CH_4, CO and N_2O mixing ratios, spectroscopic parameters and temperature and pressure to a file. The temperature and pressure measurements are used to make simple density corrections to the retrieved mixing ratios.
6. Pump out the White cell to a pressure of ~0.1Torr in readiness for the next sample analysis in the batch cycle.

The analysis of a complete set of flasks consisted of first analysing a sample of the calibration gas (from tank CC113591), then analysing the flasks in turn, and concluding with another analysis of a calibration gas sample. This bracketing by calibration samples allowed close supervision and correction (by simple linear interpolation) of any small effects due to instrument drift during the analysis of one set of flasks.

The main difference between this scheme and the one described previously (in Section 4.3) for monitoring at Cape Grim is in the pressure control. At Cape Grim, the White cell was simply filled to ambient pressure. The raw mixing ratios were later corrected for density effects due to pressure differences and a further small empirical correction due to second order pressure effects on the retrieved mixing ratios. For the OASIS experiment all samples were analysed at a uniform pressure to avoid having to make this second order correction, as it is an unnecessary source of additional uncertainty in the final results. A further difference is that in the above scheme only one empty cell reference spectrum is used for a set of analyses, instead of measuring a new reference spectrum for every sample, as was the case in the Cape Grim experiment. For batch analysis of up to 8 flasks over 2 hours a single reference was found to be acceptable both in terms of time (and throughput of samples) and analytical precision.

5.3.3 Calibration and Intercalibration

Since one of the stated aims of the OASIS project was to make comparisons between flux measurement methods that differed in sensor instrumentation as well as in scale, calibration of each instrument and intercalibration between instruments became a critical issue. Without a rigorous approach to intercalibration, meaningful intercomparison of experimental data sets becomes problematic if not impossible. For the trace gas instruments, it was decided that this end could best be achieved if all instruments were directly related to a single mixing ratio scale for each species. The CSIRO-DAR group (specifically GASLAB) provided a suite of tanks which spanned the appropriate mixing ratio range for each of CO_2, CH_4, N_2O and CO. These tanks were circulated amongst all groups involved in trace gas analysis. All trace gas instruments were calibrated against

the entire suite, several times throughout the duration of the campaign if possible. In addition to this OASIS calibration suite, the UoW_{FLASK} FTIR instrument had its own devoted tank (CC113591, see Table 5.4), also provided by GASLAB, with mixing ratios assigned on the same internationally recognised scale. This scale is traceable to primary standards generated by gravimetric and manometric methods at NOAA/CMDL. All sets of flask measurements were sandwiched between replicate analyses of this tank. The complete suite of OASIS calibration tanks was also analysed on the UoW_{FLASK} FTIR instrument, and the results used to transform the one-point calibration into a multi-point one. The tanks and their GASLAB assigned trace gas mixing ratios are listed in Table 5.4.

Tank	CO_2 (ppm)	CH_4 (ppb)	CO (ppb)	N_2O (ppb)
CC113591	358.14	1694.9	90.36	310.91
CA01692	376.54	1782.0	111.33	325.42
CC99528	339.81	1601.6	106.17	303.83
CA01628	359.6	1694.3	124.86	311.68

Table 5.4. The calibration air tanks supplied by CSIRO-DAR for the OASIS 95 experiment and their assigned trace gas mixing ratios. Tank CC113591 was the tank devoted specifically to the UoW_{FLASK} FTIR instrument.

5.4 Results and Discussion: CBL Trace Gas Profiles and Fluxes

Aircraft-borne flask sampling yielded a total of 13 trace gas mixing ratio vertical profiles (4 or 5 points each profile). A further 8 profiles (3 or 4 points each) were obtained from balloon-borne sampling. These results are tabulated in Tables C.1 and C.2, respectively, and illustrated in Figure C.1, Appendix C. In addition a total of eight profiles were

determined within the surface layer by taking flask samples from the 22m and the 4m towers. These are tabulated in Table C.3 and illustrated in Figure C.2, Appendix C.

Only the boundary layer vertical profiles from 25-27 October have been analysed by the CBL budget method, in Sections 5.4.4 and 5.4.5 below. On these days CBL depth measurements were available and, particularly for 26-27 October, the meteorology was suitable for classical CBL development, ie. sunshine, high barometric pressure, light winds. There were four profiles measured on 24 October, however the prevailing meteorology of that day was considered to be unsuitable for application of the CBL model. The two balloon-sampled profiles for 25 October are not considered in the CBL budget analysis since they are three and four point profiles, only one of them extends to above the CBL, and neither are reconcilable with the Grob-sampled profiles of that day. There are some doubts remaining about the balloon-sampling process. Similarly, only one of the balloon-sampled profiles extends above the CBL on 26 October, and there was no balloon-sampling on 27 October. Those profiles selected for CBL budget analysis are redrawn in Figures 5.2, 5.3 and 5.4.

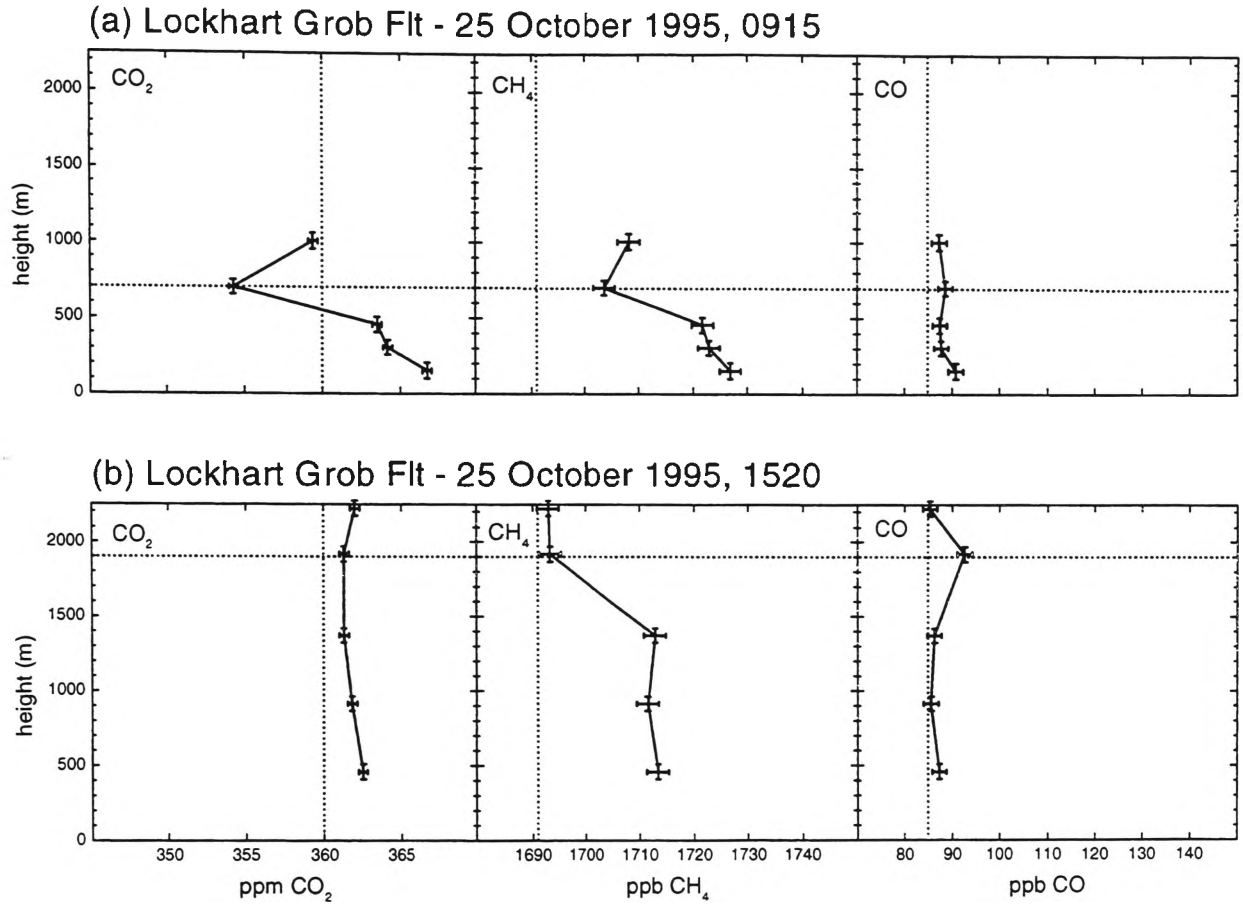

Figure 5.2. CBL trace gas mixing ratio profiles for 25 Oct 1995. Horizontal broken line is CBL depth, vertical broken line is free-troposphere mixing ratio of species. Error bars are ±50m in height, ±0.3 ppm CO_2, ±2 ppb CH_4, ±1.5 ppb CO (all ±1 std dev).

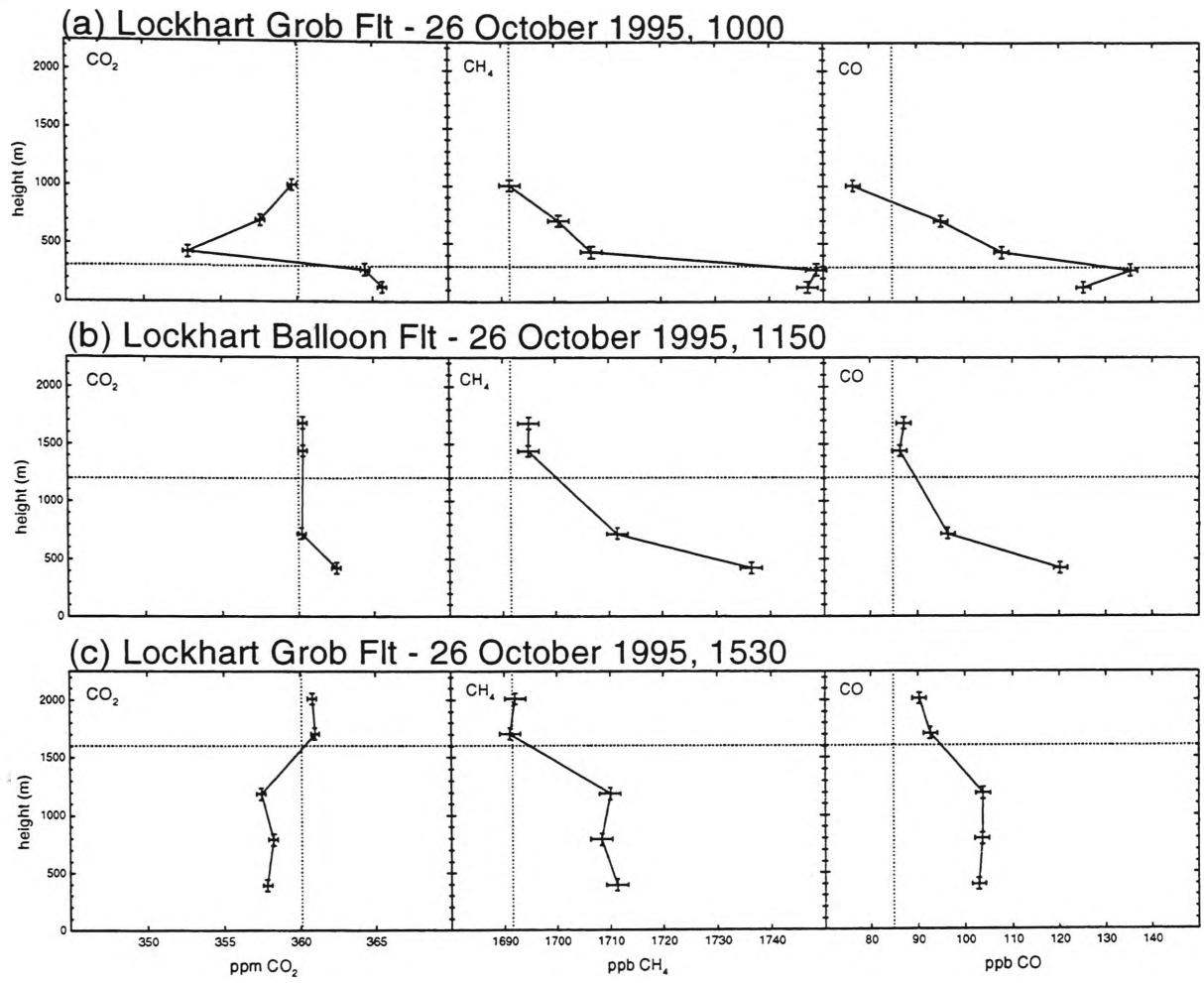

Figure 5.3. CBL trace gas mixing ratio profiles for 26 Oct 1995. Horizontal broken line is CBL depth, vertical broken line is free-troposphere mixing ratio of species. Error bars are ±50m in height, ±0.3 ppm CO_2, ±2 ppb CH_4, ±1.5 ppb CO (all ±1 std dev).

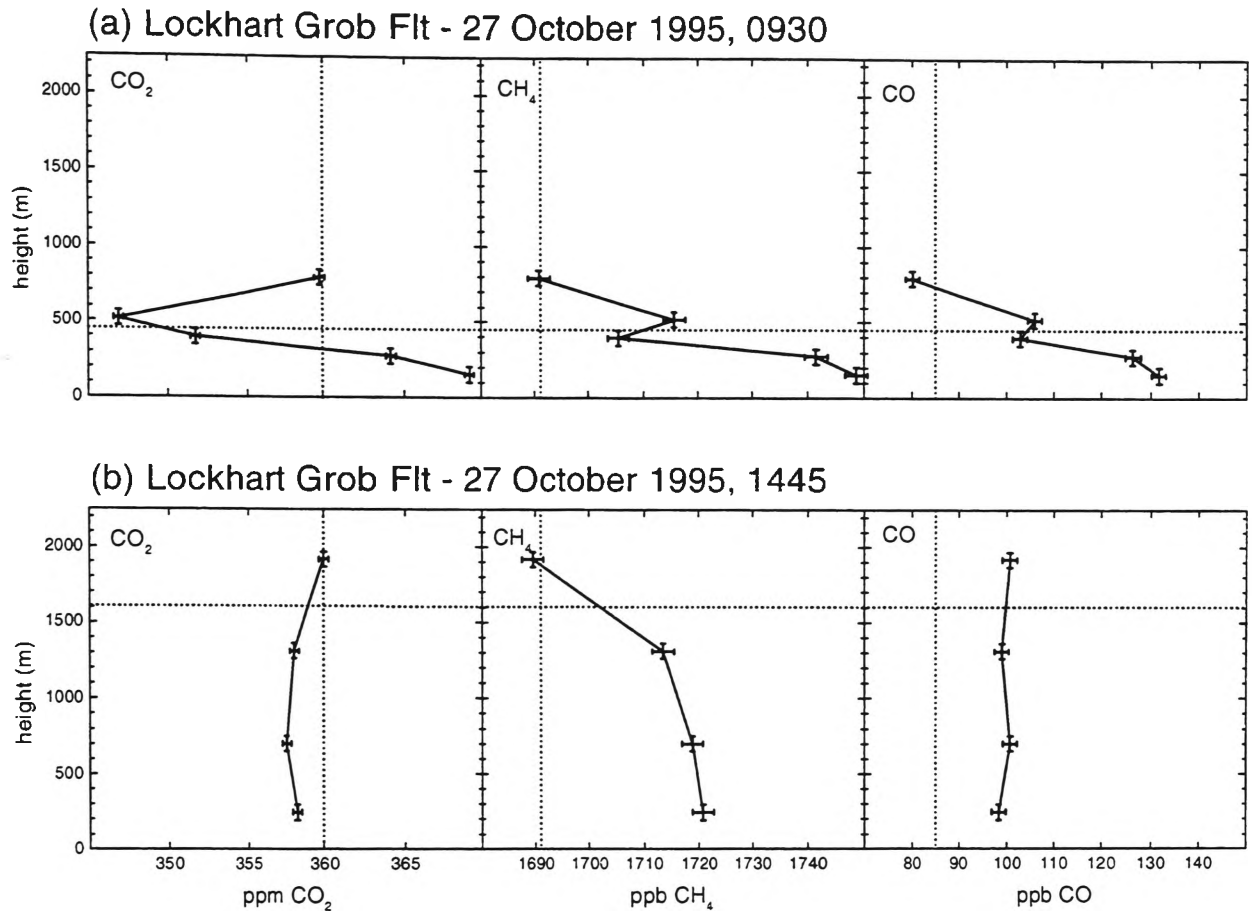

Figure 5.4. CBL trace gas mixing ratio profiles for 27 Oct 1995. Horizontal broken line is CBL depth, vertical broken line is free-troposphere mixing ratio of species. Error bars are ±50m in height, ±0.3 ppm CO_2, ±2 ppb CH_4, ±1.5 ppb CO (all ±1 std dev).

5.4.1 Precision of FTIR Mixing Ratio Analysis

In Figures 5.2 to 5.4 the y (height) error-bars, ±50m, are an estimate of the precision of the altitude (height above ground) measurement at each sampling. The x (mixing ratio) error-bars, ± 1 standard deviation, illustrate the precision of a single mixing ratio measurement based on replicate analyses of a standard. For CO_2, and CH_4 the precision of the FTIR analysis is such that depletions and enrichments due to biospheric source and sink processes may be well characterised. In addition depletions and enrichments of CO are well characterised, however these are probably anthropogenic rather than biospheric in origin. Referring to Table 5.3, the estimated minimum sensor precision required for CBL trace gas studies was ±3ppm, ±10ppb and ±0.1ppb for CO_2, CH_4 and N_2O respectively. The achieved precision using the FTIR method in this study was estimated at ±0.3ppm, ±2ppb and ±1ppb, respectively. While this is better than the required precision for CO_2 and CH_4 it is not sufficient for N_2O studies where the very small biosphere-atmosphere fluxes result in levels of enrichment in the mixed layer of the CBL that are not detectable by the FTIR instrument as it was configured here. N_2O profiles are therefore not included in Figures 5.2 to 5.4. Note that the precision of analysis by FTIR given above is significantly less than what was achieved using a very similar technique at the Cape Grim BAPS as described in Chapter 4. It has already been mentioned above that a much smaller White cell was used for the OASIS experiment, with less than half the total pathlength of the cell used at Cape Grim, leading to some loss of precision. An additional factor is that despite a thermostatted enclosure and an air-conditioned cabin, it was not possible to maintain the optimal degree of instrument temperature control during the warmest part of some days in Wagga in October.

Methods of improving field-based FTIR analysis precision for N_2O are discussed below (Section 5.4.7).

5.4.2 Measurement of CBL Depth

CBL depth, *h*, was measured directly by balloon-borne temperature sonde as the height of the capping inversion, denoted where available by the horizontal broken line in Figures 5.2, 5.3, 5.4 and C.1. Figure 5.5 illustrates the evolution of the CBL in terms of potential temperature, a conserved scalar within the CBL. The CSIRO-CEM group collected the data by airsonde at the times indicated on 26 October 1995 at the same site that the trace gas flask sampling was being performed by aircraft. The top of the CBL is clearly apparent as a discontinuity in the potential temperature profile. Although the airsondes did not always coincide with the times of flask sampling, interpolation between sondes provides a good estimate of the CBL depth.

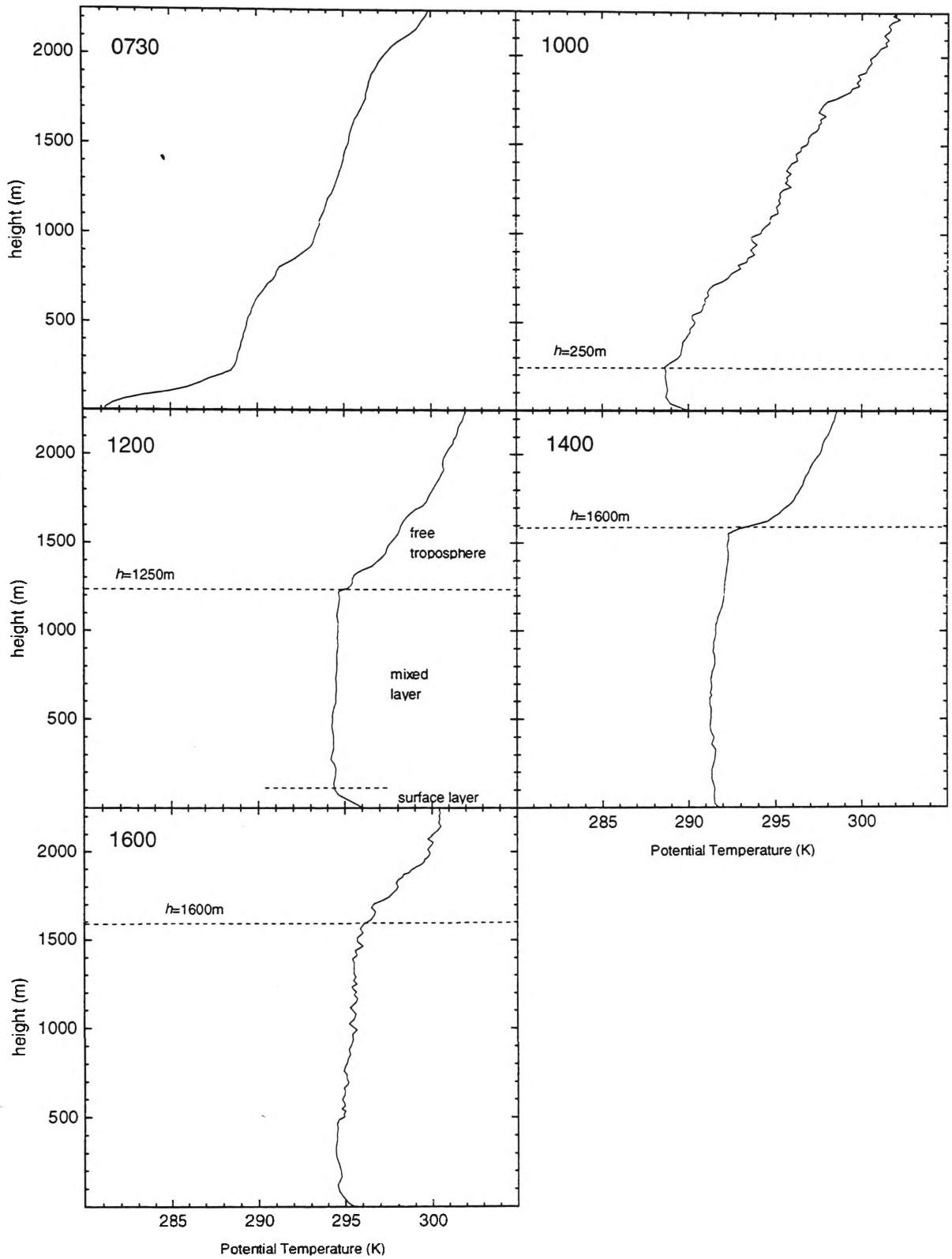

Figure 5.5. The evolution of the potential temperature profile in and above the CBL on 26 October 1995 at Lockhart. Measured by H. Cleugh and P. Briggs (CSIRO-CEM).

5.4.3 *Free Troposphere Mixing Ratios*

The vertical line in each of the profiles, Figures 5.2, 5.3, 5.4, 5.9 and C.1, indicates the typical free-troposphere mixing ratio, C_+, observed for CO_2, CH_4 and CO during the OASIS campaign. For CO_2 and CH_4 these were fairly invariant at 360 ±1 ppm and 1692 ±2 ppb respectively, measured as the mean of all C_+ observations. Cape Grim BAPS reported October 1995 monthly mean mixing ratios of CO_2 and CH_4 in the remote marine boundary layer of 359.5 ppm and 1695 ppb respectively [*Steele et al.*, 1996c], in close absolute agreement with the observed OASIS free-troposphere mixing ratios. For CO, the observed Cape Grim remote marine boundary layer baseline mixing ratio was observed to be 70 ppb [*Steele et al.*, 1996c]. The free-troposphere CO mixing ratios observed during OASIS 95 were typically significantly higher at approximately 85 ± 5 ppb. The free-troposphere CO level also showed relatively more variation than the corresponding CO_2 and CH_4 levels, due probably to its short atmospheric lifetime. *Junge* [1974], observed that variability in tropospheric trace gas concentration is inversely proportional to atmospheric lifetime. Also, CO undergoes much greater proportional enrichments than CH_4 and CO_2. A polluted airmass with elevations over baseline mixing ratios of say 10% in CO_2 and CH_4 may have CO elevated by a factor of 50 or more. This makes the application of the CBL budget method to CO somewhat more problematic than to CO_2 and CH_4. However, even though CO is not a primary focus of the OASIS experiment and its sources are not primarily biospheric, it may still serve to offer some verification of the CBL budget approach to estimation of trace gas fluxes and so is included in this discussion.

5.4.4 CBL Trace Gas Profiles 25-27 October 1995

The trace gas profiles in Figures 5.2 to 5.4, when combined with knowledge of the free troposphere trace gas mixing ratios and of the depth of the boundary layer, provide an account of the development of the CBL which broadly consistent with our understanding of its expected behaviour as outlined in Section 5.2.1 above. Consider, firstly, Figures 5.2a, 5.3a and 5.4a, the morning profiles around 0930, probably only a couple of hours after that day's CBL is first established. For all three gases there is a great deal of interpretable structure present, even in a five point profile. The morning CBL is clearly not well mixed, and is stratified in a reproducible manner. These reproducible features include apparent vestiges of the NBL of the previous night and even of the surface layer of the previous day.

For all three gases on all three days, the mixing ratios in the lowest part of the profiles are significantly elevated above the free-troposphere level. This is consistent with known NBL behaviour. At night when the ground cools down, a temperature inversion is established within the NBL, resulting in very limited vertical transport of gases. Any nocturnal biospheric emissions will be trapped under the inversion close to the ground. These may be CO_2 emissions from respiring plants, CH_4 emissions from sheep and cattle, and CO emissions from local vehicular traffic or combustion. It is not unusual, for example, to observe CO_2 mixing ratios of >500 ppm late at night in the lowest few meters of the NBL. The first effect of convective turbulence in the new day's nascent CBL will be to mix this highly trace-gas enriched air into the lower part of the mixed layer. This is apparently what is observed at altitudes of 100-300 m in the three morning profiles, Figures 5.2a, 5.3a and 5.4a.

For CO_2 but not for CH_4 or CO there is another quite distinctive feature in the morning profiles (Figures 5.2a, 5.3a and 5.4a) due to a similar effect. In each case, at altitudes quite close to the top of the nascent CBL, the CO_2 mixing ratio is significantly lower than its level in the free-troposphere. It seems probable that the air at these altitudes originates largely from the surface layer of the previous day's CBL. It is only in the surface layer of an established afternoon CBL that CO_2 mixing ratios will be 5-15 ppm lower than the free-troposphere level. The consistency of this feature suggests that the residual of the day's CBL persists while the NBL is established underneath it overnight. By about 0930 a "fossil" of the previous day's surface layer lies immediately above the residual of the NBL, at about 500m. This feature is observed for CO_2 but not for CH_4 or CO. This difference is interpreted as being due to the photosynthetic drawdown of CO_2 and the absence of any corresponding significant biospheric sink term for CH_4 or CO.

Finally, for the uppermost point of each of the morning profiles, at around 800m, the mixing ratio in most cases tends towards the free-troposphere level. The air at these altitudes is perhaps a mixture of air from the previous afternoon's CBL and of subsiding free-troposphere air. This would bring the mixing ratios at ~800 m close to the free-troposphere level, as is observed.

The midday and afternoon CBL trace gas profiles as illustrated in Figures 5.2b, 5.3b,c and 5.4b are entirely different from the corresponding morning profiles and clearly illustrate the evolution of the CBL during the day. Again there are several features common to all three days. In most cases, at least for CO_2 and CH_4, the mixing ratio above the CBL (altitudes of ~2000m) is close to the expected free-troposphere level.

Within the CBL mixed layer there is evidence of significant photosynthetic drawdown of CO_2 particularly on October 26 and 27 when the mixing ratio is depleted several ppm relative to the free-troposphere level, even at altitudes above 1300m. Significant ground-level CH_4 emissions are observed with enrichment in CH_4 of more than 20 ppb to altitudes above 1300 m on all three days. For CO, the profile on October 26 seems typical of a regional source of CO at the ground level. The CO profiles are not as straightforward to interpret on the other two days, perhaps due to the factors mentioned above pertaining to the great variability often observed in CO mixing ratios and in the intensity of CO sources.

The near midday balloon profile of October 26 shows an intermediate stage of CBL development in each of the three species. There is still some evidence of the previous night's NBL enrichment around 500m but it is less extreme than the morning profiles. By midday, it is evident that convective turbulence has not yet produced a uniform mixed layer. *Raupach et al.* [1992], remark that the CBL budget method of trace gas flux estimation is best applied in the late afternoon when both h and $C_+ - C_m$ are near their largest values. In addition, the integration of equation 5.1 assumes that the CBL is always well mixed, as this affects C_m in the $C_+ - C_m$ term. This midday profile suggests that the so-called "mixed layer" may not be very well mixed at all until late afternoon and that the CBL budget method is not applicable until then. Any estimation of C_m based on a few mixing ratio observations before the "mixed layer" is well mixed would be very sensitive to the altitudes at which those observations were made.

Encouragingly, the afternoon profiles presented here do strongly indicate that by around 1500 on typical CBL days, the trace gas mixing ratios are a conserved scalar within the

mixed layer for the purposes of the CBL budget method, i.e. that the mixed layer is indeed mixed and that trace gas fluxes can be inferred from just a few measurements above and below the top of the CBL.

5.4.5 CBL Regional Flux of CO_2, CH_4, CO 25-27 Oct 1995

Species	Date 1995	Time	C_+ ppb	C_m ppb	h m	I_C g m^{-2}	t (t_0 = 0800) s	t' (t_0 = 1800) s	F_C (t_0 = 0800) g m^{-2} s^{-1}	F_C' (t_0 = 1800) g m^{-2} s^{-1}
CO_2	25 Oct	1520	362.0E3	361.9E3	1900	-3.80E-1	26400	-	-1.44E-5	-
	26 Oct	1530	360.8E3	357.8E3	1600	-8.64	27000	-	-3.20E-4	-
	27 Oct	1445	360.0E3	358.0E3	1600	-5.76	24300	-	-2.37E-4	-
CH_4	25 Oct	1520	1692.9	1712.5	1900	2.43E-2	26400	52800	9.20E-7	4.61E-7
	26 Oct	1530	1692.1	1709.9	1600	1.87E-2	27000	77400	6.93E-7	2.42E-7
	27 Oct	1445	1689.6	1717.7	1600	2.94E-2	24300	74700	1.21E-6	3.94E-7
CO	25 Oct	1520	85.4	86.4	1900	1.90E-3	26400	52800	7.20E-8	3.60E-8
	26 Oct	1530	90.3	103.4	1600	2.40E-2	27000	77400	8.89E-7	3.10E-7
	27 Oct	1445	100.6	99.3	1600	-3.20E-3	24300	74700	-1.31E-7	-4.28E-8

Table 5.5. Calculation of regional trace gas fluxes for CO_2, CH_4 and CO using the CBL budget method on 25-27 October during OASIS 95. Two different t_0 values are considered for the cases of CH_4 and CO. The first t_0=0800 of that morning, is the standard CBL assumption. The alternative, t_0=1800 of the day before, is suggested to more realistically account for the effect of significant buildup of CH_4 and CO in the NBL, and the effect this has on the following day's CBL.

For the three afternoon profiles, Figures 5.2b, 5.3c and 5.4b, it is possible to calculate the cumulative mass flux, I_C, in g m^{-2}, and therefore the average flux F_C ($=I_C/t$), in g m^{-2} s^{-1}, for the three trace gases using the CBL budget method. Equation 5.4 is used to determine I_C. In each case C_m is calculated as the mean of the three mixing ratios within the mixed layer, C_+ is the mixing ratio of the highest air sampled from above the CBL, h is the depth of the CBL as determined by potential temperature sonding. For CH_4 and CO two different measures of elapsed time are used: t is the number of seconds elapsed since 0800 of that morning and t' is the number of seconds elapsed since 1800 of the previous day. This leads to two quite different sets of flux results, F_C and F_C', related to a consideration of the assumptions underlying the CBL budget model, discussed below. These values are listed in Table 5.5.

5.4.5.1 CH_4 and CO Regional Flux - Modified CBL Budget Method

One of major assumptions underlying the CBL budget method was that t_0 is chosen as the time when $C_m=C_+$, i.e. the trace gas concentrations within the CBL and just above the CBL are equal. This is normally taken as the time in the morning when the CBL is just forming, around 0800. This assumption might be defended for CO_2 since by about 0800 much of the respired CO_2 built up in the NBL overnight has already been consumed by photosynthesis. Figure 5.6, showing the 26 and 27 October UoW_{TOWER} profiles, illustrates the rapid decrease in CO_2 mixing ratio within the surface layer in the 2-3 hours following dawn, due to photosynthetic uptake. The dCO_2/dz gradient turns from negative to positive and the entire profile rapidly shifts back towards the free troposphere level. The excess CO_2 which remains, is gradually carried into the mixed layer as the CBL develops. Also contributing to the new CBL is that stratum of air just above the NBL which was depleted in CO_2 due to the photosynthetic drawdown of the previous day. These remnants of both CO_2 enriched and CO_2 depleted air go some way to cancelling each other as the CBL develops and they mix. For the purposes of simplicity it is still appropriate to assume t_0=0800, and to integrate the mass flux from that time when estimating F_C.

The biosphere is a significant source of CH_4 throughout the day and night, due to enteric fermentation, however biospheric sinks of CH_4 are negligibly small. During the OASIS campaign CH_4 mixing ratios of up to 2300 ppb were observed overnight within the NBL. This nocturnal buildup is sufficiently large to make a significant contribution to the CH_4 mixing ratio in the mixed layer of the following day, so that the assumption of $C_m=C_+$ at t_0=0800 is not justified. The early morning UoW_{TOWER} profiles, illustrated in Figure 5.6, show high CH_4 mixing ratios persisting within the surface layer well beyond 0800.

Applying the CBL budget method with t_0=0800 will wrongly attribute this nocturnally built up CH_4 to emissions since 0800. Thus, the CH_4 flux may be considerably overestimated.

It is suggested therefore that t_0'=1800 of the previous day is a more appropriate assumption. Rather than the time when the new CBL is being established, 1800 is approximately the time of the collapse of the previous day's CBL and the beginning of the NBL formation associated with trapping of emissions under the temperature inversion. It will still not be true to say that C_m=C_+ at this alternative time. However, in the interests of retaining a simple model, setting t_0'=1800 will take into account the nocturnal buildup of CH_4. A similar line of reasoning can be applied to CO, for which sources vastly outweigh sinks in the surface layer. Table 5.5 lists the CH_4 and CO flux calculated according to t_0'=1800 (previous day).

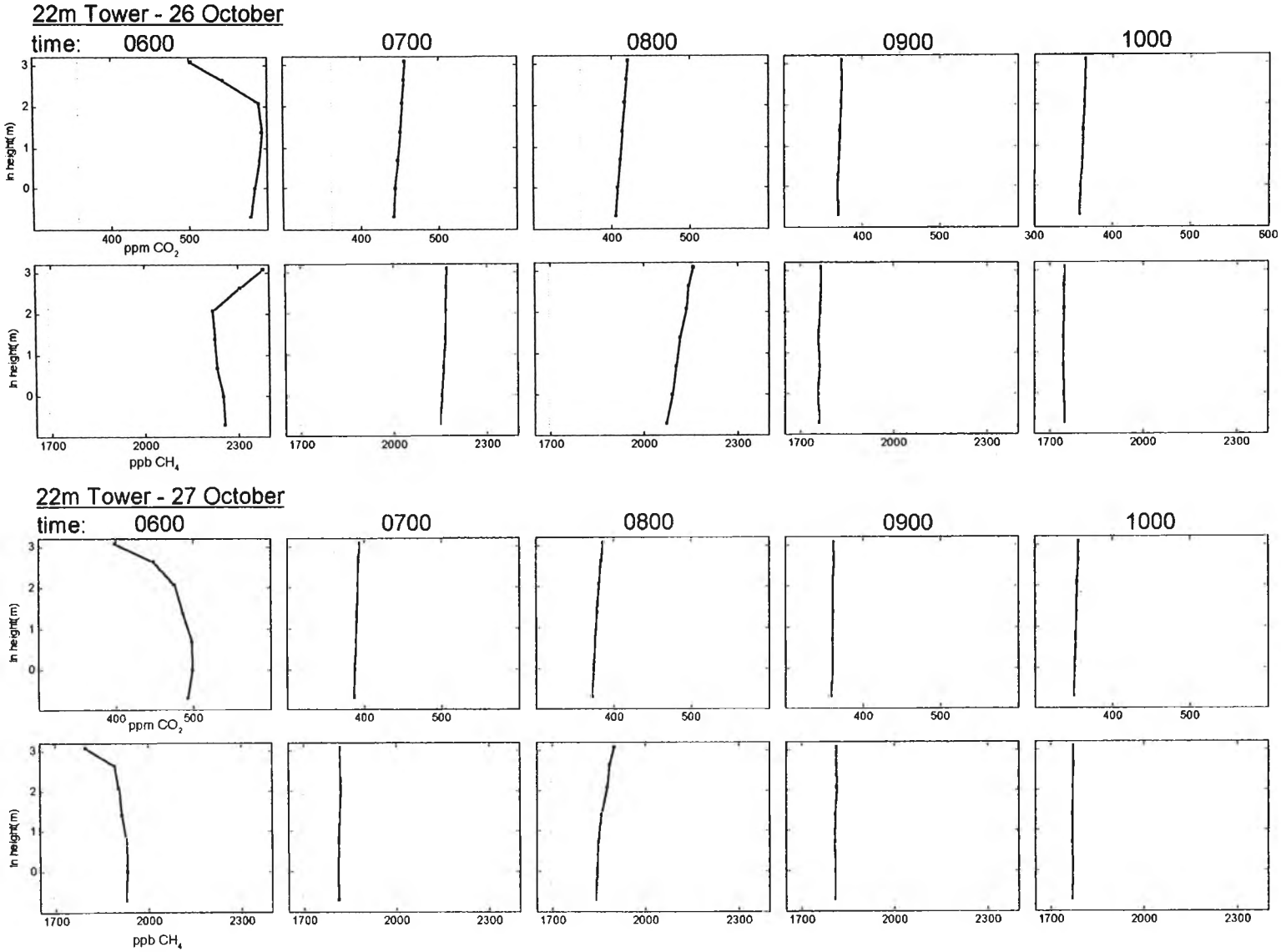

Figure 5.6. 22m tower profiles measured by UoW_{TOWER} FTIR. CO_2 and CH_4 profiles for 26 and 27 October 1995 at times 0600, 0700, 0800, 0900 and 1000.

5.4.5.2 CH_4 Regional Flux - Livestock Census Method

One other independent means of estimating the regional CH_4 flux was attempted. A visual census of the livestock present within a ~36 km^2 area around the main OASIS site was undertaken. While the "footprint" of the CBL budget method is much greater than this, the 36km^2 survey area is expected to be broadly representative of the region. The count was 4700 sheep, 110 horses and 534 beef cattle. Australia's National Greenhouse Gas Inventory Committee [*NGGIC*, 1996b] has published estimates of the CH_4 emissions associated with livestock animals, summarised in Table 5.6.

Livestock	CH_4 emissions (kg/head/year)	Beef cattle equivalent
Beef cattle	59.93	1
Sheep	6.68	0.111
Horses	18.00	0.300

Table 5.6. Average annual CH_4 emissions of Australian livestock animals

The total livestock population was equivalent to 1089 cattle, with a density of 0.3 head/ha. The expected regional CH_4 flux is 6×10^{-8} g m^{-2} s^{-1} if livestock are the only source. This flux is significantly less than the range estimated by the modified CBL budget method, $24\text{-}46\times10^{-8}$ g m^{-2} s^{-1}.

5.4.6 Analytical Uncertainty in CBL Flux Measurement

The main analytical uncertainty in the calculation of trace gas fluxes by the CBL budget method arises from the need to measure a small difference between two large quantities, namely the trace gas mixing ratios above the CBL and within the CBL. The individual

mixing ratio measurements of CO_2, CH_4 and CO have standard deviations of approximately ±0.3ppm, ±2ppb and ±1ppb respectively. The difference (C_m–C_+), where C_m is a mean of three measurements and C_+ is a single measurement, will have uncertainties of ±0.45ppm, ±2.4ppb and ±1.2ppb as standard deviations, for CO_2, CH_4 and CO respectively. The typical size of the difference (C_m–C_+) in the above table is 3ppm CO_2, 20 ppb CH_4 and 10 ppb CO. It follows that the uncertainty in the difference (C_m–C_+) is of the order of ±15% for CO_2 and ±12% for both CH_4 and CO. The depth, h, of the CBL is precise to approximately ±50m, or ±3%. Similarly, the time elapsed since the first development of the CBL is probably not more precise than half an hour, or 7% (for t_0=0800). The total combined error in the calculation of fluxes using this approach is estimated to be 17% for CO_2, and 14% for both CH_4 and CO. To this should be added any uncertainties introduced into the model itself by the potential unreality of the assumptions on which its simplicity depends. These are considered in Section 5.4.8, and are indeed seen to have a much greater impact than the combined uncertainties of the gas analysis and measurements of h and t.

The N_2O mass flux during OASIS, determined by $UoW_{CHAMBER}$ FTIR and CSIRO-DAR GC measurements, was very sensitive to soil moisture content, varying in the range 2-23 $\times 10^{-9}$ gN_2O m^{-2} s^{-1}. A daytime maximum flux of approximately $4\pm2\times10^{-9}$ gN_2O m^{-2} s^{-1} was typical (M. Meyer and D. Griffith, personal communication). Reversing the procedure applied immediately above to CO_2, CH_4 and CO, it can be shown that to measure the N_2O flux using the same CBL budget approach, the FTIR would need to have a mixing ratio measurement precision of 0.1 ppb N_2O or better, as suggested by Denmead in Table 5.3. The N_2O analysis precision achieved in fact was an order of

magnitude worse than this. Firstly, it should be noted that the challenge in determining N_2O fluxes is the very small atmospheric signature of these fluxes on a relatively large background signal of 310 ppb. CH_4 mass fluxes are about two orders of magnitude greater than those of N_2O, but CH_4 has a background signal only six times greater than N_2O. To measure an N_2O flux by this technique is an intrinsically more difficult objective than for CH_4 or CO_2.

5.4.7 Improving FTIR for CBL N_2O Measurements

It is possible to anticipate some simple improvements to the FTIR instrument which are very likely to deliver higher precision, in particular to determine N_2O fluxes. In Chapter 2 an analytical precision of ±0.3ppb for N_2O was demonstrated using the 0.5L, 9.8m White cell (see Section 2.5.1). A goal of ±0.1ppb is not unreasonable. During OASIS essentially the same optical configuration was used, however the temperature of the instrument was not as well controlled because of the practical restraints of field work as opposed to laboratory studies. The mixing ratios retrieved for N_2O during OASIS were very sensitive to temperature fluctuations. This is likely to be due to the N_2O rotational structure not being resolved in a $1cm^{-1}$ spectrum (see Figure 2.7). At the same resolution CO_2, CH_4 and CO all exhibit well resolved rotational structure. Their spectra are "information rich". By contrast, N_2O appears as a broad, unresolved and therefore "information poor" band in the spectrum. The CLS spectral fitting algorithm apparently finds it difficult to distinguish between N_2O and broad baseline features such as gradient or curvature in the region of N_2O. An unstable temperature is likely to produce such confounding baseline effects. There are several remedies to this problem which might be applied separately or in unison. Firstly, the temperature control of the instrument can be improved. Secondly, an FTIR spectrometer with higher spectral resolution, (e.g.

$0.5cm^{-1}$) may be used. While this may entail some loss in SNR, the availability of N_2O spectra with resolved rotational structure may more than compensate. Thirdly, scrubbing samples of CO_2 before analysis may be considered, perhaps using Ascarite™, if this can be done without perturbing N_2O mixing ratios. The N_2O band near 2200 cm^{-1} lies on the shoulder of, and is partly obscured by, a very strong CO_2 band. The removal of CO_2 would better ensure that retrieved N_2O mixing ratios are entirely independent of the strong CO_2 spectrum. Clearly this would be at the cost of simultaneous CO_2 measurements, currently one of the principle advantages of the FTIR technique. However, if this measure resulted in analytical precision of ±0.1ppb, FTIR spectroscopy would be the most sensitive technique available for N_2O analysis, making possible the application of flux-gradient and CBL budget methods.

5.4.8 Discussion of Regional Trace Gas Flux Estimates

5.4.8.1 CH_4

In section 5.4.5 the regional CH_4 flux was estimated in three different ways. The estimates were approximately 1 $\mu gCH_4\ m^{-2}\ s^{-1}$ by the CBL budget method (with t_0=0800), 0.4 $\mu gCH_4\ m^{-2}\ s^{-1}$ by the modified CBL budget method (with t_0=1800 day before), and 0.06 $\mu gCH_4\ m^{-2}\ s^{-1}$ by the livestock census method. The greater than order of magnitude range in estimates of the same quantity is concerning. However, there are several assumptions implicit in the methods which on closer examination may need to be reviewed.

Firstly, the livestock census method is oblivious to possible non-livestock sources (and sinks) of CH_4. One example of these is wetlands – natural or manmade (e.g. rice fields) – which have a typical flux of $1\mu gCH_4\ m^{-2}\ s^{-1}$ (e.g. [*Denmead*, 1993; *Wofsy et al.*, 1988]). However these are virtually absent from the relatively arid OASIS experimental region. Another intense source of CH_4 is fugitive fossil fuel emissions, predominantly leaks of natural gas. Agricultural CH_4 emissions (overwhelmingly due to ruminant livestock), and fugitive emissions are estimated by NGGIC to constitute approximately 59% and 23%, respectively, of total Australian CH_4 emissions [*NGGIC*, 1996a]. It is quite conceivable then, that fugitive emissions from regional centres such as Wagga and Lockhart may constitute a significant part of the regional CH_4 flux.

Secondly, it has already been recognised in section 5.4.5.1 above, that applying the CBL budget method (t_0=0800) to CH_4 will erroneously attribute CH_4 enrichment in the CBL solely to daytime emissions when the effects of NBL buildup may be equally significant. In the interests of maintaining the simplicity of the original CBL approach the somewhat *ad hoc* adjustment of setting t_0=1800 was implemented in the modified CBL method. A more rigorous approach would be to relax the assumption that C_m=C_+ at t_0 and to reintroduce the second term of equation 5.3. This would more properly account for the contribution of nocturnal buildup to daytime CH_4 mixing ratios.

$$I_C = h(C_m - C_+) \tag{5.4}$$

$$I_C = h(C_m - C_+) - h_0(C_{m0} - C_{+0}) + \frac{\gamma}{2}(h - h_0) \tag{5.3}$$

Similarly, preliminary investigations by David Griffith (personal communication) indicate that it is not necessarily appropriate to assume that C_+ is constant, thereby necessitating the reintroduction of the third term in equation 5.3. The third term may, in some

circumstances be similar in magnitude and opposite in sign to the first term. If the air just above the CBL is in fact enriched in CH_4 rather than at the free tropospheric mixing ratio, its entrainment as the CBL develops will result in an increase in C_m. Applying equation 5.4 in will in this case result in an overestimation of the regional flux.

In summary, regional methane flux may often be overestimated by the CBL method and will usually be underestimated by livestock census methods. *Ad hoc* measures such as suggested here in the modified CBL method are probably more accurate. Ideally, though the assumptions underlying the simplification of equation 5.3 to 5.4 need to be reconsidered.

5.4.8.2 CO_2

The same arguments for CH_4 apply to CO_2, although for CO_2 the situation is both simpler and more complicated. The complication arises from needing to consider biospheric sinks as well as sources for CO_2 whereas for CH_4 there is no significant biospheric sink term. Reintroducing the second and third terms of equation 5.3 will be correspondingly more complicated. On the other hand, to the extent that CO_2 sources and sinks partially cancel each other out in the surface layer in the early morning hours (as discussed in section 5.4.5.1) the CBL approach of equation 5.4 is still useful.

On the two days considered best for application of the CBL budget method, 26 and 27 October, the average daytime (0800-1500) regional CO_2 flux was estimated at approximately -0.3mgCO_2 m^{-2} s^{-1}. By way of comparison, the UoW_{FLASK} tower CO_2 flux estimates (section 5.5.1 below) were typically about -0.6mgCO_2 m^{-2} s^{-1} at 1500 over pure pasture, the part of the day when photosynthesis is close to its peak (which occurs

around midday). Considering this and that the regional flux is from an area with lower average rainfall, and correspondingly less intense agriculture, than the Wagga tower site, the two results seem mutually consistent. The results are also broadly consistent with reported Australian patch-scale CO_2 fluxes at about 1300, obtained by micrometeorological methods, of $-0.5 mgCO_2\ m^{-2}\ s^{-1}$ for a growing pasture and $-0.75 mgCO_2\ m^{-2}\ s^{-1}$ for a growing wheat crop [*Denmead et al.*, 1996].

5.5 Results and Discussion: Tower Trace Gas (and $\delta^{13}CO_2$) Profiles and Fluxes

Flask samples were collected from the 22m and 4m towers as described in Section 5.3.1.3. The gases sampled at the top of the 22m tower are probably representative of the area 1-2 km immediately upwind of the tower. Two daytime profiles from the 4m tower in the triticale crop were obtained. Five daytime and one nocturnal profile were obtained from the 22m tower in the lucerne pasture. The UoW_{FLASK} FTIR mixing ratio analysis results are listed in Table C.3 (Appendix C) and the tower profiles (in black) illustrated in Figure 5.9, at the end of the Chapter. Also illustrated in Figure 5.9 for comparison are the corresponding UoW_{TOWER} CO_2 and CH_4 profiles (in red), and the CSIRO-CEM NDIR CO_2 profiles (in blue). UoW_{FLASK} was the only instrument at OASIS analysing for CO.

5.5.1 CO_2 Tower Profiles and Fluxes

All of the daytime UoW_{FLASK} tower profiles show sub-ambient CO_2 mixing ratios and strongly positive gradients, $dCO_2/dlnz$. This is consistent with photosynthetic drawdown of CO_2. The single nocturnal profile shows CO_2 enrichment of up to 55ppm near the ground and a strongly negative gradient, $dCO_2/dlnz$. This is consistent with nocturnal plant respiration, with the emitted CO_2 being trapped within the NBL under a capping

inversion. A linear relationship between mixing ratio and log height is observed. This reflects the dominance of mixing by eddy diffusion within the surface layer. The simultaneous CO_2 tower profiles arising from three different instruments (UoW_{FLASK}, UoW_{TOWER} and CSIRO-CEM NDIR) are generally similar in shape, but not identical. Some of the discrepancies are understandably due to slight differences in time and method of sampling. However there are other significant systematic differences. UoW_{FLASK} typically reports CO_2 mixing ratios 2-8 ppm higher than both UoW_{TOWER} CSIRO-CEM. The margin seems consistent within a single profile but varies somewhat from day to day. The UoW_{TOWER} and CSIRO-CEM mixing ratio scales show similar variations relative to each other. This illustrates the practical difficulty in maintaining absolute intercalibration between several instruments, even over the relatively short period of a few weeks, and when the instruments are all located in close proximity and are calibrated against the same set of standards. Fortunately, while there was some variation in absolute calibration, flux-gradient calculations depend primarily on instantaneous differences in mixing ratio between different heights rather than on long term absolute stability.

Fluxes of CO_2 have been derived from the UoW_{FLASK} tower profiles using the flux-gradient technique (section 5.2.3), specifically equation 5.9:

$$F_{CO2} = F_{H2O} \frac{\partial CO_2}{\partial H_2O} \tag{5.9}$$

A two point gradient, $\frac{\partial CO_2}{\partial H_2O}$, was calculated from the UoW_{FLASK} CO_2 mixing ratios and the independently determined (by UoW_{TOWER} and CSIRO-CEM) H_2O mixing ratios, at the 2m and 0.5m levels on the tower. F_{H2O} was determined by CSIRO-CEM from eddy

correlation measurements of latent heat flux. The resulting UoW_{FLASK} CO_2 fluxes are noted (in black) on the profiles plots of Figure 5.9. Also noted on the profile plots, for comparison, are the corresponding UoW_{TOWER} CO_2 fluxes (in red), and the CSIRO-CEM NDIR CO_2 fluxes (in blue). In addition to the three flux-gradient results, the CO_2 flux determined directly by CSIRO-CEM eddy correlation measurements is noted (in green), where it was available. With only these few points of comparison between the UoW_{FLASK} CO_2 fluxes and those determined from UoW_{TOWER}, CSIRO-CEM NDIR and eddy correlation data, only general conclusion can be drawn. The fluxes calculated from the four different techniques are generally within ± 0.2 $mgCO_2$ m^{-2} s^{-1} of each other, without any apparent systematic differences. Examination of the extended half-hourly CO_2 flux records from the UoW_{TOWER}, CSIRO-CEM NDIR and eddy correlation records suggest that none of those techniques is more precise than about this amount, ± 0.2 $mgCO_2$ m^{-2} s^{-1}. It is reasonable to conclude that the UoW_{FLASK} instrument has enabled the measurement of patch scale CO_2 fluxes with much the same precision and accuracy as the other techniques deployed during OASIS.

5.5.2 CH_4 and CO Tower Profiles and Fluxes

The UoW_{FLASK} profiles indicate a less dynamic situation prevailing for CH_4 fluxes than for CO_2. The CH_4 mixing ratios are consistently greater than the free-tropospheric CH_4 level, during both day and night, at all heights on the tower. This is consistent with the presence of a biospheric source and the absence of a significant biospheric sink. The UoW_{FLASK} tower profiles do not generally exhibit a consistently positive or negative $dCH_4/dlnz$ gradient and tend to be more or less vertical. This tends to suggest that the biospheric CH_4 source is not in the immediate vicinity of the tower (pasture and crop) but further afield (such as livestock in other paddocks) and that CH_4 emissions reach the

tower already well mixed through the surface layer. The full UoW_{TOWER} CH_4 record (D. Griffith, personal communication) confirms that CH_4 mixing ratios were generally higher at night within the shallow NBL than during the day when the emissions are mixed into the much deeper CBL. The 18 October 1500 profile is an exception to this rule, and is likely due the short-term presence of a large mob of sheep in a nearby stockyard. Slight timing and sampling differences probably explain the small random differences between the UoW_{FLASK} and UoW_{TOWER} CH_4 profiles. The UoW_{FLASK} CH_4 mixing ratios are systematically displaced from UoW_{TOWER}'s by about -20ppb, variable from day to day. This is evidence again of the difficulty in establishing and maintaining absolute intercalibration between instruments. In this case it may be related to the fact that the UoW_{FLASK} instrument analysed dried air samples and the UoW_{TOWER} instrument analysed undried air. There is considerable overlap of CH_4 and H_2O infrared absorption features around $3000cm^{-1}$ which may account for the calibration offset. The CH_4 profile gradients were not sufficiently large relative to the CH_4 mixing ratio precision to calculate fluxes. As already mentioned, is likely that almost none of the CH_4 emissions originated near the tower.

The UoW_{FLASK} CO profiles are generally vertical near the base of the tower but show variable and high levels of enrichment near the top. Somewhat similar to the case for CH_4, this structure is consistent with the existence of intense CO sources being some distance from the immediate vicinity of the tower. Vehicular traffic is one such likely CO source.

5.5.3 $\delta^{13}CO_2$ Tower Profile in the NBL

Figure 5.7 illustrates the UoW_{FLASK} CO_2 and $\delta^{13}CO_2$ vertical profiles in the nocturnal boundary layer at 2230 on 19 October. Particular care was taken when collecting and analysing the flask set from which these data were derived. The object was to determine if analysis by the UoW_{FLASK} instrument could provide a vertical profile of the CO_2 isotope ratio $\delta^{13}CO_2$. The principle and method of $\delta^{13}CO_2$ analysis have been described in Chapter 2. A nocturnal $\delta^{13}CO_2$ profile is likely to be more easily measured than a daytime profile since nocturnal CO_2 enrichment in the surface layer due to plant respiration is normally much larger (three-four times) than daytime drawdown in the surface layer due to photosynthesis. In fact, photosynthetic drawdown is a larger CO_2 sink than plant respiration is a CO_2 source. However, the turbulent diffusion present during the day causes the concentration gradient, dCO_2/dz, to be smaller then than at night, when turbulent diffusion is largely absent. A rough guide to the expected change in $\delta^{13}CO_2$ in a body of air (typical $\delta^{13}CO_2 \approx -8‰$) due to the introduction of some CO_2 originating from fossil fuels or C3 plants (with typical $\delta^{13}CO_2 \approx 28‰$) is about -1‰ for each +20ppm change in the CO_2 mixing ratio. It follows that the nocturnal isotope ratio profile be more easily distinguished than a daytime profile using the same instrument. Table C.3 lists $\delta^{13}CO_2$ data for all the tower profiles. Due to the issues mentioned immediately above, however, and to the particular care taken with the analysis of the single nocturnal profile, the daytime isotope data is largely uninterpretable, whereas there is good reason to have more confidence in the nocturnal data.

The $\delta^{13}CO_2$ profile indicates that the CO_2 nearest the respiring pasture is depleted in ^{13}C by ~2‰ relative to the CO_2 at the top of the tower. The background tropospheric

$\delta^{13}CO_2$ was -7.85‰ during October 1995, as measured at Cape Grim [*Allison et al.*, 1996]. Photosynthesis by C3 plants causes carbon isotopic fractionation of about -20‰, resulting in the plant tissue having a carbon isotopic signature of about -28‰ [*Bowen*, 1991]. Respiration, on the other hand, proceeds with very little fractionation, and so is a source of CO_2 which has an isotopic signature of about -28‰. At night the ^{13}C-depleted respired CO_2, mixing with the CO_2 already present in the air will cause the isotopic signature of the low lying air to drop to levels more negative than -7.85‰.

Keeling [1958], has considered the case of a CO_2 source, of isotopic signature δ^{13}_{source}, diffusing into and thereby perturbing an airmass of a different CO_2 isotopic signature. He demonstrated that the relationship between $\delta^{13}CO_2$ and CO_2 concentration for the perturbed airmass is described by the equation

$$\delta^{13}_{perturbed} = \delta^{13}_{source} + \frac{m}{[CO_2]_{perturbed}} \qquad (5.10)$$

Thus, the isotopic signature of the perturbing source of CO_2 can be deduced from the y-intercept of the plot of $\delta^{13}CO_2$ vs $1/CO_2$. Figure 5.8 is such a plot for the CO_2 and $\delta^{13}CO_2$ data illustrated in Figure 5.7. The x-axis ($1/CO_2$) error-bars are derived from the CO_2 analytical precision, expressed as ±1 std deviation, of ±0.3 ppm. Most of the uncertainty lies in the y-axis, since the precision of a single $\delta^{13}CO_2$ analysis is estimated at ±0.2 per mil (as ±1 std dev). A linear regression was performed on the data and the results listed in Table 5.7. The table lists the regression parameters for the two cases where the circled data point is excluded and included. This outlier, which lies more than 10×SEP distant from the line of best fit defined by the other five points, corresponds to the sample taken at the 0.5m level, closest to the ground. Experimental error cannot be excluded as the origin of this outlier. Another possibility is that it reflects real

inhomogeneities in the sources of respired CO_2. These are likely to be more apparent close to the ground before the air is well mixed by diffusion or turbulence. For the purposes of the discussion below, this point will be neglected.

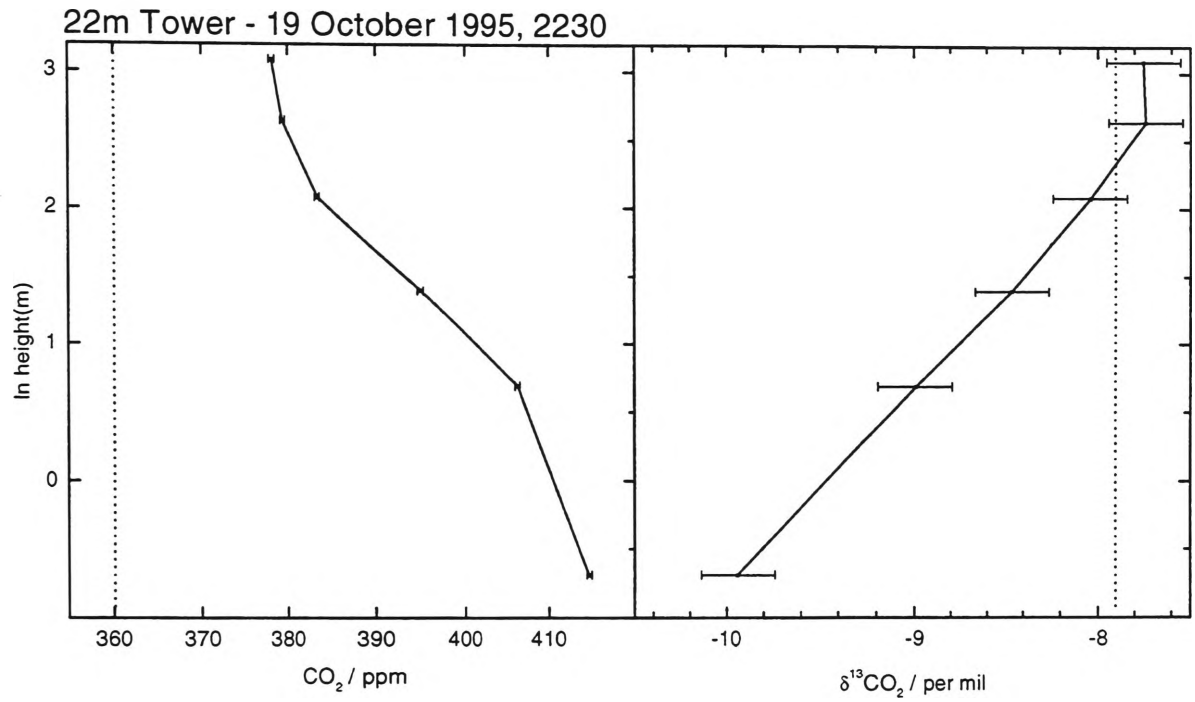

Figure 5.7. 22m Tower CO_2 and δ13CO_2 vertical profile for 19 October, 1995, 2230. Error bars are ±0.3ppm CO_2 and 0.2‰ $\delta^{13}CO_2$, (±1 std dev.)

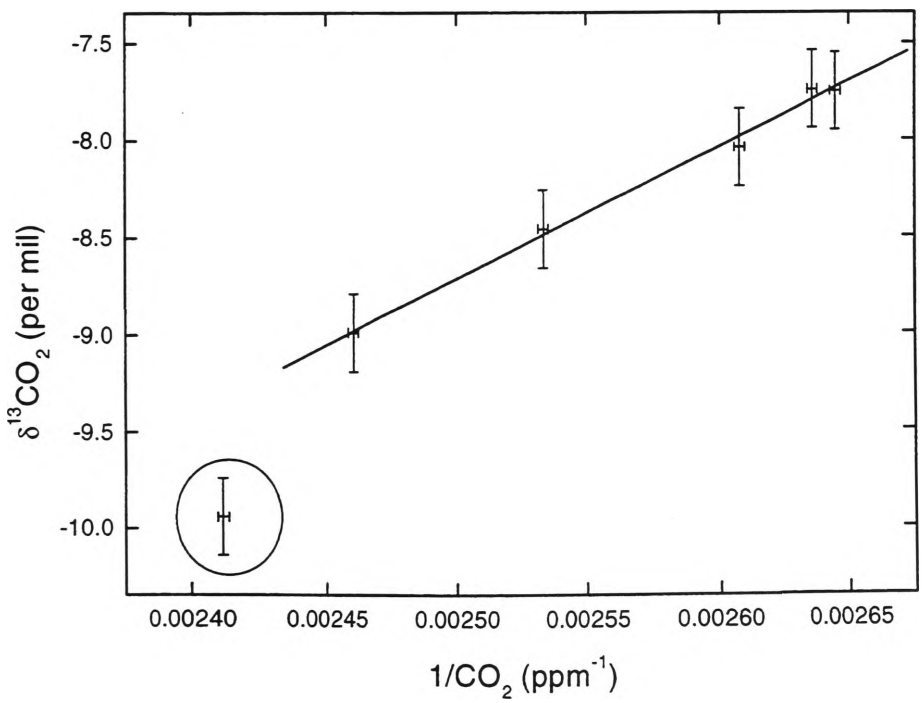

Figure 5.8. $\delta^{13}CO_2$ versus inverse CO_2 concentration for the nocturnal profile of Figure 5.7. Regression line illustrated is for the case excluding the outlier.

Regression Parameters	UoW_{FLASK} 22m Tower (Exclude Outlier)	UoW_{FLASK} 22m Tower (Include Outlier)	RSBS Ground level IRMS	CSIRO-DAR Aircraft IRMS
	nocturnal	nocturnal	nocturnal	daytime
y-intercept	-25.7 ± 0.8 ‰	-30.4 ± 2.5 ‰	-26.8 ± 0.14 ‰	-23.95 ± 0.76 ‰
slope	6780 ± 315	8600 ± 970	6878 ± 56	5720 ± 270
R^2	0.994	0.95	0.9995	0.97
SEP	0.05 ‰	0.2 ‰	0.06 ‰	0.03 ‰
N	5	6	17	26

Table 5.7. Regression statistics for $\delta^{13}CO_2$ versus $1/CO_2$ plot, Figure 5.8. The regression parameters from the FTIR data are listed for inclusion and exclusion of the possible outlier. Also listed are regression parameters of nocturnal ground-level sampling (by the RSBS group) and daytime aircraft sampling (by CSIRO-DAR) programs conducted during OASIS where the air samples were shipped to a remote laboratory (GASLAB) for analysis using isotope ratio mass spectrometry.

Two other programs within OASIS 95 were focused on stable isotope analysis. The RSBS group (see Table 5.1) collected samples within the canopies of a triticale crop and pasture at night on 10-11 October. The regression in Table 5.7 includes all of these samples [J. Lloyd, personal communication]. In addition, the CSIRO-DAR aircraft conducted automatic flask sampling flights over the OASIS transect on October 24-25 during the day. The regression in Table 5.7 includes the data from the four flights on October 25 [R. Francey and J. Lloyd, personal communication]. In both of these cases the samples were shipped to GASLAB for GC CO_2 analysis and $\delta^{13}CO_2$ analysis by IRMS.

Within the limits of precision of the FTIR $\delta^{13}CO_2$ analysis method, the UoW_{FLASK} regression slope and y-intercept results are the same as those determined by IRMS analysis of the RSBS samples. The RSBS results are, however, reported with a much

higher degree of precision. Both experiments sampled air at the patch-scale within the NBL, within or just above a vegetation canopy consisting overwhelmingly of C3 plants (i.e. triticale crop and lucerne pasture respectively). The similar $\delta^{13}CO_2$ respiration source term inferred by the two methods is understandable and lends support to the validity of the FTIR approach. The CSIRO-DAR samples, on the other hand, were collected during the day by aircraft and so are more a regional-scale probe of isotopic discrimination. The regression line of this data is shallower and has a more positive y-intercept than either of the nocturnal data regressions, to an extent which is statistically significant. One possible source of such a difference is the presence of C4 vegetation at the regional scale. The photosynthetic fractionation by these plants, about -5‰, is much less than for C3 vegetation, -20‰. C4 plants constitute about 5% of total plant biomass and include corn, sugarcane and many grasses. The greater the proportion of total vegetation consisting of C4 plants the more positive will be the regional $\delta^{13}CO_2$ sink/source term.

There are other relevant reports of the isotopic signature of biospheric CO_2 flux processes using the same $\delta^{13}CO_2$ versus inverse CO_2 concentration relationship as above. *Yakir and Wang* [1996], using a 12m tower in a wheat field during the day, estimated the $\delta^{13}CO_2$ signature of the photosynthetic sink process to be -29.4 ‰. An amazon basin study employing nocturnal sampling from a 27m tower in the forest canopy identified a respiration source of CO_2 with $\delta^{13}CO_2$ of -28 ‰ as well as a river degassing CO_2 source with $\delta^{13}CO_2$ of -22 ‰ [*Quay et al.*, 1989]. *Bakwin et al.* [1995], from measurements on a 496m tower in North Carolina, have determined a winter isotopic sink/source signature

of -23.0 ± 0.6 ‰ and a summer signature of -28.1 ± 1.0 ‰, reflecting seasonal differences in biological processes.

5.6 Conclusion

Fourier Transform Infrared Spectroscopy has been deployed *in situ* in a major field campaign to analyse flask samples of air. The CBL profiles obtained provide an account of the development of the CBL, particularly the reproducible structures present in the morning CBL. From these profiles regional fluxes of the important greenhouse gases CO_2, CH_4 and of CO were inferred using CBL budget techniques. The instrument was further applied to the determination of trace gas mixing ratio profiles and fluxes in the surface layer, demonstrating good agreement with alternative techniques. FTIR spectroscopy has also shown its utility as an alternative to isotope ratio mass spectrometry in CO_2 isotope ratio analyses of ambient air. Sampling in the NBL followed by isotopic analysis has allowed the estimation of the isotopic signature of the respiration CO_2 source. Broader application of the methods developed and applied here will contribute towards the characterisation of biosphere-atmosphere fluxes of trace gases. In turn this information will help to close the regional, national and global trace gas budgets.

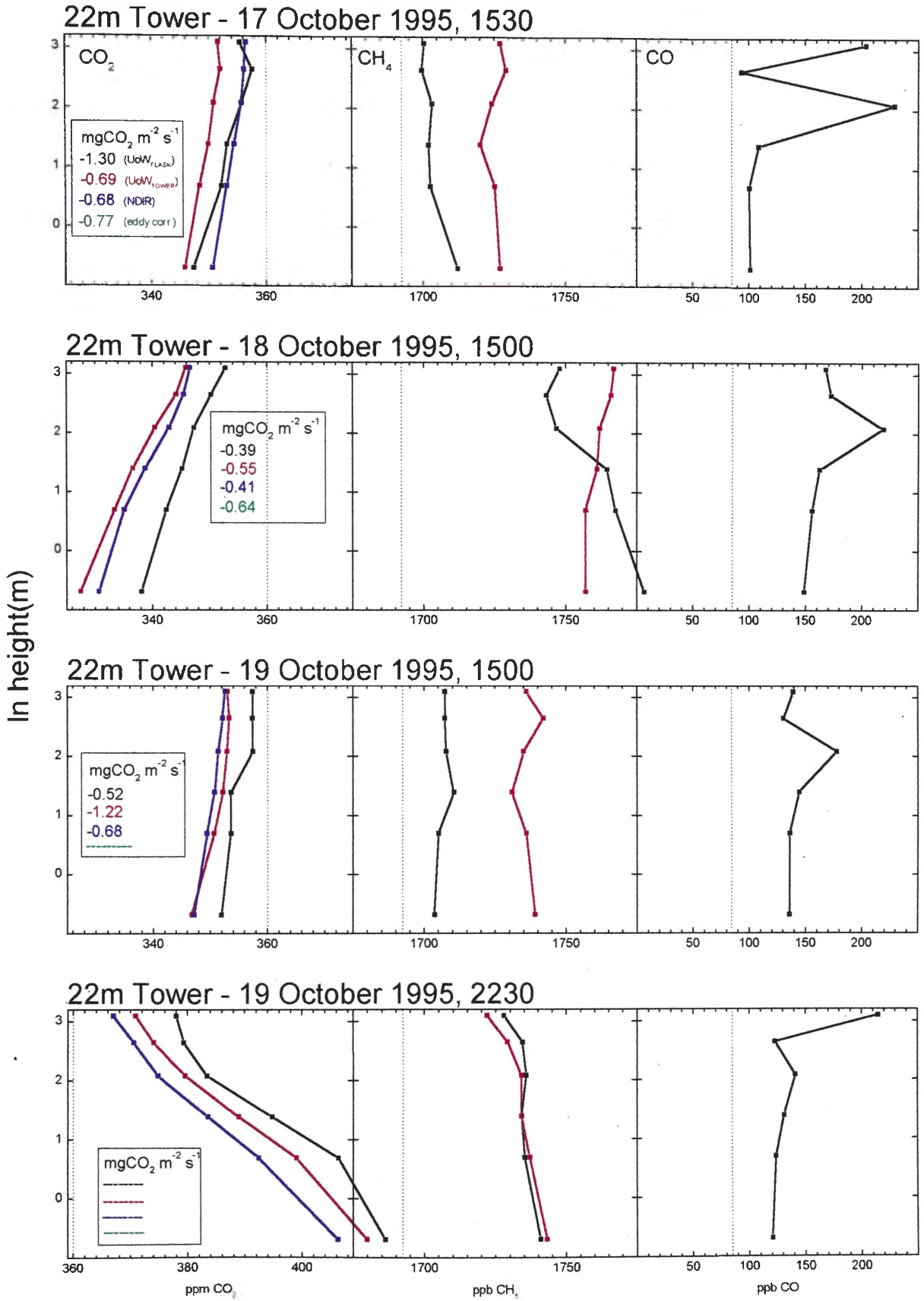
22m Tower - 17 October 1995, 1530
CO2
CH4
CO
mgCO2 m-2 s-1
-1.30 (UoW FLASK)
-0.69 (UoW TOWER)
-0.68 (NDIR)
-0.77 (eddy corr)
22m Tower - 18 October 1995, 1500
mgCO2 m-2 s-1
-0.39
-0.55
-0.41
-0.64
22m Tower - 19 October 1995, 1500
mgCO2 m-2 s-1
-0.52
-1.22
-0.68
22m Tower - 19 October 1995, 2230
mgCO2 m-2 s-1
ln height(m)
ppm CO2
ppb CH4
ppb CO

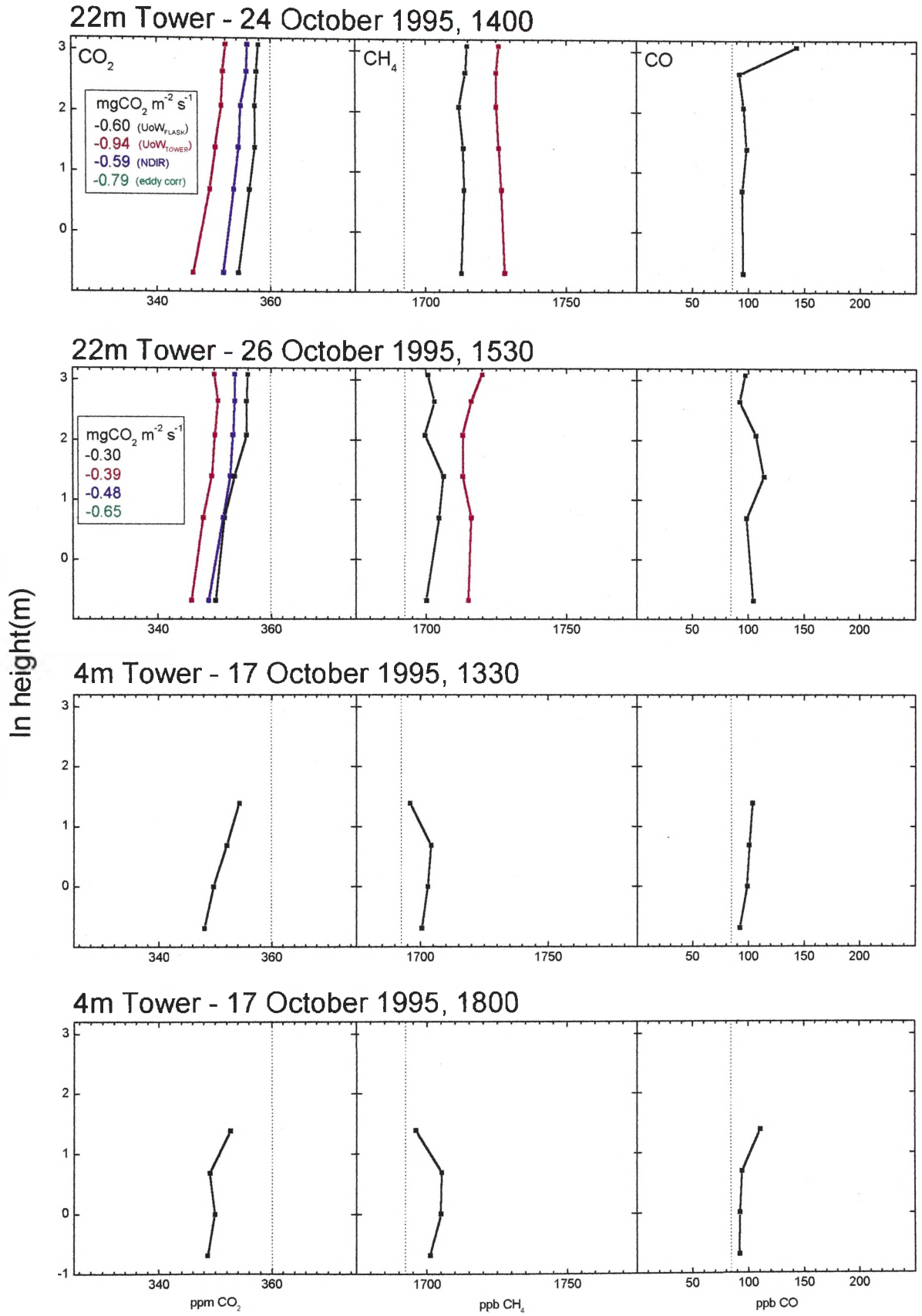

Figure 5.9. All 22m and 4m tower CO_2, CH_4 and CO profiles resulting from FTIR flask analysis on UoW_{FLASK} (in black). Also shown (in red) are the corresponding 22m tower CO_2 and CH_4 profiles resulting from realtime analysis on the UoW_{TOWER} FTIR instrument, and (in blue) the corresponding 22m tower CO_2 profiles from the CSIRO-CEM NDIR instrument. All three instruments were calibrated against a common suite of reference standards. The CO_2 fluxes calculated from the profiles by the flux-gradient method are shown where available. Also shown are the corresponding eddy correlation CO_2 flux measurements.

Chapter 6: Conclusion

The content and foci of Chapters 1 to 5 are somewhat disparate and broad-ranging. In Section 6.1, below, these Chapters are briefly summarised in an attempt to draw them together. Sections 6.2 and 6.3 then derive some general conclusions about both the strengths and the limitations of the FTIR spectroscopic method described in those chapters. Finally, Section 6.4 serves to introduce further applications and developments, both actual and potential, which flow directly from the present work.

6.1 Summary

6.1.1 Chapter 1: Introduction

Since pre-Industrial times the global average atmospheric mixing ratio of CO_2 has grown by 30%, CH_4 by 145%, N_2O by 13%, and CO by an unknown amount, through the activities of humankind. Anthropogenic emissions of these gases has resulted in radiative forcing (by CO_2, CH_4 and N_2O), as well as changes to the oxidative state of the atmosphere (by CO and CH_4) and depletion of stratospheric ozone (by N_2O). These all constitute perturbations to the Earth's atmosphere-climate system, which is in a state of metastable disequilibrium. The probable outcome is a shift in the system accompanied by potentially harmful global climate change.

There are still large uncertainties in the global budgets of CH_4, CO and N_2O. For CO_2, the important question of the relative magnitude of the terrestrial and oceanic sinks remains unanswered. Trace gas mixing ratio and isotope ratio measurements are required to reduce the budget uncertainties and so to constrain projections of models of

future climate. Standard techniques exist to measure the mixing ratios of atmospheric trace gases. For global atmospheric and climate change studies the main trace-gas analytical techniques are:

- CO_2: NDIR or GC
- CH_4, CO, N_2O: GC
- $\delta^{13}CO_2$: IRMS
- TDL techniques for CH_4, CO and N_2O are frequently used for intensive airborne and ground-based field campaigns.

6.1.2 Chapter 2: Experimental Method and Quantitative Analysis

FTIR spectroscopy and its previous atmospheric applications are reviewed briefly. A new method of high precision atmospheric trace gas analysis based on FTIR spectroscopy is described. The main instrumental components of the method are:

- maximisation of spectroscopic signal-to-noise ratio;
- rigorous control and monitoring of sample and spectrometer physical parameters: pressure, temperature, purging;
- optimisation of sample handling through: materials selection, drying, automation.

The main analytical elements are:

- the MALT program which calculates synthetic spectra from the HITRAN database;
- CLS multivariate calibration and prediction algorithm;
- optimal spectral window selection algorithm;

- absolute calibration against standard gases.

In order to achieve maximum precision, several second order effects must be considered:

- limited spectral resolution and Beer-Lambert linearity;
- temperature and pressure differences.

The short term precision of the method is estimated in a series of repeat analyses experiments. For a single analysis of a sample of clean air the precision (as $\pm\sigma$) of the simultaneously retrieved mixing ratios is of the order of:

- $^{12}CO_2$: ±0.01% (±0.04ppm)
- $^{13}CO_2$: ±0.01% (±0.0004ppm)
- CH_4: ±0.1% (±2ppb)
- N_2O: ±0.1% (±0.3ppb)
- CO: ±0.5% (±0.3ppb)
- $\delta^{13}CO_2$: ±0.02% (i.e. ±0.2‰)

In the cases of CO_2, CH_4 and N_2O these are competitive with the more commonly used NDIR and GC techniques. Importantly, for $\delta^{13}CO_2$, this level of precision is geophysically useful and better precision has only ever been achieved before by IRMS.

6.1.3 Chapter 3: Results I: Study of CSIRO-GASLAB Calibration Tanks

CSIRO's GASLAB and its methods and instrumentation for high precision trace gas analysis are reviewed briefly. The issue of calibration of trace gas measurements and the closely related issue of intercalibration across different instruments, methods, laboratories and times is raised. The method described in Chapter 2 is applied to the

analysis of a suite of tanks containing reference standards for air analysis already well characterised by GASLAB. A comparison of the FTIR analyses with the GASLAB analyses yielded the following results:

- The FTIR response function is linear within and well beyond the range of trace gas mixing ratios normally found in air;
- The FTIR technique provided an uncalibrated absolute accuracy within 5% (i.e. without reference to any calibration standards)

Stability of the FTIR instrument and method in a laboratory setting was probed by repeated analysis of an individual air tank over a two week period. Reproducibility of trace gas mixing ratio analysis was described in terms of the standard deviation in the analyses over the two week period:

- $^{12}CO_2$: ±0.19%
- $^{13}CO_2$: ±0.07%
- CH_4: ±0.17%
- CO: ±0.37%
- N_2O: ±0.28%

The same data set also revealed that ratios of mixing ratios could be determined with greater precision than would be predicted from the individual mixing ratios, due to cancellation of some systematic errors when the ratio is taken. For example, using CH_4 as the reference species the following levels of precision were achieved for ratios of mixing ratios over the two week period:

- $^{12}CO_2/CH_4$: ±0.22%

- $^{13}CO_2/CH_4$: ±0.15%
- CO/CH_4: ±0.27%
- N_2O/CH_4: ±0.20%

This method of simultaneous multi-species analysis, calculating ratios of mixing ratios, and using one species as an internal standard may have important ramifications for the propagation and maintenance of reference standards.

The standard deviation over two-weeks in the repeated analyses of the stable isotope ratio, $^{13}CO_2/^{12}CO_2$, suggests that, with calibration, the FTIR technique is of sufficient robustness and stability to provide time series of $\delta^{13}C$ measurements:

- $^{13}CO_2/^{12}CO_2$: ±0.17% (or ±1.7‰)

6.1.4 Chapter 4: Results II: Cape Grim Trace Gas Monitoring by FTIR

The Cape Grim Baseline Air Pollution Station and its operations were introduced briefly. The station's CO_2, CH_4, CO and N_2O monitoring protocols and instrumentation (NDIR, GC-FID, GC-RGD and GC-ECD, respectively) were described. The FTIR instrumental configuration and trace gas monitoring protocol were described for a five week field experiment during which the systems were run in parallel. Subsequent comparison of the parallel trace gas records revealed that the FTIR precision was competitive with that achieved by the normal Cape Grim instrumentation:

	FTIR	NDIR/GC
• CO_2:	0.03%	0.02%
• CH_4:	0.05%	0.05%
• CO:	0.5%	0.7-1.9%

- N_2O: 0.09% 0.2%

During baseline conditions the mean and standard deviation of the difference between the parallel methods indicates a very small systematic offset and a high level of agreement:

- CO_2: 0.02 ± 0.2 ppm
- CH_4: 0.5 ± 1.4 ppb
- CO: 0.6 ± 0.9 ppb
- N_2O: 0.4 ± 0.6 ppb

Correlation of trace gas mixing ratios with wind direction revealed two distinct sources of atmospheric pollution: south eastern mainland Australia to the north and Tasmania to the east of Cape Grim. Estimates of trace gas emission ratios in the easterly and northerly polluted sectors allowed some general conclusions to be drawn regarding the likely nature of the main pollutant sources. The emission ratio results are consistent with the northerly sector being more influenced by urban pollution sources and with the eastern being more influenced by agricultural pollution sources. This chapter also reports the earliest attempt in this work at measuring $\delta^{13}C$ in atmospheric CO_2 by the FTIR method, in this case a five week time series of half-hourly measurements.

6.1.5 Chapter 5: Results III: Trace Gas Flux Measurements by FTIR in the Convective Boundary Layer

The OASIS experiment was described briefly: an intensive month-long field campaign studying biosphere-atmosphere exchange of trace gases, moisture and energy in an inhomogeneous Australian agricultural ecosystem. Standard atmosphere-biosphere

exchange measurement techniques were reviewed briefly. A recently developed method for the estimation of trace gas fluxes on the regional scale was described: the CBL budget method. Some limitations in this method were identified and minor modifications proposed.

The methods by which flask air samples were obtained and subsequently analysed in-the-field for trace gas mixing ratios by FTIR was described. FTIR analysis of the flask samples allowed the construction of a dataset of trace gas vertical profiles, in both the CBL and in the surface layer of the troposphere. Application of the CBL method to the CO_2 vertical profiles and of the modified CBL method to CH_4 vertical profiles allowed the average daytime regional fluxes of these trace gases to be estimated:

- CO_2 flux: $-0.3\ mgCO_2\ m^{-2}\ s^{-1}$
- CH_4 flux: $+0.4\ \mu gCH_4\ m^{-2}\ s^{-1}$

Application of the flux gradient method to trace gas vertical profiles in the surface layer allowed the estimation of daytime and nocturnal CO_2 fluxes from a lucerne pasture. These were compared in a few instances with independently obtained, simultaneous flux-gradient and eddy correlation measurements of CO_2 flux. The different techniques were found to be in general agreement.

In one instance a nocturnal vertical profile of both CO_2 and of $\delta^{13}CO_2$ was obtained by FTIR analysis. This enabled the estimate of the isotopic signature of the CO_2 respired nocturnally by the lucerne pasture. This was consistent with the value obtained independently by IRMS analysis of ground level nocturnal air samples collected at the same site two weeks earlier:

- FTIR: $\delta^{13}C_{V\text{-}PDB} = -25.7 \pm 0.8‰$
- IRMS: $\delta^{13}C_{V\text{-}PDB} = -26.8 \pm 0.14‰$

6.2 Strengths of the FTIR Method

- **High precision:** For CH_4, CO and N_2O, FTIR precision matches or exceeds that currently achieved by the best available GC-based methods. For CO_2, FTIR almost matches the precision attainable by NDIR analysis.
- **Simultaneity:** FTIR allows simultaneous, high precision mixing ratio analysis of the important atmospheric trace gas species $^{12}CO_2$, $^{13}CO_2$, (hence $\delta^{13}CO_2$), CH_4, N_2O and CO.
- **Stable isotope analysis:** FTIR offers a new method of stable carbon isotope analysis at natural abundances with sensitivity and precision exceeded only by IRMS, which is still about an order of magnitude more precise. In addition, there is no need to pre-concentrate or separate CO_2 from the sample of whole air. Hard vacuums and rigorous drying are not required. The FTIR instrument is significantly less complex (and less expensive) than an IRMS.
- **Uncalibrated accuracy:** Without reference to any calibration gases, the FTIR method described in this work typically achieves a trace gas mixing ratio accuracy of around 5%. This makes it much closer to being an absolute technique than either GC or NDIR.
- **Linearity and dynamic range:** Because it explicitly exploits the Beer-Lambert law, the FTIR technique provides a much greater dynamic range and degree of linearity

than is typically achieved using non-spectroscopic trace gas analysis techniques which are often characterised by non-linear response functions.

- **Mobility:** The FTIR method described here relies on a relatively small, robust benchtop spectrometer which is, to some extent, mobile. This has allowed relatively easy deployment of the same instrument at a variety of laboratory and field campaign sites. It can be packed in a day and on relocation was typically installed and operating optimally again within a few days.

- **Non-destructive analysis:** Analysis by FTIR is non-destructive. In principle, further analyses could be carried out on the sample downline from the FTIR instrument.

6.3 Limitations of the FTIR Method

- **Large sample required:** In comparison with most other trace gas analysis techniques the FTIR method requires a large sample. In this work, the samples were typically either 8L.atm or 500ml.atm. For analysis of boundary layer air this is rarely a problem as there is an abundance of analyte. Reference standards, however, are usually expensive, in short supply and must be used frugally. The large sample size is also a problem when air samples need to be retrieved from above the boundary layer. Typically balloon, kite and aircraft payloads limit both the number and size of samples which can be collected.

- **Slow response:** High precision trace gas analysis by FTIR requires averaging times of 1-8 minutes. Other techniques such as NDIR and TDL spectroscopy are virtually instantaneous by comparison and are therefore more suitable for high frequency measurements such as aircraft-mounted experiments or eddy correlation studies.

6.4 Further Work

6.4.1 Atmospheric Trace Gas Mixing Ratio Studies

The present work has given rise to several further applications of FTIR instrumentation in what might be called "mini-baseline station" configurations. These are in various states of planning or execution and have in common that they exploit the simultaneity, sensitivity and mobility of this technique for trace gas analysis in the background atmosphere. In one project already running, CO_2, CO, N_2O and CH_4 are being monitored continuously at a remote site on the north coast of Australia's Northern Territory. The project aims to quantify the pollutant emissions due to biomass burning in tropical savanna ecosystems. Other FTIR trace gas projects at the planning stage include remote site monitoring in northern Europe to better constrain the European CH_4 budget; and a CO_2, CH_4 and N_2O biosphere-atmosphere flux study in New Zealand.

6.4.2 Plant Physiology Studies- Simultaneous δD and $\delta^{13}C$ in Plant Canopy

Preliminary investigations related to the present work have indicated that simultaneous analysis of δD in atmospheric water vapour and $\delta^{13}C$ in atmospheric CO_2 may be possible both in the laboratory and in the field, using a single $1cm^{-1}$ resolution FTIR instrument. It is estimated that precisions of ±1‰ for δD and ±0.2‰ for $\delta^{13}C$ may be achieved. CO_2 and H_2O are centrally involved in plant physiology through both photosynthesis/respiration and transpiration. Knowledge of CO_2 and H_2O mixing ratios with simultaneous $\delta^{13}CO_2$ and δD data, for example in a plant canopy, may provide important information about the soil-plant-atmosphere ecosystem.

6.4.3 High Resolution FTIR Stable Isotope Studies

Preliminary results from theoretical and experimental studies undertaken at the Wollongong laboratory indicate that some of the methods developed in the present work for $\delta^{13}CO_2$ analysis at moderate ($1cm^{-1}$) spectral resolution can be applied to other stable isotopes using high resolution ($0.004cm^{-1}$) FTIR spectroscopy. Species and ratios potentially amenable to quantitative analysis include:

- $\delta^{18}O$ and $\delta^{17}O$ in CO_2
- δD and $\delta^{18}O$ in H_2O
- doubly substituted CO_2 e.g. $^{18}O^{12}C^{17}O$, $^{18}O^{13}C^{16}O$
- $\delta^{13}C$ and δD in CH_4
- $\delta^{13}C$ and $\delta^{18}O$ in CO
- $\delta^{15}N$ and $d^{18}O$ in N_2O
- δD and $\delta^{15}N$ in NH_3
- $\delta^{34}S$ in SO_2
- symmetry isomers of O_3, e.g. $^{16}O^{18}O^{16}O$ and $^{16}O^{16}O^{18}O$

In some cases these analyses are in principle inaccessible to IRMS techniques because the two isotopomers will not be distinguishable by mass. For example $^{16}O^{13}C^{16}O$ and $^{17}O^{12}C^{16}O$ have easily distinguishable infrared spectra. Preliminary experimental work has been undertaken on $\delta^{18}O$ and $\delta^{17}O$ analysis of CO_2 in relation to anomalous stable isotope abundances in stratospheric CO_2. Work has also commenced on high resolution $\delta^{13}C$ and δD analysis in methane, in relation to further restraining the uncertainties in the global methane budget.

6.4.4 Biomedical Applications of FTIR Stable Isotope Analysis

A number of metabolic disorders and infections are currently diagnosed simply and non-invasively by means of isotope ratio analysis of breath samples [*Braden et al.*, 1995; *Mion et al.*, 1995]. For example, *Helicobacter pylori* is a recently discovered bacterium now believed to be responsible for the majority of stomach ulcers and implicated in stomach cancer (see, for example, http://www.helico.com). It dwells in the mucus lining of the stomach and protects itself from stomach acid by excreting a powerful urease enzyme which in turn reacts with food protein to produce ammonia and carbon dioxide. The basic ammonia gives *H. pylori* pH protection. The carbon dioxide rapidly enters the blood stream and is exhaled. Infection with H. Pylori can be diagnosed by ingestion of a small amount of ^{13}C-labelled urea. If the $\delta^{13}C$ of exhaled CO_2 is observed to rise significantly in the 20-30 minutes following ingestion of the ^{13}C-urea, the diagnosis is positive [*Klein and Graham*, 1993]. Similar ^{13}C-labelled substrates are used in breath tests for:

- carbohydrate malabsorption - ^{13}C-labelled sugars
- fat malabsorption - ^{13}C-labelled fats
- bile acid metabolism - ^{13}C-glycoholic acid
- liver function - ^{13}C-aminopyrine

Currently, breath samples must be analysed by IRMS. The complexity and expense of these instruments is limiting access to diagnosis by breath-test techniques. Preliminary studies of breath samples in the Wollongong laboratory indicate that the FTIR instrument can provide these diagnoses quickly and simply.

6.5 Overall Conclusion

A method and an FTIR spectroscopic instrument for gas-phase analysis has been developed which:

- is capable of simultaneous CO_2, CH_4, CO, N_2O and $\delta^{13}CO_2$ analysis;
- offers high precision measurement;
- is compact, robust and mobile.

The instrument has been used for:

- "mini-baseline station" studies of trace gases in the background atmosphere;
- field studies of biosphere-atmosphere exchange of trace gases;
- field and laboratory analysis of $\delta^{13}C$ in atmospheric CO_2.

The methods developed in the present work may be extended to analysis of other stable isotope ratios using both low and high resolution gas-phase FTIR spectroscopy.

Appendix A: 3-Dimensional Plots Representing Precision vs Spectral Window Edges

Refer to Chapter 2, Section 2.3.4 for an explanation of how these surfaces are derived.

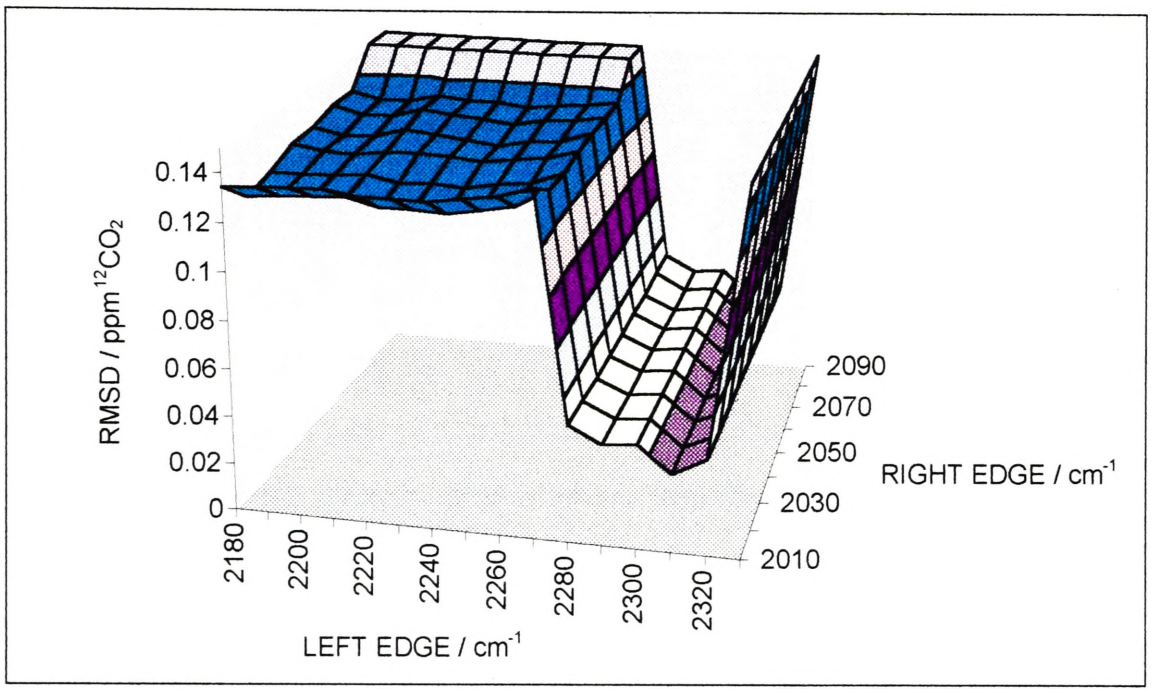

Figure A.1. $^{12}CO_2$ RMSD prediction error vs left and right edges of spectral window. Minimum on surface indicates optimal window edges.

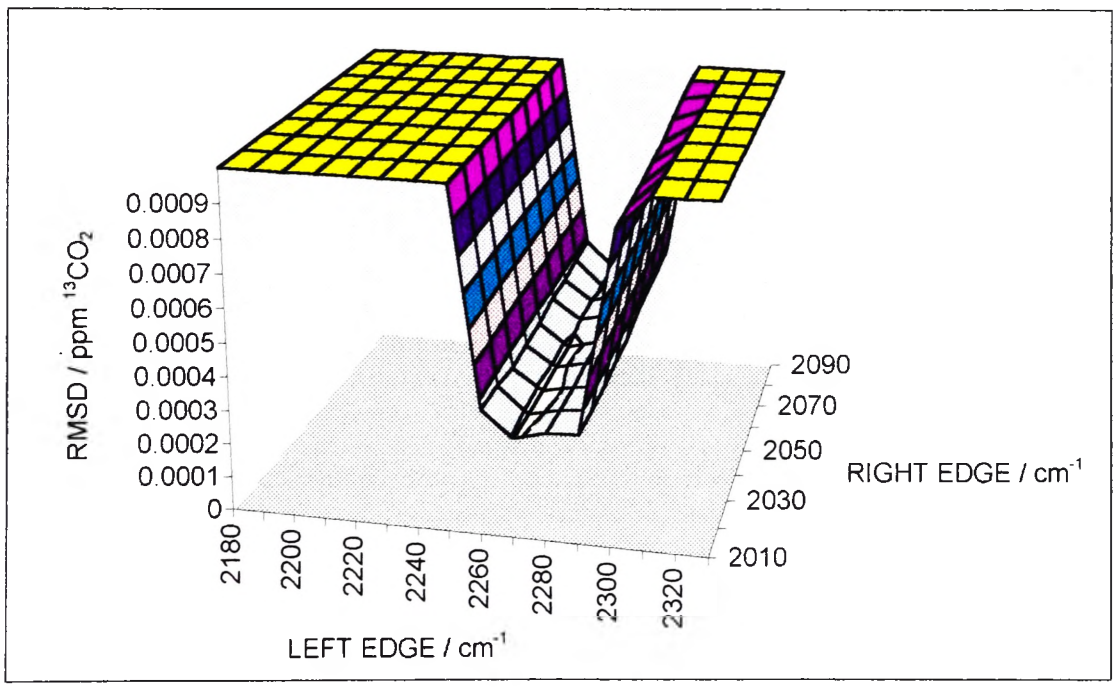

Figure A.2. $^{13}CO_2$ RMSD prediction error vs left and right edges of spectral window. Minimum on surface indicates optimal window edges.

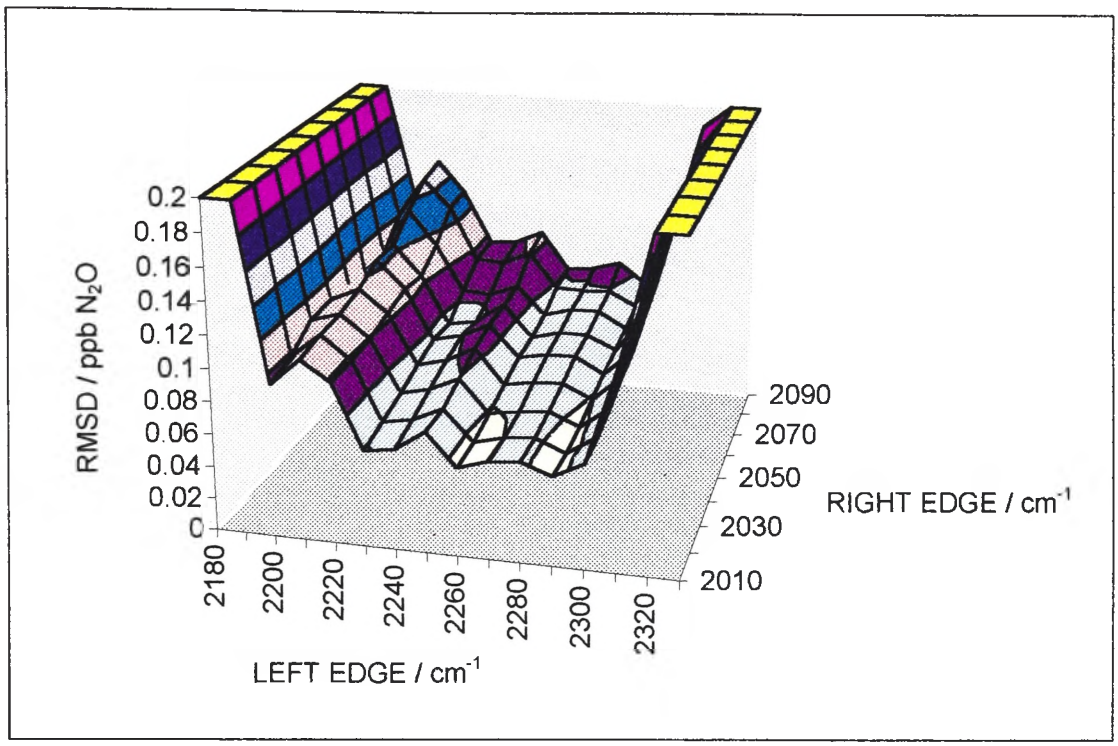

Figure A.3. N_2O RMSD prediction error vs left and right edges of spectral window. Minimum on surface indicates optimal window edges.

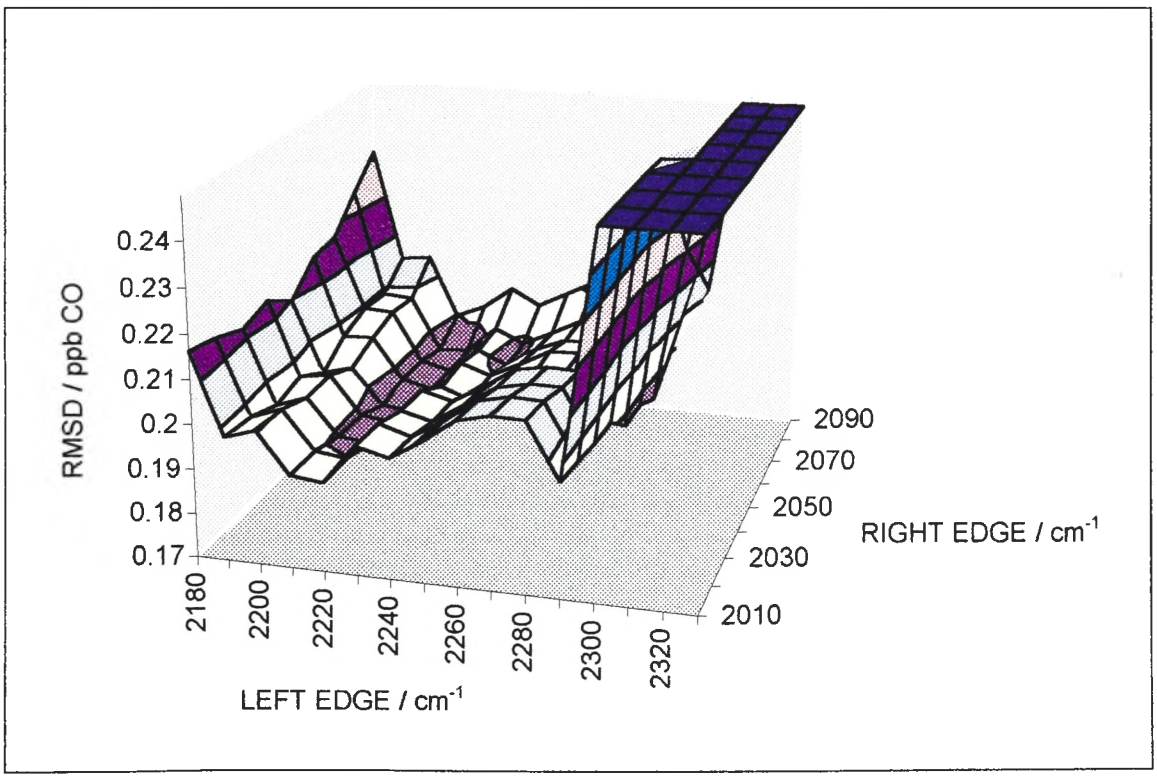

Figure A.4. CO RMSD prediction error vs left and right edges of spectral window. Minimum on surface indicates optimal window edges.

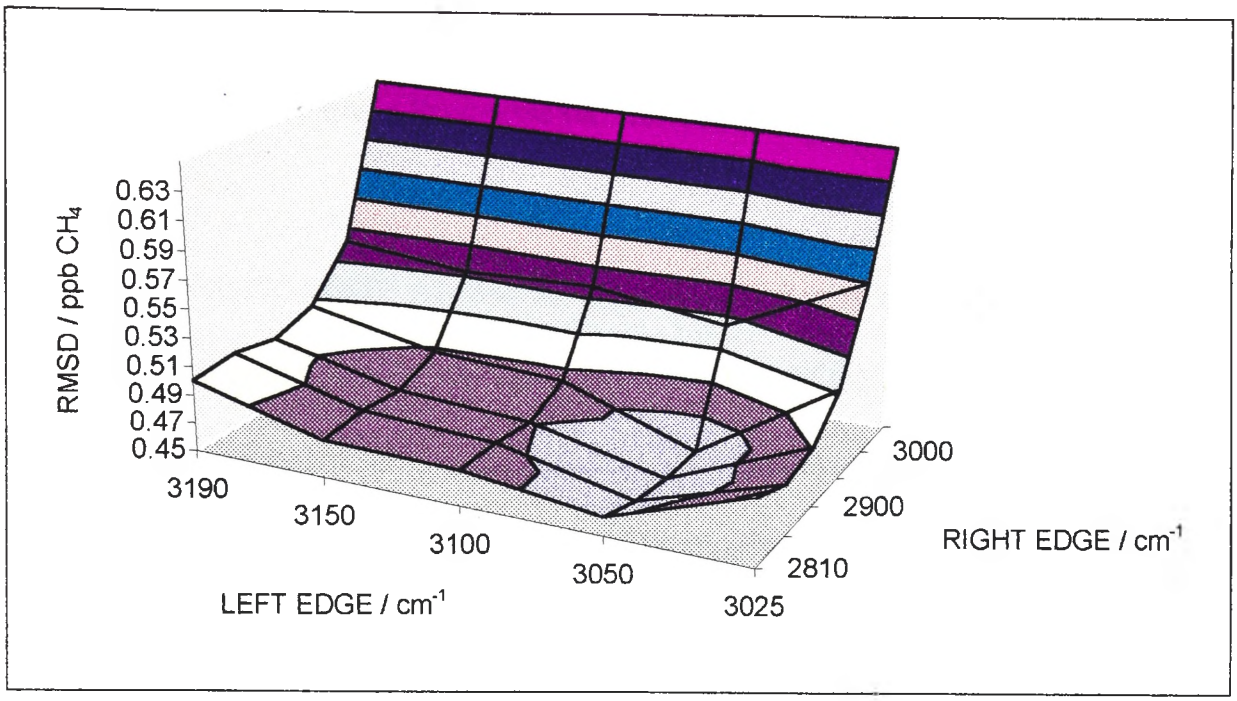

Figure A.5. CH_4 RMSD prediction error vs left and right edges of spectral window. Minimum on surface indicates optimal window edges.

Appendix B: Array Basic Programs for Automation of FTIR Trace Gas Analysis

The program AUTOMATE.AB was the first automation program written in the present work, and was used to control the unattended operation of the FTIR instrument at Cape Grim for continuous half-hourly trace gas and $\delta^{13}CO_2$ analyses of air samples drawn from a sampling line to the ambient atmosphere. The program DEL13.AB automates repeated laboratory based $\delta^{13}CO_2$ analysis of air samples drawn from a pressurised tank. FLASKS.AB facilitates the automated batch analysis of up to 8×2L glass flasks containing atmospheric samples and was used during the OASIS campaign. SUBS.AB contains valve switching and analog input reading subroutines used by all of the programs.

B.1 Array Basic Program AUTOMATE.AB

```
'       ============================================================
'       Program Automate - Controls automatic operation of the MB100
'       to sample air, measure concentrations and log to file.
'       Michael Esler, May 1994.
'       ============================================================

        free
        portout -44,-1                  'enables error messages
        Po=760.0                        'pressure in MALT (torr)
        To=303.3                        'temp in MALT (K)
        temp1i=30.0
        temp2i=30.0
        temp1f=30.0
        temp2f=30.0
        pressi=7.6
        pressf=7.6

        dim comment(80)
        dim memo1(120)
'       dim dirname(40)
        dim fname(40)
        dim logname(40)
'       dim doscomm(80)
'       dim refspc(40)                  'reference spectrum
        DIM CALNAME(40)                 'calibration file used by kp
        dim COCALIB(40)                 'calibration file for CO,N2O,CO2
        dim CH4CALIB(40)                'calibration file for CH4
```

```
'       Establish links to the Strawberry Tree DLL functions
'       ====================================================
        !link #51, "sticall.dll", "StiOpen"
        !link #52, "sticall.dll", "StiClose"
        !link #53, "sticall.dll", "SetDigitalDataInteger"
        !link #54, "sticall.dll", "SetDigitalDataLong"
        !link #55, "sticall.dll", "SetAnalogDataFloat"
        !link #56, "sticall.dll", "SetAnalogDataInteger"
        !link #57, "sticall.dll", "GetDigitalData"
        !link #58, "sticall.dll", "GetAnalogData"
        !link #59, "sticall.dll", "StiCommand"
        !link #60, "sticall.dll", "MaximumAnalogPoints"
'
        !call #51, w{R}=()                              'initializes DLL
'        dialogbeg "StiOpen Return"
'                print "R= ";R
'        dialogend

'       Initialize conditions for analog input channels
'       ===============================================
'       Sets 4 analog input channels, (first element in dig array)
'       Ch1 is for pressure
'       Ch2 is used for RTD room temp sensing
'       Ch3,4 are for RTD cell temperature sensing
        !call #53, (w{4},w{0})
        !call #59, w{R}=("N")

'       Sets the range for each analog input channel.
'       Range 2 = 0-10V for pressure sensor.
'       Range 1003 = 100 Ohm RTD with 20 KOhm set resistor.
        !call #53, (w{2},w{0})
        !call #53, (w{1003},w{1})
        !call #53, (w{1003},w{2})
        !call #53, (w{1003},w{3})
        !call #59, w{R}=("r")

'       Sets all analog inputs to low-noise, highest resolution.
        !call #53, (w{18},w{0})
        !call #59, w{R}=("a")

'       Sets delay in reading analog input channels, 0.03ms x number.
        !call #53, (w{1000},w{0})
        !call #59, w{R}=("d")

'       Initialize conditions for digital input/output channels.
'       ========================================================
'       Sets digital I/O channels to input or output according to
'       values in DLL digital array; 0 for input, 1 for         output.
        !call #53, (w{1},w{0})
        !call #53, (w{1},w{1})
        !call #53, (w{1},w{2})
        !call #53, (w{1},w{3})
        !call #53, (w{1},w{4})
        !call #53, (w{1},w{5})
        !call #53, (w{1},w{6})
        !call #53, (w{1},w{7})
        !call #53, (w{1},w{8})
```

```
        !call #53, (w{1},w{9})
        !call #53, (w{1},w{10})
        !call #53, (w{1},w{11})
        !call #59, w{R}=("S")

'       Ensure all valves and pump switched off
'       ========================================
        chain "subs.ab",1000,(1)                    'closes valve 1 to cell
        chain "subs.ab",1000,(2)                    'closes valve 2 to fast pump
        chain "subs.ab",1000,(3)                    'closes valve 3 to oil pump
        chain "subs.ab",1000,(4)                    'closes valve 4 to dryer line
        chain "subs.ab",1000,(5)                    'turns off fast pump, 5
        chain "subs.ab",1000,(7)                    'closes valve 7 to air inlet
        chain "subs.ab",1000,(8)                    'closes valve 8 to cal gas line

'       Resolution check
'       ================
'        !sdir "c:\mbdata\apr"
        driver 3, "scratch",11,1,4                  '1 scan spc, not displayed
        if {[vres]}=1 goto 5 else goto 2
2       dialogbeg "RESOLUTION ERROR"
                print "VRES is ";{[vres]}
                print "Change to 1cm-1 and restart"
        dialogend
        stop
5       driver "iput nsubs",1                       'resets scanning parameter

        onerror 6                                   'goto 6 if error occurs
        open "O",#4,"automate.def"                  'reads current defaults
'        input #4,"", $dirname
        input #4,"", $fname
        input #4,"", $comment
        input #4,"", $cocalib
        input #4,"", $ch4calib
        input #4, nscan
        input #4, ncycle
        input #4, cycletime
        close #4
        onerror -1

'       Set the parameters for this run
'       ===============================
6       close #4                                    'closes file if error
        onerror 9000
        portout -24,1                               'allows default inputs
        dialogbeg "SET THE PARAMETERS FOR THIS RUN"
'                dialogask $dirname,2,40,40, "directory name (c:\mbdata\***\)"
                dialogask $fname,2,40,40, "file name (mm/dd/yy/##), no extension"
                dialogask $comment,2,40,80, "Comment (<80 char)"
                dialogask $cocalib,2,40,40, "CO Calibration file (.cll)"
                dialogask $ch4calib,2,40,40, "CH4 Calibration file (.cll)"
                dialogask nscan,1,1,256, "Number of scans per spectrum"
                dialogask ncycle,1,1,1000, "Number of cycles"
                cyclest=2*nscan*2.14+80+120+120+240
                print "Estimated minimum cycletime: ";cyclest;" seconds"
                dialogask cycletime,1,1,3600,"Enter cycletime in seconds"
        dialogend
```

```
        open #4,"automate.def"                          'stores last entered values
'        print #4, $dirname
        print #4, $fname
        print #4, $comment
        print #4, $cocalib
        print #4, $ch4calib
        print #4, nscan
        print #4, ncycle
        print #4, cycletime
        close #4

'       Set the Collect parameters
'       ==========================
        driver "iput name",$fname
        driver "iput memo",$comment
        driver "iput scans",nscan
        driver "isetup"                                 'show Instrument/Parameters dialog box

'       Set up .CSV file and output to it
'       =================================
        driver "iget name", fname
        string $logname=$fname + ".csv"
'        ii=index0(logname)
'        string logname(ii-3,ii-1)="csv"
        open "C", #5, $logname
        print #5, "AUTOMATE.AB output for ";$logname," ";
        print @2
        print #5, "Date: ";clock(-5);"-";clock(-6);"-";clock(-7)
        print @6
        print #5, $comment
        print #5, "Calibration file for CO N2O CO2: ";$cocalib
        print #5, "Calibration file for CH4: ";$CH4calib
'        print #5, "Reference spectrum for absorbance: ";$refspc
        print #5, " "
        print #5, "";",";"Spectrum,";"time,";"[H2O],";"[CO2],";"[N2O],";"[CO],";
        print #5, "BOFF,";"BSLOPE,";"COresid,";
        print #5, "[H2O],";"[CH4],";"BOFF,";"BSLOPE,";"CH4RESID,";
        print #5, "P avg,";"T avg,";"P init,";"P final,";
        print #5, "T1 init,";"T2 init,";"T1 final,";"T2 final,";"T Room,"
        close #5

'       Set up timing
'       =============
        ispec=0
        count=0                                         'cycle counter
        CALCOUNT=1                                      'calibration frequency counter
300     if count>=ncycle goto 9000
        ispec=ispec+1                                   'multifile label counter
        time=clock(0)                                   'seconds since midnight
        starttime=(int(time/cycletime)+1)*cycletime
        if starttime >= 86400 then starttime=0          'reset at midnight
        shour=int(starttime/3600)
        sminute=int(int(starttime-shour*3600)/60)
        ssecond=starttime-shour*3600-sminute*60
        blank
        print @2
        pauseoff
```

```
        printline 12
        print "Waiting for next cycle to begin"
'       print "Is there a floppy in the A: drive????"
        printline 24
        print "Start time  : ";shour;":";sminute;":";ssecond

        if starttime=0 goto 307                                 'midnight condition
305     time=clock(0)
        if time>=starttime goto 350
        hour=clock(-4)
        minute=clock(-3)
        second=clock(-2)
        print "Current time: ";hour;":";minute;":";second
306     if not(clock(1)) goto 306
        goto 305

'       At midnight set up new output file and update spectrum name
'       ===========================================================
307     time=clock(0)
        if time<cycletime goto 309                                  'just after midnight
        hour=clock(-4)
        minute=clock(-3)
        second=clock(-2)
        print "Current time: ";hour;":";minute;":";second
308     if not(clock(1)) goto 308
        goto 307

309     close #5                                    'this closes the .csv output file at the end of day
'       onerror 320
'       string $doscomm = "command.com /c copy " + $dirname + $logname + " a:"
'       dos $doscomm
'       onerror -1
320     day=clock(-5)
        month=clock(-6)
        year=(clock(-7))-1900
        fname=0
        if month=1 then  string $fname="ja"
        if month=2 then  string $fname="fe"
        if month=3 then  string $fname="mr"
        if month=4 then  string $fname="ap"
        if month=5 then  string $fname="my"
        if month=6 then  string $fname="jn"
        if month=7 then  string $fname="jl"
        if month=8 then  string $fname="au"
        if month=9 then  string $fname="se"
        if month=10 then string $fname="oc"
        if month=11 then string $fname="no"
        if month=12 then string $fname="de"
        if day<10 then string $fname=$fname+"0"+day
        if day>9 then string $fname=$fname+day
        string $fname=$fname+year
        string $fname=$fname+"01"
        driver "iput name", $fname
        ispec=1
        calcount=1


'       dialogbeg
```

```
'               print $fname
'        dialogend
         string $logname=$fname + ".csv"
'        stop
         open "C", #5, $logname
         print #5, "AUTOMATE.AB output for ";$logname," ";
         print @2
         print #5, "Date: ";clock(-5);"-";clock(-6);"-";clock(-7)
         print @6
         print #5, $comment
         print #5, "Calibration file for CO N2O CO2: ";$cocalib
         print #5, "Calibration file for CH4: ";$CH4calib
'        print #5, "Reference spectrum for absorbance: ";$refspc
         print #5, " "
         print #5, "";",";"Spectrum,";"time,";"[H2O],";"[CO2],";"[N2O],";"[CO],";
         print #5, "BOFF,";"BSLOPE,";"COresid,";
         print #5, "[H2O],";"[CH4],";"BOFF,";"BSLOPE,";"CH4RESID,";
         print #5, "P avg,";"T avg,";"P init,";"P final,";
         print #5, "T1 init,";"T2 init,";"T1 final,";"T2 final,";"T Room,"
         close #5

350      hour=clock(-4)
         minute=clock(-3)
         second=clock(-2)

'        Take Empty Cell Reference Spectrum
'        ==================================
         driver "iget name", fname
'        strname 0, $fname= ${[qname]},spc,-1              'updates spectrum name

         memo1=0
         string $memo1 = "Last [CO]= " + int(CO)
         string $memo1 = $memo1 + " [H2Oa]= " + int(H2Oa)
         string $memo1 = $memo1 + " [H2Ob]= " + int(H2Ob)
         string $memo1 = $memo1 + " [CH4]= " + int(CH4)
         string $memo1 = $memo1 + " [N2O]= " + int(N2O)
         string $memo1 = $memo1 + " [CO2]= " + int(CO2)
         string $memo1 = $memo1 + " Press= " + int(pressavg)
         driver "iput memo", $memo1              'displays last retrieved concentrations on screen
         driver 1,$fname                         'collects a single beam reference, and saves it.
         savespc "refspc"
         savespc $fname, #ispec
'        string $refspc = $fname

'        Fill Cell and read initial T and P
'        ==================================
'        Cell empty and all valves closed at this stage
         if calcount=1 goto 1000                          'run calibration sample
         chain "subs.ab",1050,(1)                         'opens valve 1 to cell
         chain "subs.ab",1050,(7)                         'opens valve 7 to dryer line
         chain "subs.ab",1050,(4)                         'opens valve 4 to fill cell
'        Allow 140 seconds to fill cell
         time=clock(0)
400      if not(clock(140)) then 400                      'waits 140 seconds

         chain "subs.ab",1000,(4)                         'closesvalve 4to stop fill
         chain "subs.ab",1000,(1)                         'closes valve 1 to cell
         chain "subs.ab",1000,(7)                         'closes valve 7 to dryer line
```

```
'
'       Wait 120 sec before reading P,T initial values
405     time=clock(0)
410     if not(clock(120)) then 410
'
        chain "subs.ab",1100,(1,pressi)                 'reads analog channel 1, pressure
        chain "subs.ab",1100,(3,temp1i)                 'reads analog channel 3, temperature
        chain "subs.ab",1100,(4,temp2i)                 'reads analog channel 4, temperature
        chain "subs.ab",1100,(2,rtemp)                  'reads analog channel 2, room temp

'       Updates spectrum name and memo for display
'       ==========================================
'       driver "iget name", fname
'       strname 0, $fname= ${[qname]},spc,-1

'       Takes spectrum of sample
'       ========================
        driver 1,$fname                         'collects a single beam spectrum, and saves it.
                                                'this is old syntax for driver.
        Savespc "sample"
        ispec=ispec+1
        savespc  $fname, #ispec

'       Reads final T and P
'       ===================
        chain "subs.ab",1100,(1,pressf)                 'reads analog channel 1, pressure
        chain "subs.ab",1100,(3,temp1f)                 'reads analog channel 3, temperature
        chain "subs.ab",1100,(4,temp2f)                 'reads analog channel 4, temperature

'       Computes absorbance spectrum, does fits and calcs avg T and P
'       ============================================================
        pressavg=100*(pressi+pressf)/2
        tempavg=(temp1i+temp2i+temp1f+temp2f+2*1.35+2*1.55)/4
        tempavg=tempavg+273.15
        rtemp=rtemp+1.2
'               RTD B correction: +1.35C
'               RTD C correction: +1.55C
'               RTD A correction: +1.2C

        #2=absorb(#1,#2)                                'computes abs spectrum with current
background
        noshow
        STRING CALNAME=$COCALIB
        chain "kp"                                      'calls predict routine
        H2Oa=Po/pressavg*tempavg/To*Yn(0)
        CO2=Po/pressavg*tempavg/To*Yn(1)
        N2O=Po/pressavg*tempavg/To*Yn(2)
        CO=Po/pressavg*tempavg/To*Yn(3)
        BOFFa=Yn(4)
        BSLOPEa=Yn(5)
        coresid=rmsres

        noshow
        noshow
        noshow

        STRING CALNAME=$CH4CALIB
        loadspc "sample"
```

```
        loadspc "refspc"
        #2=absorb(#2,#1)
        noshow
        chain "kp"                                          'calls predict routine
        H2Ob=Po/pressavg*tempavg/To*Yn(0)
        CH4=Po/pressavg*tempavg/To*Yn(1)
        BOFFb=Yn(2)
        BSLOPEb=Yn(3)
        ch4resid=rmsres

        noshow
        noshow
        noshow

'       ii=index0(fname)
        print @6
        open "O", #5, $logname
        seek #5, -0                                         'go to end of file
        print #5, "";",";$fname;"#";ispec;",";hour;":";minute;",";
        print #5, H2Oa;",";CO2;",";N2O;",";CO;",";BOFFa;",";BSLOPEa;",";CORESID;",";
        print #5, H2Ob;",";CH4;",";BOFFb;",";BSLOPEb;",";CH4RESID;",";
        print #5, pressavg;",";tempavg;",";(100*pressi);",";(100*pressf);",";
        print #5, temp1i;",";temp2i;",";temp1f;",";temp2f;",";rtemp
        close #5

'       Empties cell
'       ============
430     chain "subs.ab",1050,(2)                            'opens valve 2 to fast pump cell
        chain "subs.ab",1050,(1)                            'opens valve 1 to fast pump line
        chain "subs.ab",1050,(5)                            'switches on fast pump
'       Allow 100 seconds to pump cell from 760t to ~80t
        time=clock(0)
440     if not(clock(100)) then     440                     'waits 100 seconds

        chain "subs.ab",1000,(2)                            'closes valve 2 to fast pump
        chain "subs.ab",1000,(5)                            'switches off fast pump
        chain "subs.ab",1050,(3)                            'opens valve 3 to oil pump
'       Allow 240 seconds for pumping from ~80t   to <10t
        time=clock(0)
460     if not(clock(240)) then 460                         'waits 240 seconds

        chain "subs.ab",1000,(1)                            'closes valve 1 to cell
        chain "subs.ab",1000,(3)                            'closes valve 3 to oil pump

        count = count+1
        calcount = calcount+1
        goto 300

'       Fill Cell with Calibration Gas
'       ==============================
'       Cell empty and all valves closed at this stage
1000    chain "subs.ab",1050,(1)                            'opens valve 1 to cell
        chain "subs.ab",1050,(8)                            'opens valve 8 to cal gas line
'       Fill cell to ~760t
1010    chain "subs.ab",1100,(1,presscal)                   'reads analog channel 1, pressure
        if presscal<7.73 goto 1010
        chain "subs.ab",1000,(8)                            'closes valve 8 to stop fill
        chain "subs.ab",1000,(1)                            'closes valve 1 to cell
```

```
        calcount=0
        goto 405
'

9000    !call #52, w{R}=()                          'closes DLL
        close #5
        chain "subs.ab",1000,(1)                    'closes valve 1 to cell
        chain "subs.ab",1000,(2)                    'closes valve 2 to fast pump
        chain "subs.ab",1000,(3)                    'closes valve 3 to oil pump
        chain "subs.ab",1000,(4)                    'closes valve 4 to air inlet
        chain "subs.ab",1000,(5)                    'turns off fast pump, 5
        chain "subs.ab",1000,(7)                    'closes valve 7 to dryer line
        chain "subs.ab",1000,(8)                    'closes valve 8 to cal gas line
        DIALOGBEG "AUTOMATE.AB PROGRAM"
                PRINT "THE PROGRAM HAS FINISHED"
        DIALOGEND
        stop
```

B.2 Array Basic Subroutines SUBS.AB

```
'================================================
'This file, subs.ab, contains a number of subroutines which are called
'from a master program to perform basic tasks such as switching a
'valve using digital output or reading a single analog input channel.
'Michael Esler, May 1994
'================================================
'
'
'This subroutine closes a valve by setting a digital output to 0.
1000    procedure vclose
        !mov v=&(vclose-1)
        !call #53, (w{0},w{v})
        !call #59, ("O")
        return
'
'
'This subroutine opens a valve by setting a digital output to 1.
1050    procedure vopen
        !mov v=&(vopen-1)
        !call #53, (w{1},w{v})
        !call #59, ("O")
        return
'
'
'This subroutine reads a single analog input channel once
1100    procedure anread,chan
        !mov a=&(anread)
        !call #53, (w{a},w{0})
        !call #59, w{R}=("h")
        !ptr q=%m(#2)              'sets pointer to start of block
'
'
'Puts the DLL analog array into the #2 memory block.
        !call #58, (&{@qx}, w{1})
'
'
'Reads the first 32-bit float element of memory block #2.
        !ptr q=%m(#2)
        chan={@qx}
        return
```

B.3 Array Basis Program DEL13.AB

```
'       ============================================================
'       Program del13.ab - Controls automatic operation of the MB100
'       to sample air, measure concentrations and log to file.
'       Specifically, this is used to repeatedly sample from a calib
'       tank to determine precision of del13 measurement.
'       Michael Esler, January 1996.
'       ============================================================

        free
        portout -44,-1                          'enables error messages

        dim comment(80)
        dim memo1(120)
        dim fname(40)
        dim logname(40)
        DIM CALNAME(40)                         'calibration file used by kp
        dim C12CALIB(40)                        'calibration file for C12-CO2
        dim C13CALIB(40)                        'calibration file for C13-CO2

'       Establish links to the Strawberry Tree DLL functions
'       ====================================================
        !link #51, "sticall.dll", "StiOpen"
        !link #52, "sticall.dll", "StiClose"
        !link #53, "sticall.dll", "SetDigitalDataInteger"
        !link #54, "sticall.dll", "SetDigitalDataLong"
        !link #55, "sticall.dll", "SetAnalogDataFloat"
        !link #56, "sticall.dll", "SetAnalogDataInteger"
        !link #57, "sticall.dll", "GetDigitalData"
        !link #58, "sticall.dll", "GetAnalogData"
        !link #59, "sticall.dll", "StiCommand"
        !link #60, "sticall.dll", "MaximumAnalogPoints"
'
        !call #51, w{R}=()                      'initializes DLL
'       dialogbeg "StiOpen Return"
'               print "R= ";R
'       dialogend
        !call #59, w{R}=("c")                   'calibrates Mini-16 board analog inputs
with Temp

'       Initialize conditions for analog input channels
'       ===============================================
'       Sets 4 analog input channels, (first element in dig array)
'       Ch1 is for pressure
'       Ch2 is used for RTD room temp sensing
'       Ch3,4 are for RTD cell temperature sensing
        !call #53, (w{4},w{0})
        !call #59, w{R}=("N")

'       Sets the range for each analog input channel.
'       Range 2 = 0-10V for pressure sensor.
'       Range 1003 = 100 Ohm RTD with 20 KOhm set resistor.
        !call #53, (w{2},w{0})
        !call #53, (w{1003},w{1})
```

```
        !call #53, (w{1003},w{2})
        !call #53, (w{1003},w{3})
        !call #59, w{R}=("r")

'       Sets all analog inputs to low-noise, highest resolution.
        !call #53, (w{18},w{0})
        !call #59, w{R}=("a")

'       Sets delay in reading analog input channels, 0.03ms x number.
        !call #53, (w{1000},w{0})
        !call #59, w{R}=("d")

'       Initialize conditions for digital input/output channels.
'       ========================================================
'       Sets digital I/O channels to input or output according to
'       values in DLL digital array; 0 for input, 1 for output.
        !call #53, (w{1},w{0})
        !call #53, (w{1},w{1})
        !call #53, (w{1},w{2})
        !call #53, (w{1},w{3})
        !call #53, (w{1},w{4})
        !call #53, (w{1},w{5})
        !call #53, (w{1},w{6})
        !call #53, (w{1},w{7})
        !call #53, (w{1},w{8})
        !call #53, (w{1},w{9})
        !call #53, (w{1},w{10})
        !call #53, (w{1},w{11})
        !call #59, w{R}=("S")

'       Ensure all valves and pump switched off
'       =======================================
        chain "subs.ab",1000,(1)                    'closes valve 1 to flask
        chain "subs.ab",1000,(2)                    'closes valve 2 to flask
        chain "subs.ab",1000,(3)                    'closes valve 3 to flask
        chain "subs.ab",1000,(4)                    'closes valve 4 to flask
        chain "subs.ab",1000,(5)                    'closes valve 5 to flask
        chain "subs.ab",1000,(6)                    'closes valve 6 to flask
        chain "subs.ab",1000,(7)                    'closes valve 7 to flask
        chain "subs.ab",1000,(8)                    'closes valve 8 to flask
        chain "subs.ab",1000,(9)                    'closes valve 9 to calib gas line
        chain "subs.ab",1000,(10)                   'closes valve 10 to oil pump
        chain "subs.ab",1000,(11)                   'closes valve 11 to White cell
        chain "subs.ab",1000,(12)                   'closes valve 12 to slow pumping

'       Resolution check
'       ================
        driver 3, "scratch",11,1,4                  '1 scanspc, not displayed
        if {[vres]}=1 goto 5 else goto 2
2       dialogbeg "RESOLUTION ERROR"
                print "VRES is ";{[vres]}
                print "Change to 1cm-1 and restart"
        dialogend
        stop
5       driver "iput nsubs",1                       'resets scanning parameter

'       Read default settings from del13.def file
'       =========================================
```

```
        onerror 6                                       'goto 6 if error occurs
        open "O",#4,"del13.def"                         'reads current defaults
        input #4,"", $fname
        input #4,"", $comment
        input #4,"", $c12calib
        input #4,"", $C13calib
        input #4, nscan
        input #4, nbatch
        close #4
        onerror -1

'       Set the parameters for this run
'       ===============================
6       close #4                                        'closes file if error
        onerror 9000
        portout -24,1                                   'allows default inputs
        dialogbeg "SET THE PARAMETERS FOR THIS BATCH OF REPEATS"
                dialogask $fname,2,40,40, "file name (mm/dd/yy/##), no extension"
                dialogask $comment,2,40,80, "Comment (<80 char)"
                dialogask $c12calib,2,40,40, "C12-CO2 Calibration file (.cll)"
                dialogask $C13calib,2,40,40, "C13-CO2 Calibration file (.cll)"
                dialogask nscan,1,1,256, "Number of scans per spectrum"
                dialogask nbatch,1,1,40, "Number of repeats in this batch"
        dialogend


        open #4,"del13.def"                             'stores last entered values
        print #4, $fname
        print #4, $comment
        print #4, $c12calib
        print #4, $c13calib
        print #4, nscan
        print #4, nbatch
        close #4


        if nbatch <= 40 goto 100
        dialogbeg "Too many repeats"
                print "40 is the maximum number of repeat injections"
                print "Start again"
        dialogend
        goto 9000

'       Set the Collect parameters
'       ==========================
100     driver "iput name",$fname
        driver "iput memo",$comment
        driver "iput scans",nscan
        driver "isetup"                                 'show Instrument/Parameters dialog box

'       Set up .CSV file and output to it
'       =================================
        driver "iget name", fname
        string $logname=$fname + ".csv"
        open "C", #5, $logname
        print #5, "del13.AB output for ";$logname," ";
        print @2
        print #5, "Date: ";clock(-5);"-";clock(-6);"-";clock(-7)
```

```
        print #5, "Time: ";clock(-4);":";clock(-3)
        print @6
        print #5, $comment
        print #5, "Calibration file for C12-CO2 : ";$c12calib
        print #5, "Calibration file for C13-CO2 : ";$c13calib
        print #5, " "
        print #5, "";",";"Spectrum,";"Time,";"[C12-CO2],";"[C13-CO2],";"C12RESID,";"C13RESID,";
        print #5, "P avg,";"T avg,";"P init,";"P final,";
        print #5, "T1 init,";"T2 init,";"T1 final,";"T2 final,";"T Room,"
        close #5


'       Pump out cell and manifold
'       ==========================
        chain "subs.ab",1050,(10)                       'opens valve 10 to pump
        !wait 36                                        'wait 2 seconds
        chain "subs.ab",1050,(11)                       'opens valve 11 to cell
        !wait 36                                        'wait 2 seconds
        dialogbeg "PUMPING DOWN CELL AND MANIFOLD"
                print "Press OK when the P < 0.1torr on Edwards gauge"
        dialogend

'       Main Loop Control for CALIB samples
'       ===================================
        fcount=1                                        'repeat counting variable
        ispec=0
300     dialogbeg "del13.AB STATUS"
                dialogloc 1,0
                print "Current Spectrum"
                print "================"
                print "Run Name:         "; $fname
                print "Number of repeats: "; nbatch
                print "Current repeat:    "; fcount
                print " "
                print "Last Spectrum"
                print "============="
                print "[C12-CO2]  = ";C12;" ppm"
                print "[C13-CO2] = ";C13;" ppm"
                print "Press = ";pressavg;" torr"
        dialogend 22
        if fcount>nbatch goto 9000

'       Take Empty Cell Reference Spectrum
'       ==================================
'       At this stage the cell is still being pumped through valves 10 and 11
        driver "iget name", fname
'        driver 1,$fname                                'collects a single beam reference, and
saves it.
'        savespc "refspc"
'        ispec=ispec+1
'        savespc $fname, #ispec                         'refspc is also appended to the multifile
'        noshow
'        noshow

'       Fill Cell with Calibration Gas for analyses at 760 torr
'       =======================================================
'       Cell empty and valves 10 and 11 open at this stage pumping on cell
        chain "subs.ab",1000,(10)                       'closes valve 10 to pump
```

```
        !wait 18                                    'waits 1 second
        chain "subs.ab",1050,(9)                    'opens valve 9 to cal gas line
'       Fill cell to ~780t
310     chain "subs.ab",1100,(1,presscal)           'reads analog channel 1, pressure
        if presscal<7.80 goto 310
        chain "subs.ab",1000,(9)                    'closes valve 9to stop fill
        chain "subs.ab",1000,(11)                   'closes valve 11 to cell
        !wait 360                                   'wait 20 seconds

        chain "subs.ab",1050,(10)                   'opens valve 10 to pump
        !wait 18                                    'waits 1 second
        chain "subs.ab",1050,(12)                   'opens valve 12 to small orifice in line
'       Pump down to ~760t
315     chain "subs.ab",1100,(1,presscal)           'reads analog channel 1, pressure
        if presscal>7.60 goto 315
        chain "subs.ab",1000,(12)                   'closes valve 12 to stop emptying
        chain "subs.ab",1000,(10)                   'closes valve 10 to pump

'       Wait 60 sec before reading P,T initial values
        time=clock(0)
340     if not(clock(60)) then 340
'
        chain "subs.ab",1100,(1,pressi)             'reads analog channel 1, pressure
        chain "subs.ab",1100,(3,temp1i)             'reads analog channel 3, temperature
        chain "subs.ab",1100,(4,temp2i)             'reads analog channel 4, temperature
        chain "subs.ab",1100,(2,rtemp)              'reads analog channel 2, room temp

'       Takes spectrum of sample
'       ========================
        driver 1,$fname                             'collects a single beam spectrum, and
saves it.
                                                    'this is old syntax for driver.
        savespc "sample"
        ispec=ispec+1
        savespc  $fname, #ispec                     'append sample spectrum to multifile

        noshow
        noshow
        noshow

'       Reads final T and P
'       ===================
        chain "subs.ab",1100,(1,pressf)             'reads analog channel 1, pressure
        chain "subs.ab",1100,(3,temp1f)             'reads analog channel 3, temperature
        chain "subs.ab",1100,(4,temp2f)             'reads analog channel 4, temperature

'       Computes absorbance spectrum, does fits and calcs avg T and P
'       ============================================================
        pressavg=100*(pressi+pressf)/2
        tempavg=(temp1i+temp2i+temp1f+temp2f+2*1.0+2*0.3)/4
        tempavg=tempavg+273.15
        rtemp=rtemp+1.25
'               RTD B correction: +1.0C
'               RTD C correction: +0.3C
'               RTD A correction: +1.25C

'       loadspc "sample"
'       loadspc "refspc"
```

```
'       #2=absorb(#2,#1)                                    'computes abs spectrum with current
background
'       noshow

'       STRING CALNAME=$C12CALIB
'       chain "kp"                                          'calls predict routine
'       C12=Yn(0)
'       C12RESID=RMSRES

'       noshow
'       noshow
'       noshow
'       noshow

'       STRING CALNAME=$C13CALIB
'       loadspc "sample"
'       loadspc "refspc"
'       #2=absorb(#2,#1)
'       noshow
'       chain "kp"                                          'calls predict routine
'       C13=Yn(1)
'       C13resid=rmsres

        noshow
        noshow
        noshow
        noshow

        print @6
        open "O", #5, $logname
        seek #5, -0                                         'go to end of file
        print #5, "";",";$fname;"#";ispec;",";clock(-4);":";clock(-3);",";
        print #5, C12;",";C13;",";C12RESID;",";C13RESID;",";
        print #5, pressavg;",";tempavg;",";(100*pressi);",";(100*pressf);",";
        print #5, temp1i;",";temp2i;",";temp1f;",";temp2f;",";rtemp
        close #5

'       Empties cell
'       ============
430     chain "subs.ab",1050,(10)                           'opens valve 10 to pump
        chain "subs.ab",1050,(11)                           'opens valve 11 to cell

'       Allow 240 seconds for pumping from ~450t to <1t
        time=clock(0)
460     if not(clock(240)) then 460                         'waits 240 seconds
        fcount = fcount+1
        if fcount > nbatch goto     9000
        dialogend -20                                       'deletes status dialog box
        goto 300

'       Finishing Off
'       =============
9000    close #5                                            'ensures .csv file closed
        for i=1   to 12                                     'closes all valves
                  chain "subs.ab",1000,(i)                  'closes valve i
                  !wait 18                                  'wait 1 second
        next
        !call #52, w{R}=()                                  'closes DLL
```

```
dialogend -20                                    'closes status dialog box
DIALOGBEG "del13.AB PROGRAM"
        PRINT "THE PROGRAM HAS FINISHED"
DIALOGEND
stop
```

B.4 Array Basic Program FLASKS.AB

```
'       ============================================================
'       Program Flasks - Controls automatic operation of the MB100
'       to sample air, measure concentrations and log to file.
'       Specifically, this is used to measure a batch of 2L flasks
'       filled to ambient pressure, e.g. OASIS flask samples.
'       Michael Esler, September 1995.
'       ============================================================

        free
        portout -44,-1                          'enables error messages

        dim comment(80)
        dim memo1(120)
        dim f1comm(80)
        dim f2comm(80)
        dim f3comm(80)
        dim f4comm(80)
        dim f5comm(80)
        dim f6comm(80)
        dim f7comm(80)
        dim f8comm(80)
        dim fname(40)
        dim logname(40)
        DIM CALNAME(40)                         'calibration file used by kp
        dim COCALIB(40)                         'calibration file for CO
        dim N2OCALIB(40)                        'calibration file for N2O
        dim CO2CALIB(40)                        'calibration file for CO2
        dim CH4CALIB(40)                        'calibration file for CH4

'       Establish links to the Strawberry Tree DLL functions
'       ====================================================
        !link #51, "sticall.dll", "StiOpen"
        !link #52, "sticall.dll", "StiClose"
        !link #53, "sticall.dll", "SetDigitalDataInteger"
        !link #54, "sticall.dll", "SetDigitalDataLong"
        !link #55, "sticall.dll", "SetAnalogDataFloat"
        !link #56, "sticall.dll", "SetAnalogDataInteger"
        !link #57, "sticall.dll", "GetDigitalData"
        !link #58, "sticall.dll", "GetAnalogData"
        !link #59, "sticall.dll", "StiCommand"
        !link #60, "sticall.dll", "MaximumAnalogPoints"

        !call #51, w{R}=()                      'initializes DLL
'       dialogbeg "StiOpen Return"
'               print "R= ";R
'       dialogend
        !call #59, w{R}=("c")           'calibrates Mini-16 board analog inputs with Temp

'       Initialize conditions for analog input channels
'       ===============================================
'       Sets 4 analog input channels, (first element in dig array)
'       Ch1 is for pressure
'       Ch2 is used for RTD room temp sensing
```

```
'       Ch3,4 are for RTD cell temperature sensing
        !call #53, (w{4},w{0})
        !call #59, w{R}=("N")

'       Sets the range for each analog input channel.
'       Range 2 = 0-10V for pressure sensor.
'       Range 1003 = 100 Ohm RTD with 20 KOhm set resistor.
        !call #53, (w{2},w{0})
        !call #53, (w{1003},w{1})
        !call #53, (w{1003},w{2})
        !call #53, (w{1003},w{3})
        !call #59, w{R}=("r")

'       Sets all analog inputs to low-noise, highest resolution.
        !call #53, (w{18},w{0})
        !call #59, w{R}=("a")

'       Sets delay in reading analog input channels, 0.03ms x number.
        !call #53, (w{1000},w{0})
        !call #59, w{R}=("d")

'       Initialize conditions for digital input/output channels.
'       ========================================================
'       Sets digital I/O channels to input or output according to
'       values in DLL digital array; 0 for input, 1 for output.
        !call #53, (w{1},w{0})
        !call #53, (w{1},w{1})
        !call #53, (w{1},w{2})
        !call #53, (w{1},w{3})
        !call #53, (w{1},w{4})
        !call #53, (w{1},w{5})
        !call #53, (w{1},w{6})
        !call #53, (w{1},w{7})
        !call #53, (w{1},w{8})
        !call #53, (w{1},w{9})
        !call #53, (w{1},w{10})
        !call #53, (w{1},w{11})
        !call #59, w{R}=("S")

'       Ensure all valves and pump switched off
'       =======================================
        chain "subs.ab",1000,(1)          'closes valve 1 to flask
        chain "subs.ab",1000,(2)          'closes valve 2 to flask
        chain "subs.ab",1000,(3)          'closes valve 3 to flask
        chain "subs.ab",1000,(4)          'closes valve 4 to flask
        chain "subs.ab",1000,(5)          'closes valve 5 to flask
        chain "subs.ab",1000,(6)          'closes valve 6 to flask
        chain "subs.ab",1000,(7)          'closes valve 7 to flask
        chain "subs.ab",1000,(8)          'closes valve 8 to flask
        chain "subs.ab",1000,(9)          'closes valve 9 to calib gas line
        chain "subs.ab",1000,(10)         'closes valve 10 to oil pump
        chain "subs.ab",1000,(11)         'closes valve 11 to White cell

'       Resolution check
'       ================
        driver 3, "scratch",11,1,4        '1 scan spc, not displayed
        if {[vres]}=1 goto 5 else goto 2
2       dialogbeg "RESOLUTION ERROR"
```

```
        print "VRES is ";{[vres]}
        print "Change to 1cm-1 and restart"
dialogend
stop
5       driver "iput nsubs",1                          'resets scanning parameter

'       Read default settings from flasks.def file
'       ==========================================
        onerror 6                                      'goto 6 if error occurs
        open "O",#4,"flasks.def"                       'reads current defaults
        input #4,"", $fname
        input #4,"", $comment
        input #4,"", $cocalib
        input #4,"", $n2ocalib
        input #4,"", $co2calib
        input #4,"", $ch4calib
        input #4, nscan
        input #4, nbatch
        close #4
        onerror  -1

'       Set the parameters for this run
'       ===============================
6       close #4                                       'closes file if error
        onerror 9000
        portout -24,1                                  'allows default inputs
        dialogbeg "SET THE PARAMETERS FOR THIS BATCH OF FLASKS"
                dialogask $fname,2,40,40, "file name (mm/dd/yy/##), no extension"
                dialogask $comment,2,40,80, "Comment (<80 char)"
                dialogask $cocalib,2,40,40, "CO Calibration file (.cll)"
                dialogask $N2Ocalib,2,40,40, "N2O Calibration file (.cll)"
                dialogask $CO2calib,2,40,40, "CO2 Calibration file (.cll)"
                dialogask $ch4calib,2,40,40, "CH4 Calibration file (.cll)"
                dialogask nscan,1,1,256, "Number of scans per spectrum"
                dialogask nbatch,1,1,8, "Number of flasks in this batch"
                dialogask $f1comm,2,40,80, "Comment Flask 1 (<80 char)"
                dialogask $f2comm,2,40,80, "Comment Flask 2 (<80 char)"
                dialogask $f3comm,2,40,80, "Comment Flask 3 (<80 char)"
                dialogask $f4comm,2,40,80, "Comment Flask 4 (<80 char)"
                dialogask $f5comm,2,40,80, "Comment Flask 5 (<80 char)"
                dialogask $f6comm,2,40,80, "Comment Flask 6 (<80 char)"
                dialogask $f7comm,2,40,80, "Comment Flask 7 (<80 char)"
                dialogask $f8comm,2,40,80, "Comment Flask 8 (<80 char)"
        dialogend


        open #4,"FLASKS.def"                           'stores last entered values
        print #4, $fname
        print #4, $comment
        print #4, $cocalib
        print #4, $n2ocalib
        print #4, $co2calib
        print #4, $ch4calib
        print #4, nscan
        print #4, nbatch
        close #4
```

```
        if nbatch<=8 goto 100
        dialogbeg "Too many Flasks"
                print "8 is the maximum number of flasks"
                print "Start again"
        dialogend
        goto 9000

'       Set the Collect parameters
'       ==========================
100     driver "iput name",$fname
        driver "iput memo",$comment
        driver "iput scans",nscan
        driver "isetup"                                 'show Instrument/Parameters dialog box

'       Set up .CSV file and output to it
'       =================================
        driver "iget name", fname
        string $logname=$fname + ".csv"
        open "C", #5, $logname
        print #5, "FLASKS.AB output for ";$logname," ";
        print @2
        print #5, "Date: ";clock(-5);"-";clock(-6);"-";clock(-7)
        print #5, "Time: ";clock(-4);":";clock(-3)
        print @6
        print #5, $comment
        print #5, "Flask 1: ";$f1comm
        print #5, "Flask 2: ";$f2comm
        print #5, "Flask 3: ";$f3comm
        print #5, "Flask 4: ";$f4comm
        print #5, "Flask 5: ";$f5comm
        print #5, "Flask 6: ";$f6comm
        print #5, "Flask 7: ";$f7comm
        print #5, "Flask 8: ";$f8comm
        print #5, "Calibration file for CO : ";$cocalib
        print #5, "Calibration file for N2O : ";$n2ocalib
        print #5, "Calibration file for CO2: ";$co2calib
        print #5, "Calibration file for CH4: ";$CH4calib
        print #5, " "
        print #5, "";",";"Spectrum,";"Time,";"[H2O],";"[CO2_1],";"[CO2_2],";"[N2O],";"[CO],";
        print #5, "BOFFN2O,";"BSLOPEN2O,";"N2ORESID,";
        print #5, "[CH4],";"BOFFCH4,";"BSLOPECH4,";"CH4RESID,";
        print #5, "P avg,";"T avg,";"P init,";"P final,";
        print #5, "T1 init,";"T2 init,";"T1 final,";"T2 final,";"T Room,"
        close #5


'       Pump out cell and manifold up to flasks
'       =======================================
        chain "subs.ab",1050,(10)                       'opens valve 10 to pump
        !wait 36                                        'wait 2 seconds
        chain "subs.ab",1050,(11)                       'opens valve 11 to cell
        !wait 36                                        'wait 2 seconds
        for i=1 to nbatch
                chain "subs.ab",1050,(i)                'opens valve i to flask
                !wait 36                                'wait 2 seconds
        next
        dialogbeg "PUMPING DOWN CELL AND MANIFOLD UP TO FLASK VALVES"
                print "Press OK when the P < 0.1torr on Edwards gauge"
```

```
        dialogend
        for i=1  to nbatch
                 chain "subs.ab",1000,(i)                    'closes valve i to flask
                 !wait 18                                    'wait 1 second
        next
        dialogbeg "OPENING FLASKS"
                 print "Open green valve on each flask by hand"
                 print "Then press OK"
        dialogend


'       Take First Empty Cell Reference Spectrum
'       =======================================
'       At this stage the cell is still being pumped through valves 10 and 11
        driver "iget name", fname
        driver 1,$fname                  'collects a single beam reference, and saves it.
        savespc "refspc"
        savespc $fname                   'refspc is also saved to the first spec of the multifile
        ispec=1
        noshow
        noshow

'       Main Loop Control for flask samples
'       ===================================
        fcount=0                                             'flask counting variable
300     dialogbeg "FLASKS.AB STATUS"
                 dialogloc 1,0
                 print "Current Spectrum"
                 print "================"
                 print "Run Name:         "; $fname
                 print "Number of flasks: "; nbatch
                 print "Current flask:    "; fcount
                 print " "
                 print "Last Spectrum"
                 print "============="
                 print "[CO]  = ";CO;" ppb"
                 print "[N2O] = ";N2O;" ppb"
                 print "[CO2] = ";CO2_2;" ppm"
                 print "[CH4] = ";CH4;" ppb"
                 print "[H2O] = ";H2O;" ppm"
                 print "Press = ";pressavg;" torr"
        dialogend 22
        if fcount=0 goto 700
        if fcount>nbatch goto 700

'       Fill Cell to 450 torr and read initial T and P
'       ==============================================
'       Cell empty and valves 10 and 11 open at this stage pumping on cell
        chain "subs.ab",1000,(10)                            'closes valve 10 to pump
        !wait 18                                             'waits 1 second
        chain "subs.ab",1050,(fcount)                        'opens valve to flask #fcount

'       Fill to ~460t
        time=clock(0)
320     chain "subs.ab",1100,(1,presscal)                    'reads analog channel 1, pressure
        if presscal<4.60 and not(clock(20)) then 320
        chain "subs.ab",1000,(11)                            'closes valve 11 to stop filling at 470torr
        !wait 18                                             'waits 1 second
```

```
        chain "subs.ab",1000,(fcount)                    'closes valve to flask #fcount
        !wait 180                                        'waits 10 secondS
        chain "subs.ab",1050,(10)                        'opens valve 10 to pump
        !wait 18                                         'waits 1 second
        chain "subs.ab",1050,(12)                        'opens valve 12 to small orifice in line

'       Pump down to ~450t
330     chain "subs.ab",1100,(1,presscal)                'reads analog channel 1, pressure
        if presscal>4.50 goto 330
        chain "subs.ab",1000,(12)                        'closes valve 12 to stop emptying
        !wait 18                                         'waits 1 second
        chain "subs.ab",1000,(10)                        'closes valve 10 to pump

'       Wait 60 sec before reading P,T initial values
335     time=clock(0)
340     if not(clock(60)) then 340
'
        chain "subs.ab",1100,(1,pressi)                  'reads analog channel 1, pressure
        chain "subs.ab",1100,(3,temp1i)                  'reads analog channel 3, temperature
        chain "subs.ab",1100,(4,temp2i)                  'reads analog channel 4, temperature
        chain "subs.ab",1100,(2,rtemp)                   'reads analog channel 2, room temp

'       Takes spectrum of sample
'       ========================
        driver 1,$fname                          'collects a single beamspectrum, and saves it.
                                                 'this is old syntax for driver.
        savespc "sample"
        ispec=ispec+1
        savespc $fname, #ispec                   'append sample spectrum to multifile

        noshow
        noshow
        noshow

'       Reads final T and P
'       ===================
        chain "subs.ab",1100,(1,pressf)                  'reads analog channel 1, pressure
        chain "subs.ab",1100,(3,temp1f)                  'reads analog channel 3, temperature
        chain "subs.ab",1100,(4,temp2f)                  'reads analog channel 4, temperature

'       Computes absorbance spectrum, does fits and calcs avg T and P
'       ============================================================
        pressavg=100*(pressi+pressf)/2
        tempavg=(temp1i+temp2i+temp1f+temp2f+2*1.1+2*0.4)/4
        tempavg=tempavg+273.15
        rtemp=rtemp+1.2
'               RTD B correction: +1.1C
'               RTD C correction: +0.4C
'               RTD A correction: +0.65C

        loadspc "sample"
        loadspc "refspc"
        #2=absorb(#2,#1)                         'computes abs spectrum with current background
        noshow

        STRING CALNAME=$COCALIB
        chain "kp"                                       'calls predict routine
        CO=Yn(3)
```

```
noshow
noshow
noshow
noshow

STRING CALNAME=$n2oCALIB
loadspc "sample"
loadspc "refspc"
#2=absorb(#2,#1)
noshow
chain "kp"                                    'calls predict routine
H2O=Yn(0)
N2O=Yn(3)
BOFFN2O=Yn(5)
BSLOPEN2O=Yn(6)
N2Oresid=rmsres

noshow
noshow
noshow
noshow

STRING CALNAME=$co2CALIB
loadspc "sample"
loadspc "refspc"
#2=absorb(#2,#1)
noshow
chain "kp"                                    'calls predict routine
CO2_1=Yn(1)
co2_2=Yn(2)

noshow
noshow
noshow
noshow

STRING CALNAME=$CH4CALIB
loadspc "sample"
loadspc "refspc"
#2=absorb(#2,#1)
noshow
chain "kp"                                    'calls predict routine
CH4=Yn(0)
BOFFCH4=Yn(1)
BSLOPECH4=Yn(2)
ch4resid=rmsres

noshow
noshow
noshow
noshow

print @6
open "O", #5, $logname
seek #5, -0                                   'go to end of file
print #5, "";",";$fname;"#";ispec;",";clock(-4);":";clock(-3);",";
print #5, H2O;",";CO2_1;",";CO2_2;",";N2O;",";CO;",";
```

```
        print #5, BOFFN2O;",";BSLOPEN2O;",";N2ORESID;",";
        print #5, CH4;",";BOFFCH4;",";BSLOPECH4;",";CH4RESID;",";
        print #5, pressavg;",";tempavg;",";(100*pressi);",";(100*pressf);",";
        print #5, temp1i;",";temp2i;",";temp1f;",";temp2f;",";rtemp
        close #5

'       Empties cell
'       ====================================
430     chain "subs.ab",1050,(10)                    'opens valve 10 to pump
        chain "subs.ab",1050,(11)                    'opens valve 11 to cell

'       Allow 240 seconds for pumping from ~450t to <1t
        time=clock(0)
460     if not(clock(240)) then 460                  'waits 240 seconds
        fcount = fcount+1
        dialogend -20                                'deletes status dialog box
        goto 300

'       Fill Cell with Calibration Gas for analyses at 450 torr
        ====================================
'       Cell empty and valves 10 and 11 open at this stage pumping on cell
700     if fcount > nbatch+1 goto 2000
        chain "subs.ab",1000,(10)                    'closes valve 10 to pump
        !wait 18                                     'waits 1 second
        chain "subs.ab",1050,(9)                     'opens valve 9 to cal gas line
'       Fill cell to ~460t
710     chain "subs.ab",1100,(1,presscal)            'reads analog channel 1, pressure
        if presscal<4.60 goto 710
        chain "subs.ab",1000,(9)                     'closes valve 9 to stop fill
        chain "subs.ab",1000,(11)                    'closes valve 11 to cell
        !wait 180                                    'wait 10 seconds

        chain "subs.ab",1050,(10)                    'opens valve 10 to pump
        !wait 18                                     'waits 1 second
        chain "subs.ab",1050,(12)                    'opens valve 12 to small orifice in line
'       Pump down to ~450t
715     chain "subs.ab",1100,(1,presscal)            'reads analog channel 1, pressure
        if presscal>4.50 goto 715
        chain "subs.ab",1000,(12)                    'closes valve 12 to stop emptying
        chain "subs.ab",1000,(10)                    'closes valve 10 to pump
        goto 335



'       Take Second Empty Cell Reference Spectrum
'       ========================================
'       At this stage the cell is still being pumped through valves 10 and 11
2000    driver 1,$fname                              'collects a single beam spectrum, and saves it.
                                                     'this is old syntax for driver.

        ispec=ispec+1
        savespc $fname, #ispec                       'append spectrum to multifile

'       Pump out manifold and all flasks ready to hand over evacuated
'       ============================================================
'       At this stage valves 10 and 11 open pumping on cell
        GOTO 9000
        chain "subs.ab",1000,(11)                    'closes valve 11 to cell
        for i=1 to nbatch
```

```
            chain "subs.ab",1050,(i)                    'opens valve i to flask
            !wait 90                                    'wait 5 seconds
        next
        dialogbeg "PUMPING DOWN ALL FLASKS FOR RETURN TO GROB"
            print "Press OK when the P < 0.1torr on Edwards gauge"
        dialogend
        dialogbeg "CLOSING FLASKS"
            print "Close green valve on each flask by hand"
            print "Then press OK"
        dialogend
        for i=1 to nbatch
            chain "subs.ab",1000,(i)                    'closes valve i to flask
            !wait 18                                    'wait 1 second
        next


'       Finishing Off
'       =============
9000    close #5                                        'ensures .csv file closed
        for i=1 to 12                                   'closes all valves
            chain "subs.ab",1000,(i)                    'closes valve i
            !wait 18                                    'wait 1 second
        next
        !call #52, w{R}=()                              'closes DLL

        dialogend -20                                   'closes status dialog box
        DIALOGBEG "FLASK.AB PROGRAM"
            PRINT "THE PROGRAM HAS FINISHED"
        DIALOGEND
        stop
```

Appendix C: Complete UoW_{FLASK} FTIR Data Set From OASIS Experiment

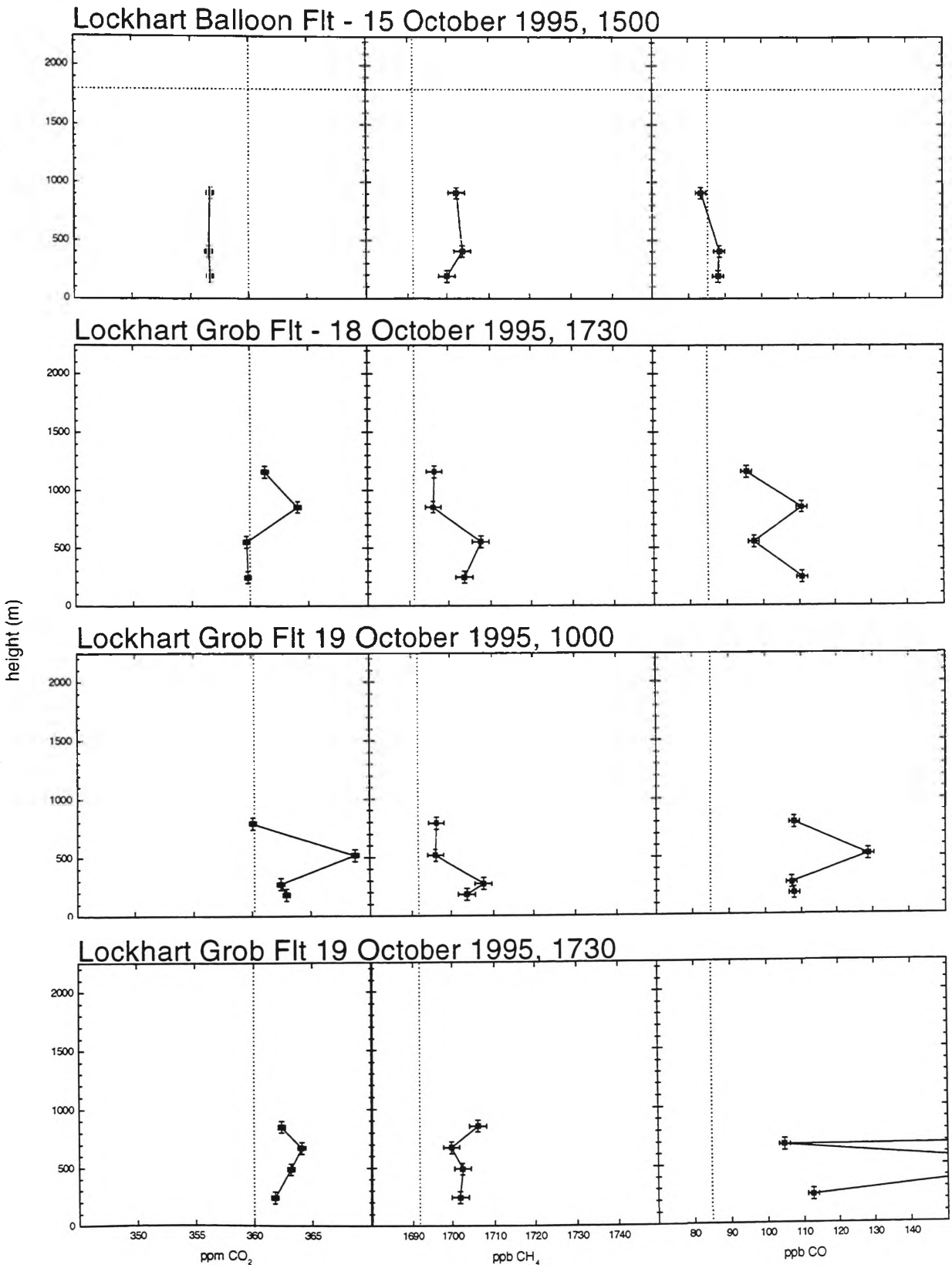

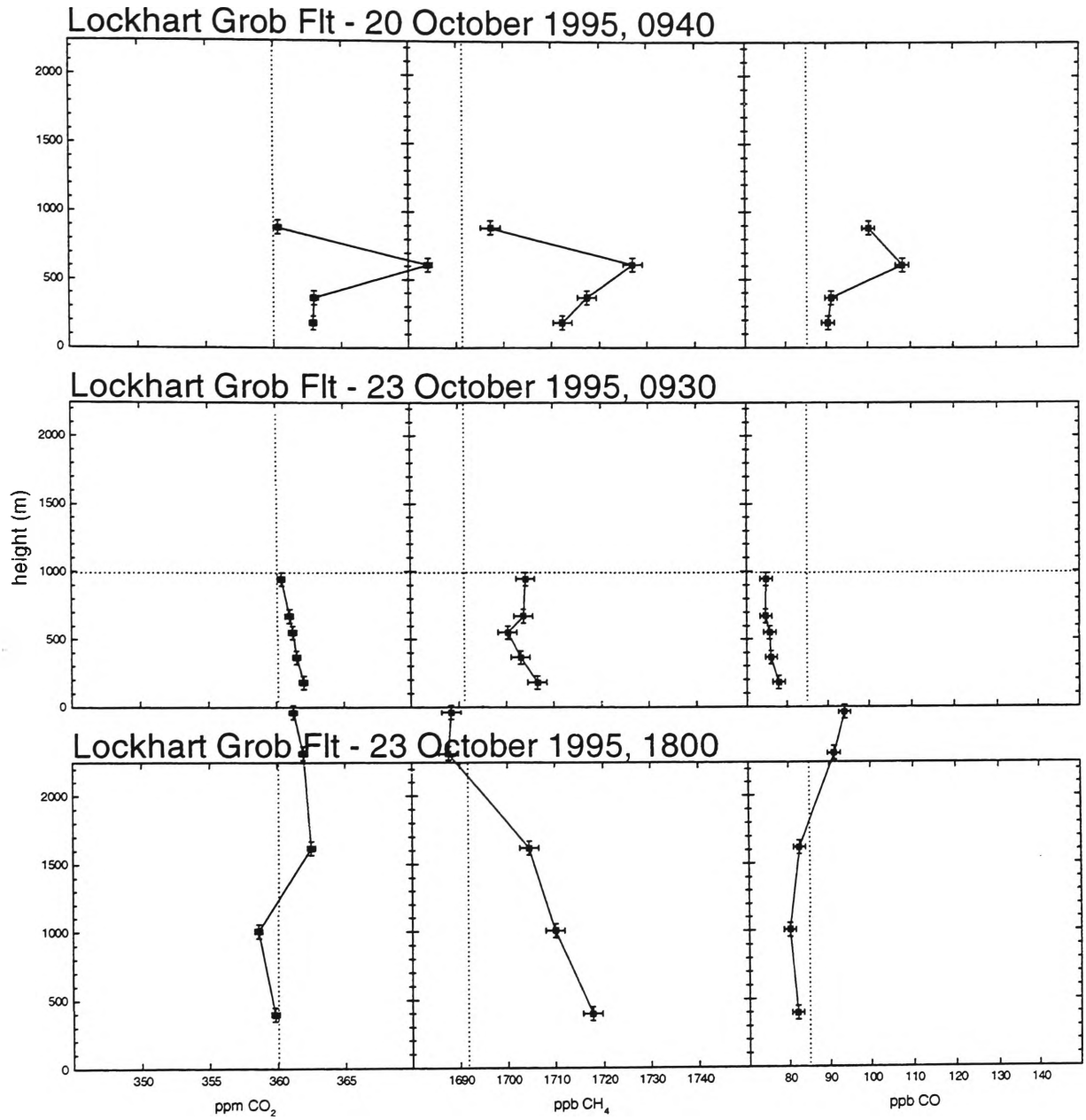
Lockhart Grob Flt - 20 October 1995, 0940
Lockhart Grob Flt - 23 October 1995, 0930
Lockhart Grob Flt - 23 October 1995, 1800
height (m)
0
500
1000
1500
2000
350
355
360
365
ppm CO_2
1690
1700
1710
1720
1730
1740
ppb CH_4
80
90
100
110
120
130
140
ppb CO

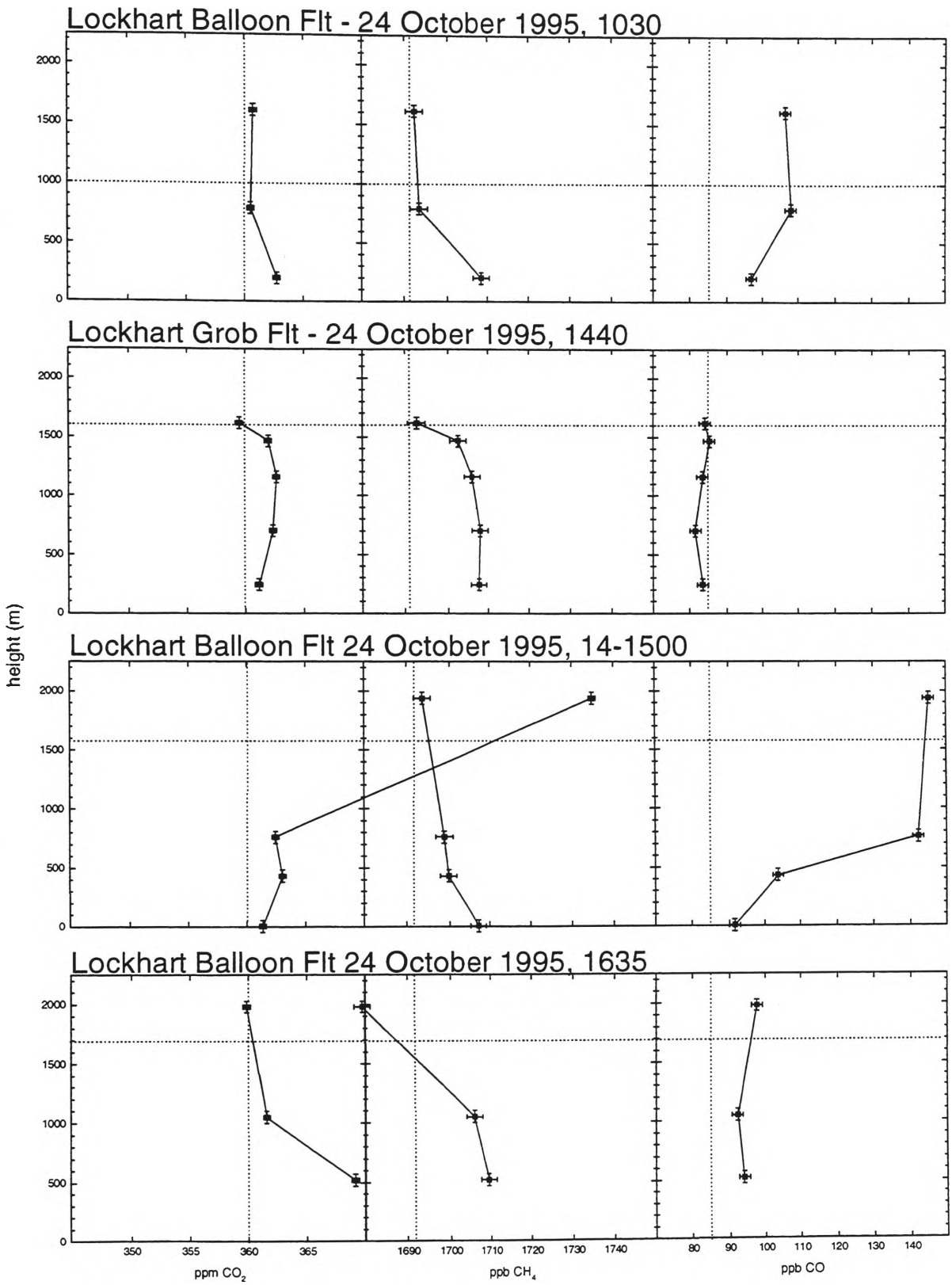
Lockhart Balloon Flt - 24 October 1995, 1030
Lockhart Grob Flt - 24 October 1995, 1440
Lockhart Balloon Flt 24 October 1995, 14-1500
Lockhart Balloon Flt 24 October 1995, 1635
height (m)
0
500
1000
1500
2000
350
355
360
365
ppm CO_2
1690
1700
1710
1720
1730
1740
ppb CH_4
80
90
100
110
120
130
140
ppb CO

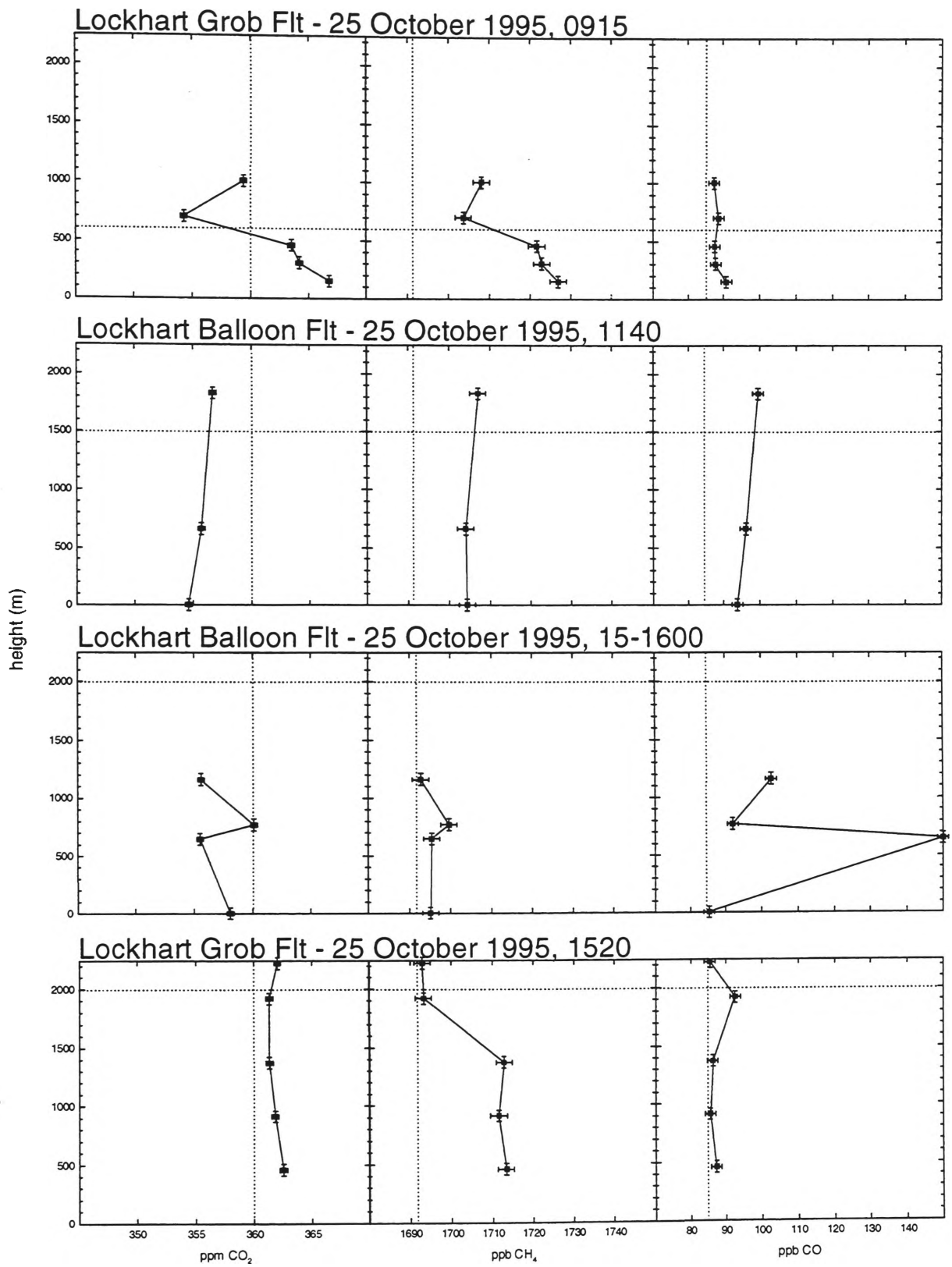
Lockhart Grob Flt - 25 October 1995, 0915
Lockhart Balloon Flt - 25 October 1995, 1140
Lockhart Balloon Flt - 25 October 1995, 15-1600
Lockhart Grob Flt - 25 October 1995, 1520
height (m)
0
500
1000
1500
2000
350
355
360
365
ppm CO_2
1690
1700
1710
1720
1730
1740
ppb CH_4
80
90
100
110
120
130
140
ppb CO

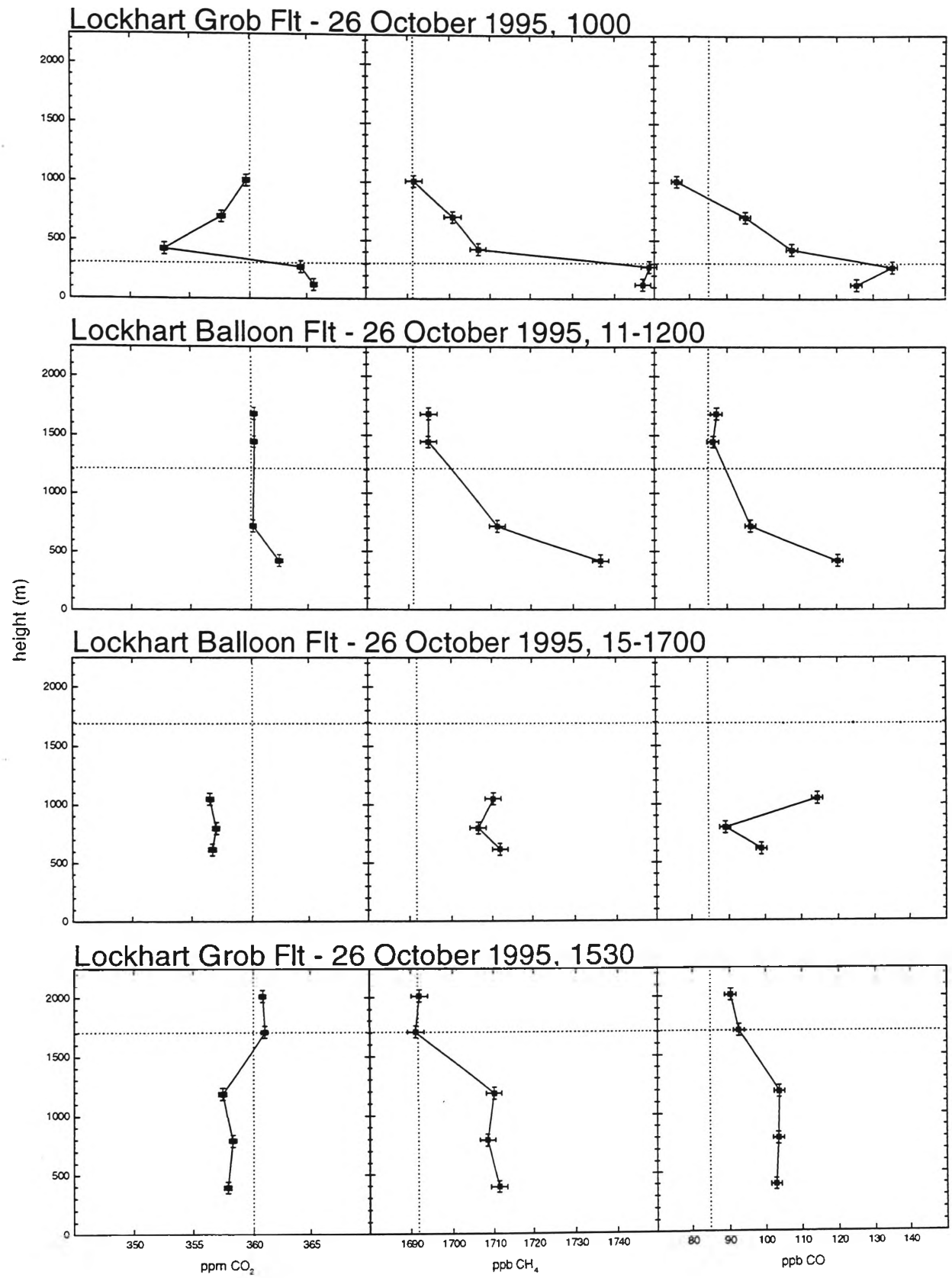
Lockhart Grob Flt - 26 October 1995, 1000
Lockhart Balloon Flt - 26 October 1995, 11-1200
Lockhart Balloon Flt - 26 October 1995, 15-1700
Lockhart Grob Flt - 26 October 1995, 1530
height (m)
0
500
1000
1500
2000
350
355
360
365
ppm CO_2
1690
1700
1710
1720
1730
1740
ppb CH_4
80
90
100
110
120
130
140
ppb CO

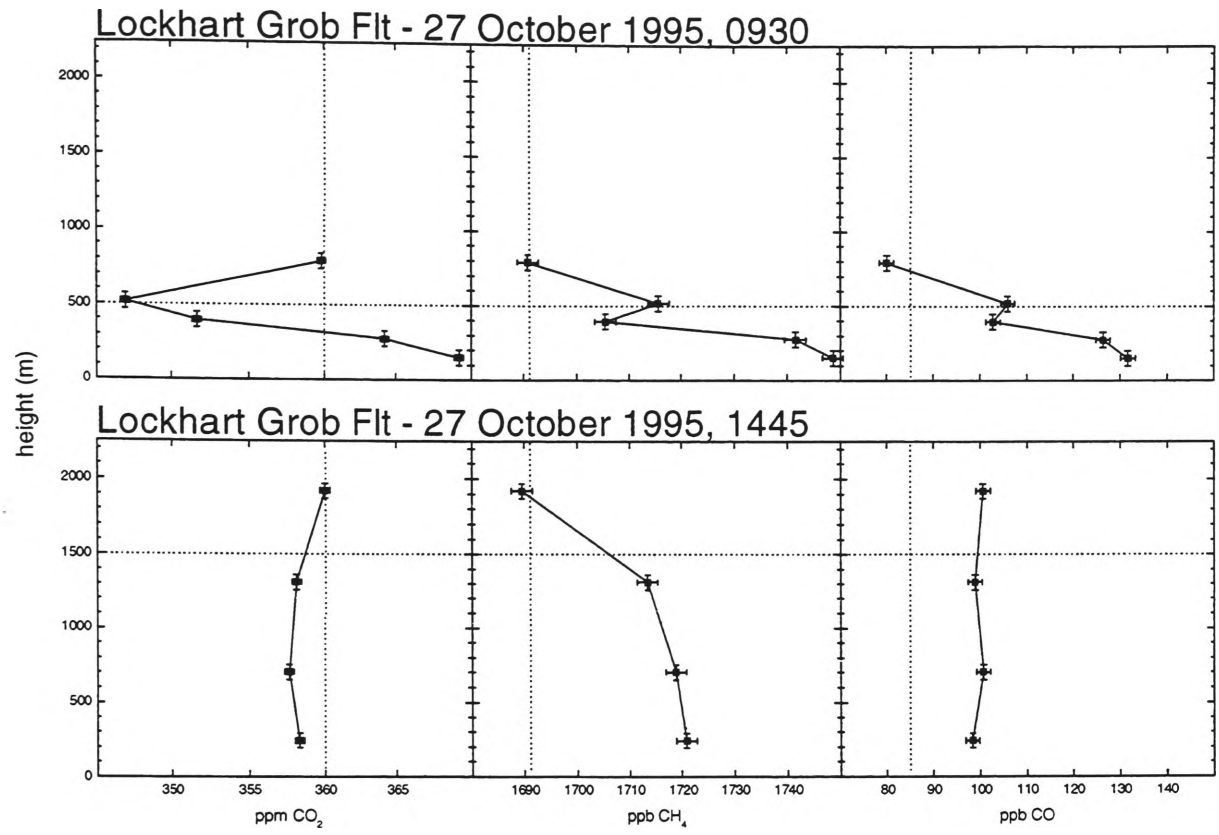

Figure C.1. Trace gas mixing ratio profiles for 15, 18, 19, 20, 23, 24, 25, 26 and 27 October 1995. This represents the complete record of flask samples collected by either Grob aircraft or balloon and analysed by FTIR during OASIS '95. Horizontal broken line is CBL depth (not always measured), vertical broken line is free troposphere mixing ratio of species. Error bars are ±50m in height, ±0.3ppm CO_2, ±2ppb CH_4 and ±1.5ppb CO (all ± 1 std dev.)

Flask sampling	Spectrum filename	Sample time	Altitude m above gnd	$[CO_2]$ ppmv	$[N_2O]$ ppbv	[CO] ppbv	$[CH_4]$ ppbv
GROB FLIGHT 17:30 18/10/95	OC199505#3	17:30	1158	361.3	*313.0*	95.5	1694.5
	OC199505#4	17:30	853	364.1	*314.1*	110.7	1701.0
	OC199505#5	17:30	549	359.7	*313.7*	97.5	1703.9
	OC199505#6	17:30	244	359.8	*311.4*	110.7	1715.0
GROB FLIGHT 10:00 19/10/95	OC209501#3	10:00	792	360.1	*315.7*	108.0	1696.5
	OC209501#4	10:00	518	368.8	*315.4*	128.8	1696.2
	OC209501#5	10:00	274	362.5	*315.1*	107.3	1707.7
	OC209501#6	10:00	183	363.0	*314.5*	108.0	1703.8
GROB FLIGHT 17:30 19/10/95	OC209502#3	17:30	853	362.4	*313.5*	1128.4	1706.1
	OC209502#4	17:30	671	364.1	*314.3*	104.8	1699.8
	OC209502#5	17:30	488	363.2	*313.6*	185.7	1702.5
	OC209502#6	17:30	244	361.8	*312.8*	112.7	1701.9
GROB FLIGHT 9:40 20/10/95	OC209502#7	9:40	884	360.3	*312.6*	100.3	1697.3
	OC209502#8	9:40	610	371.5	*313.1*	108.2	1727.0
	OC209502#9	9:40	366	363.0	*311.6*	91.2	1717.4
	OC209502#10	9:40	183	362.9	*312.9*	90.4	1712.3
GROB FLIGHT 9:30 23/10/95	OC249501#3	9:30	945	360.4	*312.1*	74.8	1704.2
	OC249501#4	9:30	671	361.0	*313.1*	74.7	1703.7
	OC249501#5	9:30	549	361.2	*313.0*	75.7	1700.4
	OC249501#6	9:30	366	361.5	*312.3*	76.0	1703.1
	OC249501#7	9:30	183	362.0	*312.3*	77.9	1706.6
GROB FLIGHT 18:00 23/10/95	OC249502#3	18:00	2621	361.2	*310.0*	94.0	1688.4
	OC249502#4	18:00	2316	361.9	*312.1*	91.3	1687.7
	OC249502#5	18:00	1615	362.5	*311.6*	82.6	1704.6
	OC249502#6	18:00	1006	358.6	*312.0*	80.1	1710.0
	OC249502#7	18:00	396	359.8	*312.3*	82.0	1717.7
GROB FLIGHT 14:40 24/10/95	OC249504#3	14:40	1615	359.5	*313.5*	84.1	1692.7
	OC249504#4	14:40	1463	361.9	*314.0*	85.3	1702.5
	OC249504#5	14:40	1158	362.6	*314.7*	83.5	1706.0
	OC249504#6	14:40	701	362.3	*313.7*	81.6	1708.0
	OC249504#7	14:40	244	361.1	*314.2*	83.6	1707.7
GROB FLIGHT 9:15 25/10/95	OC259516#3	9:15	**1006**	**359.4**	*313.1*	**87.4**	**1708.2**
	OC259516#4	9:15	**701**	**354.3**	*312.1*	**88.7**	**1703.7**
	OC259516#5	9:15	**457**	**363.5**	*313.5*	**87.5**	**1721.7**
	OC259516#6	9:15	**305**	**364.2**	*314.3*	**87.8**	**1722.9**
	OC259516#7	9:15	**152**	**366.8**	*313.0*	**90.8**	**1726.9**
GROB FLIGHT 15:20 25/10/95	OC259515#3	15:20	**2225**	**362.0**	*309.0*	**85.4**	**1692.9**
	OC259515#4	15:20	**1920**	**361.3**	*310.7*	**92.6**	**1693.2**
	OC259515#5	15:20	**1372**	**361.3**	*312.3*	**86.3**	**1712.8**
	OC259515#6	15:20	**914**	**361.8**	*313.2*	**85.6**	**1711.5**
	OC259515#7	15:20	**457**	**362.5**	*312.3*	**87.3**	**1713.3**
GROB FLIGHT 10:00 26/10/95	OC269507#3	10:00	**1006**	**359.7**	*313.2*	**76.6**	**1691.6**
	OC269507#4	10:00	**701**	**357.6**	*313.3*	**95.1**	**1700.8**
	OC269507#5	10:00	**427**	**352.9**	*312.3*	**108.0**	**1707.0**
	OC269507#6	10:00	**274**	**364.5**	*314.1*	**135.4**	**1748.7**
	OC269507#7	10:00	**122**	**365.6**	*313.8*	**125.4**	**1747.1**
GROB FLIGHT 15:30 26/10/95	OC279501#3	15:30	**2012**	**360.8**	*313.5*	**90.3**	**1692.1**
	OC279501#4	15:30	**1707**	**361.0**	*311.8*	**92.6**	**1691.1**
	OC279501#5	15:30	**1189**	**357.4**	*313.2*	**103.8**	**1710.0**
	OC279501#6	15:30	**792**	**358.2**	*312.7*	**103.6**	**1708.4**
	OC279501#7	15:30	**396**	**357.8**	*313.5*	**102.9**	**1711.3**
GROB FLIGHT 9:30 27/10/95	OC279505#3	9:30	**792**	**359.8**	*312.0*	**80.1**	**1690.9**
	OC279505#4	9:30	**518**	**346.9**	*313.7*	**106.0**	**1715.6**
	OC279505#5	9:30	**396**	**351.7**	*313.4*	**102.8**	**1705.5**
	OC279505#6	9:30	**274**	**364.2**	*314.4*	**126.4**	**1741.5**
	OC279505#7	9:30	**152**	**369.2**	*317.4*	**131.7**	**1748.6**
GROB FLIGHT 14:45 27/10/95	OC279509#3	14:45	**1920**	**360.0**	*311.1*	**100.6**	**1689.6**
	OC279509#4	14:45	**1311**	**358.1**	*313.6*	**98.9**	**1713.4**
	OC279509#5	14:45	**701**	**357.6**	*314.6*	**100.7**	**1718.8**
	OC279509#6	14:45	**244**	**358.3**	*314.4*	**98.3**	**1720.8**

Table C.1. Results of FTIR flask analysis for CO_2, N_2O, CO and CH_4 mixing ratios. Flasks obtained from aircraft (Grob) vertical profiling during OASIS 95, 18-27 October 1995. Data in bold font are illustrated in Figures 5.2, 5.3 and 5.4. N_2O mixing ratios are recorded in italics to indicate that they are not of sufficient precision to infer any flux information.

Flask sampling	Spectrum filename	Sample time	Altitude m above gnd	$[CO_2]$ ppmv	$[N_2O]$ ppmv	[CO] ppmv	$[CH_4]$ ppmv
BALLOON FLT 14:50-15:50 15/10/95	OC169503#3	15:50	907	356.7	*313.2*	83.4	1702.4
	OC169504#4	14:38	405	356.6	*311.3*	88.4	1703.7
	OC169503#4	14:47	190	356.7	*313.5*	88.1	1700.0
BALLOON FLT 10:17-10:50 24/10/95	OC249504#8	10:17	1610	360.7	*314.0*	106.5	1692.3
	OC249504#9	10:27	790	360.5	*314.4*	108.1	1693.5
	OC249504#10	10:50	200	362.7	*313.4*	96.8	1708.5
BALLOON FLT 14:04-15:14 24/10/95	OC249505#3	14:48	1940	389.6	*313.5*	145.2	1693.7
	OC249505#4	14:04	760	362.4	*314.6*	142.2	1698.8
	OC249505#5	13:55	430	363.0	*312.8*	103.8	1699.8
	OC249505#6	15:14	2	361.3	*314.4*	91.6	1707.2
BALLOON FLT 16:29-16:46 24/10/95	OC249505#7	16:46	1980	359.9	*313.5*	97.6	1679.4
	OC249505#8	16:35	1050	361.5	*313.7*	92.2	1705.9
	OC249505#9	16:29	520	369.1	*310.8*	94.0	1709.5
BALLOON FLT 11:32-11:53 25/10/95	OC259517#3	11:49	1830	356.7	*312.7*	99.6	1707.1
	OC259517#4	11:32	660	355.7	*311.9*	96.2	1704.0
	OC259517#5	11:53	2	354.6	*312.0*	93.8	1704.3
BALLOON FLT 15:01-16:07 25/10/95	OC259517#6	15:01	1160	355.6	*310.9*	102.7	1692.7
	OC259517#8	16:05	770	360.1	*312.9*	92.0	1699.6
	OC259517#7	14:46	647	355.5	*311.0*	150.1	1695.4
	OC259517#9	16:07	2	358.1	*308.7*	85.3	1695.1
BALLOON FLT 10:45-11:58 26/10/95	OC269508#3	10:45	**1680**	**360.3**	*313.7*	**87.2**	**1695.0**
	OC269508#5	11:58	**1440**	**360.3**	*312.0*	**86.3**	**1694.9**
	OC269508#4	10:31	**718**	**360.2**	*313.8*	**96.4**	**1711.6**
	OC269508#6	11:17	**420**	**362.5**	*313.9*	**120.3**	**1736.4**
BALLOON FLT 14:44-17:00 26/10/95	OC269508#7	15:00	1050	356.5	*316.5*	114.4	1710.2
	OC269508#9	17:00	800	357.0	*313.4*	89.1	1706.4
	OC269508#8	14:44	615	356.7	*312.4*	98.9	1711.9

Table C.2. Results of FTIR flask analysis for CO_2, N_2O, CO and CH_4 mixing ratios. Flasks obtained from helium balloon vertical profiling during OASIS 95, 15-26 October 1995. Data in bold font are illustrated in Figure 5.4b. N_2O mixing ratios are recorded in italics to indicate that they are not of sufficient precision to infer any flux information.

Flask sampling	Spectrum filename	Sample time	Altitude (z) m above crop	ln(z)	$[CO_2]$ ppmv	$[N_2O]$ ppbv	[CO] ppbv	$[CH_4]$ ppbv	$\delta^{13}CO_2$ per mil
4m TOWER 17/10/95	OC179502#3	13:15	4	1.39	354.3	*314.3*	103.7	1696.1	*-6.73*
	OC179502#4	13:18	2	0.69	352.1	*317.9*	100.7	1704.3	*-6.43*
	OC179502#6	13:22	1	0.00	349.7	*314.5*	99.0	1702.9	*-7.58*
	OC179502#7	13:25	0.5	-0.69	348.1	*315.1*	92.4	1700.6	*-7.08*
22m TOWER 17/10/95	OC179503#3	15:30	22	3.09	355.4	*315.4*	203.7	1700.6	*-8.03*
	OC179503#4	15:30	14	2.64	357.6	*314.9*	93.9	1699.7	*-7.96*
	OC179503#5	15:30	8	2.08	355.7	*317.7*	229.0	1703.4	*-7.83*
	OC179503#6	15:30	4	1.39	353.2	*317.4*	109.0	1702.1	*-7.59*
	OC179503#7	15:30	2	0.69	352.2	*318.0*	100.6	1702.7	*-7.80*
	OC179503#8	15:30	1	0.00	*351.1*	*316.5*	*453.2*	*1710.3*	*-7.66*
	OC179503#9	15:30	0.5	-0.69	347.4	*315.1*	101.5	1712.2	*-7.50*
4m TOWER 17/10/95	OC179504#3	18:00	4	1.39	352.7	*313.9*	111.1	1696.1	*-5.93*
	OC179504#4	18:00	2	0.69	349.1	*312.4*	94.8	1705.3	*-5.64*
	OC179504#5	18:00	1	0.00	350.0	*316.1*	92.6	1705.0	*-7.14*
	OC179504#6	18:00	0.5	-0.69	348.7	*313.2*	92.2	1701.3	*-8.40*
22m TOWER 18/10/95	**OC189508#3**	**15:03**	**22**	**3.09**	**352.8**	**313.3**	**167.6**	**1747.9**	**-7.74**
	OC189508#4	**15:04**	**14**	**2.64**	**350.3**	**314.3**	**172.4**	**1743.2**	**-6.91**
	OC189508#5	**15:06**	**8**	**2.08**	**347.3**	**315.7**	**219.0**	**1746.8**	**-6.26**
	OC189508#6	**15:01**	**4**	**1.39**	**345.2**	**314.0**	**162.5**	**1764.6**	**-6.73**
	OC189508#7	**15:00**	**2**	**0.69**	**342.4**	**312.5**	**155.9**	**1767.6**	**-7.73**
	OC189508#8	**14:58**	**1**	**0.00**	**339.0**	**313.4**	**394.3**	**1770.7**	**-7.69**
	OC189508#9	**14:56**	**0.5**	**-0.69**	**338.1**	**312.9**	**149.0**	**1777.8**	**-7.99**
22m TOWER 19/10/95	OC199506#3	15:04	22	3.09	357.4	*311.7*	139.1	1707.3	*-6.88*
	OC199506#4	15:05	14	2.64	357.4	*314.0*	130.6	1707.4	*-5.80*
	OC199506#5	15:06	8	2.08	357.5	*313.5*	177.7	1707.8	*-5.40*
	OC199506#6	15:08	4	1.39	353.7	*311.4*	144.5	1710.6	*-5.41*
	OC199506#7	15:10	2	0.69	353.7	*315.0*	136.0	1705.1	*-5.44*
	OC199506#8	15:11	1	0.00	*354.3*	*316.8*	*701.9*	*1709.3*	*-7.51*
	OC199506#9	15:13	0.5	-0.69	352.0	*314.5*	135.8	1703.8	*-7.06*
22m TOWER 19/10/95	**OC209503#3**	**22:35**	**22**	**3.09**	**378.1**	**313.6**	**215.1**	**1727.9**	**-7.75**
	OC209503#4	**22:37**	**14**	**2.64**	**379.4**	**313.0**	**122.9**	**1734.5**	**-7.74**
	OC209503#5	**22:40**	**8**	**2.08**	**383.5**	**312.9**	**141.4**	**1735.9**	**-8.04**
	OC209503#6	**22:42**	**4**	**1.39**	**394.8**	**314.9**	**131.4**	**1734.2**	**-8.46**
	OC209503#7	**22:43**	**2**	**0.69**	**406.4**	**317.3**	**124.0**	**1735.3**	**-8.99**
	OC209503#8	**22:45**	**1**	**0.00**	**410.2**	**317.4**	**383.1**	**1741.7**	**-10.11**
	OC209503#9	**22:47**	**0.5**	**-0.69**	**414.7**	**317.0**	**120.7**	**1740.8**	**-9.94**
22m TOWER 24/10/95	OC249503#3	13:50	22	3.09	357.9	*313.2*	143.4	1714.9	*-7.21*
	OC249503#4	13:50	14	2.64	357.6	*314.1*	92.4	1714.2	*-6.94*
	OC249503#5	13:50	8	2.08	357.3	*314.2*	96.2	1711.9	*-7.29*
	OC249503#6	13:50	4	1.39	357.3	*314.4*	99.1	1713.5	*-7.54*
	OC249503#7	13:50	2	0.69	356.3	*313.3*	94.9	1713.8	*-8.13*
	OC249503#8	13:50	1	0.00	*356.9*	*313.7*	*615.7*	*1721.1*	*-9.33*
	OC249503#9	13:50	0.5	-0.69	354.4	*313.4*	95.6	1712.8	*-7.83*
22m TOWER 26/10/95	OC269506#3	15:32	22	3.09	356.0	*313.7*	97.2	1700.8	*-7.28*
	OC269506#4	15:34	14	2.64	355.7	*313.3*	92.5	1703.1	*-7.33*
	OC269506#5	15:35	8	2.08	355.7	*313.0*	107.1	1699.7	*-6.08*
	OC269506#6	15:30	4	1.39	353.6	*311.1*	114.2	1706.3	*-6.59*
	OC269506#7	15:29	2	0.69	351.8	*313.1*	98.6	1704.6	*-5.97*
	OC269506#8	15:28	1	0.00	*352.7*	*315.3*	*514.4*	*1706.2*	*-7.19*
	OC269506#9	15:27	0.5	-0.69	350.2	*314.2*	104.9	1700.1	*-6.14*

Table C.3. Results of FTIR flask analysis for CO_2, N_2O, CO and CH_4 mixing ratios; and of the isotope ratio $\delta^{13}CO_2$. Flasks obtained from 22 m and 4 m tower sampling manifolds during OASIS 95, 17-26 October 1995. Data in bold font are illustrated in Figures 5.7 and 5.8. N_2O mixing ratios are recorded in italics to indicate that they are not of sufficient precision to infer any flux information. $\delta^{13}CO_2$ data are recorded in italics in most cases to indicate that they are not of sufficient quality to allow interpretation. Also, data from the sampling line at 1m height on the 22m tower are in italics as anomalously high CO mixing ratios suggest that this line is contaminated by combustion products, probably from a pump in the line.

References

Adel, A., Further detail in the rock-salt prizmatic solar spectrum, *Astrophys. J., 88*, 186-188, 1938.

Allison, C.E., R.J. Francey, R.L. Langenfelds, and E.D. Welch, Comparison of high precision Cape Grim CO_2 stable isotope measurements using two mass spectrometers, in *Baseline Atmospheric Program (Australia) 1991*, edited by A.L. Dick, and J.L. Gras, pp. 10-19, Bureau of Meteorology and CSIRO Division of Atmospheric Research, Melbourne, 1994.

Allison, C.E., R.J. Francey, and E.D. Welch, $\delta^{13}C$ of *in situ* extracted baseline CO_2, in *Baseline Atmospheric Program Australia 1994-95*, edited by R.J. Francey, A.L. Dick, and N. Derek, pp. 104-105, Bureau of Meteorology and CSIRO Division of Atmospheric Research, Melbourne, 1996.

Anderson, R.J., and P.R. Griffiths, Errors in absorbance measurements in infrared Fourier transform spectrometry because of limited instrument resolution, *Analytical Chemistry, 47*, 2339-2347, 1975.

Bakwin, P.S., P.P. Tans, C.L. Zhao, W. Ussler, and E. Quesnell, Measurements of carbon dioxide on a very tall tower, *Tellus Series B-Chemical & Physical Meteorology, 47*, 535-549, 1995.

Bange, H.W., S. Rapsomanikis, and M.O. Andreae, Nitrous oxide emissions from the Arabian Sea, *Geophysical Research Letters, 23*, 3175-3178, 1996.

Beardsmore, D.J., L.P. Steele, and G.I. Pearman, Baseline carbon dioxide monitoring, in *Baseline Atmospheric Program (Australia) 1993*, edited by R.J. Francey, A.L. Dick, and N. Derek, pp. 71-73, Bureau of Meteorology in association with CSIRO Division of Atmospheric Research, Melbourne, 1996.

Becker, J.F., T.B. Sauke, and M. Loewnstein, Stable isotope analysis using tunable diode laser spectroscopy, *Applied Optics, 31*, 1921-27, 1992.

Bergamaschi, P., and G.W. Harris, Measurements of stable isotope ratios $^{13}CH_4/^{12}CH_4$ $^{12}CH_3D/^{12}CH_4$ in landfill methane using a tunable diode laser absorption spectrometer, *Global Biogeochemical Cycles, 9*, 439-447, 1995.

Bergamaschi, P., M. Schupp, and G.W. Harriss, High-precision direct measurements of $^{13}CH_4/^{12}CH_4$ and $^{12}CH_3D/^{12}CH_4$ ratios in atmospheric methane sources by means of a long-path tunable diode laser absorption spectrometer, *Applied Optics, 33*, 7704-7716, 1994.

Boggs, P.T., and J.E. Rogers, Orthogonal distance regression, *Contemporary Mathematics, 112*, 183-194, 1990.

Bouwman, A.F., K.W. Van der Hoek, and J.G.J. Olivier, Uncertainties in the global source distribution of nitrous oxide, *Journal of Geophysical Research, 100*, 2785-2800, 1995.

Bowen, R., *Isotopes and Climates*, 483 pp., Elsevier, London, 1991.

Braden, B., S. Adams, L.P. Duan, K.H. Orth, F.D. Maul, B. Lembcke, G. Hor, and W.F. Caspary, The [^{13}C]acetate breath test accurately reflects gastric emptying of liquids in both liquid and semisolid test meals, *Gastroenterology, 108*, 1048-1055, 1995.

Brunke, E.-G., H.G. Scheel, and W. Seiler, Trends of tropospheric carbon monoxide, nitrous oxide and methane as observed at Cape Point, South Africa, *Atmospheric Environment, 24A*, 585-595, 1990.

Chackerian, C.J., and R.H. Tipping, *Journal of Molecular Spectroscopy, 99*, 431, 1983.

Ciais, P., P.P. Tans, M. Trolier, J.W.C. White, and R.J. Francey, A large northern hemisphere terrestrial CO_2 sink indicated by the $^{13}C/^{12}C$ ratio of atmospheric CO_2, *Science, 269*, 1098-1102, 1995a.

Ciais, P., P.P. Tans, J.W.C. White, M. Trolier, R.J. Francey, J.A. Berry, D.R. Randall, P.J. Sellers, J.G. Collatz, and D.S. Schimel, Partitioning of ocean and land uptake of CO_2 as inferred by delta-C13 measurements from the NOAA Climate Modelling and Diagnostics Laboratory global air sampling network[Review], *Journal of Geophysical Research, 100*, 5051-5070, 1995b.

Conny, J.M., and L.A. Currie, The isotopic characterization of methane, non-methane hydrocarbons and formaldehyde in the troposphere [Review], *Atmospheric Environment, 30*, 621-638, 1996.

Conway, T.J., P.P. Tans, L.S. Waterman, and K.W. Thoning, Evidence for interannual variability of the carbon cycle from the National Oceanic and Atmospheric Administration Climate Monitoring and Diagnostics Laboratory global air sampling network, *Journal of Geophysical Research, 99*, 22831-22855, 1994.

Craig, H., isotopic standards for carbon and oxygen and correction factors for mass-spectrometric analysis of carbon dioxide, *Geochimica et Cosmochimica Acta, 12*, 133-149, 1957.

Craig, H., and C.D. Keeling, The effects of atmospheric N_2O on the measured isotopic composition of atmospheric CO_2, *Geochimica et Cosmochimica Acta, 27*, 549-551, 1963.

Crill, P.M., J.H. Butler, D.J. Cooper, and P.C. Novelli, Standard analytical methods for measuring trace gases in the environment, in *Biogenic Trace Gases: Measuring Emissions from Soil and Water*, edited by P.A. Matson, and R.C. Harriss, pp. 164-205, Blackwell Science Ltd, Oxford, 1995.

Crutzen, P.J., The influence of nitrogen oxides on the atmospheric ozone content, *Q. J. R. Meteorol. Soc., 96*, 320-325, 1970.

Da Costa, G., and L.P. Steele, Preliminary performance of cape Grim's new low flow rate CO_2 analyser system, in *Cape Grim Baseline Air Pollution Station, Annual Meeting, 28-29 November 1996*, Stanley, Tasmania, 1996.

Denmead, O.T., Developments in flux measurements of greenhouse gases, *Journal of Agricultural Meteorology, 48*, 543-550, 1993.

Denmead, O.T., and M.R. Raupach, Methods for measuring atmospheric gas transport in agricultural and forest systems, in *Agroecosystem Effects on RadiativelyImportant Trace Gases and Global Climate Change*, edited by J.M. Duxbury, L.A. Harper, A.R. Mosier, and D.E. Rolston, pp. 19-43, American Society of Agronomy, Madison, 1993.

Denmead, O.T., M.R. Raupach, F.X. Dunin, H.A. Cleugh, and R. Leuning, Boundary layer budgets for regional estimates of scalar fluxes, *Global Change Biology, 2*, 255-264, 1996.

Derwent, R.G., P.G. Simmonds, and W.J. Collins, Ozone and carbon monoxide measurements at a remote maritime location, Mace Head, Ireland, from 1990 to 1992, *Atmospheric Environment, 28*, 2623-2637, 1994.

Dianov-Klokov, V.I., L.N. Yurganov, E.I. Grechko, and A.Z. Dzola, Spectroscopic measurements of atmospheric carbon monoxide and methane. 1: Latitudinal distribution., *Journal of Atmospheric Chemistry, 8*, 139-151, 1989.

Dlugokencky, E.J., L.P. Steele, P.M. Lang, and K.A. Masarie, The growth rate and distribution of atmospheric methane, *Journal of Geophysical Research, 99*, 17021-17043, 1994.

Dlugokencky, E.J., L.P. Steele, P.M. Lang, and K.A. Masarie, Atmospheric methane at Mauna Loa and Barrow observatories - presentation and analysis of in situ measurements, *Journal of Geophysical Research, 100*, 23103-23113, 1995.

Dunse, B., L.P. Steele, M. Lucarelli, and P. Fraser, An analysis of Melbourne pollution episodes observed at Cape Grim during 1995, in *Cape Grim Baseline Air Pollution Station Annual Meeting, 1996*, edited by A.L. Dick, Stanley, Tasmania, 1996.

Elkins, J., T. Thompson, T. Swanson, J. Butler, B. Hall, S. Cummings, D. Fisher, and A. Raffo, Decrease in the growth rate of atmopheric chlorofluorocarbons-11 and -12, *Nature, 364*, 780-783, 1993.

Elkins, J.W., J.H. Butler, T.M. Thompson, S.A. Montzka, R.C. Myers, J.M. Lobert, S.A. Yvon, P.R. Wamsley, F.L. Moore, J.M. Gilligan, D.F. Hurst, A.D. Clarke, T.H. Swanson, C.M. Volk, L.T. Lock, L.S. Geller, G.S. Dutton, R.M. Dunn, M.F. Dicorleto, T.J. Baring, and A.H. Hayden, Nitrous oxide and halocompounds, in *Climate Monitoring and Diagnostics Laboratory No. 23 Summary Report 1994-95*, edited by D. Hofmann, J. Peterson, and R. Rosson, pp. 84-111, US Department of Commerce, Boulder, Colorado, 1996.

Etheridge, D.M., G.I. Pearman, and P.J. Fraser, Changes in tropospheric methane between 1841 and 1978 from a high accumulation-rate Antarctic ice core, *Tellus, 44B*, 282-294, 1992.

Etheridge, D.M., L.P. Steele, R.L. Langenfelds, R.J. Francey, J.-M. Barnola, and V.I. Morgan, Natural and anthropogenic changes in atmospheric CO_2 over the last 1000 years from air in Antarctic ice and firn, *Journal of Geophysical Research, 101*, 4115-28, 1996.

Evans, W.F.J., and E. Puckrin, An observation of the greenhouse radiation associated with carbon monoxide, *Geophysical Research Letters, 22*, 925-928, 1995.

Foulger, B.E., and P.G. Simmonds, Ambient temperature gas purifier suitable for the trace analysis of carbon monoxide and hydrogen and the preparation of low level carbon monoxide calibration standards in the field, *Journal of Chromatography, 630*, 257-263, 1993.

Francey, R.J., C.E. Allison, and E.D. Welch, The 11-year high precision in situ CO_2 stable isotope record from Cape Grim, 1982-1992, in *Baseline Atmospheric Program (Australia) 1992*, edited by A.L. Dick, and P.J. Fraser, pp. 16-25, Bureau of Meterology and CSIRO Division of Atmospheric Research, Melbourne, 1995a.

Francey, R.J., L.P. Steele, R.L. Langenfelds, M.P. Lucarelli, C.E. Allison, D.J. Beardsmore, S.A. Coram, N. Derek, F.R. de Silva, D.M. Etheridge, P.J. Fraser, R.J. Henry, B. Turner, E.D. Welch, D.A. Spencer, and L.N. Cooper, Global Atmospheric Sampling Laboratory (GASLAB): supporting and extending the Cape Grim trace gas programs, in *Baseline Atmospheric Program (Australia) 1993*, edited by R.J. Francey, A.L. Dick, and N. Derek, pp. 8-29, Bureau of Meterology and CSIRO Division of Atmospheric Research, Melbourne, 1996.

Francey, R.J., P.P. Tans, C.E. Allison, I.G. Enting, J.W.C. White, and M. Trolier, Changes in oceanic and terrestrial carbon uptake since 1982, *Nature, 373*, 326-330, 1995b.

Fraser, P., S. Coram, and N. Derek, Atmospheric methane, carbon monoxide and carbon dioxide by gas chromatography, in *Baseline Atmospheric Program (Australia) 1991*, edited by A.L. Dick, and J.L. Gras, pp. 60-64, Bureau of Meteorology and CSIRO Division of Atmospheric Research, Melbourne, 1994.

Fraser, P.J., L.P. Steele, M.P. Lucarelli, N. Derek, and L.W. Porter, Halocarbons, nitrous oxide, methane and carbon monoxide and hydrogen- the AGAGE program, in *Baseline Atmospheric Program (Australia) 1993*, edited by R.J. Francey, A.L. Dick, and N. Derek, pp. 89-90, Bureau of Meteorology and CSIRO Division of Atmospheric Research, Melbourne, 1996.

Fried, A., B. Henry, D.D. Parrish, J.R. Carpenter, and M.P. Buhr, Intercomparison of tunable diode lasers and gas filter correlation measurements of ambient carbon monoxide, *Atmospheric Environment, 25A*, 2277-2284, 1991.

Galle, B., L. Klemedtsson, and D.W.T. Griffith, Application of a Fourier transform IR system for measurements of N_2O fluxes using micrometeorological methods, an ultralarge chamber system and conventional field chambers, *Journal of Geophysical Research, 99*, 16,575-16,583, 1994.

Garratt, J.R., *The atmospheric boundary layer*, 316 pp., Cambridge University Press, Cambridge, 1992.

Goody, R.M. and Y.L. Yung, *Atmospheric Radiation: Theoretical Basis*, 519 pp.,Oxford University Press, New York, 1989.

Graedel, T.E., and P.J. Crutzen, *Atmospheric Change: An Earth System Perspective*, 446 pp., W.H. Freeman and Company, New York, 1993.

Grant, W.B., R.H. Kagann, and W.A. McClenny, *Journal of Air Waste Management Association, 42*, 18, 1992.

Griffith, D.W.T., Synthetic calibration and quantitative analysis of gas-phase FT-IR spectra, *Applied Spectroscopy, 50*, 59-70, 1996.

Griffiths, P.R., and J.A.d. Haseth, *Fourier transform infrared spectrometry*, 656 pp., John Wiley and Sons, New York, 1986.

Haaland, D.M., Multivariate calibration methods applied to quantitative FT-IR analyses, in *Practical Fourier Transform Infrared Spectroscopy*, edited by J.R. Ferraro, and K. Krishnan, Academic Press, San Diego, 1990.

Haaland, D.M., R.G. Easterling, and D.A. Vopicka, Multivariate least-squares methods applied to the quantitative spectral analysis of multicomponent samples, *Applied Spectroscopy, 39*, 73-84, 1985.

Haaland, D.M., and E.V. Thomas, Partial least-squares methods for spectral analysis. 1. Relation to other quantitative calibration methods and the extraction of qualitative information, *Analytical Chemistry, 60*, 1193-1202, 1988.

Haisch, M., P. Hering, W. Fuss, and W. Fabinski, A sensitive isotope selective nondispersive infrared spectrometer for $^{13}CO_2$ and $^{12}CO_2$ concentration measurements in breath samples, *Isotopenpraxis, 30*, 247-251, 1994.

Hanst, P.L., and S.T. Hanst, Gas measurement in the fundamental infrared region, in *Air Monitoring by Spectroscopic Techniques*, edited by M.W. Sigrist, pp. 335-470, John Wiley and Sons, New York, 1994.

Hargreaves, K.J., U. Skiba, D. Fowler, J. Arah, F.G. Wienhold, L. Klemedtsson, and B. Galle, Measurement of nitrous oxide emission from fertilized grassland using micrometeorological techniques, *Journal of Geophysical Research, 99*, 16569-16574, 1994.

Harriss, R.C., G.W. Sachse, G.F. Hill, L. Wade, K.B. Bartlett, J.E. Collins, L.P. Steele, and P.C. Novelli, Carbon monoxide and methane in the North American Arctic and subarctic troposphere: July-August 1988, *Journal of Geophysical Research, 97*, 16589-16599, 1992.

Hurst, D.F., D.W.T. Griffith, J.J. Carras, D.J. Williams, and P.J. Fraser, Measurements of trace gases emitted by Australian savanna fires during the 1990 dry season, *Journal of Atmospheric Chemistry, 18*, 33-56, 1994a.

Hurst, D.F., D.W.T. Griffith, and G.D. Cook, Trace gas emissions from biomass burning in tropical Australian savannas, *Journal of Geophysical Research, 99*, 16441-16456, 1994b.

Hurst, D.F., D.W.T. Griffith, and G.D. Cook, Trace gas emissions from biomass burning in Australia, in *Biomass Burning and Global Change 2: Biomass Burning in South America, Southeast Asia, and Temperate and Boreal Ecosystems, and the Kuwait Oil Fires*, edited by J.S. Levine, MIT Press, Cambridge, MA, 1997.

IPCC, *Climate Change 1994: Radiative Forcing of Climate Change*, 339 pp., Cambridge University Press, Cambridge, 1995.

IPCC, *Climate Change 1995: The Science of Climate Change*, 572 pp., Cambridge University Press, Cambridge, 1996.

Johns, J.W.C., *Journal of Molecular Spectroscopy, 125*, 442, 1987.

Junge, C.E., Residence time and variability of tropospheric trace gases, *Tellus, 26*, 477-487, 1974.

Kaimal, J.C., and J.J. Finnigan, *Atmospheric boundary layer flows: their structure and measurement*, 289 pp., Oxford University Press, Oxford, 1994.

Kattenberg, A., F. Giorgi, H. Grassl, G.A. Meehl, J.F.B. Mitchell, R.J. Stouffer, T. Tokioka, A.J. Weaver, and T.M.L. Wigley, Climate Models - Projections of Future Climate, in *Climate Change 1995: The Science of Climate Change (IPCC 1995)*, edited by J.T. Houghton, L.G.M. Filho, B.A. Callander, N. Harris, A. Kattenberg, and K. Maskell, pp. 285-357, Canbridge University Press, Cambridge, 1996.

Keeling, C.D., The concentration and isotopic abundances of atmospheric carbon dioxide in rural areas, *Geochimica et Cosmochimica Acta, 13*, 322-334, 1958.

Keller, M., E. Veldkamp, A.M. Weitz, and W.A. Reiners, Effect of pasture age on soil trace-gas emissions from a deforested area of Costa-Rica, *Nature, 365*, 244-246, 1993.

Khalil, M.A.K., Decline in atmospheric carbon monoxide raises questionsabout its cause, *EOS, 76*, 353-354, 1995.

Khalil, M.A.K., and R.A. Rasmussen, Global decrease in atmospheric carbon monoxide concentration, *Nature, 370*, 639-641, 1994.

Kindness, A., and I.L. Marr, Measurement Of carbon-13/carbon-12 ratios by Fourier transform infrared spectrometry, *Analyst, 121*, 205-209, 1996.

Kindness, A., and I.L. Marr, Improved infrared spectroscopic method for the measurement of ^{13}C:^{12}C ratios, *Applied Spectroscopy, 51*, 17-21, 1997.

Klein, P.D., and D.Y. Graham, Minimum analysis requirements for the detection of Helicobacter-pylori infection by the ^{13}C-urea breath test, *American Journal of Gastroenterology, 88*, 1865-1869, 1993.

Kolb, C.E., J.C. Wormhoudt, and M.S. Zahniser, Recent advances in spectroscopic instrumentation for measuring stable gases in the natural environment, in *Biogenic Trace Gases: Measuring Emissions from Soil and Water*, edited by P.A. Matson, and R.C. Harriss, pp. 259-290, Blackwell Science, Oxford, 1995.

Koletzko, S., M. Haisch, I. Seeboth, B. Braden, K. Hengels, B. Koletzko, and P. Hering, Isotope-selective non-dispersive infrared spectrometry for detection of Helicobacter pylori infection with ^{13}C-urea breath test, *Lancet, 345*, 961-962, 1995.

Komhyr, W.D., T.B. Harris, L.S. Waterman, J.F.S. Chin, and K.W. Thoning, Atmospheric carbon dioxide at Mauna Loa observatory 1. NOAA global monitoring for climate change measurements with a nondispersive infrared analyzer, 1974-1985, *Journal of Geophysical Research, 94*, 8533-8547, 1989.

Langenfelds, R.L., P.J. Fraser, R.J. Francey, L.P. Steele, L.W. Porter, and C.E. Allison, The Cape Grim air archive: the first seventeen years, 1978-1995, in *Baseline Atmospheric Program (Australia) 1994-95*, edited by R.J. Francey, A.L. Dick, and N. Derek, pp. 53-70, Bureau of Meteorology and CSIRO Division of Atmospheric Research, Melbourne, 1996.

Lenschow, D.H., Micrometeorological techniques for measuring biosphere-atmopshere trace gas exchange, in *Biogenic Trace Gases: Measuring Emissions from Soil and Water*, edited by P.A. Matson, and R.C. Harriss, pp. 126-163, Blackwell Science, Oxford, 1995.

Livingston, G.P., and G.L. Hutchinson, Enclosure-based measurement of trace gas exchange: applications and sources of error, in *Biogenic Trace Gases: Measuring Emissions from Soil and Water*, edited by P.A. Matson, and R.C. Harriss, pp. 14-51, Blackwell Science, Oxford, 1995.

Lloyd, J., and G.D. Farquhar, ^{13}C discrimination during CO_2 assimilation by the terrestrial biosphere[Review], *Oecologia, 99*, 201-215, 1994.

Lovelock, J.E., *Gaia: a new look at life on earth*, Oxford University Press, Oxford, 1982

Lovelock, J.E., *The ages of Gaia: a biography of our living earth*, 252 pp., Oxford University Press, Oxford, 1990.

Lovelock, J.E., and S.R. Lipsky, Electron affinity spectroscopy - a new method for the identification of functional groups in chemical compounds separated by gas chromatography, *Journal of the American Chemical Society, 82*, 431-433, 1960.

Machida, T., T. Nakazawa, Y. Fujii, S. Aoki, and O. Watanabe, Increase in the atmospheric nitrous oxide concentration during the last 250 years, *Geophysical Research Letters, 22*, 2921-2924, 1995.

Mak, J.E., and C.A.M. Brenninkmeijer, Compressed air sample technology for isotopic analysis of atmospheric carbon monoxide, *Journal of Atmospheric & Oceanic Technology, 11*, 425-431, 1994.

Meieraugenstein, W., A. Hess, G.F. Hoffmann, and D. Rating, Evaluation of water removal and memory effect in $^{13}CO_2$ breath tests by isotope ratio mass spectrometry, *Isotopenpraxis, 30*, 349-358, 1994.

Merritt, D.A., J.M. Hayes, and D.J.D. Marais, Carbon isotopic analysis of atmospheric methane by isotope-ratio-monitoring gas chromotography-mass spectrometry, *Journal of Geophysical Research, 100*, 1317-1326, 1995.

Michelson, A.A., *Phil. Mag., 5*, 256, 1891.

Migeotte, M., and l. Neven, Recents progres dans l'observation du spectra solaire a la ststion scientific du Jungfraujoch, *Societie de Sciences a Liege, 12*, 165-169, 1952.

Migeotte, M.V., Spectroscopic evidence of methane in the earth's atmosphere, *Phys. Rev., 73*, 519-520, 1948.

Mion, F., P. Queneau, M. Rousseau, J.L. Brazier, P. Paliard, and Y. Minaire, Aminopyrine breath test - development of a ^{13}C-breath test for quantitative assessment of liver function in humans, *Hepato-Gastroenterology, 42*, 931-938, 1995.

Murnick, D.E., and B.J. Peer, Laser-based analysis of carbon isotope ratios, *Science, 263*, 945-947, 1994.

National Greenhouse Gas Inventory Committee, National greenhouse gas inventory 1994, Australia, National Greenhouse Gas Inventory Committee 1996, Canberra, 1996.

Nevison, C.D., R.F. Weiss, and D.J. Erikson III, Global oceanic emissions of nitrous oxide, *Journal of Geophysical Research, 100*, 15809-15820, 1995.

Novelli, P.C., J.W. Elkins, and L.P. Steele, The development and evaluation of a gravimetric reference scale for measurements of atmospheric carbon monoxide, *Journal of Geophysical Research, 96*, 13109-13121, 1991.

Novelli, P.C., K.A. Masarie, P.P. Tans, and P.M. Lang, Recent changes in atmospheric carbon monoxide, *Science, 263*, 1587-1590, 1994.

Novelli, P.C., L.P. Steele, and P.P. Tans, Mixing ratios of carbon monoxide in the troposphere, *Journal of Geophysical Research, 97*, 20731-20750, 1992.

Prather, M., R. Derwent, D. Ehhalt, P. Fraser, E. Sanhueza, and X. Zhou, Other trace gases and atmospheric chemistry, in *Climate Change 1994: Radiative Forcing of Climate Change and An Evaluation of the IPCC IS92 Emission Scenarios (IPCC 1994)*, edited by J.T. Houghton, L.G.M. Filho, J. Bruce, H. Lee, B.A. Callander, E. Haites, N. Harris, and K. Maskell, pp. 75-126, Cambridge University Press, Cambridge, 1995.

Prinn, R., D. Cunnold, R. Rasmussen, P. Simmonds, F. Alyea, A. Crawford, P. Fraser, and R. Rosen, Atmospheric emissions and trends of nitrous oxide deduced from 10 years of ALE-GAGE data, *Journal of Geophysical Research, 95*, 18369-18385, 1990.

Prinn, R.G., R.F. Weiss, F.N. Alyea, D.M. Cunnold, P.J. Fraser, L.P. Steele, and P.G. Simmonds, Advanced Global Atmospheric Gases Experiment (AGAGE), in *Climate Monitoring and Diagnostics Laboratory No. 23 Summary Report 1994-95*, edited by D. Hofmann, J. Peterson, and R. Rosson, pp. 142-43, U.S. Department of Commerce, Boulder, Colorado, 1996.

Quay, P., J. Stutsman, and D. Wilbur, The $^{13}C/^{12}C$ of atmospheric methane, in *Climate Monitoring and Diagnostics Laboratory No. 23 Summary Report 1994-95*, edited by D. Hofmann, J. Peterson, and R. Rosson, pp. 144-145, US Department of Commerce, Boulder, Colorado, 1995.

Quay, P., D. Wilbur, S. Wofsy, and J. Richey, $^{13}C/^{12}C$ of atmospheric CO_2 in the Amazon basin: forest and river sources, *Journal of Geophysical Research, 94*, 18327-18336, 1989.

Raupach, M.R., O.T. Denmead, and F.X. Dunin, Challenges in linking atmospheric CO_2 concentrations to fluxes at local and regional scales, *Australian Journal of Botany, 40*, 697-716, 1992.

Raupach, M.R., R. Leuning, J.P. Brunel, N. Clark, H.A. Cleugh, P.A. Coppin, O.T. Denmead, F.X. Dunin, G.D. Farquhar, J.J. Finnigan, I.E. Galbally, R.D. Graetz, D.W.T. Griffith, J.M. Hacker, J. lloyd, J. McAneney, K.G. McNaughton, M. Meyers, Y. Miao, W. Reyenga, P. Schwerdtfeger, and C. Wong, OASIS science plan: investigations of the biosphere-atmosphere exchanges of energy, water, CO_2, trace gases and stable isotopes in heterogeneous terrain at scales from leaf to region, CSIRO Centre for Environmental Mechanics, Canberra, 1994.

Rothman, L.S., R.R. Gamache, R.H. Tipping, C.P. Rinsland, M.A.H. Smith, D.C. Benner, V.M. Devi, J.-M. Flaud, C. Camy-Peyret, A. Perrin, A. Goldman, S.T. Massie, L.R. Brown, and R.A. Toth, The HITRAN molecular database: editions of 1991 and 1992, *Journal of Quantitative Spectroscopy and Radiative Transfer, 48*, 469-507, 1992.

Rudolph, J., D.C. Lowe, R.J. Martin, and T.S. Clarkson, A novel method for compound specific determination of d13C in volatile organic compounds at ppt levels in ambient air, *Geophysical Research Letters, 24*, 659-662, 1997.

Sachse, G.W., G.F. Hill, L.O. Wade, and M.G. Perry, Fast-response, high precision carbon monoxide sensor using a tunable diode laser absorption technique, *Journal of Geophysical Research, 92*, 2071-2081, 1987.

Schimel, D., D. Alves, I. Enting, M. Heimann, F. Joos, D. Raynaud, T. Wigley, M. Prather, R. Derwent, D. Ehhalt, P. Fraser, E. Sanhueza, X. Zhou, P. Jonas, R. Charlson, H. Rodhe, S. Sadasivan, K.P. Shine, Y. Fouquart, V. Ramaswamy, S. Solomon, J. Srinavasan, D. Albritton, I. Isaksen, M.Lal, and D. Wuebbles, Radiative Forcing of Climate Change, in *Climate Change 1995: The Science of Climate change (IPCC 1995)*, edited by J.T. Houghton, L.G.M. Filho, B.A. Callander, N. Harris, A. Kattenberg, and K. Maskell, pp. 65-131, Cambridge University Press, Cambridge, 1996.

Sebacher, D.I., and R.C. Harriss, A system for measuring methane fluxes from inland and coastal environments, *Journal of Environmental Quality, 11*, 34-37, 1982.

Smith, K.A., H. Clayton, J.R.M. Arah, S. Christensen, P. Ambus, D. Fowler, K.J. Hargreaves, U. Skiba, G.W. Harris, F.G. Wienhold, L. Klemedtsson, and B. Galle, Micrometeorological and chamber methods for measurement of nitrous oxide fluxes between soils and the atmosphere - overview and conclusions, *Journal of Geophysical Research, 99*, 16541-16548, 1994a.

Smith, K.A., A. Scott, B. Galle, and L. Klemedtsson, Use of a long-path infrared gas monitor for measurement of nitrous oxide flux from soil, *Journal of Geophysical Research, 99*, 16585-16592, 1994b.

Steele, L.P., D.J. Beardsmore, G.I. Pearman, and G.A. Da Costa, Baseline Carbon Dioxide Monitoring, in *Baseline Atmospheric Program Australia 1994-95*, edited by R.J. Francey, A.L. Dick, and N. Derek, pp. 103, Bureau of Meteorology and CSIRO Division of Atmospheric Research, Melbourne, 1996a.

Steele, L.P., R.J. Francey, R.L. Langenfelds, C.E. Allison, M.P. Lucarelli, P.P. Tans, E.J. Dlugokencky, T.J. Conway, P.C. Novelli, K.A. Masarie, J.W.C. White, and M. Trolier, An operational intercalibration experiment between CMDL and CSIRO to measure several atmospheric trace species, in *Climate Monitoring and Diagnostics Laboratory No. 23 Summary Report 1994-95*, edited by D. Hofmann, J. Peterson, and R. Rosson, pp. 148-49, US Department of Commerce, Boulder, Colorado, 1995.

Steele, L.P., P.J. Fraser, R.A. Rasmussen, M.A.K. Khalil, T.J. Conway, A.J. Crawford, R.H. Gammon, K.A. Masarie, and K.W. Thoning, The global distribution of methane in the troposphere, *Journal of Atmospheric Chemistry, 5*, 125-171, 1987.

Steele, L.P., R.L. Langenfelds, M.P. Lucarelli, P.J. Fraser, L.N. Cooper, D.A. Spencer, S. Chea, and K. Broadhurst, Atmospheric methane, carbon dioxide, carbon monoxide, hydrogen, and nitrous oxide from Cape Grim flask air samples analysed by gas chromatography, in *Baseline Atmospheric Program Australia 1994-95*, edited by R.J. Francey, A.L. Dick, and N. Derek, pp. 107-111, Bureau of Meteorology and CSIRO Division of Atmospheric Research, Melbourne, 1996b.

Steele, L.P., M.P. Lucarelli, P.J. Fraser, N. Derek, and L.W. Porter, Halocarbons, nitrous oxide, methane, carbon monoxide and hydrogen - the AGAGE program, 1993-95, in *Baseline Atmospheric Program Australia 1994-95*, edited by R.J. Francey, A.L. Dick, and N. Derek, pp. 134-140, Bureau of Meteorology and CSIRO Division of Atmospheric Research, Melbourne, 1996c.

Tans, P.P., P.S. Bakwin, T.J. Conway, R.W. Dissly, E.J. Dlugokencky, L.S. Geller, D.W. Guenther, D.F. Hurst, D.R. Kitzis, P.M. Lang, K.A. Masarie, J.B. Miller, P.C. Novelli, C. Prostko-Bell, M. Ramonet, K.W. Thoning, M. Trolier, L.S. Waterman, N. Zhang, and C. Zhao, Carbon cycle, in *Climate Monitoring and Diagnostics Laboratory No. 23 Summary Report 1994-95*, edited by D. Hofmann, J. Peterson, and R. Rosson, pp. 29-49, US Department of Commerce, Boulder, Colorado, 1995.

Tans, P.P., J.A. Berry, and R.F. Keeling, Oceanic $^{13}C/^{12}C$ observations - a new window on ocean CO_2 uptake, *Global Biogeochemical Cycles, 7*, 353-368, 1993.

Toth, R.A., *Applied Optics*, *32*, 7326, 1993.

Wahlen, M., and T. Yoshinari, Oxygen isotope ratios in N_2O from different environments, *Nature*, *313*, 780-82, 1985.

Wallace, J.M. and P.V. Hobbs, *Atmospheric science: an introductory survey*, 467 pp., Academic Press, San Diego, 1977.

Warneck, P., *Chemistry of the natural atmosphere*, 753 pp., Academic Press, San Diego, 1988.

Wayne, R.P., *Chemistry of atmospheres*, Claredon Press. Oxford, 1991.

Weeks, I.A., I.E. Galbally, P.J. Fraser, and G. Matthews, Comparison of the carbon monoxide standards used at Cape Grim and Aspendale, in *Baseline Atmospheric Program 1987*, edited by B.W. Forgan, and G.P. Ayers, pp. 21-25, Australian Government Department of Science and Technology, Canberra, 1989.

White, J.U., Long optical paths of large aperture, *Journal of the Optical Society of America*, *32*, 285-288, 1942.

White, J.U., Very long optical paths in air, *Journal of the Optical Society of America*, *66*, 411-416, 1976.

Wienhold, F.G., H. Frahm, and G.W. Harris, Measurements of N_2O fluxes from fertilized grassland using a fast response tunable diode laser spectrometer, *Journal of Geophysical Research*, *99*, 16557-16567, 1994.

Wilson, S.R., A.L. Dick, P.J. Fraser, and S. Whittlestone, Nitrous oxide flux estimates for south-eastern Australia, *Journal of Atmospheric Chemistry*, *26*, 169-188, 1997.

Wofsy, S.C., R.C. Harriss, and W.A. Kaplan, Carbon dioxide in the atmosphere over the Amazon Basin, *Journal of Geophysical Research*, *93*, 1377-1387, 1988.

Yakir, D., and X.-F. Wang, Fluxes of CO_2 and water between terrestrial vegetation and the atmosphere estimated from isotope measurements, *Nature*, *380*, 515-17, 1996.

Yoshinari, T., and M. Wahlen, Oxygen isotope ratios in N_2O from nitrification at a wastewater treatment facility, *Nature*, *317*, 349-50, 1985.

Zander, R., P. Demoulin, D.H. Ehhalt, U. Schmidt, and C.P. Rinsland, Secular increase of the total vertical column abundance of carbon monoxide above central Europe since 1950, *Journal of Geophysical Research*, *94*, 11021-11028, 1989.

D.B. AITCHISON
BOOKBINDER
122 WINDANG RD
PRIMBEE 2502
PH.42742229